



**HAL**  
open science

# Quaternary variations and origin of continental dust in East antarctica

Barbara Delmonte

► **To cite this version:**

Barbara Delmonte. Quaternary variations and origin of continental dust in East antarctica. Glaciology. Università degli studi di Milano-Bicocca, 2003. English. NNT: . tel-00701343

**HAL Id: tel-00701343**

**<https://theses.hal.science/tel-00701343>**

Submitted on 25 May 2012

**HAL** is a multi-disciplinary open access archive for the deposit and dissemination of scientific research documents, whether they are published or not. The documents may come from teaching and research institutions in France or abroad, or from public or private research centers.

L'archive ouverte pluridisciplinaire **HAL**, est destinée au dépôt et à la diffusion de documents scientifiques de niveau recherche, publiés ou non, émanant des établissements d'enseignement et de recherche français ou étrangers, des laboratoires publics ou privés.

**Università degli Studi di Siena**

*Dipartimento di Scienze della Terra*



Dottorato di Ricerca in

**Scienze Polari**

XVI Ciclo

**QUATERNARY VARIATIONS AND ORIGIN  
OF CONTINENTAL DUST IN  
EAST ANTARCTICA**

Barbara Delmonte

Tesi in Co-Tutela con  
Université Joseph Fourier – Grenoble I, Grenoble (Francia)



*Laboratoire de Glaciologie  
et Géophysique de l'Environnement (L.G.G.E.-C.N.R.S.)*



*Università degli Studi di Milano-Bicocca,  
Dipartimento di Scienze Ambientali, Milano, Italia.*



Tutori:

Dr. **Jean Robert Petit**, L.G.G.E.-C.N.R.S., St. Martin D'Hères, Francia

Prof. **Valter Maggi**, D.I.S.A.T., Università Milano-Bicocca, Milano, Italia

Università degli Studi di Siena  
*Dipartimento di Scienze della Terra*



Dottorato di Ricerca in  
**Scienze Polari**

XVI Ciclo

Collegio dei docenti

Riccardo Cattaneo-Vietti  
Silvano Focardi  
Francesco M. Faranda  
Roberto Frache  
Francesco Francioni  
Marcello Mellini  
Carlo Alberto Ricci (Coordinatore)  
Franco M. Talarico  
Sergio Tucci  
Maritza Zampi  
Tecla Zunini-Sertorio

Data dell'esame finale  
16/12/2003

Commissione giudicatrice:

Dr. **Eric Wolff**, British Antarctic Survey, Cambridge (UK)  
Prof. **Francis Grousset**, Université de Bordeaux I, Talence (F)  
Dr. **Jean Robert Petit**, LGGE-CNRS, St. Martin d'Hères, Grenoble (F)  
Prof. **Peter J. Barrett**, Victoria University of Wellington, Wellington (NZ)  
Prof. **Marcello Mellini**, Dip. Scienze della Terra, Università di Siena, Siena (I)  
Prof. **Valter Maggi**, DISAT, Università di Milano-Bicocca, Milano (I)

## RIASSUNTO

Oggetto della presente Tesi di Dottorato di Ricerca in Scienze Polari é lo studio della provenienza geografica e delle variazioni temporali degli aerosol minerali di origine continentale (polveri) trasportati nel Plateau Antartico Orientale nel Quaternario, in particolare nel corso dell'ultimo ciclo climatico.

Quattro carote di ghiaccio profonde prelevate rispettivamente a Dome C (75° 06'S, 123° 21'E), nell'ambito del progetto EPICA (*European Project for Ice Coring in Antarctica*), a Dome B (77° 05' S, 94° 55' E), a Vostok (78° S, 106° E) e a Komsomolskaia (74° 05' S, 97° 29' E) sono state analizzate.

L'origine delle polveri nei periodi glaciali e interglaciali é stata investigata attraverso l'analisi della loro segnatura isotopica ( $^{87}\text{Sr}/^{86}\text{Sr}$  versus  $^{143}\text{Nd}/^{144}\text{Nd}$ ) e la comparazione con sedimenti di origine eolica specificamente prelevati nelle potenziali aree sorgenti dell'Emisfero Australe.

L'analisi ad alta risoluzione temporale della concentrazione e della granulometria delle polveri preservate nelle quattro carote di ghiaccio ha permesso di trarre importanti informazioni sulle variazioni della circolazione atmosferica alle alte latitudini dell'Emisfero Sud, sulle condizioni ambientali alle sorgenti e sul ciclo idrologico in atmosfera.

Le vaste piane sudamericane delle Pampas e la Patagonia sono la sorgente dominante su tutto il Plateau Antartico nei periodi glaciali, mentre un contributo aggiuntivo da parte di un'altra regione é fortemente probabile durante gli interglaciali

Il flusso di polveri in Antartide Orientale nel Quaternario appare notevolmente uniforme da un sito all'altro; tale omogeneità cela tuttavia differenze significative nel trasporto, in particolare durante l'Ultimo Massimo Glaciale, ricostruite attraverso la differente granulometria del particolato.

La riorganizzazione della circolazione atmosferica nella regione polare e circumpolare avvenuta durante l'ultima transizione climatica ha influenzato il trasporto di polveri, generando variazioni asincrone e tendenze opposte da un settore all'altro del Plateau.

L'Olocene e l'ultima deglaciazione appaiono caratterizzati in tutti e quattro i siti investigati da variazioni periodiche del trasporto di polveri a scala millenaria e multi-secolare. Tali pulsazioni, che presentano le medesime frequenze da un sito all'altro ma differente fase, sembrano suggerire la propagazione circumpolare di anomalie nei sistemi oceano-ghiaccio marino-atmosfera a scale temporali multi-centennali e millenarie, in una sorta di effetto d'onda simile all'attuale movimento interannuale dell'Onda Circumpolare Antartica.

## RESUME

Les variations temporelles et la provenance des aérosols minéraux continentaux (poussières) dans l'Antarctique de l'Est au cours de la fin du Quaternaire et en particulier pendant la dernière transition climatique ont été étudiées au cours de cette thèse.

Quatre carottes de glace profondes prélevées respectivement à Dome C (75° 06' S, 123° 21' E), dans le cadre du projet Européen EPICA (*European Project for Ice Coring in Antarctica*), à Dome B (77° 05' S, 94° 55' E), à Vostok (78° S, 106° E) et à Komsomolskaia (74° 05' S, 97° 29' E) ont été analysées. L'origine géographique des poussières dans les périodes glaciaires et interglaciaires a été précisée grâce à la signature isotopique des poussières ( $^{87}\text{Sr}/^{86}\text{Sr}$  versus  $^{143}\text{Nd}/^{144}\text{Nd}$ ) et à la comparaison avec des sédiments éoliens spécifiquement prélevés dans les régions potentielles d'origine des aérosols de l'hémisphère austral.

L'analyse à haute résolution temporelle des paramètres de concentration et de distribution en taille des aérosols minéraux a permis d'obtenir d'importantes informations sur la circulation atmosphérique aux hautes latitudes de l'hémisphère Sud, ainsi que sur les conditions environnementales aux sources et sur le cycle hydrologique dans l'atmosphère.

Les plaines sud-américaines des Pampas et la Patagonie apparaissent comme étant les sources dominantes sur tout le Plateau Antarctique au cours des périodes glaciaires; par contre, on suspecte une contribution additionnelle d'une autre source durant les interglaciaires.

Le flux de poussières en Antarctique de l'Est au cours du Pléistocène et de l'Holocène est remarquablement homogène parmi les sites; par contre, des différences significatives caractérisent la granulométrie des particules, qui est un paramètre lié au transport. La réorganisation de la circulation atmosphérique dans les régions polaires et circumpolaires qui a eu lieu pendant la dernière transition climatique a influencé le transport des poussières, et a généré des variations asynchrones, voire des tendances opposés d'un secteur à l'autre du Plateau.

L'Holocène et la dernière déglaciation sont caractérisés dans toutes les carottes analysées par des variations périodiques du transport à l'échelle millénaire et multi-séculaire. Les fréquences des oscillations sont les mêmes d'un site à l'autre mais la phase est différente.

La rythmicité des advections des poussières sur le Plateau Antarctique semble suggérer la propagation circumpolaire d'anomalies dans les systèmes océan-glace de mer-atmosphère à des échelles temporelles millénaires et multi-séculaires.

## ABSTRACT

The mineral dust of continental origin windblown to the East Antarctic Plateau has been studied for its geographical provenance and variability during the Quaternary.

Four deep ice cores [EPICA-Dome C (75° 06' S, 123° 21' E), Dome B (77° 05' S, 94° 55' E), Vostok (78° S, 106° E) and Komsomolskaia (74° 05' S, 97° 29' E)] have been investigated.

Dust provenance in glacial and interglacial epochs has been identified through the  $^{87}\text{Sr}/^{86}\text{Sr}$  versus  $^{143}\text{Nd}/^{144}\text{Nd}$  isotopic signature of ice core dust and sediments from the Potential Source Areas (PSA) of the Southern Hemisphere. The isotopic method has been refined with respect to previous studies.

Dust concentration and size distribution measurements have been performed at high temporal resolution in order to examine the long-term and short-term variability of dust flux, from which important information about the conditions at the source region(s), the hydrological cycle and the transport patterns can be inferred.

For all East Antarctic sites investigated, dust originates from the southern South American regions of the Pampas and Patagonia in glacial times, but during warm interglacial periods an additional source probably contributed.

The dust input also has proved to be remarkably similar between the different sites, and shows clear relationship with environmental conditions at the source regions.

However, such an apparent uniformity of dust flux nests striking differences in dust transport, particularly during the Last Glacial Maximum.

The reorganization of atmospheric circulation in the circumantarctic during the last climatic transition generated asynchronous and even opposite changes in transport patterns in different sectors of the Antarctic Plateau.

During the Deglaciation and the Holocene epochs, millennial and secular scale pulsations in dust advection to the Plateau are omnipresent. From site to site, periodicities are the same but the phasing of the variations is different. Such rhythm suggests a circumpolar displacement of ocean-sea ice-atmosphere anomalies at these timescales, a wavering effect reminding that of present-day interannual propagation of the Antarctic Circumpolar Wave.

The rhythm of dust advection raises several questions about the modes of variability of the Southern Ocean and its capacity to propagate oceanic anomalies through the three world oceans at various timescales.

## Ringraziamenti

L'Antartide, prima mito e leggenda, poi territorio da conquistare, è oggi un meraviglioso laboratorio naturale.

Il fascino e il mistero di questa "terra di Scienza e di Pace" è molteplice, poiché nei suoi ghiacci è archiviata la storia climatica recente del nostro Pianeta. Tra i pionieri di questa recente scoperta, un ruolo di primo ordine spetta ai ricercatori del Laboratorio di Glaciologia di Grenoble, dove ho avuto il grande onore nonché il piacere di svolgere gran parte di questo lavoro.

Desidero ringraziare di cuore tutte le persone che hanno reso possibile lo svolgimento di questa tesi, e vi hanno direttamente o indirettamente contribuito. *In primis*, i miei due co-tutori.

Jean Robert Petit, che ha saputo trasmettermi con il suo rigore scientifico e coinvolgente entusiasmo, la capacità e la curiosità di leggere il codice segreto della Natura.

Valter Maggi, per avermi permesso concretamente di realizzare questi studi, per avermi dato fiducia, per i suoi consigli, le sue critiche quando necessario, e non da ultimo per avermi permesso di realizzare il mio sogno antartico a Dome C.

Un sincero grazie va anche al Prof. C.A. Ricci, per aver dato vita ai dottorati *antartici*, e al Professor Orombelli, presenza costante *dietro le quinte*, per avermi introdotta ad una disciplina così affascinante come la paleoclimatologia.

Ringrazio Isabelle Basile, per la trasmissione del suo prezioso "savoir faire" geochimico e per il suo aiuto nonostante le distanze geografiche. Non di meno, un grazie speciale ad Annie Michard per la sua infinita pazienza nell'insegnamento delle tecniche di laboratorio e di spettrometria di massa al CEREGE, a Wulfran e Kazuyo per la loro simpatia e il loro aiuto.

Grazie a Emil Jagoutz, il mago delle picco-quantità, perché da lui ho conosciuto i segreti e le astuzie delle misure isotopiche di precisione. Grazie a tutta l'équipe del Dipartimento di Cosmochimica dell'MPI di Mainz, Raimund, Olga e Oleg, per i loro consigli e la loro pazienza.

Un pensiero di ringraziamento va anche ai tre studenti con cui ho avuto il piacere di lavorare in laboratorio a Grenoble: Jeremie, Olivier e Valérie. A Gabriela Roman-Ross per le misure XRD sui sedimenti delle sorgenti.

Ringraziare tutti coloro che hanno condiviso con me le gioie e le peripezie di questi tre anni di tesi sarebbe troppo lungo. Mi scuso quindi nei confronti di tutti coloro che non sono qui menzionati, ma che porto nel cuore.

Grazie a tutti i membri dell'LGGE di Grenoble per la loro accoglienza e simpatia. Grazie ai numerosi compagni e amici di dottorato di Grenoble e Milano, Blandine e Federica in particolare. Non dimentico inoltre tutti coloro che con il loro calore umano hanno riscaldato la gelida estate Antartica a Dome C, in particolare Angela, Giggi, Luca e Adele.

Grazie a Maria Teresa, Mara M., Floriana, Giorgio, Francesca, Roberto, Giuseppe, Nadia, Mara R. e a tutti i miei amici di sempre: è anche grazie a voi che questo lavoro è stato costruito, che mi avete sempre sostenuta, incoraggiata, accolta ad ogni ritorno a casa come se non fossi mai partita.

Infine, un ringraziamento speciale ai miei genitori, alla loro generosità gratuita, pazienza e comprensione.

Dietro ad ogni bella avventura personale c'è sempre un angelo custode che indica la via e rimette tutto in prospettiva: grazie Francisco, per avermi insegnato il vero valore di ogni cosa.

## *Remerciements*

L'Antarctique, mythe et légende au début du siècle, devenu ensuite territoire à conquérir, est aujourd'hui un immense et merveilleux laboratoire naturel. Le charme et le mystère de cette « Terre de Science et de Paix » est multiple, car sa glace préserve l'histoire climatique de notre Planète.

Parmi les pionniers de cette grande et récente découverte scientifique, un rôle de premier ordre est celui des chercheurs du Laboratoire de Glaciologie de Grenoble, où j'ai eu le plaisir et l'honneur de développer la plupart de ce travail.

Je désire remercier de tout mon cœur toutes les personnes qui ont permis la réalisation de cette Thèse, *in primis* mes deux co-directeurs de Thèse.

Jean Robert Petit, qui a su me transmettre avec rigueur scientifique et enthousiasme contagieux la capacité et la curiosité de lire les codes secrets de la Nature.

Valter Maggi, qui m'a donné les outils pour réaliser ces études, en m'accordant sa confiance, en donnant toujours des bons conseils ainsi que des bonnes critiques, quand nécessaire. Merci aussi pour m'avoir permis de réaliser mon rêve Antarctique à Dome C.

Sincèrement merci à ceux qui étaient constamment présent "derrière la scène", le Professor Orombelli, qui a fait naître en premier ma passion pour une discipline si fascinante que la paléoclimatologie, et le Professeur C.A. Ricci, réalisateur de cette école doctorale *polaire*.

Je tiens à remercier Isabelle Basile, car elle m'a transmis son précieux "savoir faire" géochimique et pour son aide constant malgré, parfois, l'éloignement géographique.

Aussi, un remerciement spécial pour Annie Michard, pour sa patience infinie dans l'enseignement des techniques de laboratoire et d'utilisation du spectro auprès du CEREGE. Merci à Wulfran e Kazuyo pour leur sympathie et leur aide.

Merci à Emil Jagoutz, le magicien des picco-quantités, car c'est grâce à lui que j'ai appris les secrets et les astuces des mesures isotopiques de précision. Merci à toute l'équipe du Département de Cosmochimie de Mainz : Raimund, Olga e Oleg.

Une pensée aussi pour les trois jeunes étudiants qui m'ont aidée dans les mesures auprès du Laboratoire de Grenoble : Jeremie, Olivier e Valérie. Merci aussi à Gabriela Roman-Ross pour les mesures XRD sur les sédiments des sources.

Remercier tous ceux qui ont partagé avec moi les moments de joie et les péripéties de ces trois ans serait trop long, mais je les porte tous dans mon cœur. Je remercie les gens du LGGE pour le bon accueil et la sympathie, les copains et amis de Thèse de Grenoble et Milano, Blandine et Federica particulièrement. Merci à ceux qui ont réchauffé avec leur présence l'été Antarctique à Dome C : Angela, Gigi, Luca et Adele.

Merci à Maria Teresa, Mara M., Floriana, Giorgio, Francesca, Roberto, Giuseppe, Nadia, Mara R.: oui, c'est surtout grâce à vous que ce travail a été possible, vous qui m'avez encouragée, soutenue, dépannée.. grâce à vous, je ne suis jamais partie.

Enfin, un merci spécial à mes parents, pour leur générosité gratuite, les bons conseils et leur tolérance. C'est grâce à vous que j'ai pu faire tout cela.

Derrière toute belle histoire il y a toujours un ange gardien qui veille, indique la route, qui remet tout en proportion : merci Francisco, mon pour m'avoir appris la vraie valeur de toute chose.



## CONTENTS

### **INTRODUCTION**

Presentation of the work.....	I-IV
-------------------------------	------

### **Chap. 1 - QUATERNARY CLIMATE AND ENVIRONMENTAL CHANGES**

1.1 Quaternary climate variability .....	1
1.2 The timescales of climate changes .....	3
1.3 Quaternary environmental changes: a short overview .....	6
1.4 The natural archives of paleoclimate history	
1.4.1 Loess deposits	
1.5 Climatic tales from the Vostok ice core.....	13
1.6 Southern Hemisphere atmospheric circulation .....	16

### **Chap. 2 - MINERAL DUST IN THE CLIMATE SYSTEM, TODAY AND IN THE PAST**

2.1 Aerosol and dust.....	20
2.2 Mineralogical nature of aeolian dust .....	20
2.3 The role of mineral dust on climate .....	21
2.4 The knowledge for present time .....	23
2.4.1 Atmospheric dust load	
2.4.2 Common characteristics of source terrains identified by satellite observations	
2.4.3 Source regions at global scale	
2.4.4 Principal dust “hot spots” in the Southern Hemisphere	
2.5 The Last Glacial Maximum.....	29
2.5.1 The LGM atmospheric dust load: evidence from paleoclimate proxies	
2.5.2 The climatic and environmental conditions during the LGM	
2.5.3 The atmospheric dust load and the potential source regions: evidence from model simulations.	

### **Chap. 3 - MINERAL DUST CYCLE FROM THE SOURCE TO THE SINK: CONCENTRATION AND SIZE DISTRIBUTION CHANGES**

3.1 Dust mobilization at the source, “source strength” .....	38
3.2 The long-range transport .....	40
3.2.1. The horizontal dimension	
3.2.2 The vertical dimension	
3.3 The sink: dust in polar ice cores.....	43
3.3.1 Dust concentration: what information?	
3.3.2 Dust size distribution: what information?	

## **Chap. 4 - IDENTIFICATION OF DUST ORIGIN THROUGH THE Sr-Nd ISOTOPIC SIGNATURE**

4.1 An introduction to the Rb-Sr isotopic systems .....	47
4.1.1 Geochemistry of Rb and Sr	
4.2 An introduction to the Samarium and Neodymium isotopic systems.....	51
4.2.1 Geochemistry of Sm and Nd	
4.3 The $^{87}\text{Sr}/^{86}\text{Sr}$ versus $^{143}\text{Nd}/^{144}\text{Nd}$ isotopic ratios .....	54
4.3.1 The Sr-Nd correlation diagram	
4.4 $^{87}\text{Sr}/^{86}\text{Sr}$ - $^{143}\text{Nd}/^{144}\text{Nd}$ isotopic signature as tracer for sediment provenance.....	56
4.4.1 The conditions of applicability and limits of the method	

## **Chap. 5 - ANALYTICAL TECHNIQUES**

5.1 Dust concentration and size distribution measurements .....	63
5.1.1 Decontamination and sample preparation	
5.1.2 The measurement: principle, handling operations, limits of the technique	
5.2 Analytical procedures and Sr-Nd measurements of PSA samples.....	65
5.2.1 Size selection	
5.2.2 Leaching procedure	
5.2.3 Sr and Nd extraction	
5.2.4 Isotopic analysis of PSA samples	
5.3 Analytical procedures and Sr-Nd measurements of Ice Core Dust (ICD).....	70
5.3.1 Dust extraction from ice cores	
5.3.2 Sr and Nd extraction from ice core dust	
5.3.3 Isotopic analysis	

## **Chap. 6 - THE SAMPLES ANALYZED IN THIS STUDY**

6.1 Samples measured for dust concentration and size distribution .....	76
6.1.1 EPICA-Dome C ice core	
6.1.2 The VOSTOK BH7 (VK-BH7) ice core	
6.1.3 The Dome B (DB) ice core	
6.1.4 The Komsomolskaia (KMS) ice core	
6.2 Samples selected for Sr -Nd geochemical analysis .....	79
6.2.1 The PSA samples	
6.2.2 Ice Core Dust samples	

## **Chap. 7 - RESULTS AND DISCUSSION ABOUT DUST PROVENANCE**

7.1 The isotopic signature of ice core dust.....	92
7.1.1 Glacial dust	
7.1.2 interglacial dust	
7.2 The signature of the PSAs of the Southern Hemisphere.....	101
7.2.1 Southern South America	
7.2.2 New Zealand	
7.2.3 The non-glaciated areas of Antarctica	
7.2.4 South Africa	
7.3 Discussion.....	110
7.3.1 The dust provenance in glacial periods	
7.3.2 The interglacials	
7.3.3 The Sr contribution from carbonates	

<b><u>Chap. 8 - RESULTS AND DISCUSSION ABOUT DUST VARIABILITY</u></b> .....	128
<b><u>8A: THE LAST CLIMATIC TRANSITION</u></b> .....	129
8A.1 The first dust record from EPICA-Dome C (EDC) ice core.....	129
8A.2 High resolution EDC dust record: the last deglaciation and the Holocene.....	152
8A.3 Dome B, EDC and Komsomolskaya: two poles apart inside East Antarctica. ....	167
<b><u>8B: DUST VARIABILITY IN THE HOLOCENE</u></b> .....	190
8B.1 Holocene dust records from Vostok-BH7 and EPICA Dome C ice cores.....	191
8B.2 Holocene dust variability in the Dome B ice core .....	211
8B.3 Comparing the different sites .....	215
8B.3.1 Dome B and EDC ice cores	
8B.3.2 Dome B, EDC and Vostok dust size spectra solar variability	
8B.3.3 Periodicities nested in the dust concentration records	
<b><u>8C: A TENTATIVE SCENARIO FOR LGM AND HOLOCENE DUST TRANSPORT</u></b> .....	224
8C.1 Factors influencing dust advection.....	224
8C.2 Dust variability over East Antarctica: a response to the atmospheric circulation patterns .....	229
<b><u>8D: LATE QUATERNARY EDC DUST RECORD</u></b> .....	238
<b><u>CONCLUSIONS</u></b> .....	251
<b>Appendix I</b> : Sm-Nd dating and Sr-Nd isotopic signature of a bedrock inclusion from Lake Vostok accretion ice.....	253
<b>Appendix II</b> : Supplementary tables .....	257
<b>Appendix III</b> : List of publication outcome from this thesis .....	260
<i>References</i> .....	262

## INTRODUCTION

### *Presentation of the work*

The reconstruction of the long saga of Quaternary climatic changes with their pattern and tempo is essential to understand the present-day climate and foresee its future developments.

The memory of the Earth's paleoclimatic history can be preserved in several natural archives. In this respect, ice cores are an extraordinarily valuable proxy for past climatic, environmental and atmospheric conditions.

The longest climatic records from ice cores can be recovered from the low accumulation sites of the high East Antarctic plateau. To date, the deepest ice cores obtained are those from Vostok, spanning the last 420,000 years of climatic history (Petit et al., 1999), from Dome Fuji (Watanabe et al., 2003), going back in time to the last 330,000 years, and from the new EPICA-Dome C ice core, allowing to extend the ice core record several hundred thousand years into the past.

The key objective of this research work is to decipher the origin and the variability of the mineral dust windblown to Antarctica during late Quaternary through analysis of East Antarctic ice cores. The paleo-dust cycle allows to reconstruct the past environment and the climate and to tie together all the complex and interacting processes involving the lithosphere, the atmosphere, the cryosphere and also the hydrosphere and the biosphere.

Four deep East Antarctica ice cores have been investigated<sup>1</sup> (Fig. 1.1):

- 1 - the EPICA-Dome C (75° 06'S, 123° 21'E, 3233 m a.s.l.) ice core (EDC), drilled in the framework of the *European Project for Ice Coring in Antarctica*, to which a large part of this work has been dedicated. The drilling has been carried out in the framework of a collaboration involving 10 European countries. The ice core reached the depth of 3,200 m during the field season 2002/03, and likely preserves the climatic memory for the last one million years.
- 2 – the VOSTOK-BH7 ice core (78° S, 106° E, 3480 m a.s.l.) obtained in 1996 through a tri-partite Russia-US-France collaborative programme (Petit et al., 1999).
- 3 – The Dome B (77° 05' S, 94° 55' E) ice core, obtained during the 1987-1988 austral season by the 33<sup>rd</sup> Soviet Antarctic expedition (Jouzel et al., 1995).
- 4 – The KOMSOMOLSKAYA (74° 05' S, 97° 29' E, 3500 m a.s.l.) ice core extracted in 1983 by the Soviet Antarctic Expedition using a thermal drilling technique (Ciais et al., 1992).

---

<sup>1</sup> Each ice core and drilling site is presented in Chap.5

Through these four ice core records a comprehensive reconstruction in space and time of the past dust dynamics in Antarctica and at the high southern latitudes has been obtained.

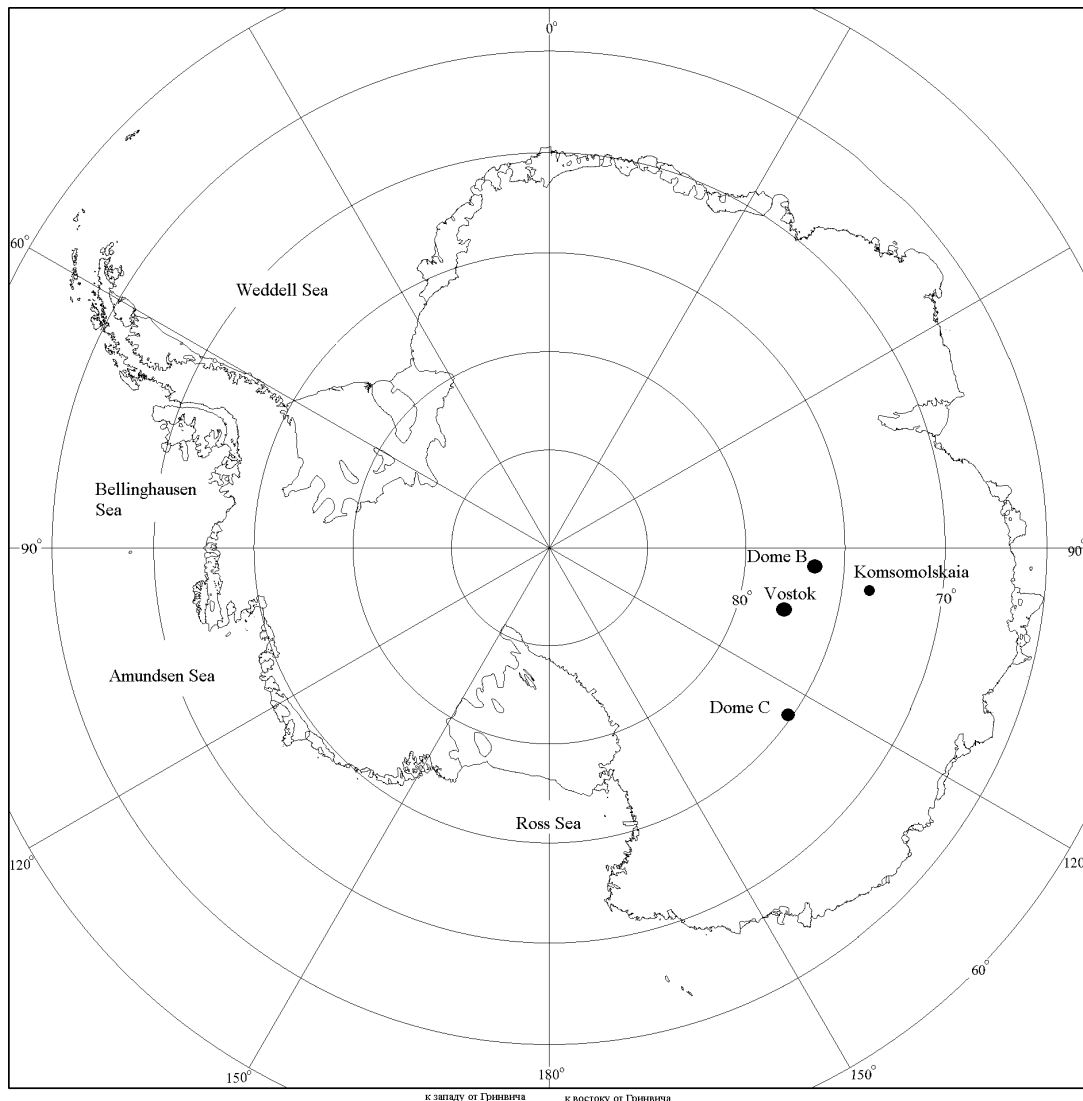


Fig. 1: Drilling sites for EPICA-Dome C, Vostok, Dome B and Komsomolskaia ice cores.

Dust variability has been investigated through a *physical approach*, consisting in the measurement of the total dust concentration and its size distribution, each of these indicators keeping different information about the paleo-dust cycle (Chapter 3).

This part of the work has been carried out in Grenoble c/o the Laboratory of Glaciology and Geophysics of the Environment of the National Center for Scientific Research (LGGE-CNRS).

The dust geographical origin, instead, has been investigated following a *geochemical approach*, first applied to the study of ice core dust provenance by Grousset et al. (1992) and largely developed by Basile in 1997 (Chapter 4).

This part of the research work has been performed in part c/o CEREGE laboratory in Aix en Provence (France) and c/o the Max Plank Institute (MPI) in Mainz.

Here below is reported the general structure of this work.

**Chapter 1 – QUATERNARY CLIMATE** - The first Chapter includes a synthetic overview of Quaternary climatic changes, their principal forcing factors, the timescales involved, and their principal environmental effects.

After a general inventory of the different typologies of natural *archives* of paleoclimate history, especially to the significance of loess-paleosol formations, a particular attention is dedicated to South American aeolian deposits.

The chapter is concluded with a summary of the climatic and atmospheric tales from the Vostok ice core for the last four glacial/interglacial cycles.

**Chapter 2 – MINERAL DUST IN THE CLIMATE SYSTEM** - The definition, the nature and the climatic role of aeolian mineral dust are considered.

The chapter contains a synthesis of all the most recent issues about present-day atmospheric dust load and an overview of the principal dust source regions with particular focus on the Southern Hemisphere.

An updated review of the LGM dust load estimations from proxy records and model simulations is presented and the salient aspects of LGM climate are resumed.

**Chapter 3 – THE DUST CYCLE** - From the continental source areas to the remote polar regions, through a *selective* atmospheric path.

The paleoclimatic significance of the dust concentration and size distribution parameters is introduced.

**Chapter 4 – THE STRONTIUM-NEODYMIUM ISOTOPIC SIGNATURE OF DUST –**

The Rb-Sr and Sm-Nd isotopic systems and their geochemical behaviour are synthetically presented. The chapter discusses the usefulness of the  $^{87}\text{Sr}/^{86}\text{Sr}$  versus  $^{143}\text{Nd}/^{144}\text{Nd}$  isotopic signature for dust as *tracer* for sediment provenance.

The limits of this method are discussed, as well as the conditions of applicability for investigating ice core dust origin.

**Chapter 5 – ANALYTICAL TECHNIQUES** - Presentation of the analytical techniques used for dust concentration and size distribution measurements and for isotopic measurements (Sr-Nd) on ice core dust and on the samples from the Potential Source Areas (PSAs).

**Chapter 6 – THE SAMPLES ANALYSED** - The ice core samples analysed in this study are presented, along with the samples from the PSAs.

**Chapter 7 – RESULTS AND DISCUSSION ABOUT DUST PROVENANCE** - The results of the isotopic measurements on ice core dust and source samples are presented. The dust provenance to the East Antarctic in glacial and interglacial times is discussed.

**Chapter 8 –RESULTS AND DISCUSSION ABOUT DUST INPUT VARIABILITY** to East Antarctica in the Late Quaternary. This chapter, that presents the main results of this thesis work, includes four sub-chapters:

*8A- Dust variability during the last climatic transition.*

*8B-Dust variability during the Holocene.*

*8C-Tentative scenario for LGM and Holocene dust transport.*

*8D-Late Quaternary dust record from EDC ice core.*

**Appendix I:** GEOCHEMICAL (Sr-Nd) SIGNATURE OF A BEDROCK INCLUSION FROM LAKE VOSTOK ACCRETION ICE AND SAMARIUM-NEODYMIUM MODEL AGE.

**Appendix II:** Additional Tables

**Appendix III:** List of publications outcoming from this work

## Chapter 1 - QUATERNARY CLIMATE AND ENVIRONMENTAL CHANGES

### 1.1 Quaternary climate variability

In the geologic timescale, the Quaternary spans a very short period of time, approximately the last two million years<sup>1</sup>, and together with the Tertiary Period forms the Cenozoic Era (spanning about the last 65 Ma).

The Quaternary is subdivided into two epochs: the Pleistocene (roughly from two million years to ten thousand years ago) and the Holocene (about the last ten thousand years to the present day). In turn, the Pleistocene is conventionally subdivided in three parts: the lower Pleistocene (1.8-0.75 Ma), the Middle Pleistocene (750-125 kyrs B.P.) and the Upper Pleistocene (125-10 kyrs B.P.).

Ice began to build up as long ago as 25-50 million years in Antarctica, but ice caps and ice sheets formed only ~2.6 million years ago in the Northern Hemisphere; this is a distinctive feature of the Quaternary, that is believed to be the only time where both poles were covered by ice simultaneously.

The Pleistocene itself is characterised by rhythmical changes of climatic conditions from cool to warm stages<sup>2</sup> (see Fig. 1.1), with different climatic effects in different parts of the world. However, what is distinctive about the Quaternary is not only the occurrence of repeated warm or cold episodes but the combination of both the high amplitude and the frequency of such variations (Williams et al., 1993).

The repeated correspondence between the rhythm of environmental changes preserved in Quaternary fossil records and Earth's orbital ones has given origin to the theory of astronomical forcing on climatic changes (Berger, 1978; Imbrie et al., 1992; Tzedakis et al., 1997)<sup>3</sup>.

The Pleistocene climatic variations had frequencies corresponding to the periodicities of three known astronomical parameters: the *eccentricity* of the Earth's orbit around the Sun (~400 kyrs and ~100 kyrs), varying from elliptical to nearly circular, the *obliquity* of the Earth's axis (~41 kyrs) respect to

---

<sup>1</sup> Its exact duration is a matter of debate with estimates of the onset of such period between 1.8 and 2.6 Ma. The first limit corresponds to the Olduvai paleomagnetic event, dated between 1.67 and 1.87 Ma, while the second one corresponds to the rapid build-up of glaciers in the Northern Hemisphere.

A survey of the literature reveals that the beginning of the Quaternary is most often put at 1.8 Ma.

<sup>2</sup> Quaternary periods can be distinguished into:

*Glacials*: Protracted cold stages with major expansions of ice sheets and glaciers

*Interglacials*: Warm intervals in which temperatures were equal or higher than during the Holocene.

*Stadials*: Shorter episodes during which local ice advances may have occurred

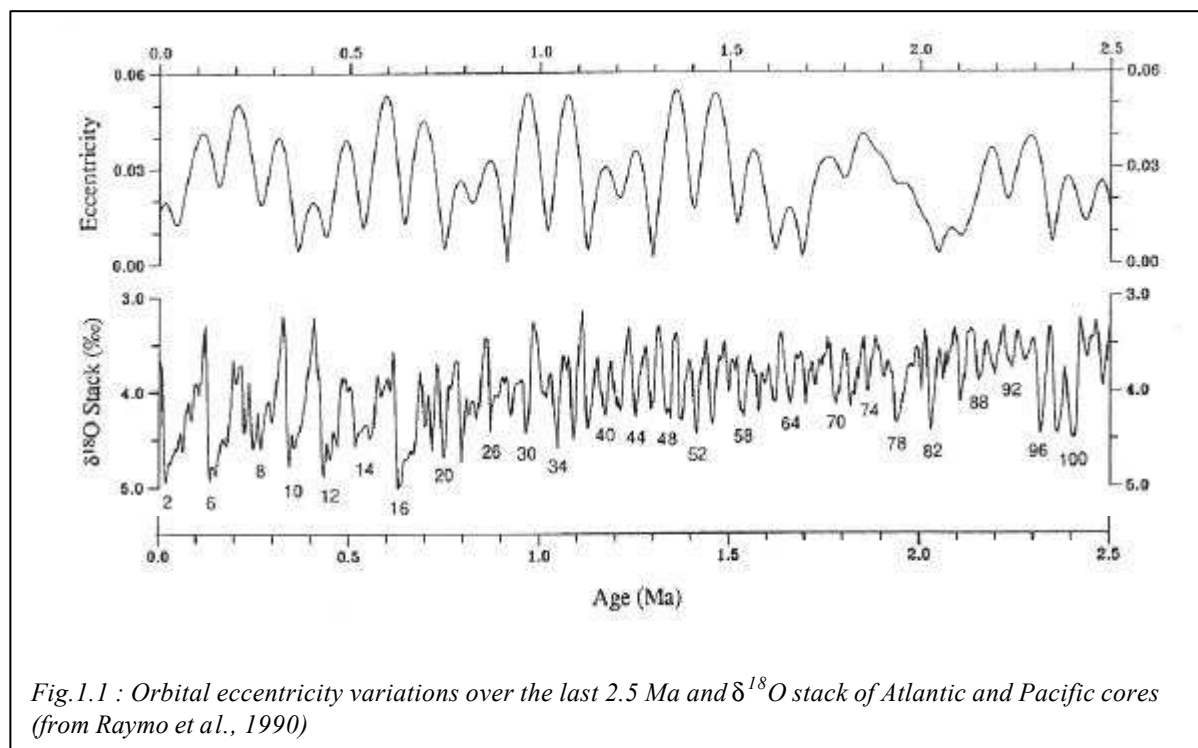
*Interstadials*: Short-lived periods of thermal improvement during a glacial phase

<sup>3</sup> The first calculations demonstrating that astronomical parameters could play a role in the Earth's Quaternary ice ages were performed by the Serbian mathematician M. Milankovitch. This theory however was not widely accepted until the 1970's.



the plane of the ecliptic cycles<sup>4</sup> and the “*precession of the equinoxes*” in the Earth’s orbit (21.7 kyrs)<sup>5</sup>. The 100- kyrs variability, in particular, became the dominant periodicity only in the late Quaternary (about the last ~800 kyrs).

The predictable and regular variations of the Earth’s orbital elements alter the latitudinal and seasonal distribution of the insolation (Berger, 1978). Such variations can be reliably determined back to ca. 5 Ma (Berger and Loutre, 1991).



If external (astronomical) variables are the slow-varying forcing factors of Quaternary climate, the variations produced are the resultant of complex positive and negative *feedback* mechanisms internal to the climate system. Such feedbacks are necessary to translate the slight changes of solar heating into climatic variations, and probably contribute to limit the magnitude of such oscillations within a limited interval, and to modulate the rapidity of the changes. As example, paleotemperature curves of the Upper Quaternary typically show a sawtooth pattern, with slow progressions into glacial phases and rapid terminations (switches from pleniglacials to warm interglacial phases). Such a pattern, evidenced

<sup>4</sup> The 41 kyrs periodical changes in the axial tilt span the range from 21.8° to 24.4° and influence the radiation at high latitudes.

<sup>5</sup> It must be noted that the periods mentioned correspond to the average of the principal periodic terms. In particular, for the precessional parameter the most important terms in the series correspond to periods of ~23.7, ~22.4 and ~19 kyrs. The 21.7 kyrs periodicity is an average of the main periods but some climatic records are capable to resolve separately the principal periods.

also in the Vostok ice core temperature profile (§1.5), probably hints positive feedback mechanisms operating during deglaciations but not during cooling stages.

The response of the climate system to any (internal or external) forcing factor is nonlinear, and the physical mechanisms by which they are translated in global climate variations are still not completely understood. This constitutes an important issue of paleoclimatological studies.

## **1.2 The timescales of climatic changes**

Climate varies on a continuum of time scales, from diurnal and seasonal ones to those associated with the tectonic evolution of the Earth (Mitchell, 1976). The different timescales of the environmental and climatic processes are usually associated to different space scales.

The impact on the climate system of plate motion, continental geography, mountain building and erosion, and the production and subduction of seafloor crust and the related changes in bio-geochemical cycles (particularly the carbon cycle) are principally investigated by geologists, looking at climate and atmospheric composition over geological timescales (hundreds of million years).

The analysis of Quaternary climate changes involves mainly processes with periodicities lower than  $10^6$  years. As previously pointed out (§ 1.1), paleoclimate reconstructions for this period have shown that the main *ice ages* are understood as primarily driven by slow orbital fluctuations to which are associated a number of positive and negative internal feedback mechanisms.

However, the late Quaternary is known to have been highly unstable and prone to rapid climatic changes of millennial scale duration. The Dansgaard-Oeshger events, the Heinrich events and the Bond's cycles are an example (see Fig. 1.2). Short-term variations can be nested in the long-term climatic variability, and sometimes the temporal resolution of the samples is insufficient for them to be resolved.

In recent years, evidences of a global climate variability at millennial and sub-millennial timescale have come out from a high number of geologic records (see Clark et al., 2000, for a general overview). In parallel, several efforts have been done for the comprehension of the mechanisms and causes for such a behaviour of the earth system. In this respect, several hypothesis have been made (e.g. Rahmstorf et al., 2001; Broecker, 1990) but many aspects remain largely unknown.

The potential mechanisms driving, amplifying and correlating variability on centennial and millennial timescales include internal ocean-atmosphere systems (Sarnthein et al., 2002). The variability in the global thermohaline circulation (THC) and its effect on the atmospheric system is one of the potential elements of climate forcing and feedback mechanisms (Broecker and Denton, 1989; Duplessy et al.,

1991). The THC variability, in turn, may have direct or indirect climate responses, and each of these can show a given phasing at regional scale (e.g. Sarthein et al., 2002).

Moreover, in the context of the global transmission of the perturbation, other internal systems are capable to provide positive or negative feedbacks (the sea ice is an example) to an initial perturbation. (e.g. Keeling and Stephens, 2001).

A general overview of the timescales of some climatic processes is reported in Fig. 1.2; this scheme is simplified, and the possible interaction between climatic variability at different timescales is not taken into account. The periodicity of external forcing factors like the Sun and the Moon are also reported.

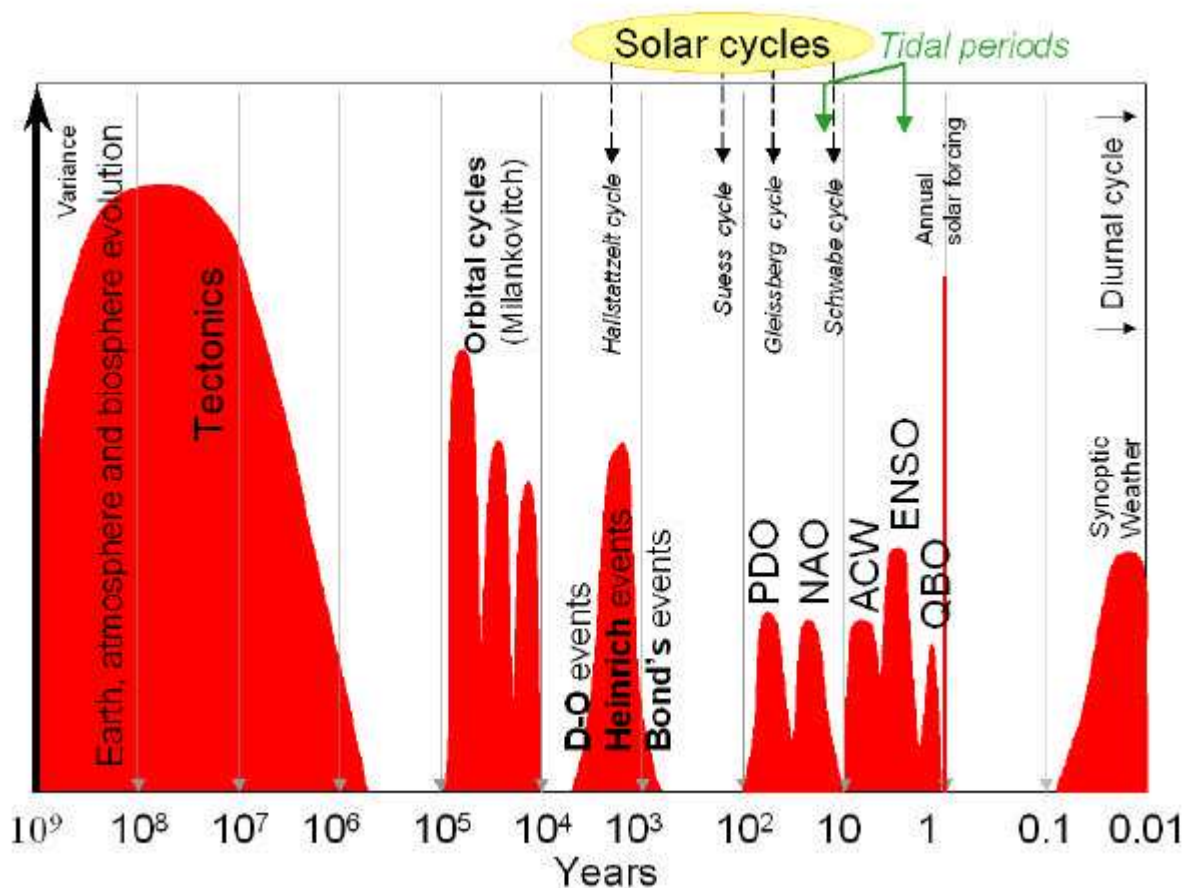


Fig. 1.2 : Timescales of climatic changes:

Milankovitch cycles: the Earth's periodical orbital variations (§1.1) are known to influence terrestrial climate at long time scales.

Dansgaard-Oeschger (D-O) events: Large amplitude and repetitive millennial-scale changes in air temperature occurring during the glacial period (from ~11 to 74 kyrs B.P.) and recorded for the first time by Willi Dansgaard and Hans Oeschger in the Camp Century Greenland ice core (Dansgaard et al., 1984). An average fundamental pacing period of ~1470 years seems to control the timing of the onset of the D-O events.

Heinrich events: succession of layers rich in Ice Rafted Detritus (IRD) observed for the first time by H. Heinrich (1988) in a sediment core from NE Atlantic.

Bond's events : events of abrupt climate shifts registered in North Atlantic deep sea cores in glacial and interglacial climates. During such events, cold and ice-carrying waters from North Iceland are advected to the South. These episodes correspond to abrupt changes in the atmospheric circulation above Greenland. The periodicity of such events is  $1374 \pm 502$  yrs for the Holocene, and  $1536 \pm 563$  years for the glacial periods. On average, the pacing of the so called Bond's events is  $1470 \pm 532$  years (Bond et al., 1997).

Pacific Decadal Oscillation (PDO): semi periodic oscillation in the spatial pattern of sea surface temperatures across the North Pacific. It seems to have return periods of 15 to 25 years and 50 to 70 years. However, research on the phenomena is less than a decade old, and not all scientists are convinced PDO is actually an oscillating feature. It has also been suggested by some researchers that PDO may be part of other features such as ENSO (e.g. Gershunov et al., 1999).

North Atlantic Oscillation (NAO): semi periodic oscillation in the atmospheric surface pressure contrast between the Icelandic low and the Azores high. It has a dominant period of 12 years and is centred in the North Atlantic (Deser, C. and M. Blackmon, 1993).

Antarctic Circumpolar Wave (ACW): Circumantarctic anomaly in surface pressure, wind stress, temperature and sea ice extent propagating eastward in the Southern Ocean with a periodicity of 4.5 years, and taking 8-10 years to encircle the Antarctic continent (White and Peterson, 1996).

El Nino-Southern Oscillation (ENSO) : quasi periodic oscillation involving large changes in air pressure patterns in the tropical pacific, associated with drastic redistribution of warm seawater at sea surface. The index commonly used is the air pressure difference between Darwin (Australia) and Papeete (Tahiti). During El-Nino events the eastern Pacific becomes abnormally warm and unusual temperature and rainfall patterns are observed all over the world.

Quasi-biennial oscillation (QBO): quasi periodic oscillation in the equatorial lower stratosphere, with associated tropical weather and climate patterns.

The annual cycle corresponds to the dominant change in several climatic parameters (e.g. temperature, precipitation) due to the Earth's rotation around the Sun, while the diurnal cycle is related to the Earth's rotation on its axis, creating the cycle of night and day. These two periodicities also influence delay between the time when the earth-atmosphere system is irradiated and the time when temperature starts to increase on the surface of the planet is called thermal response; it depends on the time of the year and the latitude, the lag can be as long as three or four hours.

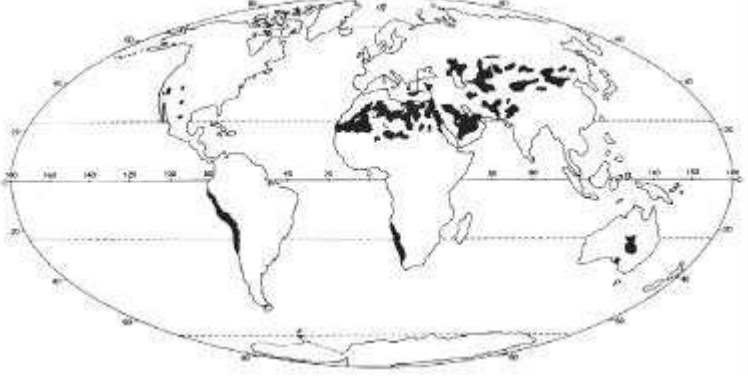
The principal periodicities of the solar variability (changes in the sun's radiation due to the sun's internal dynamics) are: the 11-years Schwabe cycle; the 88-years Gleissberg cycle, the 208-years Suess cycle, and the 2300-years Hallstattzeit cycle.

The main lunar periods are also indicated at  $\sim 4.4$  yrs, 17.7 and 18.6 yrs. The interference of these latter two master periods is 366 yrs, that corresponds to  $\frac{1}{4}$  of the 1470-yrs cycle (Berger et al., 2002).

### 1.3 Quaternary environmental changes: a short overview.

Quaternary climate variations generated several environmental processes. Synthetically, they can be summarized as follows:

<i>Process</i>	
<i>Glaciations</i>	<p>Snowlines fluctuated and two large ice sheets grew and decayed (Laurentide Ice Sheet and the Scandinavian Ice Sheet).</p> <p>At 1.2 Ma the Patagonian Ice Cap was 300,000 km<sup>2</sup> wide, respect to the 100,000 km<sup>2</sup> of the last glaciation.</p> <p>The cold phases of the Pleistocene were accompanied by an extension of the <i>permafrost</i> limit.</p>
<i>The sea level changes and isostatic readjustments</i>	<p>During the glacial maxima about 5.5% of world's water was in the form of ice (cf. today 1.7%), and when such large and thick ice sheets grew the underlying bedrock depressed and the level of the oceans lowered of ca. 170 m.</p>
<i>Land aridity during cold periods</i>	<p>The coldest Quaternary periods have been associated to an enhanced aridity on land. Sand dunes were periodically active well beyond their present-day limits (Fig. 1.3 and 1.4) and widespread loess deposits formed (see §1.4.1 and Box 1). The bigger aridity on continents associated to the high wind intensity lead to an enhanced atmospheric dustiness.</p> <div data-bbox="646 1317 1396 1691" data-label="Figure"> </div> <p><i>Fig. 1.3: Global distribution of active sand dunes at ~18 kyrs B.P. (After Sarnthein, 1978)</i></p>

	 <p data-bbox="579 589 1441 618">Fig. 1.4: Global distribution of sand dunes at present time (After Goudie, 1983).</p>
<p data-bbox="185 640 563 719"><i>Changes in the atmospheric circulation and windiness</i></p>	<p data-bbox="579 640 1452 819">The position of the Intertropical Convergence Zone (ITCZ), the Westerlies belt, and the major oceanic and continental anticyclones varied within the Quaternary, in association with changes of wind strength (§ 1.6).</p> <p data-bbox="579 842 1452 920">The past atmospheric circulation can be reconstructed through multiproxy indicators for the different regions of the globe.</p> <p data-bbox="579 943 1452 1066">Regional syntheses for the Southern Hemisphere can be found in Bowler et al. (1976), Clapperton (1993), McGlone et al. (1993), Wright et al. (1993) and Partridge (1993).</p>
<p data-bbox="185 1099 523 1128"><i>Local hydrological changes</i></p>	<p data-bbox="579 1099 1452 1178">The climatic fluctuations of the Quaternary had regional and local responses in river, lake and groundwater level fluctuations.</p>
<p data-bbox="185 1200 563 1279"><i>Terrestrial fauna and flora changes</i></p>	<p data-bbox="579 1200 1452 1323">The environmental changes induced by temperature and rainfall fluctuations induced variations of the non-marine plant assemblages and the animal populations.</p> <p data-bbox="579 1346 1452 1424">The Quaternary climatic changes are associated with the disappearance of terrestrial megafauna.</p>

Tab. 1.1: Major environmental changes linked with Quaternary climate variations.

Within the Quaternary, *Homo* species developed. *Homo erectus* appeared and introduced innovations, among which the discovery of fire that allowed him to move out of Africa and occupy new territories in Europe and Asia (~1 Ma B.P.). The first evidences of *Homo Sapiens* are dated about 300-200 kyrs B.P.; the human evolution, migrations, development and cultural advancements have always been intimately associated with climatic and environmental changes. One of the most exhaustive examples is given by the history of the occupation of Lake Mungo (Southeast Australia), that started at ca. 46-50 kyrs B.P. (i.e. after glacial stage 4 during which such lacustrine environment was submerged), developed at its maximum between 45 and 43 kyrs B.P., and declined thereafter in response to increasing aridity and fluctuations in lake levels (Bowler et al., 2003).

#### **1.4 The natural archives of paleoclimate history**

Natural materials accumulating progressively over time and responding to environmental and climatic conditions constitute natural archives of paleoclimate history (Oronelli, 1996).

Paleoclimate *proxies* of different typologies and characteristics exist on Earth, and each of them is useful for specific purposes, and for a particular area and time interval.

The sequences of interest should be continuous in time, unaltered, and the “real” climatic signal must be separable from non-climatic “noises”. Moreover, the climatic dependency of each proxy has to be *calibrated* in order to estimate as precisely as possible the magnitude of climatic variations associated to each response.

A synthetic overview of the most important types of proxies is reported in Tab. 1.2. From each of them several variables can be measured, each one responding to one or more specific parameters of the Earth’s climate system. Ice cores are extremely valuable paleo-record, and are the unique proxy preserving the past atmospheric compositions, recorded in the entrapped air inclusions of the ice (Petit et al., 1999; see § 1.5).

The sample resolution and the length of the record that can be obtained from each proxy spans different orders of magnitude. Instrumental and historical records provide the finest sample resolution but are unable to go back in the past over a few hundred or thousand years respectively.

Tree rings provide sequences up to  $\sim 10^4$  years, pollen records can overstep  $\sim 10^5$  years and marine records potentially provide the longest climatic sequences - in the order of  $\sim 10^6$  years or more – but with the lowest temporal resolution.

Polar ice cores provide climatic records of variable length (until some hundred thousand years) and time resolution (from seasonal to annual). Ice core records are comparable to some rare highly-resolved marine records.

Tab. 1.2 – Natural archives of paleoclimate history

<i>Nature</i>	<i>Environment</i>	<i>Proxy data source</i>
<i>Geological and geomorphological</i>	Terrestrial	Glacial deposits, periglacial features Shorelines Aeolian deposits ( <i>loess</i> [§ 1.4.1], dunes, sand plains, desert dust) Lacustrine sediments Pedological features (relict soils) Speleothems Evaporites
	Marine	Ocean sediments (organic and inorganic) Continental dust Fluvial inputs
<i>Biological and biogeographical</i>	Continental	Tree rings Pollens Microfossils and fossils (vertebrate and invertebrate) Diatoms Insects Population distribution
	Marine	Corals Diatoms Foraminifera Biogenic dust Faunal and floral abundance Morphological variations
<i>Glaciological</i>	Polar and mid-latitude	Ice cores Mountain glaciers Glacial deposits and features of glacial erosion (moraines,..) Periglacial features Glacio-eustatic features
<i>Human</i>	Archaeological (prehistorical)	Written records Plant and animal remains Artefacts
	Historical	Written documents Phenological records



### 1.4.1 Loess deposits

Transport of silt and clay by wind is an universal process, occurring under all climates, mainly in desertic and sub-desertic regions. The accumulation of such materials can produce loess, which is defined as a structured loam or loamy silt, spanning a size range between 20 and 60  $\mu\text{m}$ , and mostly constituted by quartz silt, feldspars and micas (Pye, 1984, 1987).

During cold climatic periods the loess accumulation was rapid and soil formation at minimum, while warm phases were associated to weathering of loess mantles and pedogenesis. Therefore, loess sequences can potentially provide a quantitative record of mineral dust deposition under changing climate regimes that is complementary to ice core records.

The Chinese loess plateau (440,000  $\text{km}^2$ , 33-40°N , 98-115°E, Kohfeld and Harrison, in press) is undoubtedly one of the most extensive areas of loess deposition of the world, and with its 100-300 m of thickness it provides some of the most studied loess/paleosol sequences (Kukla et al., 1989, 1990).

Outside China, other wide loess deposits in the Northern Hemisphere are located in North America (Great Plains), in south-central Europe, Ukraine and central Asia. In the Southern Hemisphere, the thicker and more extensive loess and aeolian deposits occur in Argentina. Thick Pleistocene loess-paleosol deposits are present also in New Zealand (e.g. Graham et al., 2001; Berger et al., 2001 and 2002, see Fig. 1.5).

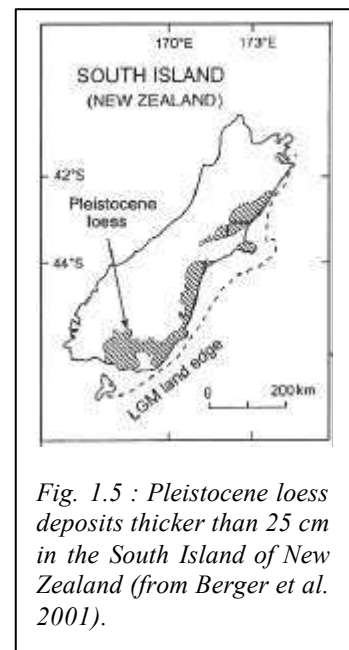


Fig. 1.5 : Pleistocene loess deposits thicker than 25 cm in the South Island of New Zealand (from Berger et al. 2001).

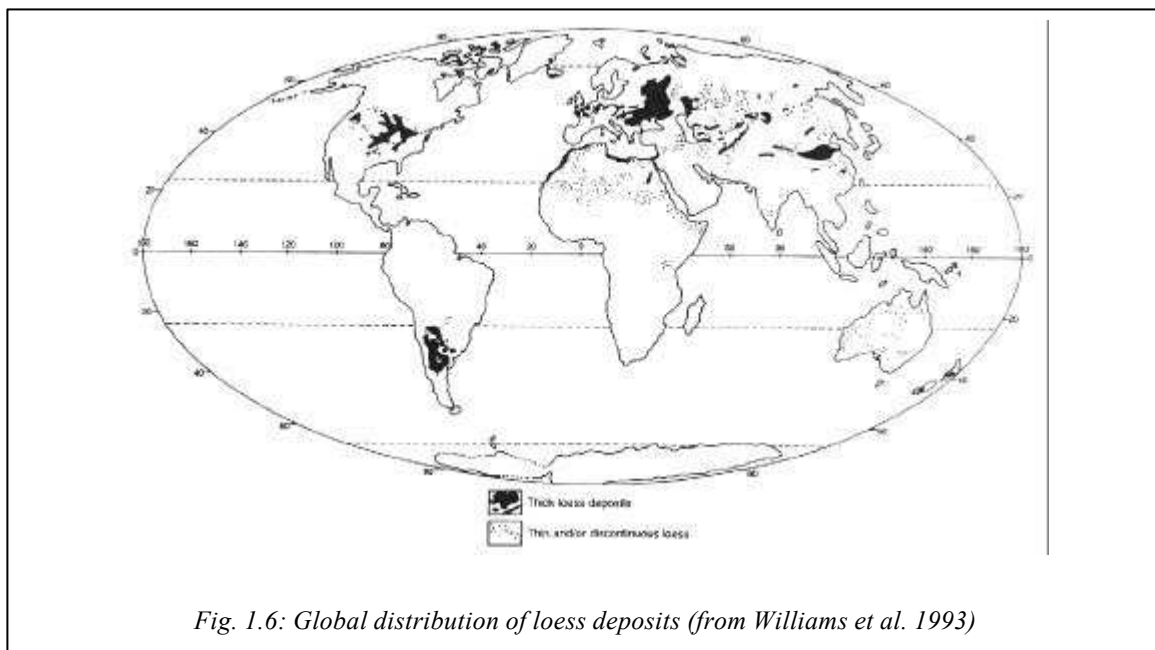


Fig. 1.6: Global distribution of loess deposits (from Williams et al. 1993)

The main stages for loess deposit formation can be resumed as follows (Claridge and Campbell, 1988):

- 1 - Production of rock debris through weathering (glacial and periglacial);
- 2 - Removal of debris by fluvial action;
- 3 - Wind deflation;
- 4 - Accumulation;
- 5 - Formation of a structure;

These steps can be composed by substages and/or some of them can be missing.

Most loess deposits are associated with former glacial conditions, and it is assumed that the main processes responsible for their formation are associated with glacial and periglacial processes (like frost thawing). However, other non-glacial formation processes are capable of generating such fine silty particles in a variety of environments, both in hot and warm conditions (Smith et al., 2002).

#### **Box 1 - The Pampean Loess and other Quaternary aeolian deposits in South America**

Southwest and south of the Paraná-Rio de la Plata estuary, extensive formations of loess and sand covering an area of ~1000-1100 km<sup>2</sup> constitute the so called *Pampean loess formation* (e.g. Clapperton, 1993, Imbellone and Terruggi, 1993).

This loess formation covers a wider area than the Pampas *sensu stricto*, extending over the western Chaco plains (NW Argentina). Further south, in the Argentine Pampas, a relatively thin (5-15 m) deposit of very fine sand, characterized by longitudinal dunes, constitutes the "*Pampean sand sea*" formation. Both this latter and the loess belt constitute the *Pampean Aeolian System* (as defined by Iriondo, 1993, 1999), a sedimentary body covering a total of 600,000 km<sup>2</sup>.

It has been suggested that the sediments deposited on the Pampas plains by the Andean rivers swollen with glacial meltwater were subsequently reworked by winds from S-SW. The sand sea formation would then constitute the proximal deposit while a finer loessic component close to the Parana river would represent the distal one.

Sayago et al. (2001) observed that the loessic substrate is sandier towards the south and southwest within the Chaco-Pampa region, while in the northeast it is enriched in the fine (silty and clay) fraction (Fig. 1.6). This confirms previous hypothesis that the sediments (between 40 and 25°S) have been transported by southwesterly winds from the Andean chain.

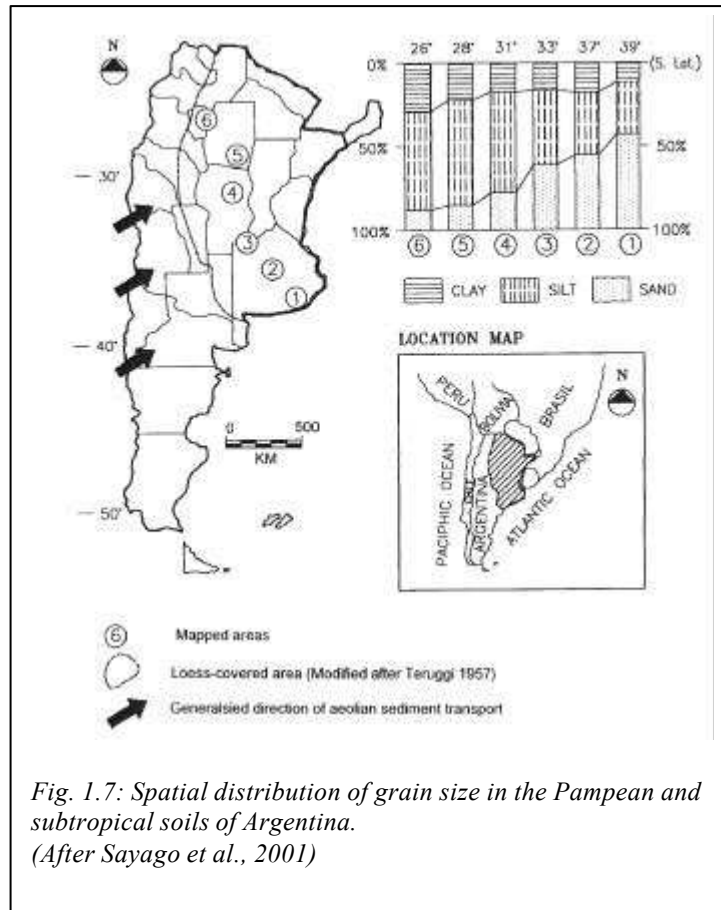
The Pampean loess is similar in texture and color to loesses of the Northern Hemisphere but differs from these for its mineralogical composition<sup>6</sup> (Gallet et al., 1998) since it is primarily derived from volcanic parental rocks<sup>7</sup>.

The thickness of such formation is 30-40 m on average, but even more at local scale and its stratigraphy consists typically of superposed loess beds (1 to 2 m) separated by palaeosols or erosional discontinuities.

The processes leading to alternation these formations are intimately linked with climatic conditions:

loess deposition dominates during dry and windy phases while pedogenesis development characterizes more humid intervals (Carignano, 1999).

Other paleo-aeolian features of late Quaternary origin can be found in southern south America further south, in Patagonia, where the wind action permitted the removal and transport of the weathered rocks within the southern plains.



<sup>6</sup> The so called Pampean loess, representative for South America windblown sediments of late Pleistocene-Holocene age is related to the last glacial events in Patagonia. It differs in mineralogy and grain size from the so called "Neotropical loess", widespread formation of (primary and reworked) loessic sediments that can be found in the region between 20 and 30°S, under subtropical climate conditions. Both the Argentine loess and the Neotropical loess display rhythmic sequences of paleosols developed over loess according to the climatic conditions (Sayago, 1995).

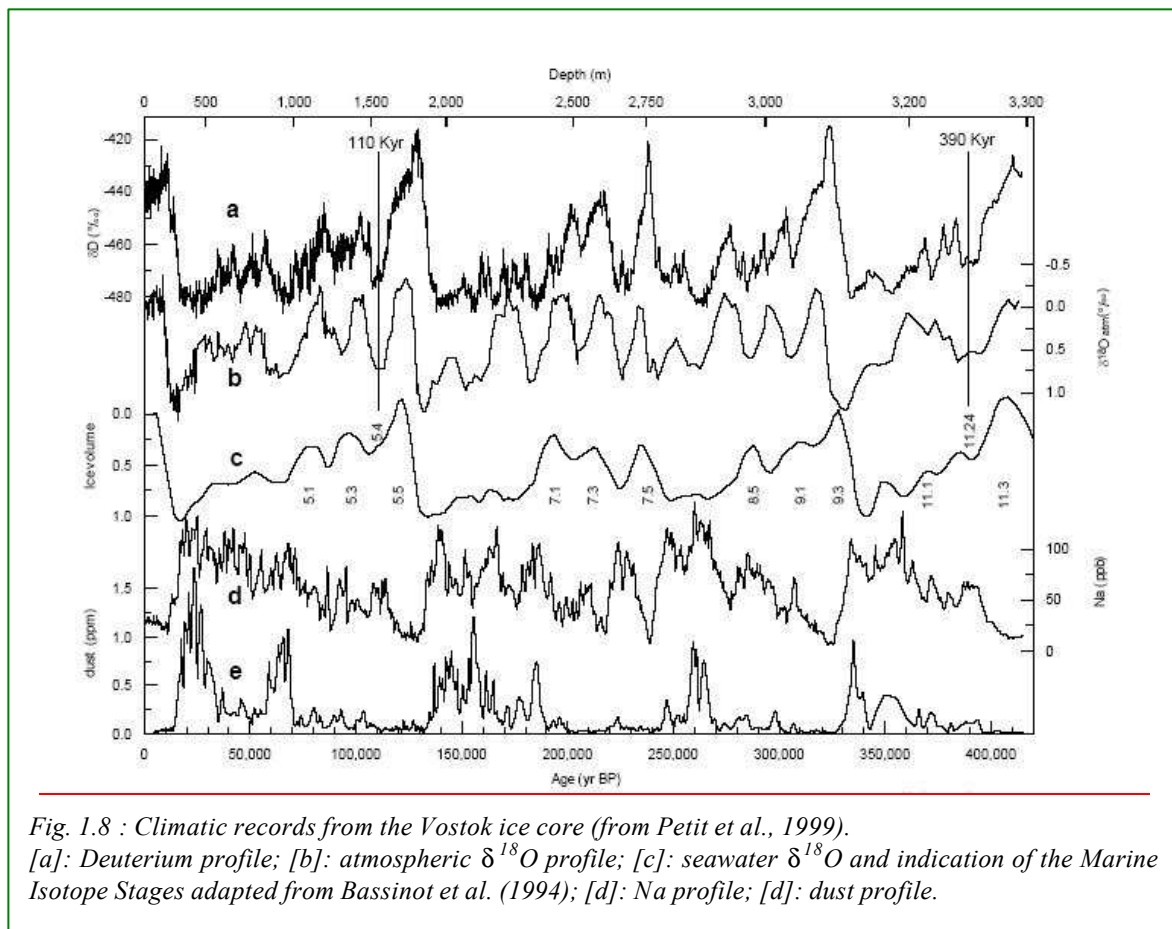
<sup>7</sup> It is assumed that the Andean explosive volcanism had a direct influence on the composition of the Argentine loess (Sayago et al., 2001).

## 1.5 Climatic tales from the Vostok ice core

The first 3310 m of the 3623 m deep Vostok ice core preserve the climatic memory of the last 420 kyrs. The climatic and atmospheric records provided by this ice core (Petit et al., 1999) have a spatial significance spanning from regional to hemispheric or even global scale.

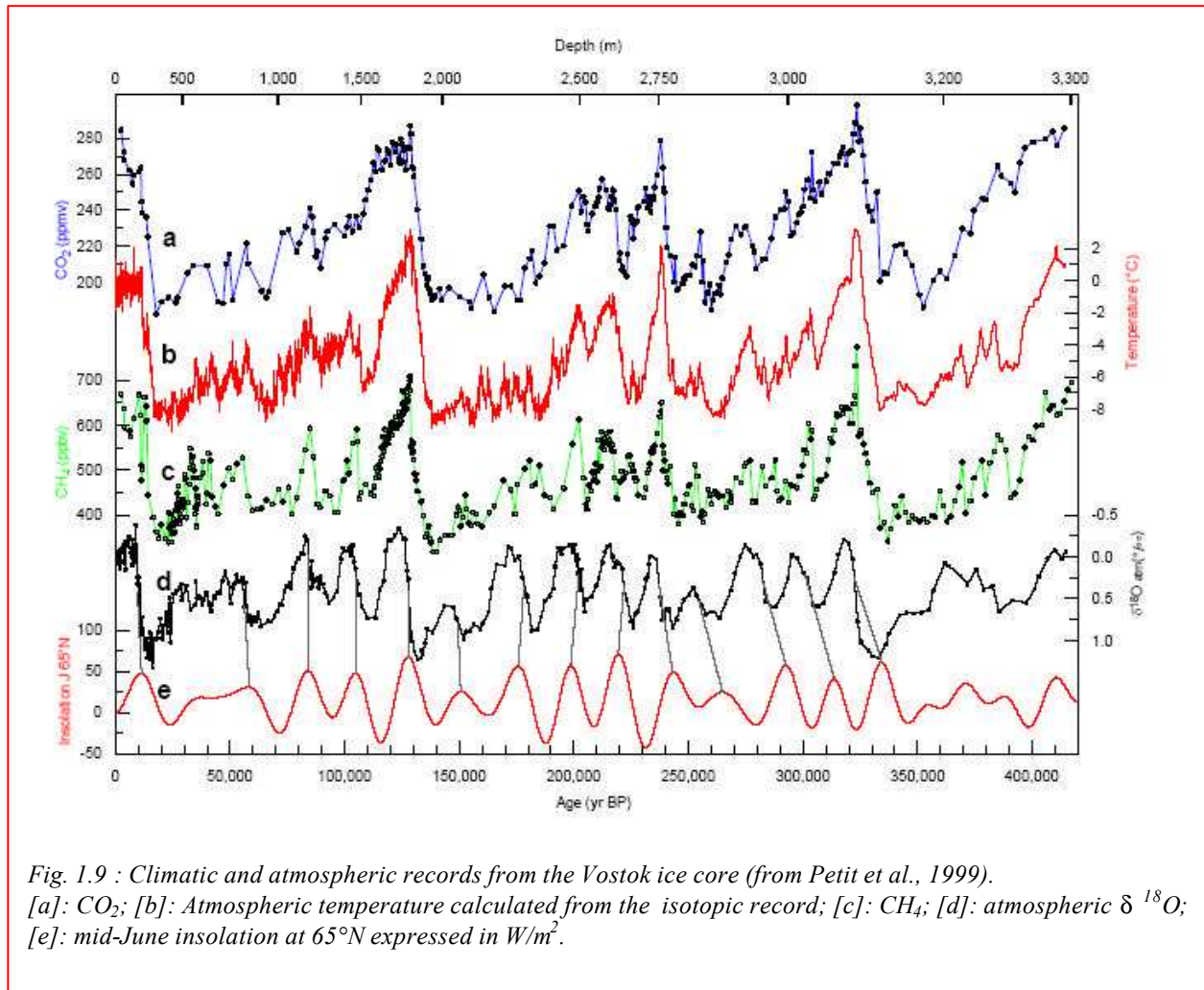
The stable isotope record (Fig. 1.8a), proxy for temperature variations (Fig. 1.9b), shows four glacial-interglacial cycles, characterized by a rapid “sawtooth” sequence of warm interglacials (Stages 11.3, 9.3, 7.5 and 5.5) followed by glacial periods increasingly colder and punctuated by cool interstadials. The end of each cycle is marked by a rapid (5-10 kyrs) return to warmer interglacial conditions.

The first-order variability of the marine and terrestrial aerosols is anti-correlated with the temperature record (Fig. 1.7d and 1.7e). In particular, the input of marine Na and dust is highest in glacial periods, lower in interstadials and minimum in interglacials. The enhanced dust input during cold periods was primarily associated to the widespread aridity on the continents, to the high wind speeds and the reduced hydrological cycle. In such cold periods the mineral particles reaching Vostok likely had a southern South American provenance (Basile et al., 1997).



Greenhouse gases  $\text{CO}_2$  and  $\text{CH}_4$  almost covary with temperature. The major and most rapid changes of these two gases occur during glacial-interglacial transitions ( $\text{CO}_2$  switched from 180 to 280-300 ppmv and methane from 320-350 to 650-770 ppbv). During glacial inception, the temperature and the methane decrease almost in phase while  $\text{CO}_2$  lags by several thousand years.

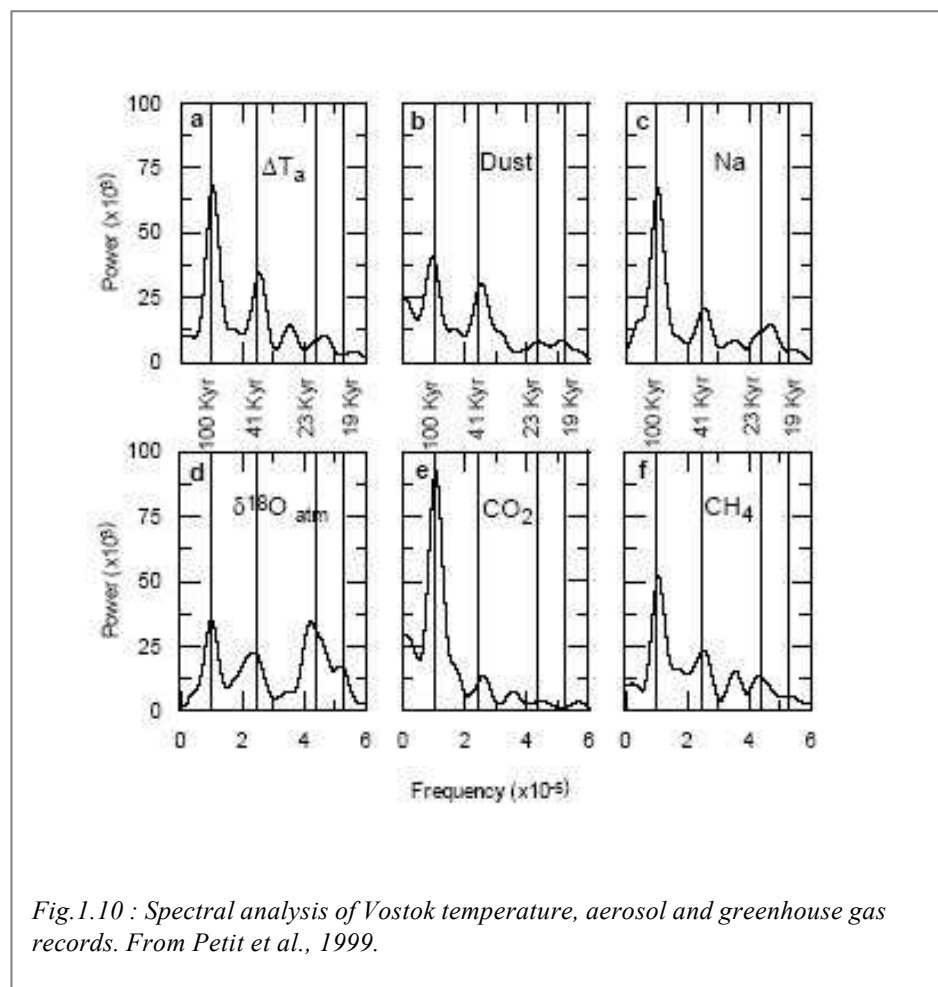
It must be noted that the present-day atmospheric levels of  $\text{CO}_2$  (~370 ppmv at Mauna Loa, Keeling and Whorf, 2002) and  $\text{CH}_4$  (~1760 ppbv, Steele et al., 2002) have never been reached during the four glacial-interglacial cycles. This is of relevant importance with respect to the evolution of Earth's climate.



The spectral analysis of the Vostok climatic and atmospheric records are reported in Fig. 1.10 (from Petit et al., 1999). All of them evidence peaks corresponding to the Earth's orbital parameters (§ 1.1), i.e. around 100, 41 and 20 kyrs. A large part of the variance of the temperature record is concentrated in the 100 kyrs and 41 kyrs bands, corresponding to the eccentricity of Earth's orbit and the obliquity of its axis. This latter is in phase with the annual insolation at Vostok site, suggesting a tight link between the variability of the annual insolation at high southern latitudes (that is in the order of 7%)

and the temperature at Vostok. Peaks within the orbital frequencies characterize also the  $\text{CO}_2$  and  $\text{CH}_4$  power spectra, but for both of them the 100 kyrs component is the dominant one.

While the marine aerosol is tightly correlated with temperature and shows a major concentration of variance in the 100 kyrs spectral band, the dust variability occurs both in the 100 and 41 kyrs bands. Petit et al. (1999) observe an interestingly similarity with the periodicities of the tropical Atlantic dust record (De Menocal, 1995), interpreted as characteristic for the progressive deglaciation of the Northern Hemisphere and re-activation of the deep ocean circulation. The Vostok dust peaks are associated to the periods of increased sea ice extent in the South Atlantic, that in turn is influenced by the thermohaline circulation (THC).



## **1.6 Southern Hemisphere atmospheric circulation**

To understand variations in climate and atmospheric circulation in time and space, some of the salient features of the Southern Hemisphere (SH) circulation have to be taken into consideration.

The SH is characterized by relatively small continental land masses over a large oceanic extent. These continental regions are mostly located at tropical and subtropical latitudes, and except the Antarctic continent only few sizable landmasses occur in the Southern Ocean south of 35°S.

### ***General pattern for present-day***

The atmospheric circulation in the SH follows the general scheme of Hadley and Ferrel cells, the first thermally-direct with ascending motion in equatorward regions and subsidence on its poleward extremity, the second with its ascending branch in the poleward side and the subsiding one in its equatorward side (Tyson, 1986).

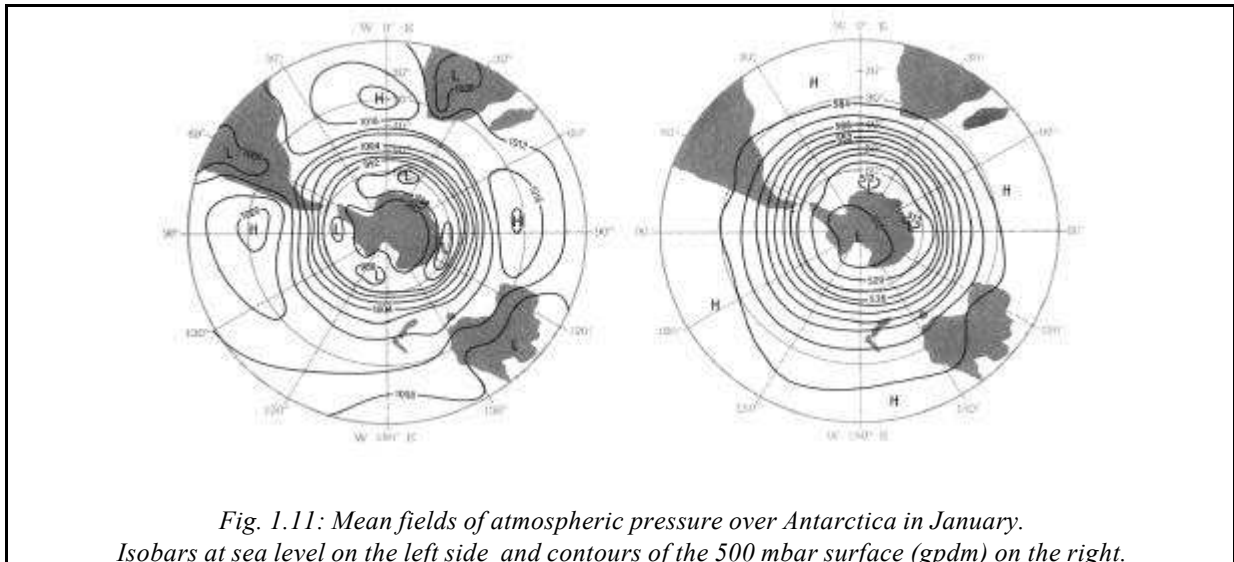
The maximum subsidence and surface divergence is situated at about 30 °S, where the surface pressure field is characterised by large anticyclonic cells (South Atlantic, South Indian, and East Pacific anticyclones). These semi-permanent oceanic anticyclones control the weather between ~15°S and ~40°S, generating areas of reduced cloudiness and anti-clockwise direction of winds. Anticyclones occurring on the continental landmasses instead, are weaker, smaller and much more sensitive to climatic changes. Today the strongest continental high pressure cell is the Australian anticyclone, covering two thirds of the continent; the South African and south American ones are smaller and less stable.

South of the latitudes dominated by the oceanic and the continental ridges, the pressure drops to a minimum (60-70°S), forming a belt of cyclonic cells - the circumpolar trough - whose axis oscillates around 65°S (Schwerdtfeger, 1984), and probably around 62°S between 30°E and 150°E.

Antarctica is characterized by a surface anticyclone and a permanent polar vortex<sup>8</sup> at high altitude (Fig. 1.11).

---

<sup>8</sup> In the analysis of zonal standing waves the wavenumber 1 corresponds to the eccentricity of the Polar vortex.



The SH is under the influence of the two major wind regimes surrounding the globe: (1) the permanent Easterlies, marking the central position of the Intertropical Convergence Zone (ITCZ), and (2) the Westerlies.

The ITCZ is a region of pronounced convective activity, associated to abundant precipitation; the width of such system spans ca. 15 degrees of latitude, and its modern average position is close to the equator.

However the dominant feature of the SH atmospheric circulation is the large tropospheric circumpolar vortex of Westerly winds, that reaches its maximum in the upper troposphere. The vortex is embedded at any time with perturbations taking the form of *waves*<sup>9</sup> and eddies which control the daily weather.

The belt of cyclonic waves is an unstable area (400-800 km in diameter) propagating from west to east formed by winds rotating in a clockwise direction and encircling the globe (Tyson, 1986).

Low levels of perturbation superimposed to the mean westerly flow enhance a more *zonal circulation* while intense perturbations favour more *meridional circulation* patterns<sup>10</sup>.

A particular feature of the SH atmospheric circulation is the Walker Circulation, which oscillates in time between high and low phases, with important consequences over all the globe. During the so called high phase of the Southern Oscillation pressure rises in eastern Pacific and falls over Indonesia.

<sup>9</sup> This is the principal difference between the ITCZ, that consists in simple winds.

<sup>10</sup> The wave perturbations are extensively studied (e.g. Trenberth, 1981, 1982) since they are important features of the Westerlies. Two kinds of waves exist: (1) large scale semi-stationary forced waves, which appear to maintain a similar location and amplitude year round, and (2) transient disturbances, which are guided by the semi-stationary waves.

Longer waves are generally associated with the zonal component of velocity and shorter waves with the meridional component. In the analysis of zonal standing waves the eccentricity of the Polar vortex is associated to wavenumber 1.



A descending limb of the Walker circulation develops over the former region and an ascending limb on the latter. Near surface easterlies intensify and upper westerlies close the cell. During the low phase the Walker circulation weakens and sometimes weak westerlies can occur. During this phase the Pacific Hadley cell and consequently the subtropical jet stream intensifies. During the low phases of the Southern Oscillation index the pressure rises over Indonesia and the consequent weakening or reversal of the pressure gradient sets in motion complex dynamical responses from the ocean, leading to warm water anomalies off Ecuador and Northern Peru (El Niño). The warm water anomaly is associated with a depression of the thermocline and a diminution of the upwelling, with important consequences worldwide (IPCC 2001).

### ***The Last Glacial Maximum***

Numerous evidences suggest a northward shift of the climatic belts during the LGM (see Wright et al., 1993 for a general overview). The ITCZ displacement is supposed to have been as large as 10 degrees of latitude north respect to its present position, as evidenced in northern South America and in the western African Sahel (e.g. Talbot, 1980). Australia was not reached by humid air masses during LGM. In parallel, the northern limit of the Westerlies shifted 5 to 10 degrees north respect to its present position (Iriondo, 1999). It is possible however that locally and in an unstable pattern the anticyclones of Australia and Africa pushed the westerlies to the south (e.g. Harrison and Dodson, 1993).

Anticyclonic centers seem to have migrated slightly eastward during the LGM. Iriondo and Garcia (1993) suggested a northeast shift of Patagonian climate of about 650 km, probably linked to major influence in South America of the South Pacific anticyclone.

It is likely this contributed to the reinforcement of the catabatic winds from the ice caps of the North Patagonian Cordillera and also to the formation of the *pampean sand sea* deposits in the southwestern Pampas and the adjacent loessic belt over the remaining area (see Box 1).

The continental anticyclones also shifted to the north during the LGM. The central Australian anticyclone was probably also stronger and sand dunes were active at that time (Wasson, 1986).

### ***The middle Holocene***

Several continental evidences from the SH suggest particularly warm period in the middle Holocene that is generally called *hypisothermal*. For example, Southeastern Australia registered high temperatures and low rainfall between 8 and 6 kyrs B.P. (Dodson and Ono, 1997), the Argentine Pampas experienced a tropical/subtropical climate with active pedogenesis, development of fluvial belts and typical Brazilian fauna (Iriondo and Garcia, 1993). Mangroves grew up to at least 39°S latitude in New Zealand (300 km south of the present position) between 10 and 7 kyrs B.P., and sand dunes did not form in central Australia between 8 and 4 kyrs B.P. (e.g. Wasson, 1986). Tasmania lakes were

lower than present and temperatures were higher from Tasmania to New Guinea along the eastern coast of Australia (Harrison and Dodson, 1993).

It is believed that in the early to middle Holocene the atmospheric circulation was different from the late Holocene and present day. Iriondo (1999) estimated southward displacement of the central position of the ITCZ 10-11 degrees further south respect to the LGM, and shift of 5 degrees south of the westerlies belt.

Shulmeister (1999) suggests an enhanced Walker circulation since 5 kyrs B.P.; the increased polar-equator pressure gradient (as result of increased seasonality) and the consequent intensification of Easterlies and Westerlies in the late Holocene could have contributed to enhance the east-west contrast across the Pacific and made the circulation “flip” from an Early Holocene to a late Holocene mode.

\*\*\*\*\*    \*\*\*\*\*    \*\*\*\*\*

### Summary

*The Earth's climate and environmental history has been punctuated ever since by variability at different timescales. Quaternary changes can be reconstructed through several natural archives. Polar ice cores from the East Antarctic plateau constitute a potential source of information for climate and atmospheric history.*

## Chapter 2 - MINERAL DUST IN THE CLIMATE SYSTEM, TODAY AND IN THE PAST.

### 2.1 Aerosol and dust

In general terms, aerosols are suspended liquid or solid particles in a gas. Natural aerosols generated directly from the Earth's surface (continents or oceans) are called *primary* aerosols, while those formed by chemical reactions of atmospheric gases and vapors are *secondary* aerosols. Primary and secondary aerosol can interact within the atmosphere and generate complex mixtures (e.g. Raynaud et al., 2003).

Primary aerosol can be subdivided in two categories: sea salts and dust. Beside sporadic contributions from volcanic material and soot and a negligible input of extraterrestrial materials, dust is mainly composed by the windblown mineral aerosol from continental areas. This latter is the object of interest for this work, and the terms continental, aeolian, or mineral dust will be used indistinctly.

### 2.2 Mineralogical nature of aeolian dust

The mineral particles injected into the atmosphere from continental erosion are mainly composed of quartz, feldspars, carbonates, clays and salts (gypsum, halite), and eventually volcanic materials (Pye, 1987, Maggi 1997).

While quartz, feldspars and carbonates are abundant in the coarse fractions, clays dominate the fine fraction that is transported long range.

During the transport from the source to the sink however the composition of the dust plume is subject to mineralogical variations. Schutz and Seibert (1987) observed an increasing clay/quartz ratio in function of the distance from the African continent and attributed that to the more rapid sedimentation of the large isometric quartz particles in contrast to the more plate-like clay minerals. Actually, clay minerals with their small mass and optimal aerodynamic properties are the more diffuse aeolian minerals all around the globe (Tegen and Fung, 1994).

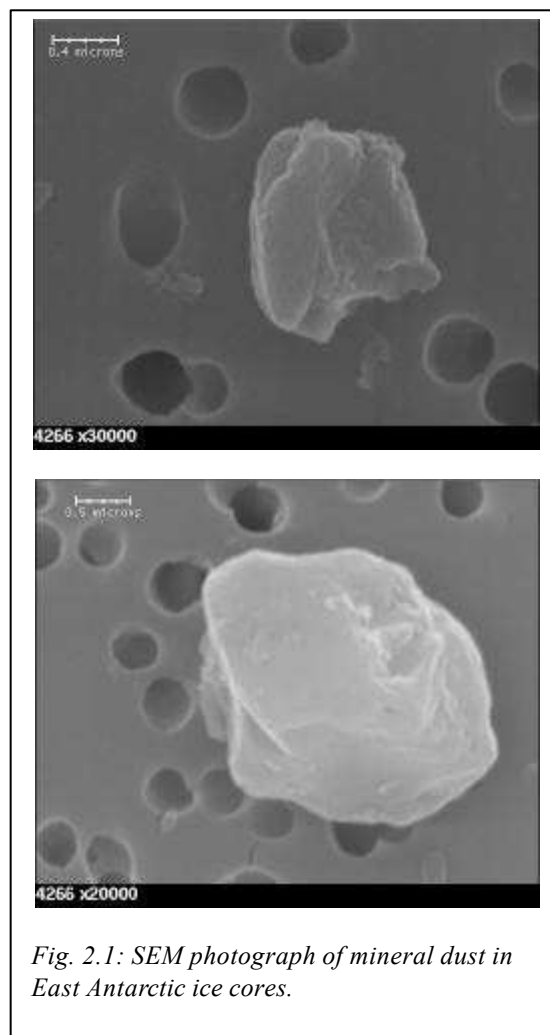


Fig. 2.1: SEM photograph of mineral dust in East Antarctic ice cores.

An important second-order effect of the dust settling within the atmosphere in function of particle mass is the heavy mineral fractionation: the rapid gravitational settling of heavy minerals (like magnetite, garnet, hornblende, zircon, rutile, epidote for example) makes them relatively more abundant in sands and sandstones and, generally speaking, in sediments with an overall larger grain size (Taylor and McLennan, 1987).

Minerals entrapped in East Antarctic ice (at the end of the dust cycle) are mainly clays (about 40% of the total number of particles), followed by about 15% of crystalline silica and a comparable amount of feldspars, and other minor components like pyroxenes and amphiboles, metallic oxides, volcanic glasses (Gaudichet, 1986, 1988). Among clays, illite is the most abundant (>60%) in Vostok and South Pole ice (Gaudichet et al., 1992), while smectite, chlorite and kaolinite vary in minor proportions.

### **2.3 The role of mineral dust on climate**

It is now well established that the windblown mineral aerosol (dust) has a considerable influence on the climate system. However, there are still important uncertainties in the quantitative estimation of direct and indirect effects of dust on the global energy balance (IPCC, 2001) both in magnitude and sign.

The radiative impact of aerosols depends on its concentration within the atmosphere, but is also strongly dependent on its particle size distribution, shape and chemical composition. Actually, only particles smaller than 20  $\mu\text{m}$  (in diameter) are considered for calculations of radiative effects since the atmospheric lifetime of larger particles is too short (Tegen and Lacis, 1996).

Dust scatters and partially absorbs incoming sunlight, playing a “greenhouse effect” in absorbing thermal radiation outgoing from the Earth. Changes in the amount of dust in the atmosphere therefore are capable to induce changes in radiation balance and consequently surface temperatures.

However, the sign and magnitude of radiative changes induced by mineral dust depend on many factors. Beside the vertical distribution of dust in the atmosphere, the presence of clouds and the brightness of the surface underlying the dust plume, a crucial role is exerted by the optical properties of the dust, depending in turn on the size and mineral composition (e.g. Sokolik and Toon, 1996; Claquin et al., 1998). Moreover, it has been previously observed (§ 2.2) that the shape and size (hence a different mineralogical nature) of the minerals composing the dust plume can vary significantly, and therefore the spatial and temporal forcing estimates are highly uncertain.

In order to translate aerosol burdens into aerosol optical depths, and subsequently in radiative perturbation, four quantities have to be accurately known as function of wavelength (IPCC 2001): the

mass light-scattering efficiency, the functional dependence of light-scattering on relative humidity, the single-scattering albedo and the asymmetry parameter.

There are also several indirect influences of mineral dust, on climate and atmospheric chemistry. The large specific surface areas provided by airborne minerals result in abundant crystallographic sites for heterogeneous condensation and subsequent reaction of gaseous species (e.g. Dentener et al., 1996). Moreover, dust can influence cloud droplet formation, with subsequent effects on cloud brightness and rainfall (e.g. Zhang and Carmichael, 1999). Dust can also moderate the photochemical processes (Dickerson et al., 1997). One important indirect radiative forcing is associated with the role of dust particles, and clays in particular, as ice forming nuclei (e.g. Rogers and Yau, 1989).

Mineral dust has also an important role on terrestrial (e.g. Swap et al., 1992) and marine (e.g. Hutchins and Brunland, 1998) ecosystems by providing nutrients. Some trace metals on dust are of crucial importance for some marine biological communities. Iron for example represents the limiting nutrient for phytoplankton communities in some ocean regions (e.g. Fung et al., 2000; Falkowski et al., 1998). The dust input consequently can potentially influence the global carbon cycle and the atmospheric greenhouse gas content. However, the magnitude of such a possible impact of dust is still highly uncertain.

## **2.4 The knowledge for present time**

The importance of mineral aerosol on climate has led scientists to improve the study of physical and radiative characteristics of dust, and to improve dust-cycle models in order to assess the dust impacts on climate. The major progresses in the matter have been made in the last four-five years, but actually the available data sets used for model input parameters and for validating the simulations are still very limited<sup>1</sup>.

### **2.4.1 Atmospheric dust load**

Global simulations of the modern dust cycle are capable to reproduce the first-order pattern of dust transport and deposition under modern climate conditions.

The estimates of the global dust emissions for present climate published in the literature span a very large range, from about 100 Mt/yr to about 3000 or even 5000 Mt/yr on a global scale (IPCC 2001, Tegen et al., 2002a), and 800-1700 Mt/yr according to one of the most recent estimates assembling the largest compilation of quantitative observations of the modern global dust cycle (Tegen et al., 2002a).

The IPCC 2001 estimates the mineral (soil) dust emission in ~2150 Mt/yr on global scale, with very high spatial and temporal variability. The estimate for the dust emission in the Southern Hemisphere is less than 1/5 the emission estimated for the Northern Hemisphere (about 350 and 1800 Mt/yr respectively).

These uncertainties are linked to the scarcity of global datasets used to determine the model input parameters and to validate model simulations: observations around the globe are very scarce and they are often representative of a limited period of time. Local observations are often extrapolated to yield a global estimate even if they come from specific regions having conditions that are not necessarily typical of all dust-source regions. Moreover, there are many desert areas in the world that are still too poorly studied.

---

<sup>1</sup> A recent workshop held in Germany (Max Plank Institute for Biogeochemistry, Jena, 24 May 2002) has brought together dust experts coming from many disciplines (Geology, physics, remote sensing, etc.) in order to formulate strategies for using existing datasets and creating new ones to improve model parametrization and evaluation. Some of the issues of the present thesis work have been presented, and an inter-comparison project for paleoclimate simulation is perspected [Tegen et al., 2002b].

#### **2.4.2 Common characteristics of source terrains identified by satellite observations**

In general terms, the regions providing the bigger dust fluxes at present time are primarily those with little or no ground cover, easily wind-erodible soils and associated to seasonal wetness (Mahowald et al., 1999).

A worldwide geographical mapping of major atmospheric dust sources has been recently provided by Prospero et al. (2002) on the basis of data from TOMS (Total Ozone Mapping Spectrometer) sensor on NIMBUS-7 satellite for a period of 13 years (1980-1992). The authors evidenced that the major sources for long-range transported dust are located in arid regions and are centered over topographical lows or on lands adjacent to topographical relief. Dry lake beds, relics of extensive lakes in the past, are a good example since lacustrine sediments are characteristically fine-grained, but also glacial outwash plains, riverine floodplains, alluvial fans and all areas where the recent geomorphological history has favoured the concentration of fine-grained material and the creation of large areas with low surface roughness are preferential sources (Tegen et al., 2002a).

Despite the arid (from semi-arid to hyper-arid) conditions of these environments at present time, these sources had either a relatively recent (Pleistocene) pluvial history or are associated with water features, such as ephemeral rivers and streams, alluvial fans, playas and saline lakes. Chemical weathering is enhanced by the abundance of water, and liquid transport is an efficient mechanism for production of small particles, separated from the soil or from the primary rock and carried to a depositional basins or an alluvial plain where, after drying, become mobilizable by wind (Prospero et al., 2002). Vegetation cover and soil crusting are also two important factors that can sensibly lower or suppress dust emission.

Sand dune systems do not appear good sources for long range transported dust (Prospero et al., 2002). This is not paradoxical, since they are relatively coarse grained, from tens to several hundred micrometers (Lancaster, 1995), and are already impoverished in the fine fraction. The coarse sandy particles have a high settling velocity in air and therefore are not carried more than few hundred kilometers away by winds; however, the role of sandy particles in generation of dust particles by saltation is crucial (Gillette et al., 1982).

Terrains with a recent history of aridity therefore, appear much more active sources than old arid sandy areas.

#### **2.4.3 Source regions at global scale**

The major global dust sources have been identified by Prospero et al. (2002) through TOMS Absorbing Aerosol Index (AAI). The authors constructed a world map, reported in Fig. 2.2, on the

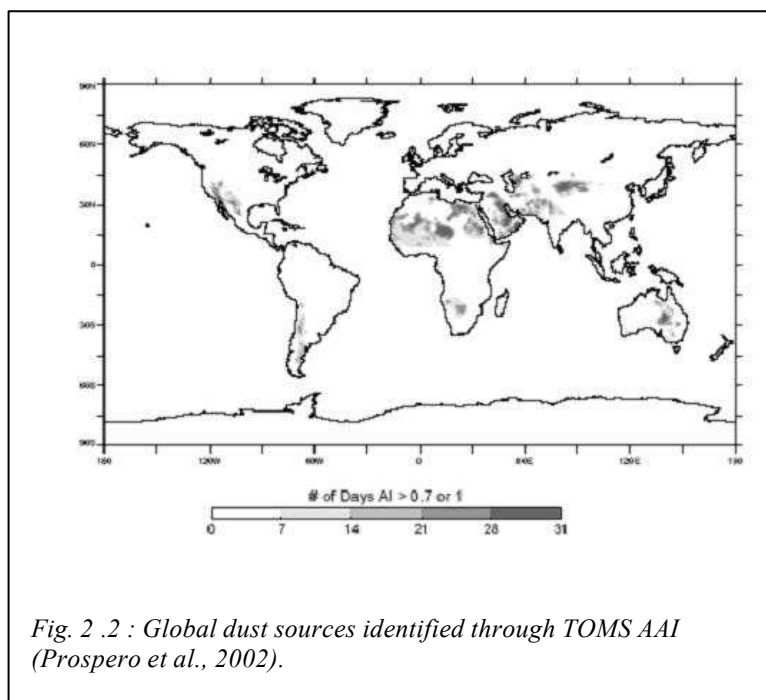
basis of the long term frequency of occurrence (FoO) distribution<sup>2</sup> for each source, and therefore is not representative of a particular period of the year. The sources, in fact, show a large variability and characteristic geometries in function of the seasons.

The principal sources for dust that can potentially be transported long-distance are located in the Northern Hemisphere, in particular in North Africa, in the Middle East, in central Asia and in the Indian subcontinent.

For the Southern Hemisphere, observations evidence that it is devoid of major dust sources impacting on large areas. This observations are consistent with concentration of dust-derived Al element in southern-ocean waters, that is much lower than in northern oceans (Measures and Vink, 2000) and with the flux of aeolian materials in deep sea sediments (Rea, 1994).

Interestingly, TOMS observations (Prospero, 2002) have evidenced that many sources are associated with areas where human impacts are well documented (e.g. the Caspian and Aral Seas, South-Western North America, the loess-lands in China), but the largest and most active sources however are located in remote areas without human activity.

Therefore, the present-day dust mobilization seems to be dominated by *natural* sources on global scale.



#### 2.4.4 Principal dust “hot spots” in the Southern Hemisphere

The theme of this thesis work is the transport of mineral dust in the Late Quaternary towards the Antarctic continent, therefore it is useful to focus on the most recent issues coming from satellite observations on the present-day dust sources for the Southern Hemisphere.

This paragraph is inspired to the observations of Prospero et al. (2002), from which the three figures here reported (Australia, South Africa and South America) have been taken.

<sup>2</sup> TOMS AAI frequency of occurrence (FoO) distribution is expressed in Prospero et al. (2002) as days per month when the AAI equals or exceeds 0.7.



## *Australia*

In the Australian continent (Fig. 2.3) continuous dust deflation is detected in the Great Artesian Basin feeding Lake Eyre, that today constitutes a large *playa*<sup>3</sup>. The most active dust area is located North-East of present-day Lake Eyre, corresponding to the pluvial Lake Dieri (ancestral Lake Eyre).

Interestingly, the large Simpson Desert does not appear as persistent source for dust but only an occasional region for large dust events. There are only other minor active regions within the continent.

At first glance, it could seem surprising that such a large and arid continent is devoid of major sources for long-range transported dust. The authors found an explication for this in the flat topography of the continent, and the lack of renewal of small particles (§ 2.2.1).

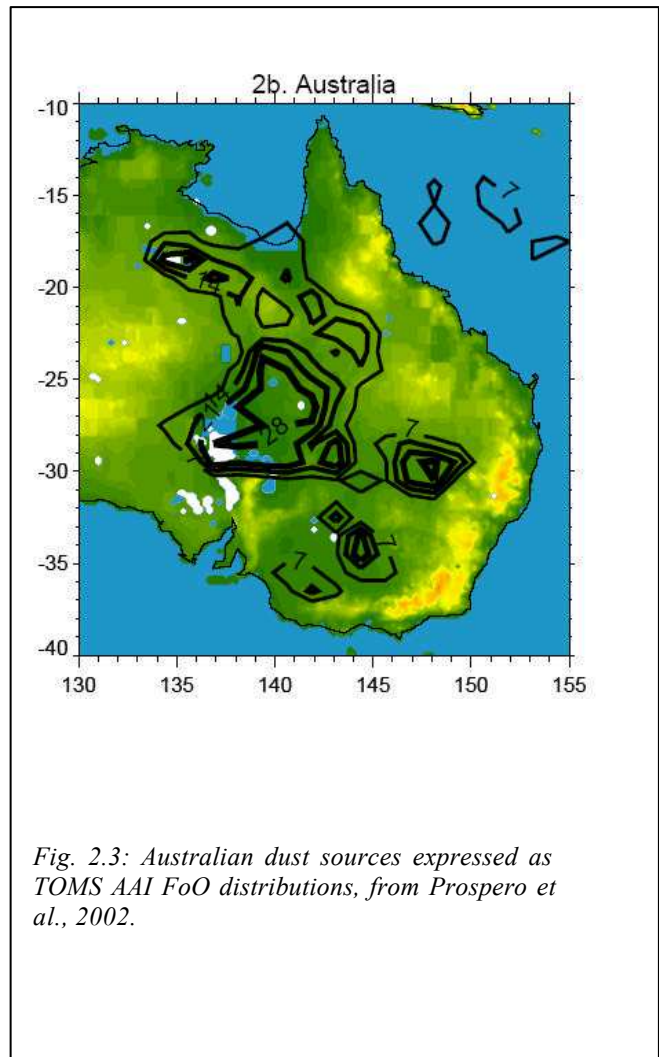


*Fig. 2.3: Australian dust sources expressed as TOMS AAI FoO distributions, from Prospero et al., 2002.*

<sup>3</sup> Playas are shallow, short-lived lakes that form where water drains into basins with no outlet to the sea and quickly evaporates. Playas are common features in arid (desert) regions and are among the flattest landforms in the world (USGS Geologic Glossary).

### ***South Africa***

For South Africa (Fig. 2.4), a continuous source for dust is located in Botswana in the region centered at 21°S, 26°E.

Dust activity is centered over the western end of the Makgadikgadi Depression, occupied during the Pleistocene by a great lake, the Palaeo-Makgadikgadi (Goudie, 1996).

A second small but persistent source is centered at 16°E, 18°S over the Etosha Pan, Northern Namibia, at the extreme northwest of the Kalahari basin. During the Pleistocene also the Etosha Pan basin was occupied by a large lake (Goudie, 1996).

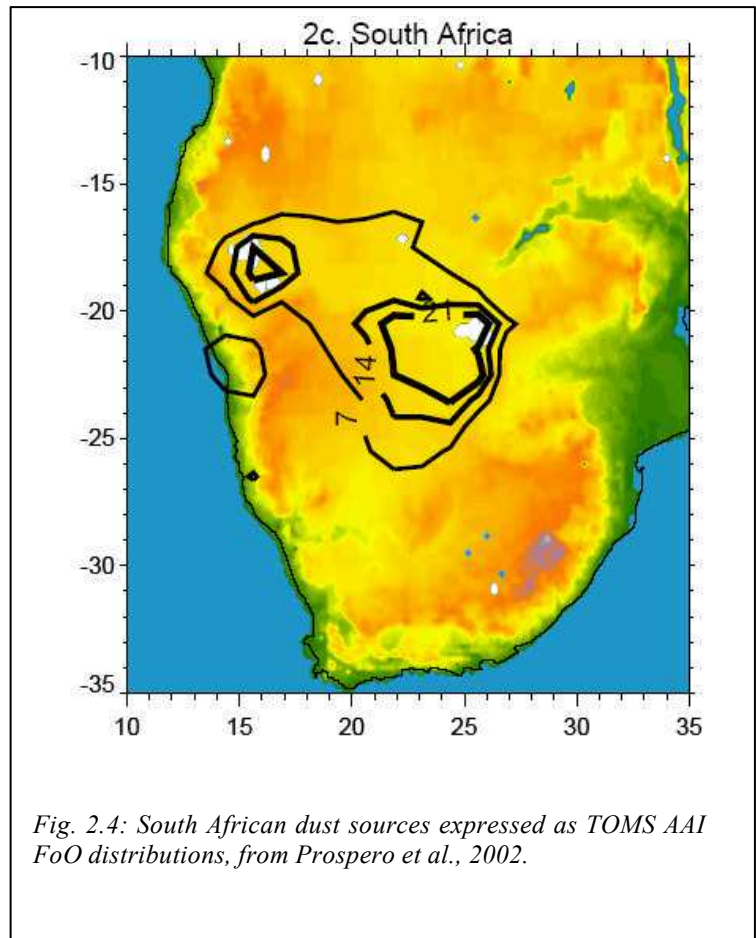


*Fig. 2.4: South African dust sources expressed as TOMS AAI FoO distributions, from Prospero et al., 2002.*

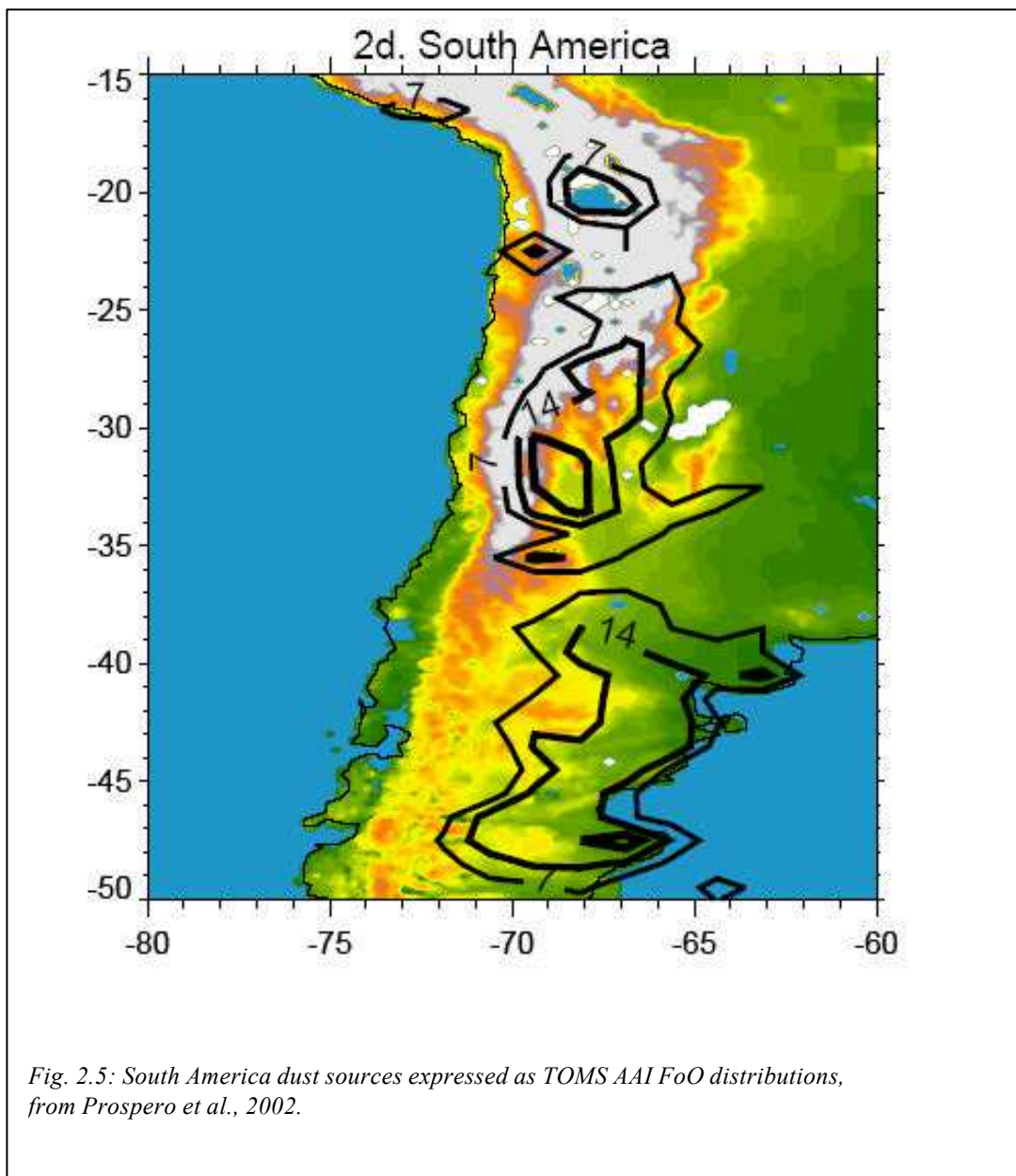
### ***South America***

For South America (Fig. 2.5) three dust source regions can be observed.

The first is located in the Bolivian Altiplano, around ~20°S and 68°W, in an arid intermountain basin situated at about 3750-4000 m of altitude that includes two of the largest salt flats (*salars*) of the world. A large part of the Altiplano was occupied in the Pleistocene by a lake, whose sediments are exported today by the strong winds blowing over the region.

The second major dust source area in South America is located in Argentina along the eastern flanks of the Andes (27-34°S, 67-70°W). Dust activity is centered in an intermountain area between the Andes (West) and the Sierra de San Luis - Sierra de Cordoba (East). It can be observed that the most active area lies in the western part of this region.

Finally, a large dust source region is located between 38°S and 48°S, and includes the Southern Pampas and Northern Patagonia, semiarid to arid region spanning from the eastern flanks of the Andean Cordillera to the Atlantic coast. Within this vast region a particular active area is located further south, close to Santa Cruz (46°-48°S), but dust emission here has been attributed mostly to anthropogenic activities reducing vegetation cover and activating wind erosion over large areas of the province.



## **2.5 The Last Glacial Maximum**

### **2.5.1 The LGM atmospheric dust load: evidence from paleoclimate proxies**

There is unequivocal and widespread evidence all over the Earth, from terrestrial (e.g. Ding et al., 1994; Kukla, 1989), marine (e.g. Rea, 1994) and polar (e.g. Petit et al., 1999) paleoclimate records for the Quaternary period, that the atmospheric dust load was considerably higher in glacial periods than during interglacials. Such increases however were neither globally uniform nor ubiquitous.

Among the cold periods of the Pleistocene, the Last Glacial Maximum (onward LGM ~21 kyrs B.P.) has become a major focus for dust cycle modeling, largely because of the considerable amount of evidences documenting deposition rates and transport paths of aeolian lithogenic material, that are necessary for evaluation of model results.

The most recent compilation of literature data on dust accumulation rates for the LGM and the Holocene from ice cores, loess sediments, marine sediment traps and marine sediments is assembled in the DIRTMAP database<sup>4</sup> (Kohfeld et al., 2001). Marine sediment records from low- and mid- latitudes show a smaller increase (maximum 5 times that of present time), and some equatorial regions actually show a decreased dust flux. Sediments from the North Pacific show an increase of 1-3 times during LGM, while those from the North Atlantic 2-5 times. A 2 to 9 fold increase in dust is found in LGM records downwind of Australian dust sources.

The DIRTMAP table with ice core data fluxes is reported here below (Tab. 2.1).

The average increase in dust deposition rates during the LGM with respect to the Holocene indicated by Greenland and Antarctic ice cores is 2 to 20-fold. However, the total amount of dust deposited was 10 to 500 times less than at locations closer to the sources of dust.

It can be observed however that Antarctica is poorly documented with respect to the paleo-dust flux, and only three records (one from the West and two from the East) are included in the DIRTMAP database.

---

<sup>4</sup> The Version 1 of DIRTMAP database (Kohfeld et al., 2001) has now been refined in the Version 2 that estimates also the non-carbonate accumulations in marine sediments which in some cases can be used as first-order estimates of dust accumulation rates. Potentially contaminated sites have been detected in a specific list.

<b>Core ID</b>	<b>Lon</b>	<b>Lat</b>	<b>Modern g/m<sup>2</sup>/yr</b>	<b>LGM/ Modern</b>	<b>LGM g/m<sup>2</sup>/yr</b>	<b>Reference</b>
Byrd	-120	-80	0.003	4	0.012	Cragin et al., 1977
Byrd	-120	-80		1.5		Thompson and Mosley-Thompson, 1981
Camp Century	-61	77	0.04	2	0.08	Cragin et al., 1977
Camp Century	-61	77		2.4		Thompson and Mosley-Thompson, 1981
Devon, Canada	-66	67		7		Fisher, 1979
Devon, Canada	-66	67		10		Fisher, 1979
Dome C	124	-75	0.001	11	0.011	Petit et al., 1981
Dome C	124	-75		12		Petit et al., 1981
Dome C	124	-75		6		Petit et al., 1981
Dome C	124	-75	0.0009	8.5	0.00765	Royer et al., 1983
Dome C	124	-75		3		Thompson and Mosley-Thompson, 1981
Dunde, China	97	38		1.5		Thompson et al., 1989
Dunde, China	97	38		4		Thompson et al., 1989
Dye 3	-44	65	0.02	1.5	0.03	Hammer et al., 1985
Dye 3	-44	65	0.02	17	0.34	Hammer et al., 1985
GRIP, Summit	-38	73	0.008	68	0.544	Steffensen, 1997
Guliya, China	82	35		0.2		Thompson et al., 1997
Huascarán, Peru	-78	-9	0.2	200	40	Thompson et al., 1995
Renland	-27	71	0.06	2	0.12	Hansson, 1994
Sajama, Bolivia	-69	-18		0.2		Thompson et al., 1998
Vostok	107	-78	0.0007	18.5	0.01295	DeAngelis et al. 1984
Vostok	107	-78		15		Petit et al., 1990

*Tab. 2.1: Table reporting modern and LGM dust fluxes from ice core records included in the DIRTMAP database (Kohfeld et al., 2001).*

### **2.5.2 The climatic and environmental conditions during the LGM**

Several aspects of the glacial climate have to be considered in order to understand the reasons for the observed increase of the dust cycle during the LGM.

Large ice sheets covered much of the Northern Hemisphere mid- to high- latitudes and developed also in the Southern Hemisphere (see box. 2). The ice formation contributed to the lowering of sea level, that is considered to have been on average 120 m lower than today (e.g. Shackleton, 1987). As consequence, wide additional landmasses were exposed.

The colder and drier climate affected land surface conditions, generating a reduction in the total area forested and the expansion of the area of grass- or shrub- dominated vegetation (Tegen et al., 2002a). Fine-grained lacustrine material was exposed in many areas where lake levels decreased, and as the present day satellite observation indicate (e.g. Prospero et al., 2002), and today this kind of deposits are powerful providers for long-range transported dust.

An important aspects of glacial climate that must also be evidenced is the strengthening of dust source areas, mainly due to the increase in the primary production of silt-sized material through glacial and periglacial processes. This material is susceptible to aeolian deflation and redistribution through glacial discharge.

The climate was globally colder and drier, with regional exceptions, wind speeds generally increased and the atmospheric circulation was globally more zonal. These factors probably affected the dust cycle by modifying the transport times and by affecting the transport pathways. Moreover, the reduced hydrological cycle also moderated the amount of dust removed en route through precipitation.

## Box 2 - The ice growth in the Southern Hemisphere during the LGM

The reconstruction of ice development in the Southern Hemisphere during the LGM is more fragmentary and less well dated than in the North.

The largest area of ice growth was southern South America: while in the northern part of the Cordillera of Chile and Argentina valley glaciers developed, calving sometimes into the Pacific ocean, further south (from 38°S to 55°S) a ~500,000 km<sup>2</sup> wide ice sheet of ca. 1.2 km of thickness formed (Hulton et al., 2002, see Fig. 2.6). The authors estimated a contribution of the Patagonian ice sheet to global sea level of ca. 1.2 m.

In the southwest Pacific the largest ice covered area was in the Southern Alps of New Zealand (South Island), where a 40,000 km<sup>2</sup> wide

ice cap of lower thickness (100-200 m) formed (see Fig. 2.7, from McGlone et al., 1993).

In New Guinea, Australia, and Tasmania, that were linked by land bridges, the snowlines were lowered. Small ice caps and valley and cirque glaciers formed in Tasmania, while southeastern Australia was briefly glaciated during the LGM and deglaciated well before the Holocene (Barrows et al., 2002).

The growth of the Antarctic ice sheet during the LGM is quite uncertain; a recent reconstruction for the LGM constrained by geological data (Denton and Hughes, 2002) shows little inland change but expansion of the continental shelves. The additional ice volume on the Antarctic Ice Sheet during

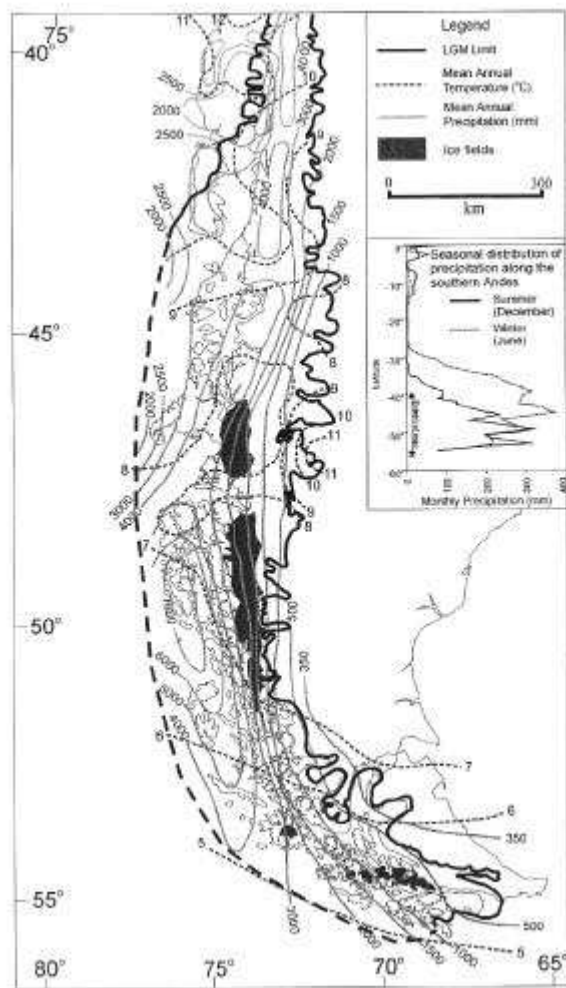


Fig. 2.6: LGM limit and distribution of the Patagonian icefield with present-day precipitation distribution in function of latitude. (After Hulton et al., 2002).

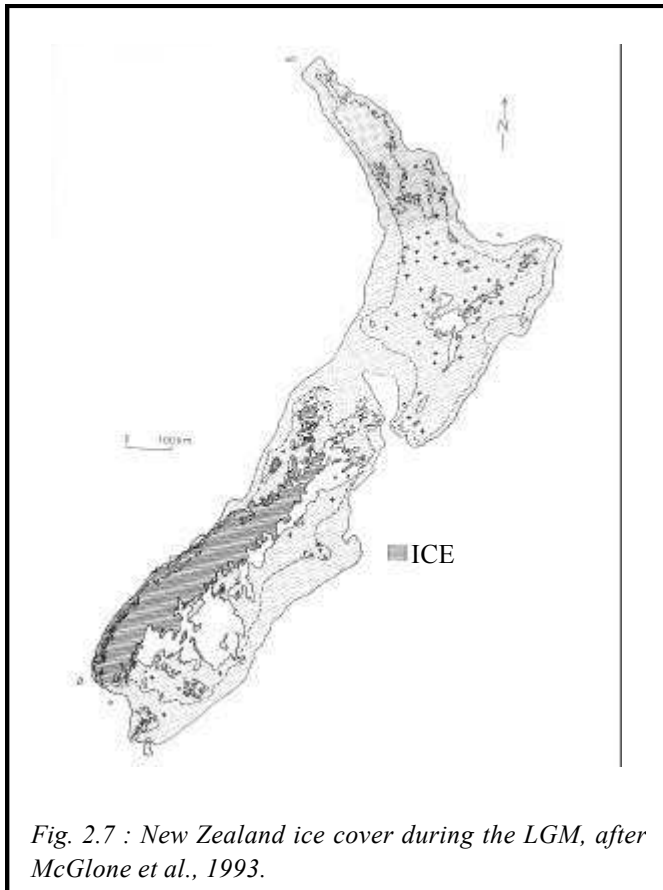
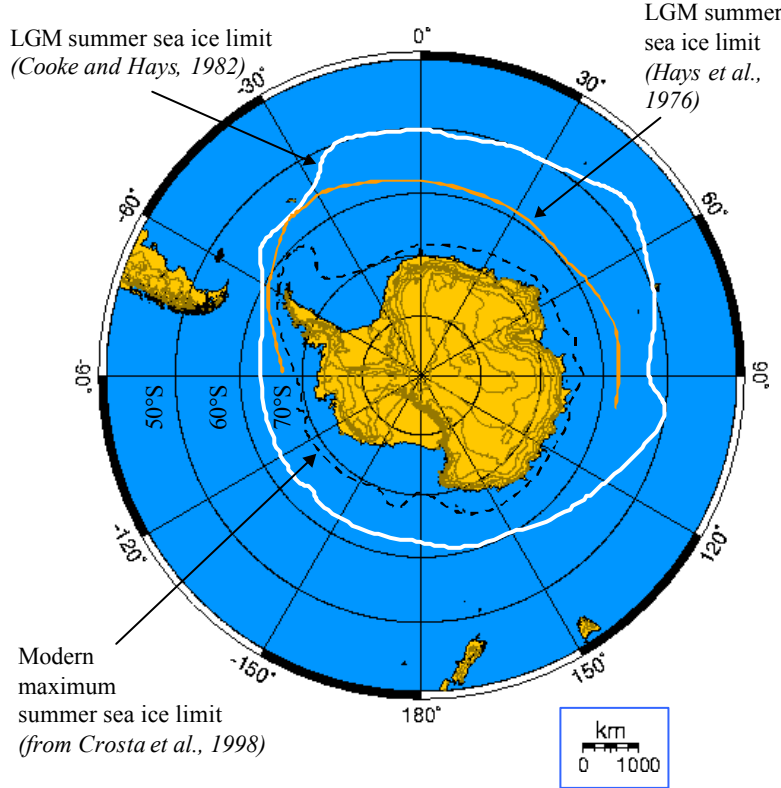


Fig. 2.7 : New Zealand ice cover during the LGM, after McGlone et al., 1993.

LGM is estimated in  $15 \times 10^6 \text{ km}^3$  (Denton and Hughes, 2002), corresponding to a contribution to the global sea level of  $\sim 14 \text{ m}$ .

On the other side, circum-Antarctic sea ice (Fig. 2.8) was considerably more extended than at present (e.g. Crosta et al., 1998).





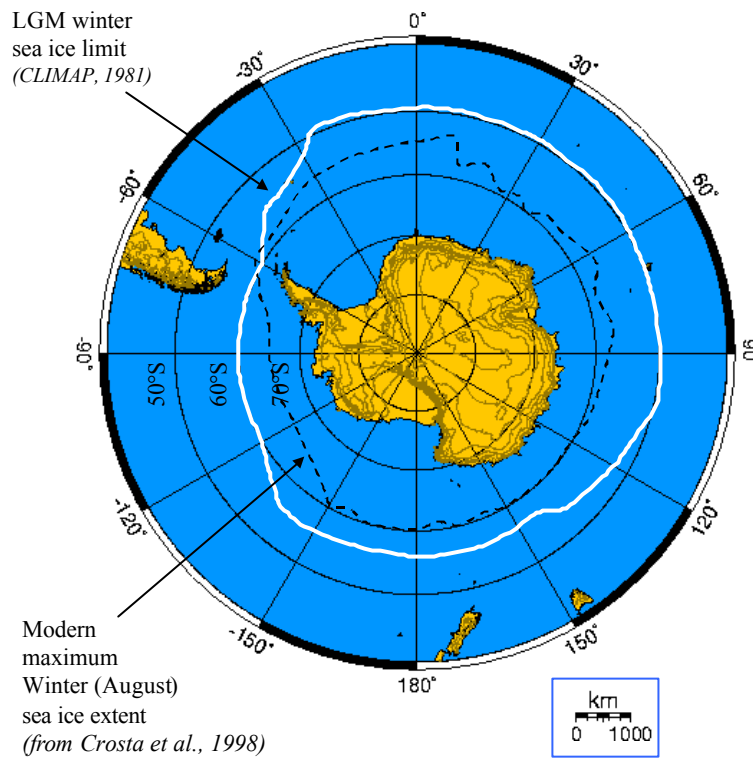


Fig. 2.8: Summer (Top) and winter (Bottom) sea ice extent around Antarctica during LGM and at present-day.

### 2.5.3 The atmospheric dust load and the potential source regions: evidence from model simulations.

Several model simulations have been performed in an attempt to reproduce the paleo dust cycle. Those taking into account changes in wind regimes and the reduced intensity of the hydrological cycle (e.g. Joussaume et al., 1989, Genthon et al., 1992) were unable to reproduce the observed increase in dust deposition at high latitudes. Also the addition of the exposed continental land areas as extra source does not account for the magnitude of the observed changes (Andersen et al., 1998).

A simulation performed by Mahowald et al. (1999)<sup>5</sup>, taking into account the effect of increasing dust surface areas as well as the climate-induced change

in vegetation cover, has been capable of reproducing a 20-fold increase at high latitudes, and the more moderate (2 to 5- fold) increase at low latitudes, broadly in agreement with observations. On global scale, the LGM/Holocene increase in atmospheric dust loading has been estimated about 2.5.

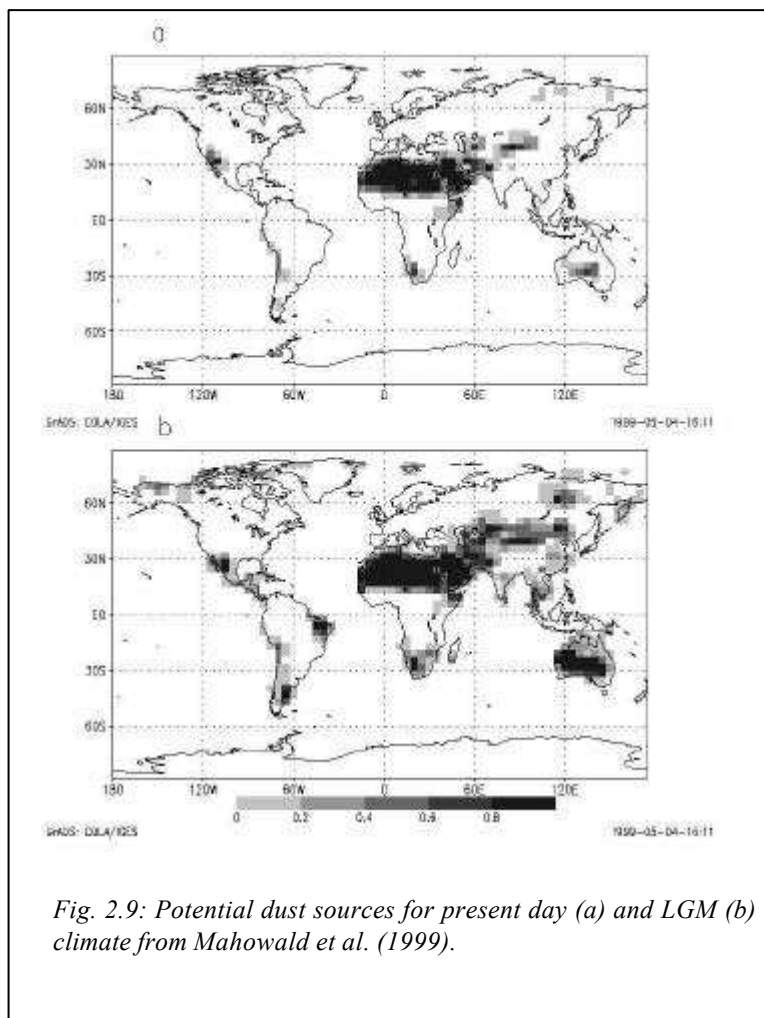


Fig. 2.9: Potential dust sources for present day (a) and LGM (b) climate from Mahowald et al. (1999).

For dust flux to Antarctica however, some discrepancies occur. Modelled rates are underestimated if modern dust source regions are considered, while they are slightly overestimated when LGM source areas are considered.

<sup>5</sup> Mahowald et al. (1999) performed a model simulation on the basis of the BIOME3 terrestrial biosphere model (Haxeltine and Prentice, 1996) and using the climatic parameters of temperature, precipitation and insolation fields derived from ECHAM3 general circulation model (Roegner et al., 1992).

Potential source regions are estimated fixing threshold values for vegetation, in terms of leaf area index (LAI), and taking into consideration specific soil criterion from Tegen and Fung (1994), and orographic changes.

The authors attributed the differences to an oversimplification of the dust entrainment model that did not include some important factors like soil moisture, the different erodability properties, and vegetation cover. This latter in particular has proved to be of primary importance for present climate both in seasonal and interannual variability (Tegen et al., 2002a).

Mahowald's simulations for LGM and present day climate show a geographical distribution for dust source areas that is reported in the fig. 2.9.

The comparison with satellite observations (Fig. 2.2) evidences that the model does capture the general pattern of dust sources (Fig.2.9a) for present day climate, despite the underestimation of dust deposition fluxes (not reported) off east Asia and the slight overestimation off the coast of Africa and in Southeast Australia.

Comparison with paleo-environmental evidences suggests that the simulated source area increases during LGM are plausible. In particular, the eastward expansion of the desert region in Asia is confirmed by pollen data from BIOME6000 project compilation (Prentice and Webb, 1998), although an overestimation of about 10° of latitude seems to occur for the modelled northern limit of the desert. The very small southward expansion of the Sahara desert is also confirmed by pollen and lake-level data.

An improvement in simulation on LGM dust cycle has been recently provided by Werner et al. (2002) that took into account also vegetation phenology, affecting the seasonality of dust sources and hence dust emissions. This model provided a good explanation for the observed LGM dust changes even at regional scale.

However, up to now there is no model taking into account also the increase in dust primary production through glacial processes. Periglacial and glacial processes enhancing production of debris and their transport via glacially-fed river system zones were a significant dust source during cold periods, as many loess deposits suggest.

Mahowald et al. (1999) model has been used by Claquin et al. (2003) to estimate the direct radiative effect of the increased dust loading at the LGM, taking also into account the mineralogical properties of dust according to its origin. The computation showed that incoming solar radiation was highly reduced at LGM because of the higher atmospheric dustiness, especially at tropical latitudes.

\*\*\*\*\*      \*\*\*\*\*      \*\*\*\*\*

### Summary

*Mineral dust of continental origin is an ubiquitous component of the atmosphere, and contributes to the climate forcing.*

*The Southern Hemisphere is characterized by a lower atmospheric dust load than its Northern counterpart, and modern satellite data allow to distinguish some active dust emission areas in South America, South Africa and Australia.*

*During the IGM, continental aridity was widespread and the atmospheric dustiness considerably higher than at present.*

## Chapter 3 - MINERAL DUST CYCLE FROM THE SOURCE TO THE SINK: CONCENTRATION AND SIZE DISTRIBUTION CHANGES

### **3.1 Dust mobilization at the source, “source strength”**

The so called *source strength* is a complex parameter depending on many factors, like the availability of particles and their renewal in time (primary production), the surface conditions in terms of moisture, surface roughness (depending on soil obstacles), snow cover, and crusting. An important role is played by vegetation cover with its typology as well as seasonal and interannual variations.

The surface extension of the dust-supplying regions also must be considered when the source strength at continental scale has to be determined.

The *source strength* determines the magnitude of dust amount injected into the atmosphere.

Soils and sediments generally include materials of various sizes, like gravels (>2mm in diameter), sands (0.063-2.0 mm), silts (63-4 μm), and clays<sup>1</sup> (<2 μm). The smallest diameter measured for clays is about 0.02 μm. The relative proportions of these classes determines the *texture* of the soil material.

The deflation of dust is strongly dependent on surface wind speed<sup>2</sup>. Empirical studies (e.g. Gillette, 1978) have demonstrated that the amount of uplifted dust varies as the 3<sup>rd</sup> power of the surface wind speed, following the equation:

$$Q_a = C(u-u_{tr})u^2$$

Where  $Q_a$  is the dust flux from the surface,  $u$  is the surface wind speed,  $u_{tr}$  is the threshold velocity, and  $C$  is a dimensional parameter linked to soil properties and typical for each soil.

Dust mobilization therefore occurs only when the surface wind speed exceeds a threshold velocity, which depends on surface properties and particle size.

Tegen (in press) evidenced that particles with diameter between 120 and 200 μm have the lowest threshold velocity, while coarse particles with diameter >200 μm as well as very small particles require the higher wind speeds to be mobilized. For these latter, the increased surface area enhance adhesive and cohesive forces, but on the other side, their mobilization is favored by processes of saltation of larger particles. Clays agglomeration and sticking to form larger particles leads to decrease the availability for wind erosion of particles smaller than a critical dimension. The magnitude of this effect however is difficult to estimate. Tegen and Fung (1994) estimated that if all clays with diameter

---

<sup>1</sup> *Granulometrical* clays are intended here as the category of particle-size used in pedological studies. They can include *mineralogical* clays as well as other fine grained sediments.

<sup>2</sup> The highest wind speeds in the ECMWF data are about 100-150 km/hr, but peak wind speeds really occurring during dust storms can be considerably higher.

larger than 0.8  $\mu\text{m}$  are considered available for wind erosion, about 1/6 of the total clay mass of a soil is available for uplift.

D'Almeida and Schutz (1983) observed a direct relationship between surface wind speeds and the size distribution of the airborne dust for the  $>10 \mu\text{m}$  size fraction. During long range transport, dust is graded around a modal value of about  $2\mu\text{m}$  (Schulz et al., 1998), hence the size distribution of particles measured at the sink (e.g. in polar ice cores) can be considered independent from that of particles uplifted from the source (Ruth et al., 2003).

The dust emission can be drastically reduced or suppressed when soil moisture is abundant, and the moisture threshold is usually texture dependent (in press).

Gillette et al. (1999) however pointed out that high wind speeds can dry the first few mm of soils and allow dust production even when the rest of the soil is saturated.

Another important factor that can increase wind threshold velocity for dust emission is the surface roughness, caused by obstacles that partly absorb wind energy. A typical example is vegetation cover. Typically, wind erosion is favoured where the vegetation cover is low and sparse (deserts, shrubland or grassland).

## 3.2 The long-range transport

### 3.2.1. The horizontal dimension

The long-range dust transport depends on the large scale wind regime. Dust transport models usually do not take into account localized small scale processes like dust injection into jet streams, that nevertheless can occur in summer months in some regions like the Sahel (Pye, 1987).

During long range transport the decrease in particle concentration (from a to b) can be described as :

$$C_b = C_a * f * e^{-t/T}$$

Where t is the transit time between the source a and the sink b, T is the residence time in the atmosphere, governed by wet and dry depletion processes en route (see below),  $C_a$  and  $C_b$  the atmospheric dust concentrations at the source and the sink respectively, and f a correction factor. Therefore, the longer the transport time, the lower will be the concentration of dust at the sink.

Particles can be removed from the atmosphere by *dry* or *wet* deposition. Dry deposition includes gravitational settling, where the settling velocity depends on the square of particle size, and turbulent mixing to the surface, while precipitation-related events like sub-cloud scavenging and in-cloud removal determine the *wet deposition*.

The removal efficiency is size dependent, hence during transport the size distribution changes. For sands and coarse silts the gravitational settling<sup>3</sup> alone (dry deposition) determines the sedimentation velocity, while for clays the lifetime in the atmosphere is mainly controlled by wet deposition and turbulent mixing.

A parametrization of uplift and deposition (using analyzed winds and rainfall statistics) has been performed by Tegen and Fung (1994) and Tegen and Lacis (1996). The authors obtained atmospheric lifetimes spanning a very large interval, from one hour to about ten days, in function of particle size (Tab. 3.1).

---

<sup>3</sup> In a fluid regime the particle settling velocity is governed by the Stokes law equation which can be expressed:

$$V = [\Delta\rho g / 18\mu] d^2$$

V= settling velocity (cm\*s-1)  
 $\Delta\rho$ = particle-fluid density difference (g\*cm-3)  
g= acceleration due to gravity (cm\*s-1)  
 $\mu$ = viscosity (poise)  
and d= particle diameter (cm)

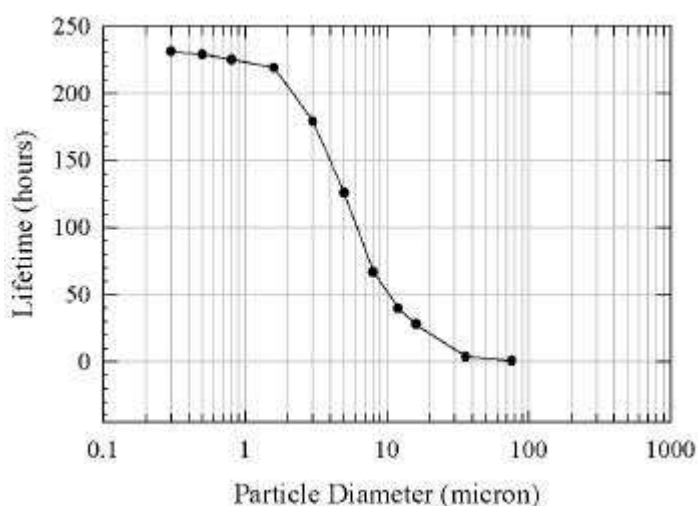
Coarse silts<sup>4</sup> are mainly removed by gravitational settling, as occurs for sands, these latter having a lifetime generally lower than 1 hour. A direct consequence of the different residence times of particles in function of size is an enrichment in clays respect to silty and sandy particles at the dust sink.

The residence time in the atmosphere T is governed also by the efficiencies of depletion processes (wet and dry deposition) occurring en route. Therefore, the change in the size distribution of particles within a dust plume can reflect changes in the strength of such processes in the atmosphere.

However, the magnitude of this effect on particles with high atmospheric lifetimes is not known.

On global scale, Mahowald et al. (1999) estimated that ~78% of dust aerosol is centered around a mean mass diameter (MMD) of 2.5  $\mu\text{m}$ , while extremely large and small particles distributed around a MMD of 38  $\mu\text{m}$  and 0.01  $\mu\text{m}$  may reasonably be neglected.

Particle Diameter ( $\mu\text{m}$ )	Atmospheric Lifetime (hours)
<b>0.30</b>	<b>231</b>
<b>0.50</b>	<b>229</b>
<b>0.80</b>	<b>225</b>
<b>1.6</b>	<b>219</b>
<b>3</b>	<b>179</b>
<b>5</b>	<b>126</b>
<b>8</b>	<b>67</b>
12	40
<b>16</b>	<b>28</b>
36	4
76	1



Tab. 3.1 and Fig. 3.1: Atmospheric lifetimes for particles of different diameter (data from Tegen and Lacis, 1996 and Tegen and Fung, 1994).

<sup>4</sup> The silty fraction of soils is often subdivided into fine silt (<10  $\mu\text{m}$ ) and coarse silt (>10  $\mu\text{m}$ ), an assumption that is justified by their different atmospheric lifetimes (from days to hours).



### 3.2.2 The vertical dimension

Tegen and Lacis (1996) observed a decrease in dust concentration with increasing atmospheric height, as large particles are removed by gravitational settling before they can reach the higher atmospheric levels.

Size distribution is also altitude dependent, since the higher atmospheric levels are depleted of large particles. The decrease in the mode of size distribution observed by the authors is  $1.4 \mu\text{m}$ , from a mode of  $3 \mu\text{m}$  at 970 mbar, to  $1.6 \mu\text{m}$  at 40 mbar.

An interesting issue from Tegen and Fung (1994) is the modeled vertical distribution of dust concentration for individual classes of particles, that exhibits increased concentration of small particles (clays) respect to larger ones (silts and sands) with height, due to the high sedimentation velocity of these latter.

Only clays and small silts therefore are transported within the mid to high troposphere levels and have therefore the potential to reach the interior of the East Antarctic Plateau.

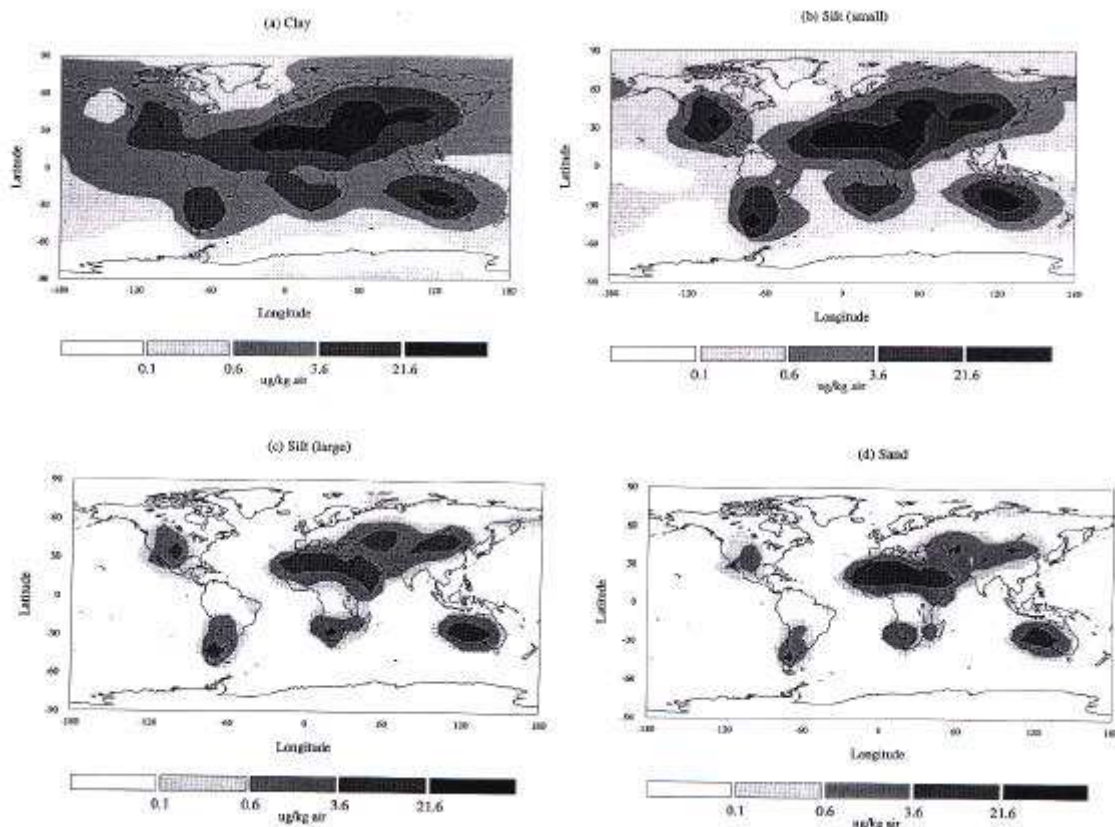


Fig. 3.2: Modeled annual mean dust concentration for different size classes: clays ( $<2 \mu\text{m}$  diameter), small silts ( $2\text{-}20 \mu\text{m}$ ), large silts ( $20\text{-}50 \mu\text{m}$ ) and sand ( $>50 \mu\text{m}$ ).

### **3.3 The sink: dust in polar ice cores**

#### **3.3.1 Dust concentration: what information?**

In synthesis, it can be assumed that the dust concentration in ice cores depends on the synergical action of many factors. These can be grouped in four main categories.

1-The *source strength* (§ 3.1), depending on the physical parameters of the deflated terrains and on surface wind speeds.

2-The *transport*, in terms of transport time and residence time of particles in the atmosphere (§ 3.2.1).

3- The *hydrological cycle*, since very active wet deposition processes can produce an efficient washout of atmospheric impurities.

4- The *snow accumulation rate* at the sites. It is possible to get rid of this factor by converting the dust concentration into fluxes, and produce a quantity comparable with fluxes calculated from other terrestrial and marine proxies. The disadvantage of converting concentrations to fluxes is that this calculation relies upon estimated ice accumulation rates.

### 3.3.2 Dust size distribution: what information?

#### 3.3.2.1 The air-to-snow transfer

When dust deposition in ice depends both on wet and dry deposition processes, its size distribution can be affected by the different magnitude of these processes during the air-to-snow transfer, as evidenced for Greenland ice by Unnerstad and Hansson (2001).

If wet deposition processes can be considered so efficient to have no size-fractionation potential, dry deposition can induce a particle size fractionation as follows:

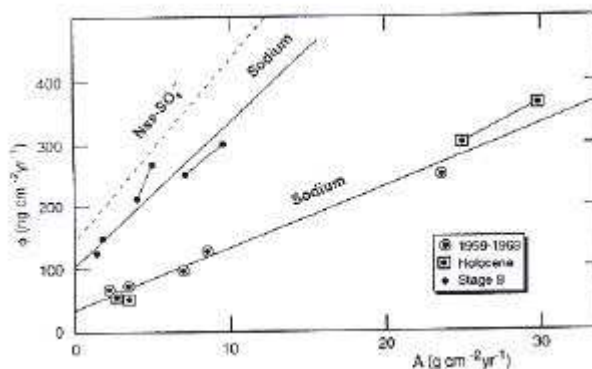
$$V_d = kd^n$$

Where  $V_d$  is the dry deposition velocity,  $k$  and  $n$  are constants and  $d$  is the particle diameter.

The dry-to-wet deposition ratios varied in Greenland in the different climatic periods. A quantitative estimation of the possible effect of this on particle modal value (Ruth et al., 2003) has evidenced that it is very low ( $<0.1 \mu\text{m}$ ) and accounts only 3% to 20% of the observed changes.

For East Antarctica, the deposition of dust is exclusively dry (Legrand and Mayewski, 1997, Legrand et al., 1997) for all climatic periods, and this effect has not to be taken into account.

Fig. 3.3: Average annual Na deposition flux ( $\text{ng cm}^{-2} \text{yr}^{-1}$ ) versus snow accumulation rates ( $\text{g cm}^{-2} \text{yr}^{-1}$ ) over the Antarctic plateau under present-day and LGM conditions. The dashed line represents the deposition flux of non-sea-salt sulfate for present-day over Antarctica. (Legrand et al, 1997)



### 3.3.2.2 The size distribution of dust in ice cores

The mineral dust transported long range is well graded; the first studies on polar ice cores (e.g. Royer et al., 1983 , Steffensen, 1997) already showed a log-normal distribution for particles around a mean mass diameter of 1.5-2  $\mu\text{m}$ .

$$dV/d \ln D = a * \exp [-0.5*(\ln (D/D_v)/(\sigma_g))^2] \quad (1)$$

Where

$$a = V/ [(2\Pi)^{1/2} * \sigma_g ] \quad (2)$$

Beside the total volume  $V$ , there are two important parameters defining the particle size distribution: the modal diameter  $D_v$  (also called *mode*) where the derivative is null, and  $(\sigma_g)$  the Geometric Standard Deviation ( $\sigma_g = \ln \sigma$ ) which describes how closely the particle volume is distributed around the mean.

According to Ruth et al. (2003) a dusty air mass characterized by  $(D_i, \sigma_i)$  at the source, transforms during transport in  $(D_f, \sigma_f) * f * e^{-t/T}$  (with  $T$  size-dependent).

Its new modal diameter  $D_f$  is characterized by

$$\ln (D_f/D_i) = -n * \sigma_g^2 * t/T * v_d/(v_w+v_d) \quad (3)$$

where  $v_w$  and  $v_d$  reflect depletion processes for wet and dry deposition en route, and  $n$  is a coefficient linked to dry deposition. The different efficiency of wet and dry processes en route plays only a minor effect when particles with high atmospheric lifetimes (clays) are considered.

At the beginning of the transport, the mode  $D_f$  decreases rapidly in function of time, but as soon as particles start to be more well-classed around their modal value (low  $s$ ) the rate of size diminution decreases.

In conclusion, while the dust concentration in Antarctic ice is a complex variable depending on the combination of several parameters, its size distribution is essentially linked to the transport; the investigation of the changes in time and space of these two elements can provide new insights into the paleo-dust cycle.

\*\*\*\*\*

### Summary

*The initial dust input in the atmosphere is modulated essentially by the source strength. Particles initially injected in the atmosphere vary in concentration and size distribution during the atmospheric transport from the source to the sink and in function of the altitude of advections.*

*The measurement of these two parameters in polar ice provides important information about dust source(s) environmental conditions and atmospheric transport.*

## Chapter 4 - IDENTIFICATION OF DUST ORIGIN THROUGH THE Sr-Nd ISOTOPIC SIGNATURE

### 4.1 An introduction to the Rb-Sr isotopic systems

Rubidium and Strontium are dispersed elements belonging to Group IA and IIA respectively.

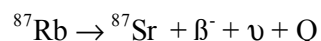
Rubidium (Rb, Atomic Weight<sup>1</sup> 85.46776) is an alkali metal whose ionic radius (1.48 Å) is very similar to that of K (1.33 Å). Therefore, Rb can replace K in many minerals, and for this reason it is particularly abundant in K-bearing minerals such as micas, K-feldspar, clay minerals, and evaporite minerals. Its concentration ranges from about 1 ppm or less in ultramafic rocks and carbonates, to more than 170 ppm in low-calcium granitic rocks.

Strontium (Sr, Atomic Weight 87.62) has a ionic radius (1.13 Å) very similar to Ca (0.99 Å) and therefore is mainly concentrated in Ca-bearing minerals (e.g. carbonates, plagioclase, apatite). Moreover, it can also replace K<sup>+</sup> ions in K-feldspars. The similarity of its geochemical behaviour with Calcium is also evident from its concentrations, spanning from a few ppm in ultramafic rocks to more than 460 ppm in basaltic rocks and even up to 2000 ppm or more in carbonate rocks.

<i>Atomic number Z</i>	<i>Element</i>	<i>Mass number A</i>	<i>Abundance (%)</i>
37	Rb	85	72.1654
37	Rb	87	27.8346
38	Sr	88	82.53
38	Sr	87	7.04
38	Sr	86	9.87
38	Sr	84	0.56

*Tab. 4.1: Rb and Sr atomic number<sup>2</sup>, mass number<sup>3</sup>, and isotopic abundances (see Faure, 1986 and references therein).*

Rb has two natural isotopes, whose abundances are reported in the Tab. 4.1. <sup>87</sup>Rb is radioactive and decays into the stable isotope <sup>87</sup>Sr by emission of a Beta particle and an antineutrino.



(Where  $\beta^{-}$  is the Beta particle,  $\nu$  is an antineutrino and Q the decay energy).

---

<sup>1</sup> The Atomic Weight of an element is the sum of the masses of its naturally occurring isotopes, weighted in accordance with the abundance of each isotope; it is measured in "Atomic Mass Unit" (amu). One amu corresponds to one-twelfth of the mass of <sup>12</sup>C.

<sup>2</sup> the atomic number is the number of protons defining an element

<sup>3</sup> the mass number A is the sum of protons and neutrons in the nucleus of an atom. Atoms of different elements having the same A are called "isobars".

The decay constant ( $\lambda$ ) of  $^{87}\text{Rb}$  internationally used is  $1.42 \cdot 10^{-11} \text{ y}^{-1}$ , corresponding to a half-life of  $48.8 \cdot 10^9$  years.

Sr has four naturally occurring isotopes all stables. The isotopic abundance of these isotopes are variable because of the formation of  $^{87}\text{Sr}$  by the decay of  $^{87}\text{Rb}$ .

The growth of radiogenic  $^{87}\text{Sr}$  from Rb decay can be described by the following equation derived from the law of radioactivity decay:

$$^{87}\text{Sr} = ^{87}\text{Sr}_i + ^{87}\text{Rb} (e^{\lambda t} - 1)$$

( $^{87}\text{Sr}$  = abundance of  $^{87}\text{Sr}$  at present time,  $^{87}\text{Sr}_i$  = abundance of  $^{87}\text{Sr}$  at the time of formation of the mineral,  $^{87}\text{Rb}$  = abundance of  $^{87}\text{Rb}$  at present time,  $\lambda$  = decay constant of  $^{87}\text{Rb}$ , and  $t$  is the time)

that can be divided by the abundance of the stable  $^{86}\text{Sr}$  isotope, obtaining the basic equation for Rb-Sr age determination:

$$^{87}\text{Sr}/^{86}\text{Sr} = (^{87}\text{Sr}/^{86}\text{Sr})_i + (^{87}\text{Rb}/^{86}\text{Sr})(e^{\lambda t} - 1)$$

### 4.1.1 Geochemistry of Rb and Sr

The isotopic composition of Sr in rocks has varied with time, becoming more and more heterogeneous since an initial substantial homogeneity in the Earth.

The initial  $^{87}\text{Sr}/^{86}\text{Sr}$  ratio of the Earth has been estimated to be about  $0.69897 \pm 0.00003$  (McCulloch and Black, 1984) on the base of studies of stony meteorites and lunar samples. Geological processes actually have destroyed, altered by metamorphism or buried deep in the mantle the rocks formed on Earth at the beginning of geologic time.

The continental crust started forming around four billion years ago by internal differentiation of the mantle and has become more and more enriched in radiogenic  $^{87}\text{Sr}$ , in contrast with the lower increase of  $^{87}\text{Sr}/^{86}\text{Sr}$  in the upper mantle. The present-day Sr in the mantle has lower  $^{87}\text{Sr}/^{86}\text{Sr}$  and is isotopically more homogeneous than Sr that resided in the continental crust for long periods of time. However, also the mantle has significant heterogeneities within a narrow interval of  $^{87}\text{Sr}/^{86}\text{Sr}$  of  $0.704 \pm 0.002$ , implying that some parts of it were depleted in Rb relative to Sr in the early history of the Earth, while other parts were probably undepleted or less depleted.

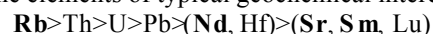
Rubidium and Strontium (parent and daughter elements) present a different geochemical behavior, that makes them strongly fractionated within the crust and the mantle. Rubidium is a Large Ion Lithophile (LIL) element and is more incompatible<sup>4</sup> than Sr. Therefore, it is more concentrated in the crust relative to the mantle than Sr.

This explains the different evolution rates of Sr in these two reservoirs: crustal rocks with high Rb/Sr ratio acquires high  $^{87}\text{Sr}/^{86}\text{Sr}$  in the course of time, while the upper mantle has become depleted.

---

<sup>4</sup> Elements whose charge or size differs significantly from that of available lattice sites in the mantle minerals will partition into the melt phase and are termed *incompatible* elements. K, Rb, Sr, Ba, the Rare Earth Elements, Ta, Hf, U, Pb, are an example. On the opposite, elements remaining in the solid (like Ni, Cr, Co, Os) are called *compatible* elements.

The order of incompatibility for some elements of typical geochemical interest is for example:



The compatibility of an element indicates the extent to which an element is fractionated into the crust relative to the depleted mantle.



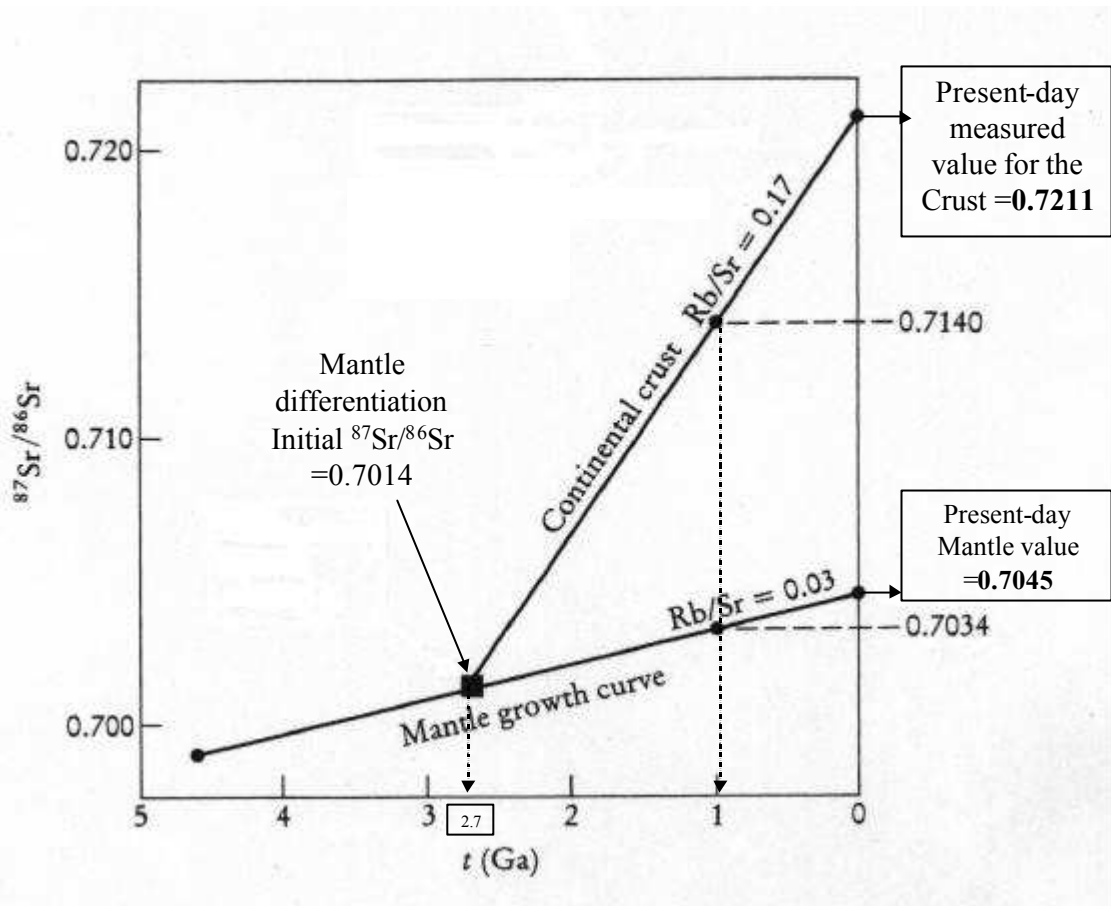


(Fig. 4.1: the evolution of  $^{87}\text{Sr}/^{86}\text{Sr}$  in time in the continental crust and in the mantle. The example shows a differentiation occurred at 2.7 Ga, leading to the formation of new continental crust with an initial  $^{87}\text{Sr}/^{86}\text{Sr}$  of 0.7014. The crust – that acquired higher Rb/Sr than the mantle – developed a higher  $^{87}\text{Sr}/^{86}\text{Sr}$  evolution with time, so that their present-day values differ substantially. The initial ratios of melts from the crust and the mantle formed at 1 Ga are shown as example (from Rollinson, 1993, modified).

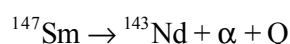
Within the continental crust, moreover, Sr and Rb are further separated by geological processes related to igneous activity, metamorphism, sedimentation and diagenesis, where Rb is preferentially partitioned into the melt or fluid phase.

Therefore, the isotopic evolution of Sr in the continental crust cannot be described by means of simple models because of the heterogeneity in the age of crustal rocks, their different Rb/Sr ratios, and the variety of geological processes that cause destruction rocks and allow recombination of material to form new rocks.

## 4.2 An introduction to the Samarium and Neodymium isotopic systems

Samarium (Sm, Atomic Weight 150.36) and Neodymium (Nd, Atomic Weight 144.24) are both Light Rare Earth Elements occurring as trace elements in common rock-forming minerals in which they replace major ions; in particular, they tend to be concentrated in biotite, feldspar and apatite.

Samarium has seven naturally occurring isotopes reported in Tab. 4.2, three of which are radioactive:  $^{147}\text{Sm}$ ,  $^{148}\text{Sm}$  and  $^{149}\text{Sm}$ . However, only  $^{147}\text{Sm}$  (decay constant  $6.54 \times 10^{-12} \text{ yr}^{-1}$ , Lugmair and Marti, 1978) has a half-life sufficiently short ( $1.06 \times 10^{11}$  yrs) to produce measurable variations in the daughter stable isotope  $^{143}\text{Nd}$ .



This decay scheme is at the base of rock datation and has found wide geological applications.

The changing isotopic composition of Nd in the Earth has been described with a model that assumes an evolution of terrestrial Nd in a uniform reservoir called CHUR (CHondritic Uniform Reservoir) having Sm/Nd ratio as that of Chondritic meteorites. The present value of  $^{143}\text{Nd}/^{144}\text{Nd}$  in CHUR is 0.512638 (Jacobsen and Wasserburg, 1980), normalized to  $^{146}\text{Nd}/^{144}\text{Nd}$  of 0.7219. The isotopic ratios of Nd in CHUR for the present-day, normalized to this ratio, are reported in Tab. 4.3 (from Faure, 1987).

<i>Atomic number</i> <i>Z</i>	<i>Element</i>	<i>Mass number</i> <i>A</i>	<i>Abundance (%)</i>
60	Nd	142	27.16
60	Nd	143	12.18
60	Nd	144	23.8
60	Nd	145	8.29
60	Nd	146	17.19
60	Nd	148	5.75
60	Nd	150	5.63
62	Sm	144	3.1
62	Sm-r	147	15
62	Sm-r	148	11.2
62	Sm-r	149	13.8
62	Sm	150	7.4
62	Sm	152	26.7
62	Sm	154	22.8

*Tab. 4.2: Nd and Sm atomic number, mass number, and isotopic abundances (see Faure, 1986 and references therein).*

$^{142}\text{Nd}/^{144}\text{Nd}$	1.141827
<b><math>^{143}\text{Nd}/^{144}\text{Nd}</math></b>	<b>0.512638</b>
$^{145}\text{Nd}/^{144}\text{Nd}$	0.348417
<b><math>^{146}\text{Nd}/^{144}\text{Nd}</math></b>	<b>0.7219</b>
$^{148}\text{Nd}/^{144}\text{Nd}$	0.241578
$^{150}\text{Nd}/^{144}\text{Nd}$	0.236418

Tab. 4.3: Nd isotope ratios compatible with normalization to  $^{146}\text{Nd}/^{144}\text{Nd} = 0.7219$

#### 4.2.1 Geochemistry of Sm and Nd

Sm and Nd have very similar geochemical properties, and therefore they are not highly fractionated. However, Nd is slightly more incompatible than Sm<sup>5</sup>, and this slight difference is sufficient to imprint in typical crustal rocks a lower Sm/Nd ratio than rocks originated from the upper mantle.

The Sm/Nd concentration ratio in terrestrial rocks shows very low variations, spanning from about 0.1 to 0.5. Such ratio decreases during fractional crystallization of the magma.

Rocks in the Earth are extremely variable in their isotopic composition and a comparison can be made only if samples are of the same age. In order to make the samples comparable, the  $^{143}\text{Nd}/^{144}\text{Nd}$  ratios are normalized to the chondritic model of Earth composition (CHUR), that evolves in time.

For this reason, DePaolo and Wasserburg (1976) introduced the Epsilon ( $\epsilon$ ) parameter, normalizing the isotopic ratio of  $^{143}\text{Nd}/^{144}\text{Nd}$  measured in the rocks at present time [ $(^{143}\text{Nd}/^{144}\text{Nd})_{\text{meas}}$ ] to the value of CHUR at the same time as follows:

$$\epsilon_{\text{Nd}}(0) = ((^{143}\text{Nd}/^{144}\text{Nd})_{\text{meas}} / (^{143}\text{Nd}/^{144}\text{Nd})_{\text{CHUR}} - 1) \times 10^4$$

(With present time  $(^{143}\text{Nd}/^{144}\text{Nd})_{\text{CHUR}} = 0.512638$ , according to Jacobsen and Wasserburg, 1980).

An  $\epsilon_{\text{Nd}}$  is *positive* indicates that rocks were derived from sources that were *depleted* in LIL elements, while *negative*  $\epsilon_{\text{Nd}}$  values indicate that the rocks were derived from sources *enriched* in LIL elements, i.e. that the rocks derived or assimilated old crustal rocks whose Sm/Nd ratio had been originally lowered when they separated from the uniform reservoir.

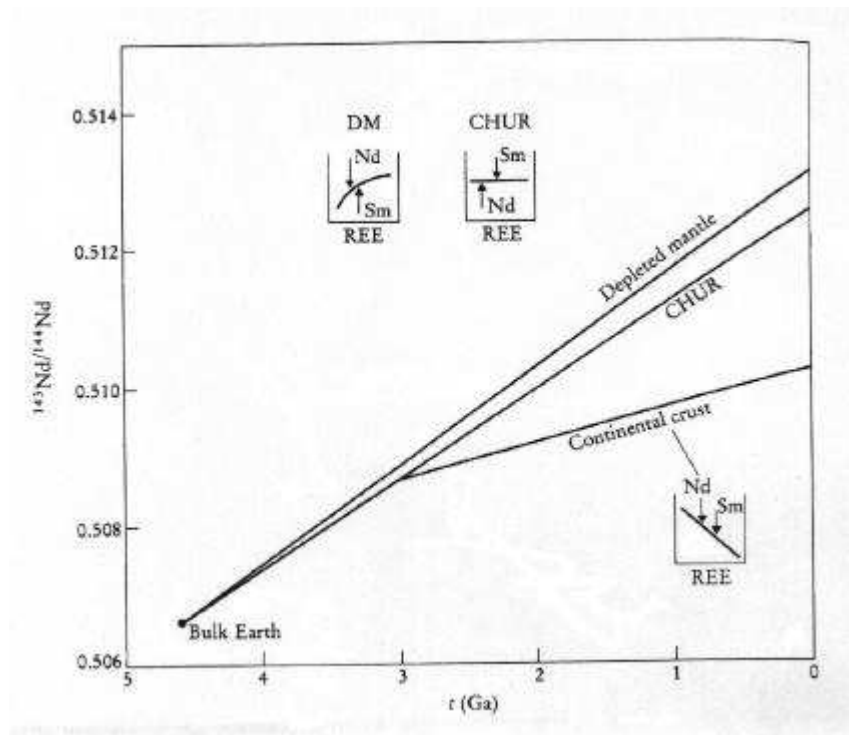
<sup>5</sup> Contrary to the Rb-Sr isotopic system, in this case the daughter element (Nd) is more incompatible than the parent element (Sm).

Fig. 4.2: the evolution of  $^{143}\text{Nd}/^{144}\text{Nd}$  isotopes with time.

Respect to the bulk Earth (CHUR) the Depleted Mantle (DM) has higher Sm/Nd ratio and therefore acquires higher  $^{143}\text{Nd}/^{144}\text{Nd}$  with time.

The crust, enriched in Nd respect to Sm, shows a delayed  $^{143}\text{Nd}/^{144}\text{Nd}$  evolution respect to the mantle.

The inserts evidence the Nd depletion in the mantle and enrichment within the crust. (from Rollinson, 1993, modified).



Since Sm-Nd isotopic system is not altered by geological processes in the crust (such as metamorphism, sedimentation, erosion etc.) it has found widespread application in geology for determination of “model ages”, representing the time elapsed since the rock had the same isotopic composition than CHUR.

Model ages therefore can be interpreted as estimates for crustal residence times.

However, when samples are composed by a mixture of many different rocks, as in the case of the aeolian dust deposited in Antarctica, for example, the model age has no geological significance, and it reflects an *average* residence time in the continental crust of rocks having different geological histories (Arndt and Goldstein, 1987).

### 4.3 The $^{87}\text{Sr}/^{86}\text{Sr}$ versus $^{143}\text{Nd}/^{144}\text{Nd}$ isotopic ratios

The Nd and Sr isotopic systematics has found wide application in geochemistry for studying the origin of igneous rocks.

The  $^{143}\text{Nd}/^{144}\text{Nd}$ , commonly expressed in the form of  $\epsilon_{\text{Nd}}(0)$ , and the  $^{87}\text{Sr}/^{86}\text{Sr}$  ratios are negatively correlated for uncontaminated basaltic rocks in the ocean basins (e.g. De Paolo and Wasserburg, 1976; Richard et al., 1976; O’Nions et al., 1977). The correlation line of  $\epsilon_{\text{Nd}}(0)$  versus  $^{87}\text{Sr}/^{86}\text{Sr}$  of basaltic rocks from Mid Ocean Ridges (MORB) and selected Oceanic Island basalts (OIB) has been defined as the “*Mantle Array*”.

This colinearity evidences that some magma sources are slightly enriched in Nd/Sm and Rb/Sr while others, such as MORBs, are depleted. Magma sources in the mantle have low  $^{87}\text{Sr}/^{86}\text{Sr}$  ratio and high  $^{143}\text{Nd}/^{144}\text{Nd}$  relative to the Bulk Earth, and this can be explained by the extraction of continental crust.

The various mantle and crustal reservoirs have different isotopic character respect to Nd, Sr and Pb isotopes. With respect to Sr and Nd in particular, some distinctions can be made between oceanic mantle sources and continental crustal sources.

Young magmatic rocks register the isotopic composition of their source and have no time to allow the parent isotopes to decay and produce additional daughter isotopes to add to those inherited from the source. Oceanic basalts are a good proxy to identify the isotopic composition of the mantle reservoirs. Basically five mantle sources have been identified (Zindler and Hart, 1986):

<i>Reservoir</i>	Rb/Sr	$^{87}\text{Sr}/^{86}\text{Sr}$	Sm/Nd	$^{143}\text{Nd}/^{144}\text{Nd}$ ( <sup>6</sup> )
1-Depleted mantle (DM)	low	low	high	High
2-HIMU mantle	low	=0.7029	intermediate	<0.51282
3a-Enriched mantle (EM I)	low	~0.705	low	<0.5112
3b-Enriched mantle (EM II)	high	>0.722	low	0.5111-0.5121
4-PREMA (PREvalent MAntle reservoir)		=0.7033		0.5130
5-Bulk Silicate Earth (BSE)		=0.7052		0.51264

Continental crustal sources are the Upper Continental Crust (UCC), the middle and the lower crust, and the subcontinental lithosphere. The UCC has high  $^{87}\text{Sr}/^{86}\text{Sr}$  ratios and low (negative)  $\epsilon_{\text{Nd}}(0)$ , as consequence of the enrichment in light REE and the low Sm/Nd ratio that characterizes the continental crust. The Mid-continental crust presents  $^{87}\text{Sr}/^{86}\text{Sr}$  lower than the upper crust, and the lower crust, depleted in Rb, and has lower  $^{87}\text{Sr}/^{86}\text{Sr}$  ratios that the middle crust (0.702-0.705), not very different from modern mantle values. These rocks have retarded Nd evolution with respect to CHUR.

The subcontinental lithosphere, poorly characterized, presents low Sm/Nd but very variable Rb/Sr.

<sup>6</sup> All  $^{143}\text{Nd}/^{144}\text{Nd}$  are normalized to  $^{146}\text{Nd}/^{144}\text{Nd}=0.7219$

### 4.3.1 The Sr-Nd correlation diagram

The Sr-Nd correlation diagram can be divided in four quadrants respective to  $\epsilon_{Nd}(0) = 0$  and  $\epsilon_{Sr}^7$  to facilitate the interpretation of data (see fig. 4.3).

Quadrant I and III are the spaces of enrichment (I) and depletion (III) in both in Sm and Rb; the covariance of such elements is contrary to their geochemical properties, and for this reason very few rocks occur therein.

Quadrant II includes all rocks having higher Sm/Nd than CHUR and lower Rb/Sr than the Uniform Reservoir, i.e. all rocks whose magma sources are the residual solids after withdrawal of a partial melt from undifferentiated mantle.

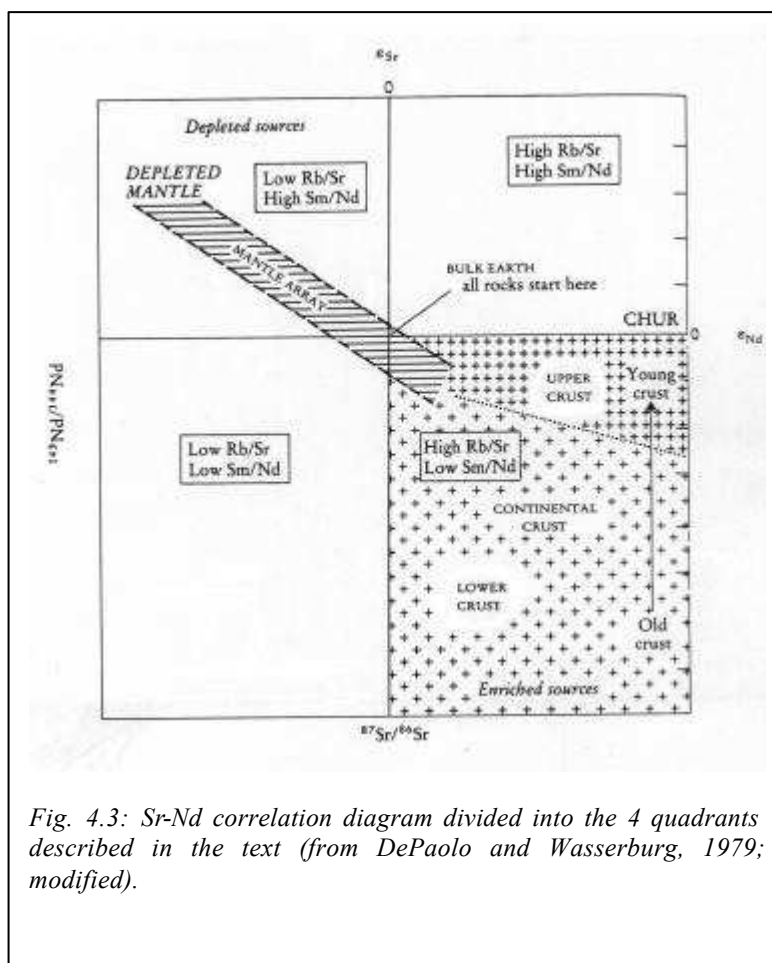


Fig. 4.3: Sr-Nd correlation diagram divided into the 4 quadrants described in the text (from DePaolo and Wasserburg, 1979; modified).

The IV quadrant includes most crustal rocks derived from sources that were depleted in Sm and enriched in Rb, that over time have developed high  $^{87}\text{Sr}/^{86}\text{Sr}$  and low  $^{143}\text{Nd}/^{144}\text{Nd}$ .

It includes continental rocks, that are the final product of geochemical differentiation of the mantle, and basalts derived from enriched sources or contaminated by magma.

It can be observed in the figure that upper and lower crustal rocks tend to plot in different positions of this quadrant.

<sup>7</sup> De Paolo and Wasserburg (1976) calculated an unfractionated mantle (Bulk Earth)  $^{87}\text{Sr}/^{86}\text{Sr}$  of 0.7045 [ $(^{87}\text{Sr}/^{86}\text{Sr})_{\text{UR}}$ ] from the intersection of the chondritic  $\epsilon_{Nd}$  line ( $\epsilon_{Nd} = 0$ ) with the mantle Nd-Sr correlation line defined only with MORBs. When other data from oceanic islands are used to construct this correlation line (see Faure, p 218), the  $(^{87}\text{Sr}/^{86}\text{Sr})_{\text{UR}}$  is between 0.7045 and 0.7055.

#### 4.4 $^{87}\text{Sr}/^{86}\text{Sr}$ - $^{143}\text{Nd}/^{144}\text{Nd}$ isotopic composition as tracer for sediment provenance

The use of  $^{87}\text{Sr}/^{86}\text{Sr}$  versus  $^{143}\text{Nd}/^{144}\text{Nd}$  isotopic composition has found wide application in the identification of aeolian dust and sediment provenance. First applied in oceanography (e.g. Grousset et al., 1988, Revel, 1996), the Sr-Nd fingerprint was subsequently adopted to identify the origin of aeolian dust at polar latitudes (e.g. Grousset et al., 1992, Basile et al., 1997, Biscaye et al., 1997, Bory et al., 2002).

Whatever the nature (isotopic, mineralogical...) a dust *tracer* should be:

- 1) *representative* for a geographical region.
- 2) *distinctive* for that region respect to other areas.
- 3) *conservative* from the source to the sink.

There is no a universal or ideal tracer, and each approach has its limits.

Biscaye et al. (1997) associated to Sr and Nd tracers the  $^{206,207,208}\text{Pb}/^{204}\text{Pb}$  ratios and a mineralogical indicator based on the relative abundance of kaolinite and chlorite clays to decipher dust provenance in Greenland ice cores.

On the other hand, the Rare Earth Elements (REE) profile seems to be quite an unsuitable tracer for mixed materials like loesses and sediments, since the profile resembles that of the upper continental crust (Gallet et al., 1998). Grousset et al. (1992) and Basile et al. (1997) evidenced the same flat pattern is typical also for dust in Antarctic ice cores.

In this thesis work the  $^{87}\text{Sr}/^{86}\text{Sr}$  versus  $^{143}\text{Nd}/^{144}\text{Nd}$  isotopic ratios are used as tracers, and the signature of dust at the source has been compared with that of dust reaching Antarctica.

The rationale is that soils and sediments keep at first order the Sr-Nd isotopic imprint of the rock(s) from which they derive, which in turn depends on lithology and geologic age (Biscaye et al., 1997).

Respect to classical approaches, the significance of the isotopic signature of mixed sediments is primarily *geographical* and not necessarily *geological*, since different types of rocks can have contributed to the formation of the sediments.

#### 4.4.1 The conditions of applicability and limits of the method

The use of the geochemical fingerprints for identification of the dust origin is a powerful tool, provided that some conditions are satisfied.

The basic requisites for the correct application of this geochemical approach, as well as its limits, are detailed in the following paragraphs.

They can be synthetically resumed as follows:

- 1) The PSAs samples must be adequately collected in order to be *representative* for a geographical region.
- 2) The PSA particles analyzed must be of *equivalent granulometry* than the ice core dust since it does exist an isotopic fractionation in function of particle size.
- 3) The eventual presence of *carbonates* in the PSA samples has to be taken into account.

##### *The requisites of the PSA samples*

Each PSA sample has to be representative for a geographical region. The samples collected however do not pretend to be exhaustive of all potential source regions within a continent, and many areas forming the present-day continental shelves were partially exposed during glacial periods and are not available to us.

A PSA sample can be either (1) a primary source for mineral aerosol, derived directly from the mechanical and/or chemical alteration of the parent material (e.g. moraines) or (2) a secondary source for dust, that is a mixture of particles already subjected to a phase of aeolian (e.g. loess and loess-like deposits) and/or liquid (e.g. fluvioglacial sediments) transport, or (3) a mixture of one (many) primary and one (many) secondary sources.

In any case, the dust deposit from which a PSA sample has been collected should be – or should have been in the past – an active source for dust. Climatic conditions influence greatly the dust source strength: weak sources at present time could have been very important in the past and vice versa. It is the case for instance of the thick loess deposits buried under vegetated soils that are common for example in the plain of Argentina east of the Andean Cordillera. Beside pedogenesis and vegetation cover, other factors potentially reducing the strength of a source are the lack of renewal of small particles, surface crusting, soil moisture, and surface roughness (Tegen et al., 2002a).

Areas where the recent geomorphological history has allowed concentration of fine-grained material, like paleolake beds, glacial outwash plains, riverine floodplains, alluvial fans, are powerful dust sources (Tegen et al, 2002a).



### ***Particle size and isotopic signature from the source to the sink***

From the parent rock to the dust transported long range and archived in Antarctic ice, several processes lead to particle *size selection*, in most cases corresponding to a change in the mineralogical (hence isotopic) composition; such processes are basically weathering and the transport.

The consequences of such effect on the isotopic signature of dust have to be taken into account (e.g. Derry and France Lanord, 1996, see Basile, 1997, and references therein), and for this reason it is essential to compare the isotopic (Sr-Nd) composition of the fine ice core dust (onward ICD) samples with that of samples from the source regions of equivalent grain size.

The size-dependent isotopic shift can be significant and concerns almost only Sr isotopes. Graham et al (1997) separated three granulometric fractions and observed an increase in  $^{87}\text{Sr}/^{86}\text{Sr}$  ratios between the  $>63\ \mu\text{m}$ , the  $63\text{-}4\ \mu\text{m}$  and the  $< 4\ \mu\text{m}$  fractions. In that experiment, the Sr signature spanned ranges from 0.7039-0.7092 for the coarser group of samples to 0.7092-0.7153 for the finest one.

#### *Size and mineralogical differentiation induced by rock weathering*

Physical/Mechanical weathering<sup>8</sup> consists in fragmentation of rocks (through generally inorganic mechanisms) without changes in their chemical composition. Chemical weathering<sup>9</sup> instead alters the minerals that make up the rocks and dissolve them or transforms them to other minerals. Chemical weathering of a parent rock acts preferentially on minerals like biotite, Ca-plagioclase and feldspars. Alteration also induces the formation of neoformed minerals (clays), that register the  $^{87}\text{Sr}/^{86}\text{Sr}$  ratio of the environment of alteration. The final sediments resulting from alteration are enriched in the non-altered minerals (e.g. quartz) in their silty and sandy fractions and in neoformed clays for their fine fraction.

In synthesis, the direct effect of weathering is a reduction of particle size and a mineralogical differentiation. This has important isotopic consequences in the Rb-Sr isotopic system, since this latter is more soluble than the former. Sm and Nd, on the contrary, have very similar behavior, being both elements with very low solubility. The neoformed minerals (clays) will acquire therefore high Rb/Sr ratio and a higher  $^{87}\text{Sr}/^{86}\text{Sr}$  ratio in the long (geological) time.

Finally, the sediments will be composed by:

---

<sup>8</sup> Examples of physical weathering are frost wedging, heat/cold cycles, unloading (often called exfoliation), and abrasion by wind, waves, rain, glaciers, and so on.

<sup>9</sup> Examples of chemical weathering are oxidation, hydration (feldspars in particular tend to hydrate and change to clay), and dissolution processes. This latter, often called leaching, implies that ions from rocks exposed to rainwater are put in solution in the water, and are carried away with it. Both chemical and physical weathering processes can be accelerated by the action of living organisms, like tree roots and bacteria for instance.

- 1- the non-altered minerals, keeping the original signature of the parent rock (different from that of whole-rock)
- 2- the neoformed clays, enriched in Rb, that register at their formation the  $^{87}\text{Sr}/^{86}\text{Sr}$  signature of the leaching environment,
- 3- the neoformed clays, that have acquired after a sufficient time a high  $^{87}\text{Sr}/^{86}\text{Sr}$ .

#### *Size and mineralogical differentiation induced by transport*

The effects of long range transport on dust grain size and mineralogy are discussed in Chap. 3. In synthesis, it can be stated that liquid and aeolian transport processes exert an important size selection. During long range aeolian transports, like those from the continental areas of the Southern Hemisphere to Antarctica, dust is graded around a modal value of about 2-2.5  $\mu\text{m}$  (Schulz et al., 1998). In terms of mineralogy, the atmospheric transport leads to an enrichment in clays respect to quartz and feldspars (see chap. 3).

Chemical weathering processes, moreover, can continue en route, in particular during aqueous transport.

#### ***The Sr contribution from carbonates***

The mineral particles and amorphous materials that constitute a PSA sample can be mixed with authigenic compounds as carbonates and sulfates that are typical in soils or sedimentary deposits. The  $^{87}\text{Sr}/^{86}\text{Sr}$  ratio of these formations, that are extremely widespread in arid and semiarid climates, depends on the source of calcium in the host material.

Various studies (e.g. Chiquet et al., 1999) have shown that calcium can derive either from in-situ weathering of the parent rocks or from an allochthonous source, that can be continental calcareous aerosol transported by wind or seawater. In this latter case, the Sr isotopes keep the seawater signature<sup>10</sup>, and for this reason they are commonly used as tool for investigation of Ca origin in carbonate accumulations (Hamidi et al., 2001).

The Sr concentration in carbonates is very high (>600 ppm), and even a small percentage of  $\text{CaCO}_3$  in a PSA sample would influence the signature of the remaining (aluminosilicate) fraction.

With respect to this problem, previous studies followed two different approaches for the ice core dust-PSAs comparison.

---

<sup>10</sup> Strontium signature of seawater changed over time; extreme low values of  $^{87}\text{Sr}/^{86}\text{Sr} = 0.7068$  were reached in the Late Permian, while high values of 0.7091 characterised the Late Cambrian. The modern seawater  $^{87}\text{Sr}/^{86}\text{Sr}$  ratio is 0.7092.

In Greenland ice cores, where the carbonate contribution is important and makes the ice pH slightly alkaline (Steffensen et al., 1997), a ‘*leached-leached*’ strategy of comparison has been adopted (Biscaye et al., 1997). Both ice and source samples were decarbonated and the residual aluminosilicate fractions compared.

For Antarctica, the situation is different than for Greenland, since chemical (Legrand et al., 1987; De Angelis et al., 1992) and CO<sub>2</sub> measurements (Anklin et al., 1995) evidenced that there are no carbonates in East Antarctic ice. The pH of ice is slightly acid (about 5.5) even in glacial periods, and filtered dust (>0.4 µm) from the Old Dome C core evidenced a Ca/Al ratio impoverished respect to the upper continental crust (De Angelis, personal communication).

One leaching test has been performed in this work on a glacial (LGM) dust sample from Antarctic ice, and results evidence no differences in Sr between the leached and the unleached fractions (see Chap. 7). Calcite, however, could have been present to a certain extent at the source and during the first stages of the aeolian phase, and totally lost en route through interaction with acid aerosol. These considerations lead previous authors (Basile et al., 1997) to adopt an unleached-unleached strategy for Antarctic ice.

One important aspect concerning leaching has to be taken into account: the procedure is supposed to remove only calcite from samples, but a possible *bias* effect on clays, that are abundant in polar ice, (and where Strontium resides adsorbed on mineral surfaces and in interlayer sites), or on the most labile phases different from carbonates (e.g. volcanic glasses) cannot be excluded. Graham et al. (1997) for instance observed that mild leaching procedures, although intended to remove all and only carbonate and seawater Sr, may in some cases lead to extraction of small amounts of Sr from the leached residue. In that study, since the highest Sr shifts were observed in samples containing high proportions of volcanic materials, the hypothesis of a *leachable component* probably derived from volcanic glass or authigenic clays has been advanced.

In the case of ICD-PSA leached-leached comparison, the possible bias introduced by the leaching procedure is probably supposed to play the same effect in both groups of samples. This aspect however has not been commented in these studies.

### *The strategy adopted in this work*

In this work the method of investigation has been refined, according to the following strategy:

- 1) **Increase of the PSA sampling** through collection of a high number of PSA samples, especially from regions not previously documented (New Zealand and in the Antarctic Dry Valleys), and from South America, that appeared from previous investigations the dominant source at Dome C and Vostok in Glacial periods.  
The PSA samples have been specifically selected in order to be as much representative as possible for a given region: they mainly consist of loesses, aeolian deposits, silts, sands, fluvio-glacial deposits.
- 2) Selection and analysis of the **fine (<5 $\mu$ m) fraction** from all PSA samples, in order to build a new database suitable for comparison with the fine-grained ICD.
- 3) Due to the heterogeneous strategies adopted by previous authors for ICD-PSAs comparison, in this work some **leaching tests** have been performed on PSA samples in order to remove the eventual calcite and estimate for each of them an isotopic interval ( $\Delta$  Sr and  $\Delta$  Nd) for calcium carbonate contribution.

\*\*\*\*\*

### Summary

*The geographical provenance of æolian mineral dust in Antarctic ice can be identified by comparing its Sr-Nd isotopic fingerprint to that of sediments from the potential source regions.*

*The accurate choice of the samples, their granulometry, as well as the presence of carbonates are some aspects that have to be taken into consideration when this exercise is performed.*

## Chapter 5 - ANALYTICAL TECHNIQUES

### 5.1 Dust concentration and size distribution measurements

#### 5.1.1 Decontamination and sample preparation

Dust concentration and size distribution measurements have been performed on samples of about 6-8 cm of length, on average. Before dust measurements, the ice samples have to be carefully decontaminated. First, the external part of the ice sample has been removed through a band saw in cold room at LGGE-CNRS laboratory (Grenoble, France). The inner core has been put in clean plastic bags hermetically closed, and transferred in a class 100 clean room.

The second step of decontamination consists in three repeated washings in ultra-pure water (MilliQ®). The decontaminated samples are put in plastic beakers and let at room temperature until melting (1-2 hours)<sup>1</sup>. Afterwards, they have been put into plastic accuvettes pre-cleaned through three repeated washing in ultra-pure water.

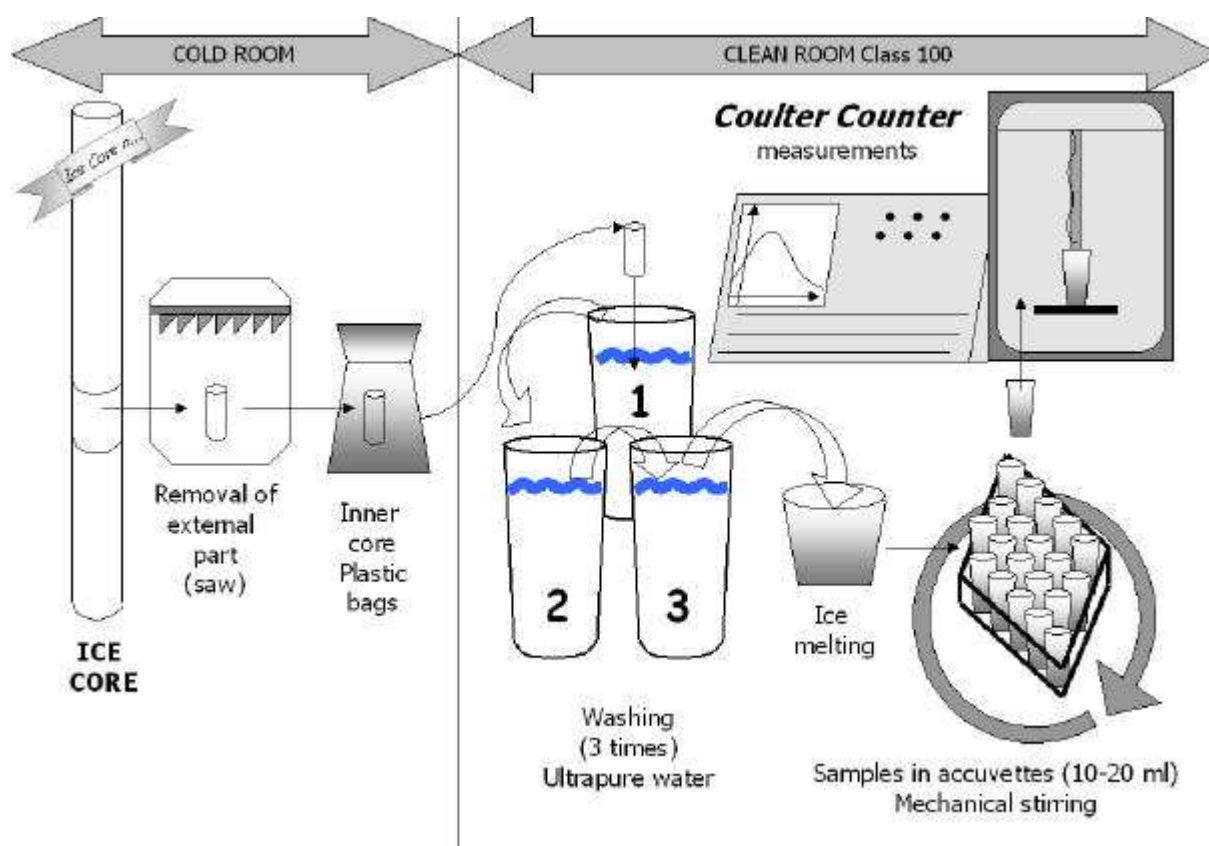


Fig. 5.1: Sketch of the analytical procedure used for ice samples analysed by Coulter Counter.

<sup>1</sup> Some tests were made on porous firm samples, that were decontaminated by scraping away the outer part of the core (about 2 mm) using a lathe, and put directly into pre-cleaned plastic beakers.

The laboratory blanks were carefully checked before and during each series of measurements and represented always <1 ppb of total dust. They consist of MilliQ water used for sample decontaminations, the dust content of the beakers for ice melting and the dust content of the accuvettes.

### **5.1.2 The measurement: principle, handling operations, limits of the technique.**

The measurements of dust concentration and size distribution were performed using a Coulter Counter (CC) Multisizer IIe© set up in the class 100 clean room of LGGE.

The instrument works on the basis of the detection of the electric signal generated by the particles that are forced to flow through a small aperture tube (50  $\mu\text{m}$  in diameter). The melted ice sample is made conductive by addition of a pre-filtered 20% NaCl electrolyte solution giving a 1% concentration in the final solution.

Melted samples were continuously stirred (mechanically) before the analysis in order to prevent dust sedimentation in the accuvettes. At least three consecutive countings were performed on each volume of 500  $\mu\text{l}$ . After each sample a blank solution (ultra-pure water added with the electrolyte) has been measured some minutes for cleaning of the orifice tube, and checked through a single measurement.

The instrument was set for measurements of particles with diameters from 0.7 to 20  $\mu\text{m}$  in 256 channels on a logarithmic scale.

The particle size is expressed by the diameter of a sphere of equivalent volume, and the mass was calculated from the measured volume assuming an average crustal density for particles of 2.5  $\text{g}/\text{cm}^3$ . These two assumptions constitute the main limit of the method. Actually, particles transported long-distance and archived in Antarctic ice are not regular and isometric but are typically those with the best aerodynamic properties, like the plate phyllosilicate minerals.

The density is also adopted arbitrarily, considering that clays and quartz are the most abundant mineral phases of long-range transported dust and that heavy minerals ( $>2.8 \text{ g}/\text{cm}^3$ ) with high settling velocity concentrate mostly in sandy and silty sediments (Chap. 2).

Coulter Counter measurements are highly precise<sup>2</sup>: for highly concentrated samples (ca. 50,000 particles per g, i.e. ~300-400 ppb) the scattering between three repeated measurements is usually < 2%; for very low concentrated samples (1,000 particles per g, i.e. ~10 ppb), however, it can increase to 20%.

---

<sup>2</sup> The *precision* of the analysis refers to the closeness of agreement between results obtained by repeating an analytical procedure several times under the same conditions. An analysis is precise if the random error associated with the analysis is small, independently of the *true* value.

The CC was initially calibrated with certified reference latexes (2.07 and 9.6  $\mu\text{m}$ ) to check the accuracy and prevent analytical bias<sup>3</sup>. The calibration has been periodically checked but no instrumental drift has ever been detected during the three years of this thesis work; this confirms the high stability in time of the instrument. The samples were always processed in random for all ice cores investigated.

The CC technique does not allow to perform measurements continuously like new laser detectors (e.g. Ruth et al., 2003) and the preparation of samples is more time-consuming. However, the technique has the advantage to perform precise measurements even for very low dust concentrations, and to provide a size distribution of particles very highly resolved in size. An analogue technique was used by Steffensen (1997) to perform measurements on the GRIP ice core.

## **5.2 Analytical procedures and Sr-Nd measurements of PSA samples**

All chemical treatments for PSAs samples have been performed c/o CEREGE laboratory (Aix en Provence, France).

### **5.2.1 Size selection**

The bulk PSA samples have added with MilliQ water and submitted to an ultrasonic bath for about 10 minutes for aggregate dispersion, under temperature control ( $T < 30^\circ\text{C}$ ).

The fine fraction has been then separated from the bulk through humid sedimentation, and extracted with a syringe.

The size of particles recuperated was carefully checked with a Laser particle Counter, and only samples presenting at least 95% of the total mass ( $>99.8\%$  of total number) finer than 5  $\mu\text{m}$  have been accepted. Then, the liquid suspension of the sample ( $\sim 30$  ml) has been frozen and lyophilised. The average weight of the dry samples was  $\sim 5$  to 10 mg.

### **5.2.2 Leaching procedure**

After size selection, some samples have been splitted in two aliquots, one of which has been added with Acetic Acid buffered at pH 5, let  $\frac{1}{2}$  hour at room temperature, and then centrifuged.

The supernate has been subsequently removed and the particles recuperated. These have been re-washed three times and centrifuged, each time discarding the supernate. This procedure is supposed to remove calcite from the samples (e.g. Biscaye et al., 1997).

---

<sup>3</sup> The *accuracy* of the analysis refers to the deviation of a measurement from the *true* value. When the error is systematic it is called *bias*. The main method to estimate the bias is analysing a certified reference material.



### 5.2.3 Sr and Nd extraction

Dissolution of dust has been made in pre-cleaned teflon beakers through two acid attacks, heating the sample on a hot plate with beaker hermetically closed and drying the dissolved sample after each step. The first acid solution added to the samples consisted in a mixture of [HNO<sub>3</sub> + HF + HClO<sub>4</sub>], while the second [HNO<sub>3</sub> + HCl].

The Sr and Nd have been then extracted by single passage through primary and secondary ionic chromatographic columns.

The total blanks of the whole procedure were ~ 1 ng for Sr and ~0.2 ng for Nd. Assuming UCC concentration for Sr (350 ppm) and Nd (26 ppm), the Sr concentration of the sample spans ~1.5-3.5 µg and Nd ~0.10-0.25 µg.

### 5.2.4 Isotopic analysis of PSA samples

The Sr and Nd samples have been loaded on pure<sup>4</sup> filaments of Re before insertion inside the mass spectrometer (*filaments of evaporation*).

The procedure followed for Strontium loading and analysis is basically the same described by Birck (1986). Sr has been loaded within two layers of an activator (composed of a solution of TaF<sub>5</sub>) that retards the evaporation of the element and enhances ionization. Nd instead was loaded without activator.

Isotopic measurements on PSA samples have been made using a multiple Faraday cup Thermo-Ionization Mass Spectrometer (TIMS) Finnigan© MAT 262 c/o CEREGE Laboratory (Aix en Provence, France). For a detailed description of the principle and characteristics of a mass spectrometer refer to e.g. Dickin (1995) and Thirlwall (1997). Here below only some fundamental aspects are indicated.

#### 1- The source

The filaments are then put in a turret and inserted into the ion source that is pumped to high vacuum of 10<sup>-7</sup> mbar and more (achieved over ca. 2 hours) through a primary and a turbomolecular pump.

The filament is subsequently heated to the (absolute) temperature **T** that produces evaporation of **n** neutral atoms from the filament, accompanied by **n+** positive ions according to the equation

$$n+/n = e^{(W-E)/kT}$$

---

<sup>4</sup> The purity of the filament is certified by the manufacturer, but before sample loading the filaments are heated under vacuum to eliminate organics and other impurities.

Where  $E$  is the first ionization energy of the material evaporated (eV),  $k$  is the Boltzmann's constant and  $W$  is the work function of the metal filament.

The so called *ionization efficiency*, that is the principal limitation of the sensitivity of TIMS, is the ratio of ions produced to atoms loaded. Alkalis and other volatile elements with ionization energies less than the filament metal work function ( $W > E$ ) produce many ions at low evaporation temperature (~700-800°C). Ideally  $W$  should be higher than  $E$ , but this is rarely the case. Many elements (e.g. the REE) actually have high first ionization energy ( $W < E$ ) and would require high filament temperatures to be emitted. For this reason metals as Re, W (Tungsten), and Ta with rather high  $W$  and sufficiently high melting temperature are currently used as filaments. Here are reported the values of  $E$  for Sr and Nd and  $W$  for the three most common metals used for filaments in this kind of analysis.

Element to be analysed	E (eV)
Sr	5.69
Nd	5.51

Metal for filament	W (eV)
Re	5.1
W (Tungsten)	4.5
Ta	4.19

When the filament is heated, the sample is subjected to evaporation and ionization. The temperatures at which these two phenomena take place are often very different, and in some cases the element is evaporated but not ionized. For this reason in some cases a *double filament* technique can be used; a second pure filament (ionization filament) is placed very close to the evaporation filament where the sample has been loaded, in a way that the atoms evaporating from one are ionized by the second, which is heated at higher temperature.

For Nd analysis on PSA samples we used a double filament technique; the element was evaporated at about 1200°C and the ionization filament heated up to about 2000°C. However, for very small samples like those of ice core dust, this technique is not suitable and the single filament technique was used (§ 5.3.3).

The ions are accelerated to the mass analyzer by a high voltage applied between the source assembly and accelerator slit, and collimated into a tight ion beam by applying smaller potentials to a series of slits.

## 2-The magnetic sector

The TIMS source is coupled to an analyzer tube pumped to high vacuum ( $10^{-8}$  to  $10^{-9}$  mbar) curved into an arc of circle of radius  $r$  between the poles of an electromagnet. The magnetic field deflects the ion beam into a curved path of radius  $r$ , according to the equation:

$$m/z = B^2 r^2 / 2U$$

With  $m/z$  = ionic mass/charge ratio,  $B$  is the magnetic flux density, and  $U$  is the accelerating voltage (high potential) through which the ions pass (Thirlwall, 1997).

The mass spectrometer must resolve ion beams of similar  $m/z$  and focus them separately into the detector system. For the collection of ions to be efficient, as many as possible ions of a given  $m/z$  are focused by the electromagnet into the collection slit, located diametrically opposite to the source slit, on a straight line through the center of curvature of the analyser tube.

## 3-The ion beam detection

Ion detection systems are designed in a way that the ionic masses of interest are resolved and their ion currents amplified to an extent where useful precision is attained.

The TIMS used for PSA analysis was equipped with multiple collectors for the simultaneous measurement of the intensity of several ion beams over an array of five collectors. Before each series of analysis it was checked that the shape of the beam for a specific isotope generates a “flat-topped peak”, to keep stability to the signal.

Most of the major TIMS instrument functions were controlled through a computer: from the heating of the filament, the peak searching, setting the magnetic field, data collection and reduction. Focusing was made manually.

Strontium was measured in static mode. This means that the magnetic field is constant and each collector receives a different mass simultaneously. It is important that each detector responds with equal sensitivity to different masses, and a “gain calibration” has been daily performed before each series of measurements. The isotopes 84,86,87 and 88 were measured simultaneously, together with the  $^{85}\text{Rb}$ :

$^{84}\text{Sr}$	External cup 6
$^{85}\text{Rb}$	cup 5
$^{86}\text{Sr}$	central (immobile) cup 4
$^{87}\text{Sr}$	cup 3
$^{88}\text{Sr}$	External cup 2

Since  $^{87}\text{Rb}$  produces isobaric interferences with  $^{87}\text{Sr}$ , it had to be assured - before starting the acquisition of Sr data – that the (eventual) residual Rb deriving from imperfect purification had been totally burnt off. The presence of Rb was monitored through the interference-free isotope  $^{85}\text{Rb}$ , but anyway the system was set in a way to correct the  $^{87}\text{Sr}$  from any  $^{87}\text{Rb}$ .

Other corrections to the measured peak intensities that were automatically made by the software programme for data treatment are (1) correction for linearity (i.e. correction for the linear change in the ion beam intensity with time), and (2) the correction for mass fractionation (normalizing on the  $^{86}\text{Sr}/^{88}\text{Sr}=0.1194$ , Steiger and Jager, 1977).

Neodymium has been measured in dynamic mode; this means that different multicollection measurements are performed one after the other, and the same isotope changes collector according to the configuration defined by the operator. This mode allows to make the analysis independent from the cup efficiency. The initial configuration of the Faraday cups is:

$^{143}\text{Nd}$	external cup 6
$^{144}\text{Nd}$	cup 5
$^{145}\text{Nd}$	central (immobile) cup 4
$^{146}\text{Nd}$	cup 3
$^{150}\text{Nd}$	external cup 2

Before each analysis it was checked the absence of Samarium, that has isobaric interference with Nd, by scanning the mass 147. Corrections for linearity and for mass fractionation were automatically made, this latter normalising on  $^{146}\text{Nd}/^{144}\text{Nd}=0.7219$ .

## 5.3 Analytical procedures and Sr-Nd measurements of Ice Core Dust (ICD)

### 5.3.1 Dust extraction from ice cores

The decontamination procedure for ice core sections selected for geochemical analyses is the same used for preparation of CC samples (§ 5.1.1). However, due to the large volumes of ice involved, spanning from 300 g to 2-3 kg of ice, samples have been melted in large plastic bottles pre-cleaned with suprapure acid.

A small aliquot (ca. 10 ml) of the sample has been used for dust concentration and size distribution measurements, to estimate the total dust content of the samples.

The extraction of mineral dust could have been made by evaporation, lyophilization or centrifugation. The first two methods present the inconvenient that soluble Sr and Nd deriving from seawater would be recuperated. Therefore, the samples have been centrifuged (9000 and 4000 rpm) c/o the clean room of LGGE, and after each centrifugation cycle the supernate has been discarded with a syringe, while the bottom part (~20-30 ml) has been frozen and kept apart for evaporation.

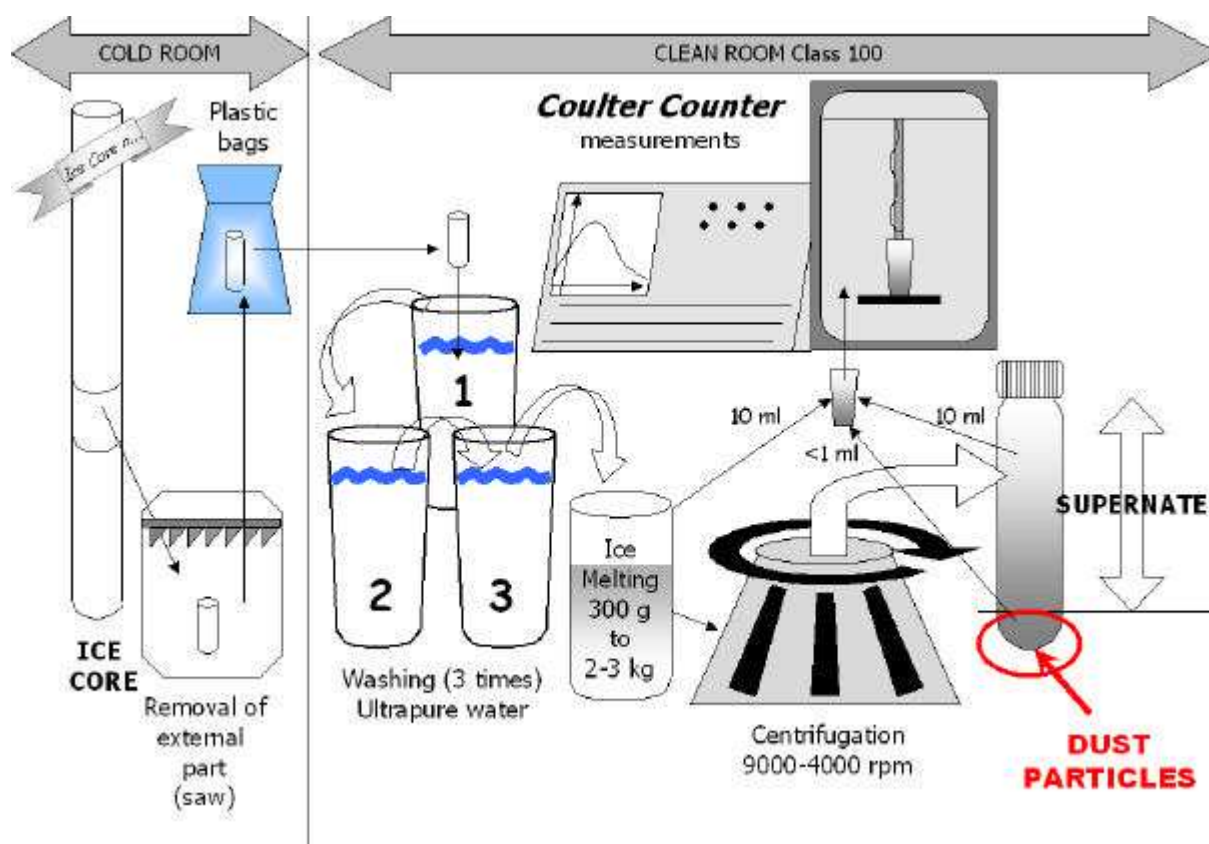


Fig. 5.2: Sketch view of the analytical procedure for preparation of ice core dust samples for isotopic analysis.

The quantity of dust in the concentrated solution and the supernate has been estimated by CC measurements.

The size distribution of the initial (whole) sample, that of the supernate and the concentrated solutions have been compared in order to prevent size (hence mineralogical and isotopic) fractionation due to centrifugation, and no significant differences have been detected.

However, some supernates were filtered in Nuclepore filters (0.4 micron), and particles recuperated after ultrasonic bath of the filter in ~10 ml of ultrapure water. This series of samples has been used as *control sample* (“filtered samples”) to check for eventual isotopic fractionation by centrifugation.

The total amount of mineral dust extracted by centrifugation spanned from a maximum of about 150 µg to about 10-15 µg for very small (interglacial) samples, and therefore it is 100 to 1000 times less concentrated than the average source samples (10 mg). These differences, and in particular the limiting amount of Nd in ICD samples, impose a special laboratory environment adapted for the treatment of very small samples. Procedural blanks have to be minimised and the instrument of measure should be highly sensitive.

Only a few laboratories in the world fulfil these requisites. One of them, where the chemical treatment and the isotopic measurements of ice core dust have been performed, is the laboratory of the Cosmochemistry Department of the Max Plank Institute (MPI) in Mainz (Germany): there, the group of Dr. Emil Jagoutz refined the chemical procedures for sample preparation, thus making possible the investigation of samples as little as a few hundred pg of Nd, and a special mass spectrometer has been conceived (§ 5.3.3).

### **5.3.2 Sr and Nd extraction from ice core dust**

The chemical treatment of ICD samples has been performed under clean laboratory conditions c/o the MPI. The procedure of chemical preparation of samples for isotope analysis is described in Jagoutz et al. (1990).

After complete evaporation of the 20-30 ml concentrated solution obtained through centrifugation, the dust dissolution was made by a mixture of concentrated [HF + HClO<sub>4</sub>] in hermetically closed Teflon beakers on a hot plate. After that, the dissolution mixture was dried and then re-dissolved in HCl. The separations of Sr and the REE and the subsequent extraction of Nd from these latter have been made through ion exchange columns (primary and secondary columns).

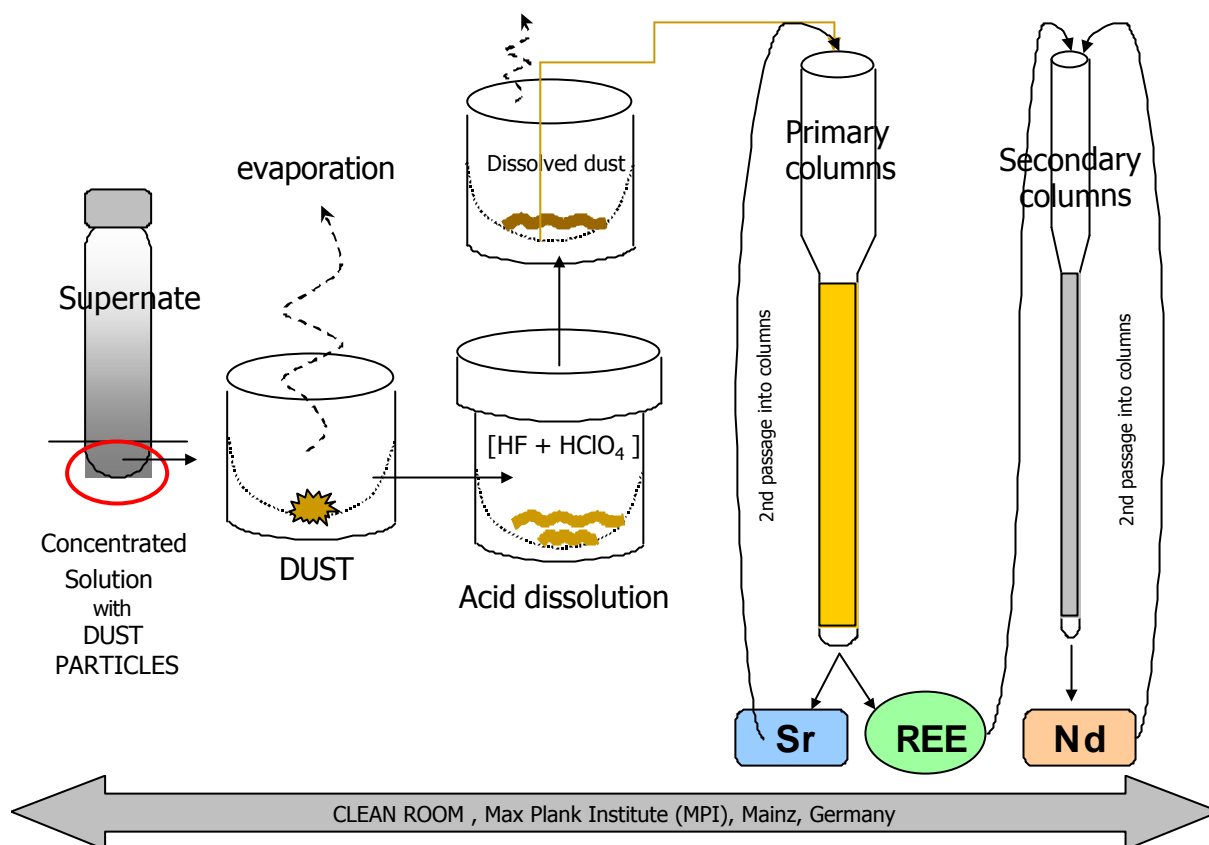


Fig. 5.3: Sketch view of the analytical procedure for Sr and Nd extraction from ice core dust samples.

Primary columns were made from pure quartz and filled with ca. 4 cm<sup>3</sup> of Bio-Rad 50W-x8 resin, after careful cleaning. The height of the resin is 17 cm and the inner diameter of the columns about 8 mm. After each passage of sample through primary columns these were cleaned with concentrated HCl and backwashed before use.

For isolation of Nd, reverse phase chromatography has been used. The REE were loaded into secondary columns (Micro-columns) also made from pure quartz and filled with teflon-powder as inert phase, coated with an ion-exchanger (HDEHP). The height of the exchanger into the columns is 10 cm and the inner diameter of the columns ca. 5 mm. As for primary columns, also secondary columns were washed with strong HCl after each passage of sample.

Purification of the elements is very important and for this reason all samples have been processed through two passages into the columns, carefully washed after each passage.

All acids and water used were specially cleaned: deionised water was thrice distilled in a quartz distiller with the last step sub-boiling and all acids used were distilled twice by sub-boiling. This, among other things, allows to reduce procedural blanks, that never exceeded 20 pg for both elements.

Assuming an average UCC concentration for Sr and Nd in the sample and a 95% recover from each passage of sample into the columns, the final Sr samples spanned from 4 to 50 ng, and the final Nd samples from 300 pg to 3-4 ng.

#### ***A leaching test on one ICD sample***

One ICD sample (*DB-St2-2Filtered*, see § 6.2.2) was split in two aliquots, one of which has been added with suprapure Acetic Acid buffered at pH 5, let ½ hour at room temperature, and then centrifuged.

Once removed the supernate and recuperated the particles, these have been re-washed three times with ultrapure water and centrifuged, each time discarding the supernate. This procedure is supposed to remove calcite from the samples (e.g. Biscaye et al., 1997).

The very limited amount of dust extracted from the ice cores did not allow to perform leaching on more samples as was done on some PSA samples.

#### **5.3.3 Isotopic analysis**

The extremely small samples of Nd have been loaded on single filament of Re under binocular loop since in most cases they are invisible by eye.

For Strontium, the procedure described by Birck (1986) was followed; the sample was loaded on a flat-top single filament of W, within a double layer of a specific activator composed by a solution of Ta (about 1% of Ta-2% H<sub>3</sub>PO<sub>4</sub>, 1% HF, 2% HNO<sub>3</sub>). Several dilutions and mixtures of activator were tested, in order to find the best one for the samples.

Isotopic measurements on ICD have been performed through a highly-sensitive single-collector Thermo-Ionisation Mass Spectrometer (TIMS) c/o the MPI that was especially modified by E.Jagoutz on the basis of Finnigan Mat 261, in order to perform precise measurements of small (few hundred pg) terrestrial and extraterrestrial samples (e.g. Bodganovski, 1997).

The high sensitivity of this mass spectrometer is provided by modifications of the ionization system, the vacuum and the registration systems, all detailed in Bodganovski (1997).

The temperature of the filament was controlled during the whole heating phase by an optical pyranometer.

Very slow heating and maximum purification of the elements are of crucial importance for very small samples. Purification is particularly important to minimise isobaric interferences and maximise



ionisation efficiency of the analyte. After a first purification step consisting in the double passage of each element into chromatographic columns, a second one is achieved by leaving the sample at a temperature of about 800°C for about 10 hours, for purification from organics and other residual impurities.

After this step, the samples have been heated very slowly (from 1 to 3-4 hrs depending on the quantity of sample) to 1200°C, the temperature at which the emission of Nd and Sr starts. Since the isotope analysis of Nd using NdO<sup>+</sup> ion beam is much more sensitive than using Nd<sup>+</sup> ion beam, an inlet of pure oxygen into the source area was applied for measurements of Nd. From this temperature onward, the beam of the most abundant isotope (<sup>88</sup>Sr and <sup>142</sup>Nd) can be manually searched and focalization can be made. When emission reaches a sufficient intensity analysis can be started.

The registration system of the mass spectrometer was equipped with a Keithley-642<sup>5</sup> electrometer, that has very low noise and fast response.

The time of analysis of each sample spanned between 17-24 hours for each sample of Sr and Nd, and each ratio usually represents the average of 600 individual ratios (120 blocks of 5 scans).

---

<sup>5</sup> Keithley Instruments, Inc., Cleveland, Ohio, USA

\*\*\*\*\*      \*\*\*\*\*      \*\*\*\*\*

### **Summary**

*The analytical techniques used in this work are presented.*

*Dust concentrations and size distributions have been measured by Coulter Counter technique, while isotopic analysis have been performed by Thermal Ionization Mass Spectrometry. These latter were performed in two different laboratories for PSAs and ice core dust samples, since the different amount of material available (a factor  $10^3$ ) makes necessary to reduce procedural blanks and to use a highly-sensitive spectrometer for these latter.*

## Chapter 6 - THE SAMPLES ANALYZED IN THIS STUDY

### 6.1 Samples measured for dust concentration and size distribution

#### 6.1.1 EPICA-Dome C (EDC) ice core

The drilling of the first EPICA (European Project for Ice Coring in Antarctica) ice core (Core EDC96) in Dome Concordia (3233 m a.s.l., mean annual temperature: -54.5 °C, ice thickness: 3309 ±22 m) started during the 1996-1997 field season.

At the depth of 788 m the ice corer stuck, and a new drilling (Core EDC99) started in 1999 and is still in progress. During the 2002/2003 field season it reached a depth of 3200 m.

Cores EDC96 and EDC99 were drilled 10 m apart, both are located at 75° 06'S, 123° 21'E.

More than 1100 samples have been analyzed for dust concentration and size distribution in this thesis work over the whole core length, as reported in Tab. 6.1.

<i>Depth (m)</i>	<i>N. of samples</i>	<i>Average Resolution (m)</i>	<i>Climatic period</i>	<i>Core</i>
0-94 (firn)	16 (*)	5.3	Last 2000 yrs	EDC96
94-520	352	1.2	~2-20 kyrs B.P.	EDC96
520-600	41	1.95	~20-30 kyrs B.P.	EDC96
600-786	158	1.2	~30-45 kyrs B.P.	EDC96
786-2201	257	5.5	~45-220 kyrs B.P.	EDC99
2201-3138	286	3.3	>220 kyrs B.P.	EDC99

*Tab. 6.1: EPICA samples analyzed in this work for dust concentration and size distribution: depth of the samples (m), number of samples analyzed within the given depth interval, depth resolution, relative climatic period and core from which the samples have been selected.*

(\*) Each of the 16 values documenting the porous *firn* part of the core represents the average of a number of measurements on the whole 55 cm bag<sup>1</sup>, as shown in the Tab. 6.2.

---

<sup>1</sup> The EPICA ice core is divided into sections of 0.55 m called Bags. The bottom depth of each bag is obtained multiplying per 0.55 m the bag number.

#Bag	Depth (top, m)	Depth (bottom, m)	Number of samples
22	11.55	12.1	8
30	15.95	16.5	3
42	22.55	23.1	4
52	28.05	28.6	4
63	34.1	34.65	3
71	38.5	39.05	4
81	44	44.55	4
91	49.5	50.05	4
102	55.55	56.1	4
112	61.05	61.6	4
122	66.55	67.1	3
131	71.5	72.05	3
142	77.55	78.1	3
151	82.5	83.05	3
163	89.1	89.65	3
172	94.05	94.6	3

Tab. 6.2: Firn samples analyzed in this study from EDC96 ice core

Apart from the main sampling, seven bags of 55 cm of length have been measured every 2-3 cm (yearly resolution) to document the interannual variability, for a total of 119 samples.

Details on these continuous sections are reported in Tab. 6.3a.

Moreover, three bag (#708, # 242, #618) have also been analysed with the same resolution to look for volcanic dust events (Tab. 6.3b).

#Bag	Depth (top, m)	Depth (bottom, m)	N. samples
193	105.60	106.15	16
207	113.30	113.85	14
242	132.55	133.10	11
265	145.20	145.75	15
275	150.70	151.25	16
293	160.60	161.15	16
477	261.80	262.35	15
479	262.90	263.45	16

Tab. 6.3a: sections analyzed in continuous from EDC96 ice core

#Bag	Depth (top, m)	Depth (bottom, m)	N. samples
242	132.55	133.10	18
618	339.35	339.90	15
708	388.85	389.40	11

Tab. 6.3b: sections with volcanic events analyzed in continuous from EDC96 ice core

### **6.1.2 The VOSTOK BH7 (VK-BH7) ice core**

The ice drilling project at the Vostok station in East Antarctica (78°28' S, 106°48' E; 3480 m a.s.l.) was undertaken in the framework of a long-term collaboration between Russia, France and USA. The site is located at 3488 m of altitude on the East Antarctic plateau. Vostok is the coldest place on Earth, and the mean annual temperature at the site is  $-55^{\circ}\text{C}$ .

In January 1998 the ice core drilling reached 3623 m of depth, providing the deepest ice core ever recovered. The drilling stopped ca. 120 m above the surface of the large Vostok subglacial lake.

The Vostok ice core climatic record spans the last 420 kyrs, and the complete climatic record has been published by Petit et al. (1999) and for dust the Holocene period was not documented in detail (15 samples).

In this work about 140 samples have been selected between 104 to 250 m (with a sampling resolution of ca. one sample per 1 m) from shallow (235 m) Vostok-BH7 (VK-BH7) ice core, extracted in 1996. The average annual accumulation rate is about  $2.2\text{ g cm}^{-2}\text{ y}^{-1}$  for the Holocene period.

This core is particularly suitable for analysis of very low dust concentrations since it was obtained without drilling fluid.

### **6.1.3 Dome B (DB) ice core**

The site of Dome B (77° 05' S, 94° 55'E, 3650 m a.s.l.) is located about 320 km upflow from Vostok and 870 km far from Dome C. The ice core has been obtained during the 1987-1988 austral season by the 33<sup>rd</sup> Soviet Antarctic expedition through a thermal drilling.

A total of 385 samples have been analyzed from 89 to 719 m of the core, corresponding to the period between 1,800 and 26,400 yrs B.P.

The sampling resolution is one sample per 1.38 m from 89 to 600 m (about 19.5 kyrs B.P.), and from 600 to 719 m the average sampling resolution is one sample per 9.15 m.

Each sample measured 6 to 10 cm in length and is representative of ~2-3 years of accumulation during the Holocene and ~4-5 years during the last glacial maximum, assuming the same accumulation rate at the site as in Dome C.

### **6.1.4 The Komsomolskaia (KMS) ice core**

The 850 m deep KMS ice core was extracted in 1983 by the 28<sup>th</sup> Soviet Antarctic Expedition at the summer camp of Komsomolskaia (74°05'S, 97° 29'E, 3500 m a.s.l.) using thermal drilling technique. The average annual temperature at the site is  $-52.6^{\circ}\text{C}$ , and the average annual accumulation rate is

twice that of Vostok (about  $5 \text{ g cm}^{-2} \text{ y}^{-1}$  according to Young et al., 1982). The deuterium profile was measured (Ciais et al., 1992).

A set of 103 samples have been selected from the core, from 662 m to 870 m depth, spanning from 11,200 to 16,400 yrs B.P. The average sampling resolution is about one sample per 3.3 m from 662 to 770 m (11.2-13.5 kyrs B.P.) and one sample per 1.36 m from 770 to 870 m (13.5-16.4 kyrs B.P.).

Each sample (6-8 cm in length) is representative of  $\sim 2$  years of accumulation during the period investigated, corresponding to the last deglaciation (assuming for this period an accumulation rate of  $\sim 4 \text{ cm/yr}$ ).

## **6.2 Samples selected for Sr -Nd geochemical analysis**

*In this paragraph are reported in detail the samples selected for isotopic analysis in the present thesis work. It can be noticed that the quantity of dust extracted varies of a factor  $\sim 100$  between PSA and glacial ice core dust samples, and a factor  $\sim 1000$  between PSA and interglacial dust samples.*

### **6.2.1 The PSA samples**

The collection of PSA samples has been particularly focused on South America, indicated as principal dust source by previous studies (Grousset et al., 1992; Basile et al., 1997). New Zealand and the Dry Valleys of Antarctica are here documented for the first time.

No sample from Australia has been analyzed in this study, but a joint project with Dr. M.Revel-Rolland (Australian National University, Canberra, Australia) is in course.

All the samples presented here have been selected and analyzed exclusively for their  $<5 \mu\text{m}$  fraction (§ 5.2.1). Very few bibliographic data exist for the fine fraction of PSA, among which the studies of Grousset (1992), Basile (1997) and Gemmiti (2000).

In this work we got an aliquot of some samples previously analysed by Gemmiti (2000) for their  $<5 \mu\text{m}$  (unleached) fraction (indicated with [\*]) and some of them have been re-analyzed in this study to check the reproducibility of the measurements, or leached and analyzed to evaluate the  $\Delta \text{Sr}$  or  $\Delta \text{Nd}$  for carbonate contribution.

## *South America*

A set of 16 samples from South America south of 31°S (Tab. 6.4) have been collected and analysed for their fine fraction; some of them have been decarbonated and analysed also for their leached fraction.

Other isotopic data on the fine fraction of south American deposits can be found in Gemmiti (2000) [8 samples from Argentina] and in Grousset et al. (1992) [1 sample from the Pampas].

<i>Original code</i>	<i>Geographical area</i>	<i>Geographic coordinates</i>	<i>Age</i>
P.A.	Puerto Madryn	42° 46' S, 65° 03' W	Pleistocene-Holocene
AR-MDP-1	Pampas 1	37° 57' S, 57° 38' W	20-25 kyrs B.P.
AR-GOR-2	Pampas 2	34° 54' S, 58° 01' W	20-25 kyrs B.P.
AR-HUD-3	Pampas 3	25 km NW from AR-GOR-2	<23 kyrs B.P.
AR-BAR-4	Pampas 4	33° 49' S, 59° 31' W	ca. 20 kyrs B.P.
AR-LOZ-5	Cordoba area	31° 39' S, 64° 08' W	10-20 kyrs B.P.
CH1	S.Carlos de Bariloche	41° 09' S, 71° 18' W	
CH3	Isla Grande de Chiloe	48° 38' S, 74° 06' W	Holocene
CH4	Isla Grande de Chiloe	48° 38' S, 74° 06' W	Holocene
CH5	Isla Grande de Chiloe	48° 38' S, 74° 06' W	modern
CH6	Torres del Paine N.Park	51° 04' S, 73° 09' W	
CH7	Torres del Paine N.Park	51° 04' S, 73° 09' W	pre-Holocene
CH9	Punta Arenas	53° 09' S, 70° 55' W	
CH10	Tierra del Fuego	53° 18' S, 70° 22' W	
CH11	Punta Arenas	53° 09' S, 70° 55' W	
OLA0	Aeolian dust event		

*Tab. 6.4: South America samples analyzed in this study.*

*The first column reports the original code of each sample; the second one the region where samples have been collected, the geographic coordinates and the age of the deposit when available.*

Sample named P.A. (provided by A. Aristarain) consists of Pleistocene-Holocene aeolian sediments from Puerto Madryn region, called “Cramwy deposits” lying on top of the so called “Rodados Patagonicos” formation (see Trombotto, 1996).

Samples AR-MDP-1 to AR-LOZ-5 in Tab. 6.4 (provided by M.Zaraté) have been collected in the Pampas area between latitudes 31° S and 37° S, and are part of a transect throughout the central part of Argentina. Many authors (e.g. Gallet et al., 1997) call the whole region “Patagonia”, that is actually located 400 km south and show very different environmental characteristics. All samples roughly correspond to Isotope Stage 2 or Late Glacial times (M. Zaraté, personal communication).

Samples CH1 to CH11 have been provided by Prof. F. Previtali and R. Comolli (University of Milano-Bicocca, Italy). CH1 consists of yellow silt (loess-like) from San Carlos de Bariloche, Argentina. CH3 to CH5 have been collected in the western coast of Isla Grande de Chiloé (Pirulil, Cucao); they consist of cemented fine grey sands of the Holocene period (CH3), yellowish brown sands (medium-fine) of the Holocene (CH4) and modern aeolian deposits composed by dark grey sands.

CH6 consist of grey sands, collected on the left side of a frontal moraine, about 50-60 m above the level of Lake Grey in the Torres del Paine National Park; in this region also grayish-brown sands of lateral moraine of pre-Holocene epoch have been collected (CH7).

Sample CH9, consisting of light olive brown silt with brownish yellow patches, is probable a bottom moraine, buried under a 30-40 cm soil (*La Pinguinera*, Punta Arenas).

CH10 is light brownish gray silt of a bottom moraine with salty encrustations from marine aerosol, collected in Tierra del Fuego in the western periphery of Porvenir.

CH11 consists of yellowish-brown sandy silt (loess-like) deposit collected at about 4.5 km west from Punta Arenas.

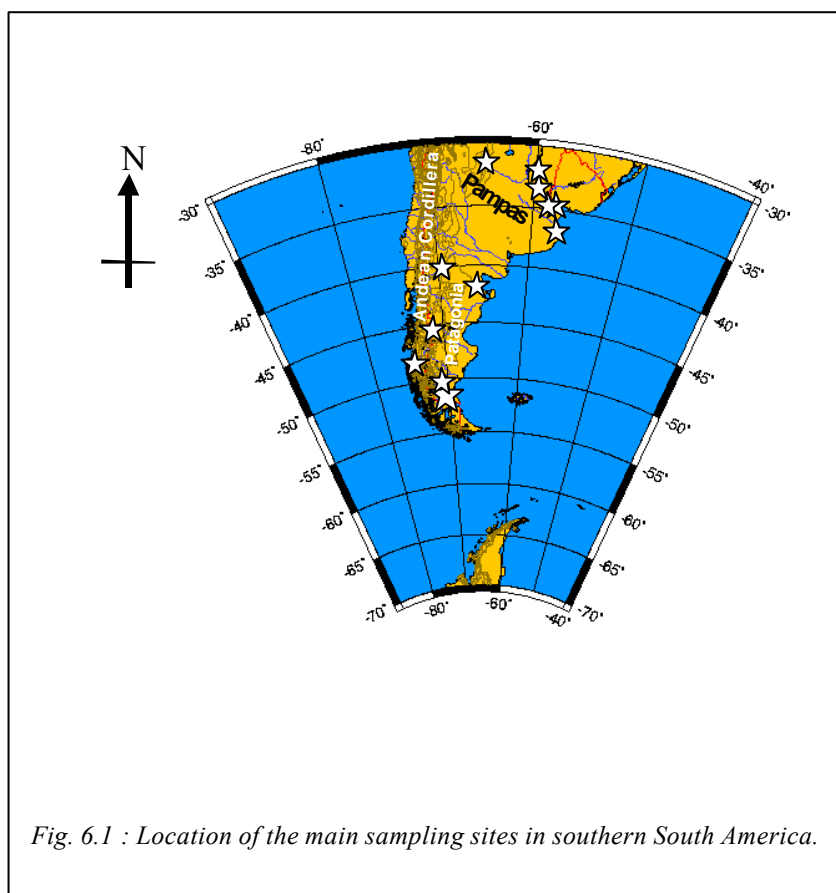


*Fig. 6.1 : Location of the main sampling sites in southern South America.*

Dust of sample OLA0 (provided by M. Mazzoni) consists of an aeolian dust event on the city of Buenos Aires occurred the 20<sup>th</sup> August 1997. The exact geographical dust provenance is unknown.

Eight samples (P.A., AR-MDP-1, AR-GOR-2, AR-HUD-3, AR-BAR-4, AR-LOZ-5, CH7 and CH9) have been analyzed both for their leached and unleached fraction.



## *New Zealand*

Samples from New Zealand analysed in this work have been collected in the South Island (Fig. 6.2). Other data on fine samples from the North Island are provided by Gemmiti (2000).

<i>Original Code</i>	<i>Geographical area</i>	<i>Geographical coordinates</i>
NZ12	Southland - Te Anau	45° 24' S, 167° 42' E
NZ22	Otago	44° 38' S, 168° 59' E
NZ136	Raikaia river mouth	43° 44' S, 172° 02' E
NZ143	South Island - ChC area	43° 28' S, 172° 31' E
NZ37	Arthur's Pass	43° 17' S, 171° 42' E
NZ15	Otago district	44° 48' S, 169° 20' E
NZ121	Canterbury plains	44° 18' S, 171° 15' E
NZ7B	Dart Valley Moraine - High valley	44° S, 168° E

*Tab. 6.5: New Zealand samples analyzed in this study.*

*The first column reports the original code of each sample; the second and third columns indicate the sites where samples have been collected and the geographic coordinates are also indicated.*

NZ12 has been collected in the Te Anau zone (District of Southland), from the border of a terrace dominating the plain over Lake Manapouri, at about 200 m a.s.l.

NZ22 consist of fluvial sediments (sandy) from the bed of the Matukituki river, descending from Mt. Aspiring in the District of Otago.

NZ136 is a deposit from the mouth of Raikaia River, collected at about 20 m a.s.l.

NZ143 is a brown loess-like deposit above a layer of gravel and buried under a soil.

NZ37 has been collected close to Arthur's Pass in the District of Westland, at about 850 m a.s.l., while

NZ15 derives from the district of Otago, at mid-way between Wanaka and Queenstown.

NZ121 consists of fine clay collected at about 20 m a.s.l. close to the sea (Christchurch area).

NZ7b is the coarser fraction of a sample of moraine collected in the Dart Valley (District of Otago).

Samples NZ12, NZ 22 and NZ 15 have been analysed both in their leached and unleached fractions.

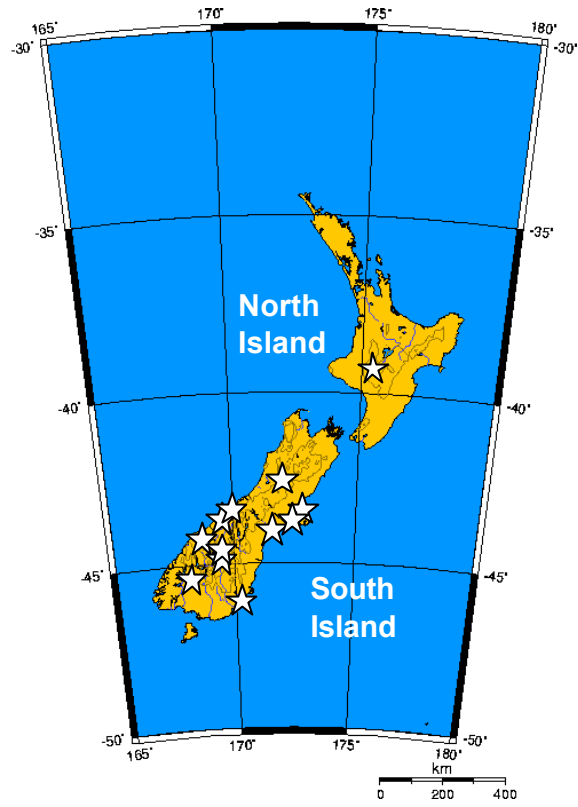


*Fig. 6.2 : Location of New Zealand sampling sites.*

*The star in the North Island indicates roughly the location of the Taupo volcanic zone, where the samples analysed by Gemmiti (2000) have been collected.*

## *Antarctica*

The ice free areas of Antarctica correspond to about 2% of the surface of the continent, an area equivalent to the size of New Zealand. They occur as isolated patches of rocks around the coast of East Antarctica, in the Transantarctic Mountains, crossing the Continent from Cape Adare to the Shackleton Mountains, and in the Antarctic Peninsula.

The McMurdo Dry Valleys occupy the southern portion of the Victoria land and the Scott Coast. This region is roughly defined as extending from 76° 30'S to 78° 30'S, and from 160° 00' E to 164° 30' E (USGS National Mapping Information system).

In this work a set of 10 samples from the McMurdo Dry Valleys region and one sample from the Northern Victoria Land have been collected. Some of them were analysed by Gemmiti (2000) for their fine and unleached fraction (samples A1-A2-A4-A5-A6-A7-A8), and have been re-selected for their fine fraction and re-analysed in this study to check for the repeatability of the measurements. Moreover, samples A2-A4-A5-A9-A10 have been re-selected for their <5 µm fraction, leached and analysed.

All samples consist of mixed surface sandy sediments. For these samples no further information are available.

<i>Original code</i>	<i>Geographical area</i>	<i>Ref</i>	<i>Geographical coordinates</i>
A1	Pearse Valley		77° 43' S, 161° 23' E
A2	Pat's peak ridge - Cape Crozier	[*]	77° 31' S, 169° 24' E
A4	Hanson Ridge		77° 17' S, 163° 15' E
A5	Mc Murdo	[*]	77° 30' S, 165° E
A6	Mc Murdo	[*]	77° 30' S, 165° E
A7	Lake Hoare, Taylor Valley	[*]	77° 37' S, 163° 11' E
A8	South Shore lake Fryxell	[*]	77° 38' S, 162° 51' E
A9	Bull pass		
A10	Simmonds Valley		
NVL	Northern Victoria Land (NVL), Terra Nova Bay		74° 50' S, 164° 30' E

*Tab. 6.6: Samples from coastal Antarctica analyzed in this study.*

*In the first and second columns are reported the original code of each sample and the corresponding code reported in Delmonte et al.(submitted). The area where samples have been collected and the geographic coordinates are also indicated.*

*[\*] = samples analysed by Gemmiti (2000)*

## South Africa

Five samples have been collected in southern Africa. Four of them (NA1, NA2, NA3, NA4) are sands from Namibia. NA1 and NA4 consist of dune sands from Sesriem and from Sossusvlei respectively.

Sample S.AF. (provided by Prof. Ann Wintle) consists of modern mineral aerosol collected in a transect from Port Elisabeth to Cape Town.

<i>Original code</i>	<i>Geographical area</i>	<i>Geographical coordinates</i>
NA1	Sesriem, Namibia	24° 29' S, 15° 48' E
NA2	Sossusvlei, Namibia	24° 42' S, 15° 17' E
NA3	Kuiseb River, Namibia intermittent stream.	23° 07' S, 14° 30' E
NA4	Sossusvlei, Namibia	24° 42' S, 15° 17' E
S.AF.	Windblown dust from transect Port Elisabeth-cape Town	34° 42' S, 26°32' E to 33° 55' S, 18°25'E

Tab. 6.7: Samples from Southern Africa analyzed in this study.

In the first and second columns are reported the original code of each sample and the corresponding code reported in Delmonte et al.(submitted). The area where samples have been collected and the geographic coordinates are also indicated.

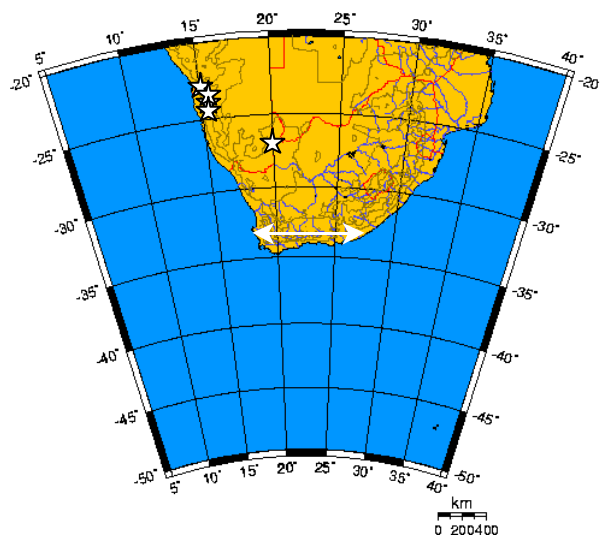


Fig. 6.3 : Location of the main sampling sites in south Africa.

## 6.2.2 Ice Core Dust samples

Prior to the selection of ice core sections for isotopic analysis a careful inspection of the ECM profile (EPICA Dome C 2001-02 Science and drilling teams, 2002) has been necessary to avoid sampling of sections containing volcanic events.

### *Dust from glacial periods*

Tables 6.8 to 6.11 give the detailed list of the ice core increments for glacial periods selected from the different ice cores. The respective depth and periods are reported, along with the sample weight after decontamination. The total mass of dust extracted, reported in the last column, is estimated by Coulter Counter measurements and varies from ~65-70  $\mu\text{g}$  to ~160  $\mu\text{g}$ .

### EPICA-Dome C ice core

Sample	EPICA core (# Bag)	EPICA Depth (m)	Climatic period	Weight (grams)	Dust recover ( $\mu\text{g}$ )
EP-St2-1	943	518.10-518.65	Stage 2	690	~65-70
	947	520.3-520.85			
EP-St2-2	1037	569.8-570.35	Stage 2	280	~100
EP-St4-1	1742	957.55-958.10	Stage 4	770	~110-120
	1752	963.05-963.6			
EP-St4-2	1812	996.05-996.60	Stage 4	770	~150
	1822	1001.55-1002.10			
EP-St6-1	3252	1788.05-1788.60	Stage 6	600	~160
	3262	1793.55-1794.10			
EP-St6-2	3422	1181.55-1882.10	Stage 6	830	~150
	3432	1887.05-1887.6			
"test"	3132	1722.05-1722.6	Stage 6 +Stage 5.5	830	~100
	3142	1727.55-1728.10			
	3252	1788.05-1788.60			

Tab. 6.8: EPICA ice core pieces selected for Sr-Nd analysis

### VOSTOK-5G ice core

Sample	Vostok 5G core	Vostok Depth (m)	Climatic period	Weight (grams)	Dust recover ( $\mu\text{g}$ )
VK-St6-1	2054	2054	Stage 6	900	70
VK-St6-2	2107	2107	Stage 6	1200	>150

Tab. 6.9: Vostok-5G ice core pieces selected for Sr-Nd analysis

Dust extraction was done by centrifugation. Moreover, the particles from the supernate of centrifugation have been filtered and recuperated as *control* sample (§ 5.3.1). They are called respectively *VK-St6-1Filtered* (filtered sample from core 2054) and *VK-St6-2Filtered* (filtered sample from core 2107).

#### DOME B ice core

Sample	Dome B Core	Dome B Depth (m)	Climatic period	Weight (grams)	Dust recover (µg)
DB-St2-1	581	581	Stage 2		110
DB-St2-2	641	641	Stage 2	860	100

Tab. 6.10: Dome B ice core pieces selected for Sr-Nd analysis

The supernate of centrifugation of both samples has been filtered and the *DB-St2-1Filtered* and *DB-St2-2Filtered* (filtered samples from cores 581 and 641) have been obtained.

#### KOMSOMOLSKAIA ice core

Samples from the KMS ice core span the last deglaciation period.

Sample	Komsomolskaia Core	Komsomolskaia Depth (m)	Climatic period	Weight (grams)	Dust recover (µg)
KMS-d-1	56	825.01-825.83	End of Deglaciation	800	10
KMS-d-2	57 58	850.08-851.23	End of Deglaciation	870	30

Tab. 6.11: KMS ice core pieces selected for Sr-Nd analysis

Filtered samples obtained from the centrifugation supernate are called *KMS-d-1Filtered* and *KMS-d-2Filtered*.

Assuming an average UCC concentration for Sr (350 ppm) and Nd (26 ppm) [Taylor and Mc Lennan, 1985], and a recovery of 99% after each passage through columns, the total quantity of Sr and Nd in each sample and the amount recovered after chemical separation have been estimated (Tab. 6.12).

<b>Sample</b>	<b>Sr tot (ng)</b>	<b>Nd tot (ng)</b>	<b>Sr recover (ng)</b>	<b>Nd recover (ng)</b>
<b>EPICA ice core</b>				
EP-St2-1	22,8	1,7	<b>22,3</b>	<b>1,7</b>
EP-St2-2	35,0	2,6	<b>34,3</b>	<b>2,6</b>
EP-St4-1	38,5	2,9	<b>37,7</b>	<b>2,8</b>
EP-St4-2	52,5	3,9	<b>51,5</b>	<b>3,8</b>
EP-St6-1	56,0	4,2	<b>54,9</b>	<b>4,1</b>
EP-St6-2	52,5	3,9	<b>51,5</b>	<b>3,8</b>
“Test”	35,0	2,6	<b>34,3</b>	<b>2,6</b>
<b>Vostok ice core</b>				
VK-St6-1	23,3	1,7	<b>22,9</b>	<b>1,7</b>
VK-St6-2	52,5	3,9	<b>51,5</b>	<b>3,8</b>
<b>Dome B ice core</b>				
DB-St2-1	37,3	2,8	<b>36,6</b>	<b>2,7</b>
DB-St2-2	35,0	2,6	<b>34,3</b>	<b>2,6</b>
<b>Komsomolskaya ice core</b>				
KMS-d-1	3,3	0,2	<b>3,2</b>	<b>0,2</b>
KMS-d-2	10,5	0,8	<b>10,3</b>	<b>0,8</b>

Tab 6.12: Total Sr and Nd (ng) recuperated from the samples and after passage through separation columns.

***Dust from interglacial periods (Holocene and Stage 5.5)***

The extremely low concentration of mineral dust in the interglacial periods makes necessary to increase in the quantity of ice used (2-3 kg) for each sample. This makes every sample representative of the atmospheric dust load for a longer period of time. The quantity of dust recuperated is about 10 to 20 µg for each sample (Tab. 6.13).

<b>Sample</b>	<b>EPICA core (# Bag)</b>	<b>EPICA Depth (m)</b>	<b>Climatic period</b>	<b>Weight ** (grams)</b>	<b>Dust recuperated*** (µg)</b>
EP-Hol-1	349 355 357 359 365 367 369	191.4-191.95 194.7-195.25 195.8-196.35 196.9-197.45 200.2-200.75 201.3-201.85 202.4-202.95	Holocene	2870	13
EP-Hol-2	597 605 607 609 617 619	327.8-328.35 332.2-332.75 333.3-333.85 334.4-334.95 338.8-339.35 339.9-340.45	Holocene	3260	20
EP-5e-1	2922 2932 2942 2952 2962 2972 3152 3152	1606.55-1607.1 1612.05-1612.6 1617.55-1618.1 1623.05-1623.6 1628.55-1629.1 1634.05-1634.6 1733.05-1733.60 1738.55-1739.1	5.5	3310	20
5e-volc “Volcanic”	3102 3112 3122	1705.55-1706.10 1711.05-1711.6 1716.55-1717.1	5.5 volcanic	650	nm

*Tab. 6.13: EPICA ice core pieces selected for Sr-Nd analysis*



From a visual inspection of the ECM profile in the field, the interglacial Stage 5.5 (of 5e, or Eemian) was estimated to span ~200 m in the EPICA core, between ca. 1550 and 1750 m of depth. The quantity of ice available for dust measurements from the main core was therefore very limited<sup>2</sup>.

The inspection of the ECM profile (EPICA Dome C 2001-02 Science and drilling teams, 2002) evidenced volcanic peaks in several bags, and for this reason only one sample representative for continental (background) dust measurements has been made for that climatic stage. A second sample, named “volcanic” has been obtained from three Bags (3102-3112-3122) that contained volcanic peaks. This sample therefore is not representative of a specific volcanic event but is aimed to show the difference between background aerosol and (generic) volcanic signature in the period investigated.

Particles in the supernate of sample EP-Hol-1 have been filtrated sample *EP-Hol-1Filtered* has been obtained.

As for glacial dust, the total quantity of Sr and Nd recovered from the small interglacial samples has been estimated (Tab. 6.14).

<b>EPICA ice core sample</b>	<b>Sr tot (ng)</b>	<b>Nd tot (ng)</b>	<b>Sr recover (ng)</b>	<b>Nd recover (ng)</b>
EP-Hol 1	4,7	0,3	4,6	0,3
EP-Hol 2	6,8	0,5	6,6	0,4
EP-5e-1	7,0	0,5	6,9	0,5
EP-5e-Volc	4,6	0,3	4,5	0,3

*Tab. 6.14: Total Sr and Nd (ng) recuperated from the samples and after passage through separation columns.*

---

<sup>2</sup> From 780 to 2200 m the ice sections assigned to dust measurements were 1 Bag every 10, i.e. a 55 cm section of the main core every 5.5 m of depth.

\*\*\*\*\*

### Summary

*The samples analysed in this study are presented.*

*More than 1700 samples from four different ice cores in East Antarctica have been measured for dust concentration and size distribution. Isotopic measurements have been performed on more than 35 samples from the continental regions of the Southern Hemisphere and 17 ice core dust samples from glacial and interglacial periods.*

## Chapter 7 - Results and discussion about dust provenance

### 7.1 The isotopic signature of ice core dust.

The  $^{87}\text{Sr}/^{86}\text{Sr}$  and  $^{143}\text{Nd}/^{144}\text{Nd}$  isotopic composition of the ice core glacial and interglacial dust (ICD) samples measured in this thesis work are reported in the following paragraphs<sup>1</sup>.

Dust has been extracted by centrifugation (§ 5.3.1) but for some samples the particles recuperated from the supernate have been also measured; they represent the so called “*filtered samples*” and their signature has been compared to that of centrifuged samples to check for eventual isotopic fractionation.

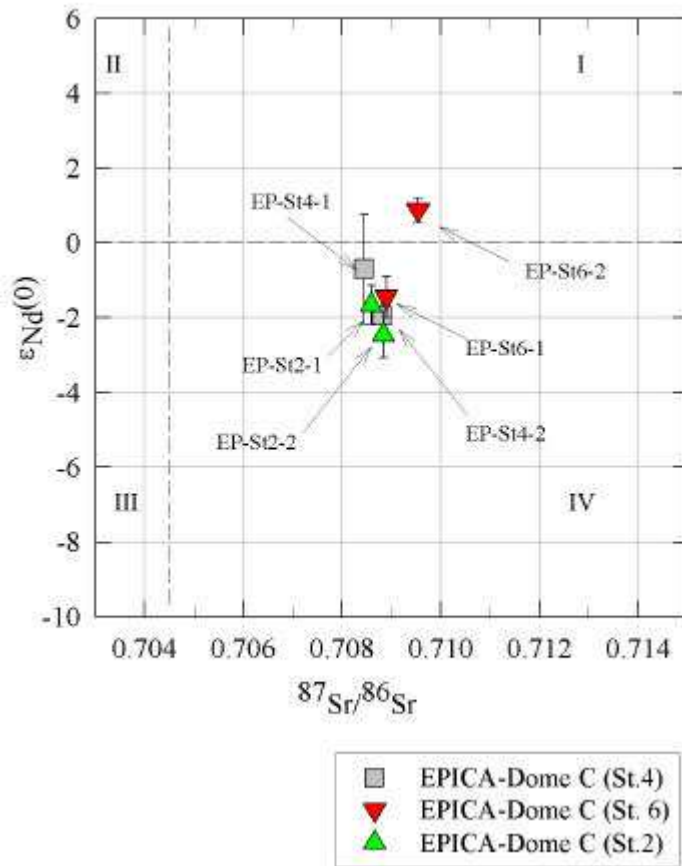
Also, some samples have been split in two aliquots to check the reproducibility of the measurement. One sample from Dome B ice core has been divided in two aliquots, one of which has been leached, and Sr has been measured from both.

---

<sup>1</sup> The measured  $^{143}\text{Nd}/^{144}\text{Nd}$  ratios have been corrected for mass fractionation by normalizing to  $^{146}\text{Nd}/^{144}\text{Nd}=0.7219$ , while the  $^{87}\text{Sr}/^{86}\text{Sr}$  ratios have been normalized to  $^{86}\text{Sr}/^{88}\text{Sr}=0.1194$ .

## 7.1.1 Glacial dust

### EPICA-Dome C: Stage 2, 4, 6



The signature of EDC glacial dust (Stage 4, 6 and 8) is restricted into a very narrow range of

$$0.7084 < {}^{87}\text{Sr}/{}^{86}\text{Sr} < 0.7095$$

and  $\epsilon_{\text{Nd}}(0)$

$$-2.4 < \epsilon_{\text{Nd}}(0) < 0.88$$

as shown in Fig. 7.1 and Tab. 7.1.

All samples except EP-St6-2 are included in the IV quadrant (see § 4.3.1). Sample EP-St2-2 was split in two aliquots each of which was subjected to a separate chemistry treatment.

The similarity of the Sr values evidence the measurements are highly reproducible ( ${}^{87}\text{Sr}/{}^{86}\text{Sr} = 0.708834 \pm 37$  and  $0.709033 \pm 81$ ).

Fig. 7.1: scatter plot of  ${}^{87}\text{Sr}/{}^{86}\text{Sr}$  versus  $\epsilon_{\text{Nd}}(0)$  ratios for EPICA glacial samples.

EPICA Sample	${}^{87}\text{Sr}/{}^{86}\text{Sr}$ ( $\pm 2\sigma \times 10^6$ )	${}^{143}\text{Nd}/{}^{144}\text{Nd}$ ( $\pm 2\sigma \times 10^6$ )	$\epsilon_{\text{Nd}}(0)$ ( $\pm 2\sigma \times 10^6$ )	Number of Sr ratios	Number of Nd ratios
EP-St2-1	0.708595 (21)	0.512553 (27)	-1.658 (0.53)	570	600
EP-St2-2	0.708834(37)	0.512512 (32)	-2.458 (0.62)	604	385
EP-St2-2, repeated	0.709033 (81)			980	
EP-St4-1	0.708443(19)	0.512602(75)	-0.70(1.46)	902	95
EP-St4-2	0.708803(20)	0.512538(26)	-1.95(0.51)	603	515
EP-St6-1	0.708897(20)	0.512564(28)	-1.44(0.55)	620	600
EP-St6-2	0.709537(17)	0.512683(16)	0.88(0.31)	691	600

Tab. 7.1:  ${}^{87}\text{Sr}/{}^{86}\text{Sr}$ ,  ${}^{143}\text{Nd}/{}^{144}\text{Nd}$  and  $\epsilon_{\text{Nd}}(0)$  isotopic values of EPICA glacial samples

### Dome B: Stage 2

The two samples from Dome B (Stage 2) are very similar and fall into the IV quadrant as EDC ones.

The DB-St2-1 sample has been split in two aliquots each of which has been subjected to an independent chemistry treatment. The results (Tab. 7.2a) evidence the reproducibility of the measurement is very good ( $^{87}\text{Sr}/^{86}\text{Sr} = 0.708383$  and  $0.708316$ ).

For both samples, the particles remaining in the supernate after centrifugation have been analysed and their signature proved to be identical to dust from the bottom of centrifugation ( $\Delta^{87}\text{Sr}/^{86}\text{Sr} = 0.000096$  between DB-St2-1 and DB-St2-1-Filtered;  $\Delta^{87}\text{Sr}/^{86}\text{Sr} = 0.000163$  between DB-St2-1

repeated and DB-St2-1-Filtered;  $\Delta^{87}\text{Sr}/^{86}\text{Sr} = 0.001242$  between DB-St2-2 and DB-St2-2-filtered not leached;  $\Delta \epsilon_{\text{Nd}}(0) = 0.10$  between DB-St2-1 and DB-St2-1-Filtered, see Tab 7.2a and Fig. 7.2).

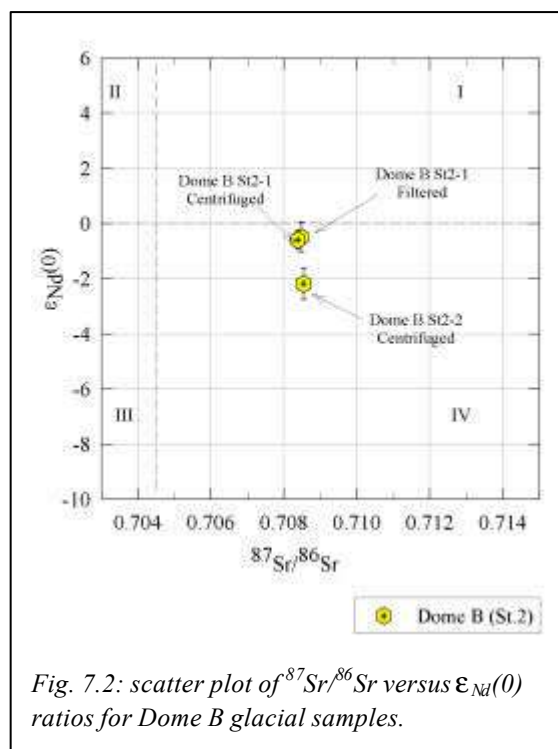


Fig. 7.2: scatter plot of  $^{87}\text{Sr}/^{86}\text{Sr}$  versus  $\epsilon_{\text{Nd}}(0)$  ratios for Dome B glacial samples.

Tab. 7.2a:  $^{87}\text{Sr}/^{86}\text{Sr}$ ,  $^{143}\text{Nd}/^{144}\text{Nd}$  and  $\epsilon_{\text{Nd}}(0)$  isotopic values of Dome B glacial samples

DOME B Sample	$^{87}\text{Sr}/^{86}\text{Sr}$ ( $\pm 2\sigma \times 10^6$ )	$^{143}\text{Nd}/^{144}\text{Nd}$ ( $\pm 2\sigma \times 10^6$ )	$\epsilon_{\text{Nd}}(0)$ ( $\pm 2\sigma \times 10^6$ )	Number of Sr ratios	Number of Nd ratios
DB-St2-1	0.708383 (32)	0.512608 (18)	-0.58(0.35)	213	675
DB-St2-1-repeated	0.708316 (39)			760	
DB-St2-1-Filtered	0.708479 (18)	0.512613 (28)	-0.49(0.55)	733	600
DB-St2-2	0.708544 (28)	0.512526 (29)	-2.18(0.57)	715	540

The difference in Sr between the unleached and the leached sample from Stage 2 also is very small ( $\Delta^{87}\text{Sr}/^{86}\text{Sr} = 0.000246$ ) and it is lower than the difference between the Sr signatures of the centrifuged and the supernate samples.

Tab. 7.2b:  $^{87}\text{Sr}/^{86}\text{Sr}$  ratios of leached and unleached DB-St 2-2F sample.

DOME B Sample	$^{87}\text{Sr}/^{86}\text{Sr}$ ( $\pm 2\sigma \times 10^6$ )	Number of Sr ratios
DB-St2-2Filtered, <i>not leached</i>	0.709786(26)	515
DB-St2-2Filtered, <i>Leached</i>	0.709540(35)	425

***Komsomolskaia: the deglaciation***

The samples from KMS ice core are the smallest analyzed in this work, and this justifies the limited number of Nd measurements on such extremely reduced samples (few hundred pg of Nd each, see Tab. 6.12).

These samples span the deglaciation period.

It can be observed from Fig. 7.3 and Tab. 7.3 that the signature of the two samples is very similar to that of EPICA and Dome B glacial dust.

Strontium ratios span the interval

$$0.7081 < {}^{87}\text{Sr}/{}^{86}\text{Sr} < 0.7096$$

and  $\epsilon_{\text{Nd}}(0)$  is slightly negative (-1.5 to -3).

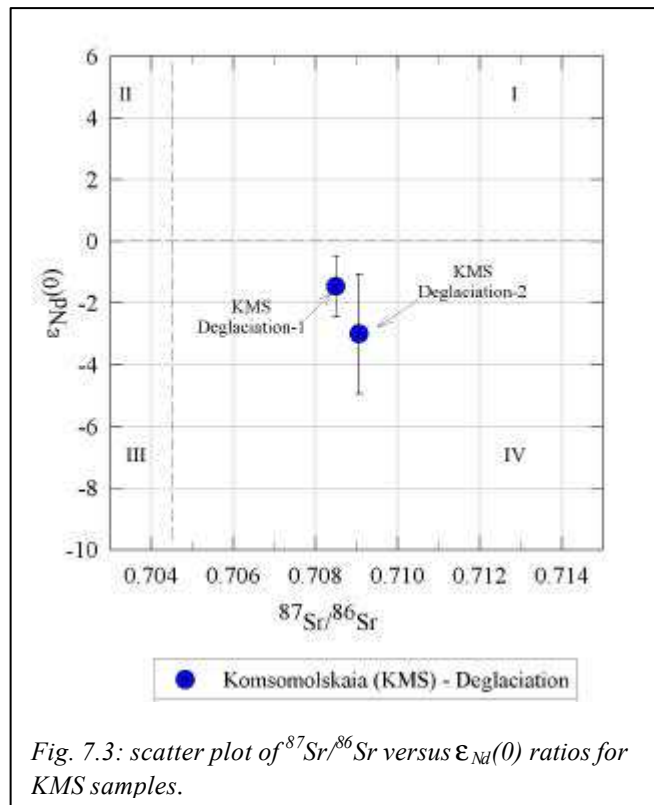


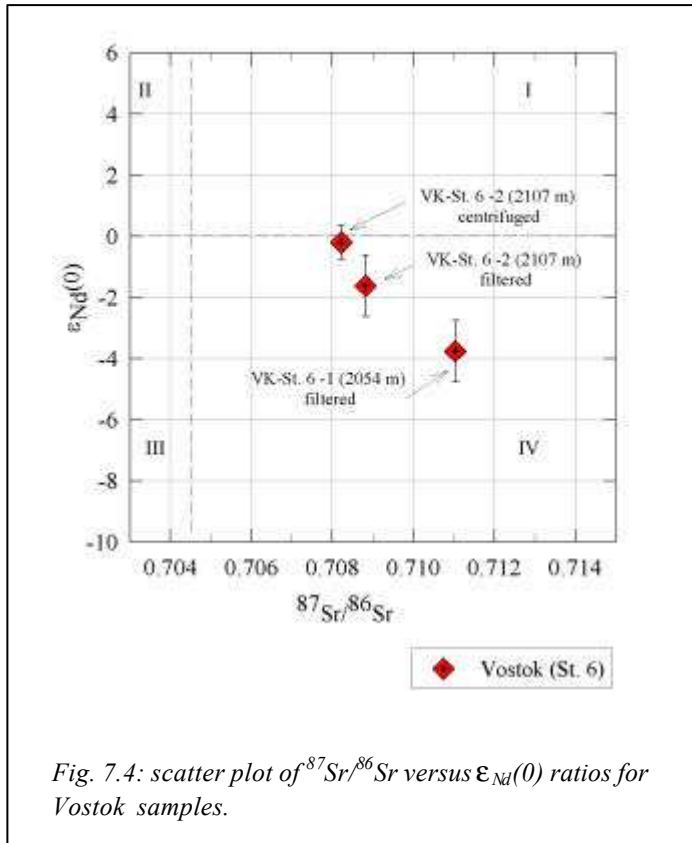
Fig. 7.3: scatter plot of  ${}^{87}\text{Sr}/{}^{86}\text{Sr}$  versus  $\epsilon_{\text{Nd}}(0)$  ratios for KMS samples.

The difference in Sr between the filtered and the centrifuged samples is very small ( $\Delta {}^{87}\text{Sr}/{}^{86}\text{Sr} = 0.000414$  for KMS-d-1 and KMS-d-1-filtered;  $\Delta {}^{87}\text{Sr}/{}^{86}\text{Sr} = 0.000574$  for KMS-d-2 and KMS-d-2-filtered). The number of measurements performed on the filtered samples, however, is very limited for both.

Tab. 7.3:  ${}^{87}\text{Sr}/{}^{86}\text{Sr}$ ,  ${}^{143}\text{Nd}/{}^{144}\text{Nd}$  and  $\epsilon_{\text{Nd}}(0)$  isotopic values of KMS samples

KMS Sample	${}^{87}\text{Sr}/{}^{86}\text{Sr}$ ( $\pm 2\sigma \times 10^6$ )	${}^{143}\text{Nd}/{}^{144}\text{Nd}$ ( $\pm 2\sigma \times 10^6$ )	$\epsilon_{\text{Nd}}(0)$ ( $\pm 2\sigma \times 10^6$ )	Number of Sr ratios	Number of Nd ratios
KMS-d-1	0.708493 (22)	0.512563 (51)	-1.46(0.99)	680	245
KMS-d-1 Filtered	0.708079(69)			90	
KMS-d-2	0.709058 (38)	0.512484 (99)	-3.00(1.93)	680	165
KMS-d-2 Filtered	0.709632(78)			27	

**Vostok: Stage 6**



Two glacial samples from Vostok (Stage 6) have been analysed.

The signature of the glacial dust from this core was previously documented in detail by Basile, 1997 and Basile et al., 1997.

As for the previous ICD samples, the difference between the filtered and the centrifuged samples is very small ( $0.000598 < \Delta ^{87}\text{Sr}/^{86}\text{Sr} < 0.001675$ ;  $\Delta \epsilon_{\text{Nd}}(0) = 1.42$ ).

Tab. 7.4:  $^{87}\text{Sr}/^{86}\text{Sr}$ ,  $^{143}\text{Nd}/^{144}\text{Nd}$  and  $\epsilon_{\text{Nd}}(0)$  isotopic values of Vostok samples

Vostok Sample	$^{87}\text{Sr}/^{86}\text{Sr}$ ( $\pm 2\sigma \times 10^6$ )	$^{143}\text{Nd}/^{144}\text{Nd}$ ( $\pm 2\sigma \times 10^6$ )	$\epsilon_{\text{Nd}}(0)$ ( $\pm 2\sigma \times 10^6$ )	Number of Sr ratios	Number of Nd ratios
VK-St6-1	0.709579(17)				780
VK-St6-1 Filtered	0.711035(38)	0.512445(52)	-3.76(1.01)	190	420
VK-St6-1 Filtered (2 <sup>nd</sup> bottle)	0.711254(91)				455
VK-St6-2 Filtered	0.708818(19)	0.512555(52)	-1.62(1-01)	270	1000
VK-St6-2	0.708220(15)	0.512628(28)	-0.20(0.55)	670	1017

## Comparison with bibliographic data

### Isotopic signature of Vostok and old Dome C glacial dust

Previous results from Grousset et al. (1992), Basile et al. (1997) and Basile (1997) on glacial dust from the old Dome C (Stage 2) and the Vostok (Stage 4, 6, 8, 10, 12) ice cores are reported in Fig.7.5 and in Tab.7.5.

Data from Grousset et al. (1992) and from Basile et al. (1997) have been obtained from dust samples extracted by evaporation and measured in Toulouse. They appear slightly more radiogenic in Nd with respect to the samples extracted by centrifugation and measured in Mainz (Basile, 1997 and this work).

The different method of dust extraction is unlikely the cause for this shift. On the opposite, evaporation could probably have affected the Sr signature through contribution of marine Sr. However, the contribution of this latter is negligible ( $0.000291 < \Delta^{87}\text{Sr}/^{86}\text{Sr} < 0.000119$ , see Basile 1997).

Such difference was already observed by Basile (1997) and attributed to natural variability of the samples.

Overall, the Sr-Nd isotopic ratios for EDC, Vostok, Dome B and KMS glacial samples analyzed in this work are coherent with previous results from Basile (1997). The dust extracting technique is the same (centrifugation), as well as the equipment for dust separation and measurement.

The similarity can be better appreciated comparing the results for the same climatic stage (Stage 6) from the Vostok ice core (see Tab. 7.4 and 7.5).

Overall, the ice core dust field is restricted into a very narrow range of  $0.708 < ^{87}\text{Sr}/^{86}\text{Sr} < 0.711$  ( $0.709035 \pm 0.000954$  on average) and a relatively more significant interval of  $\epsilon_{\text{Nd}}(0)$  ( $-5 < \epsilon_{\text{Nd}}(0) < +5$ ), slightly negative (between 0 and -3) for the majority of samples.

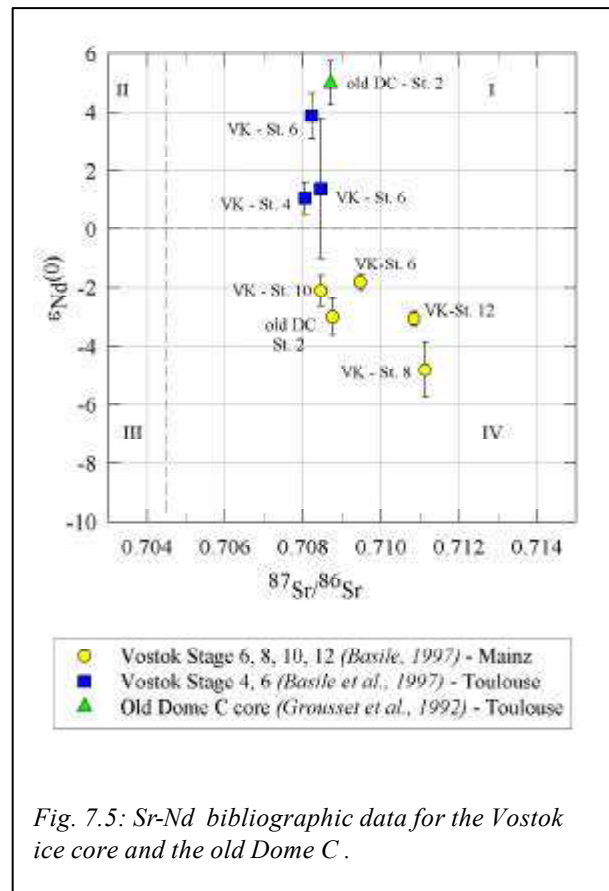


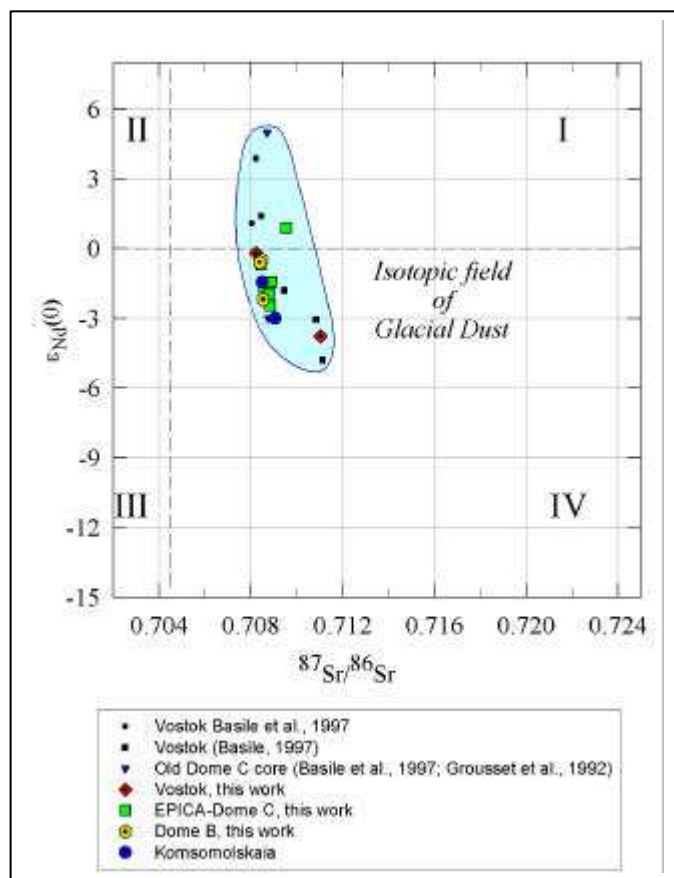
Fig. 7.5: Sr-Nd bibliographic data for the Vostok ice core and the old Dome C.



Tab. 7.5 :  $^{87}\text{Sr}/^{86}\text{Sr}$ ,  $^{143}\text{Nd}/^{144}\text{Nd}$  and  $\epsilon_{\text{Nd}}(0)$  isotopic values of Vostok samples

Sample	$^{87}\text{Sr}/^{86}\text{Sr}$ ( $\pm 2\sigma$ )	$^{143}\text{Nd}/^{144}\text{Nd}$ ( $\pm 2\sigma$ )	$\epsilon_{\text{Nd}}(0)$ ( $\pm 2\sigma$ )	Source	Lab.	Extraction method
Vostok stage4 (I)	0.708047(09)	0.512694(28)	1.09(0.55)	Basile et al. (1997)	Toulouse	evaporation
Vostok stage4 (II)	0.708404(12)			Basile et al. (1997)	Toulouse	evaporation
Vostok stage 6 (I)	0.708219(11)	0.512836(40)	3.86(0.78)	Basile et al. (1997)	Toulouse	evaporation
Vostok stage 6 (II)	0.708452(12)	0.512710(121)	1.40(2.36)	Basile et al. (1997)	Toulouse	evaporation
Vostok stage 6	0.709468(32)	0.512545(14)	-1.81(0.27)	Basile (1997)	MPI-Mainz	Centrifug.
Vostok stage 8	0.711129(33)	0.512393(48)	-4.78(0.94)	Basile (1997)	MPI-Mainz	Centrifug.
Vostok stage 10	0.708460(36)	0.512530(27)	-2.11(0.53)	Basile (1997)	MPI-Mainz	Centrifug.
Vostok stage12	0.710846(46)	0.512481(12)	-3.06(0.23)	Basile (1997)	MPI-Mainz	Centrifug.
Old Dome C stage 2	0.708707(60)	0.512894(39)	4.99(0.76)	Grousset et al. (1992)	Toulouse	evaporation
Old Dome C stage 2 (516 m)	0.708753(56)	0.512484(32)	-3.00(0.62)	Basile, 1997	Mainz	Centrifug.

Fig. 7.6: Glacial dust field for all sites and for all glacial stages investigated.



## 7.1.2 Interglacial dust

### *EPICA-Dome C: Holocene and Stage 5.5*

The Sr and Nd abundance for the interglacial samples is extremely low (see §6.2.2). The number of measurements therefore is more limited with respect to glacial samples and the error is higher, in particular for Nd that represents the “*limiting element*”.

The results on the interglacial samples are reported in Tab. 7.6.

Tab. 7.6:  $^{87}\text{Sr}/^{86}\text{Sr}$ ,  $^{143}\text{Nd}/^{144}\text{Nd}$  and  $\epsilon_{\text{Nd}}(0)$  isotopic values for interglacial samples.

Sample	$^{87}\text{Sr}/^{86}\text{Sr}$ ( $\pm 2\sigma \times 10^6$ )	$^{143}\text{Nd}/^{144}\text{Nd}$ ( $\pm 2\sigma \times 10^6$ )	$\epsilon_{\text{Nd}}(0)$ ( $\pm 2\sigma \times 10^6$ )	Number of Sr ratios	Number of Nd ratios
EP-Hol-1	0.710013(55)	0.512407(101)	-4.51(1.97)	475	160
EP-Hol-2	0.709435(37)	0.512347(95)	-5.68(1.85)	700	190
EP-5e-1	0.710213(26)	0.512211(172)	-8.29(2.48)	590	130
5.5 “Volcanic”	0.704983(36)	0.512823(53)	3.61(1.03)	324	500

The three interglacial samples from EPICA Dome C ice core appear significantly more negative in Nd respect to glacial samples even considering the error bars.

The sample containing volcanic peaks (§ 6.2.2) actually shows a typical volcanic signature highly radiogenic in Nd, and low radiogenic in Sr, therefore very different from the other interglacial samples.

**Comparison with bibliographic data**

Two Holocene samples (as well as one Nd ratio from Stage 5.5) from Vostok ice core were measured by Basile (1997), and the results are shown in Tab. 7.7.

The isotopic field defined by interglacial samples altogether is reported in Fig. 7.7.

Sample	Depth (m)	Climatic period	$^{87}\text{Sr}/^{86}\text{Sr}$ ( $\pm 2\sigma \times 10^6$ )	$^{143}\text{Nd}/^{144}\text{Nd}$ ( $\pm 2\sigma \times 10^6$ )	$\epsilon_{\text{Nd}}(0)$
Vostok	32	Holocene	0.711200(35)	0.512126(17)	-9.99
Vostok	99	Holocene	0.709289(50)	0.512379(44)	-5.05
Vostok	1676	St. 5.5		0.512261(75)	-7.35

Tab. 7.7 Bibliographic data for interglacial dust in Vostok ice core (Basile, 1997)

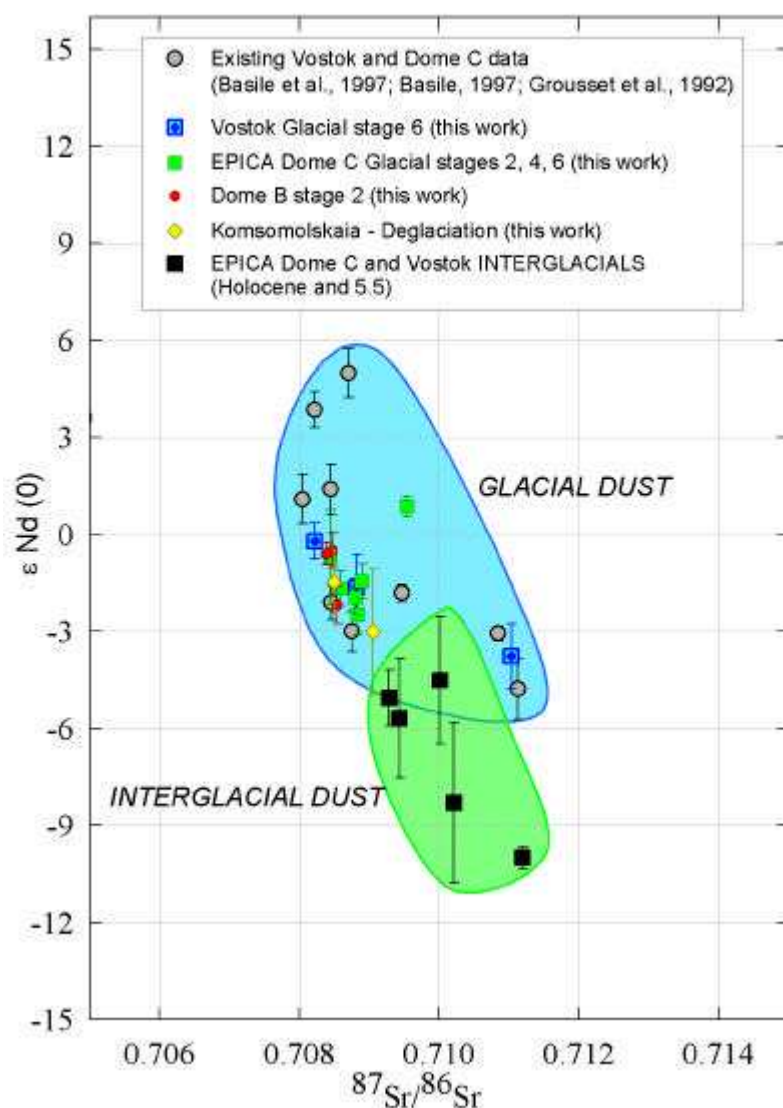


Fig. 7.7: Isotopic field for interglacial dust (this work and Basile 1997)

## 7.2 The signature of the PSAs of the Southern Hemisphere

The Sr-Nd signature of the Southern Hemisphere potential source areas is documented in the literature, mainly for South American loesses and aeolian deposits, but it refers to the bulk (all sizes) or to the coarse-grained fraction of sediments. In order to be suitable for comparison with the ice core dust, the isotopic composition of each continent of the Southern Hemisphere had to be re-defined in the same grain size than the ice core dust (<5 $\mu$ m).

### 7.2.1 Southern South America

The isotopic ratios for the southern South America samples analyzed in this work are reported in Tab. 7.8 and in Fig.7.8.

*Tab. 7.8 Sr-Nd signature of South America samples.*

<i>Original code</i>	$^{87}\text{Sr}/^{86}\text{Sr}$ ( $\pm 2\sigma \times 10^6$ )	$^{143}\text{Nd}/^{144}\text{Nd}$ ( $\pm 2\sigma \times 10^6$ )	$\epsilon_{\text{Nd}}(0)$
P.A.	0.707320 (23)	0.512644 (09)	0.12
Ar-MDP-1	0.708547 (19)	0.512628 (11)	-0.20
AR-GOR-2	0.710311 (16)	0.512524 (15)	-2.22
AR-HUD-3	0.709908 (21)	0.512541 (11)	-1.89
AR-BAR-4	0.711218 (26)	0.512496 (14)	-2.77
AR-LOZ-5	0.709357 (22)	0.512483 (08)	-3.02
CH1	0.704604 (18)	0.512777 (09)	2.71
CH3	0.707207(20)	0.512709 (17)	1.38
CH4	0.706891 (16)	0.512726 (12)	1.72
CH5	0.70715 (24)	0.512597 (29)	-0.80
CH6	0.707298 (19)	0.512489 (15)	-2.91
CH7	0.70862 (14)	0.512552 (14)	-1.68
CH9	0.70988 (19)	0.512569 (08)	-1.35
CH10	0.711806 (21)	0.512439 (07)	-3.88
CH11	0.705364 (21)	0.512743 (10)	2.05
OLA0	0.713088 (28)	0.512227 (08)	-8.02

Overall, the isotopic field of aeolian dust from Argentina and Chile is restricted into the

$$0.7045 < ^{87}\text{Sr}/^{86}\text{Sr} < 0.7130$$

and

$$-5 < \epsilon_{\text{Nd}}(0) < +3$$

isotopic ranges.

It is not possible to distinguish clear geographic sub-groups since the signatures of samples from the 31°S - 37°S zone and those the southern latitudes (>40° S) partially overlay (Fig. 7.8).

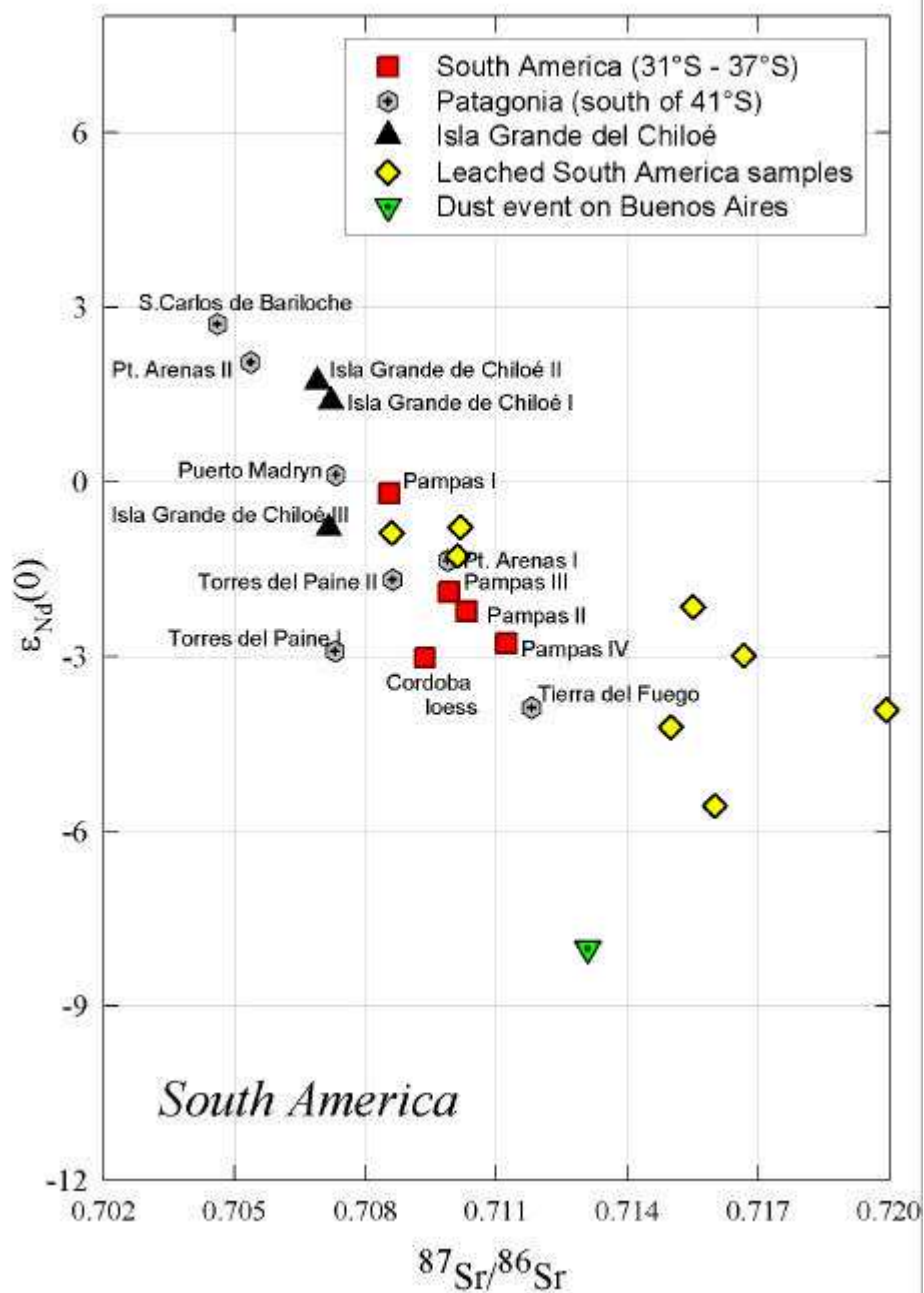


Fig. 7.8: Isotopic field for South America

The three samples from Isla Grande de Chiloé (Code CH3-CH4-CH5) are restricted to low radiogenic Sr values ( $^{87}\text{Sr}/^{86}\text{Sr} < 0.7072$ ). The sample of the dust event on Buenos Aires occurred in August 1997 (OLA1) is quite different from all the others since it is very low radiogenic in Nd and seems to fall off the main field defined by all the other samples.

The measurements performed on the leached samples (Tab. 7.9) show a systematic shift towards more highly radiogenic  $^{87}\text{Sr}/^{86}\text{Sr}$  values. The difference ( $\Delta ^{87}\text{Sr}/^{86}\text{Sr} = ^{87}\text{Sr}/^{86}\text{Sr}_{\text{leached}} - ^{87}\text{Sr}/^{86}\text{Sr}_{\text{unleached}}$ ) spans the interval  $0.0013 < \Delta ^{87}\text{Sr}/^{86}\text{Sr} < 0.0087$ , and is on average 0.004.

In the same way the Nd difference ( $\Delta \epsilon_{\text{Nd}}(0) = \epsilon_{\text{Nd}}(0)_{\text{leached}} - \epsilon_{\text{Nd}}(0)_{\text{unleached}}$ ) has been calculated. On average it is around one Epsilon unit, and hence are considered negligible. The  $\Delta \epsilon_{\text{Nd}}(0)$  is negative for all samples except CH7.

Original code	$^{87}\text{Sr}/^{86}\text{Sr}$ ( $\pm 2\sigma \times 10^6$ )	$^{143}\text{Nd}/^{144}\text{Nd}$ ( $\pm 2\sigma \times 10^6$ )	$\epsilon_{\text{Nd}}(0)$	$\Delta ^{87}\text{Sr}/^{86}\text{Sr}$	$\Delta \epsilon_{\text{Nd}}(0)$
P.A.-Leach	0.708600(15)	0.512593(26)	-0.88	<b>0.001280</b>	<b>-0.99</b>
AR-MDP-1- Leach	0.710172(12)	0.512598(09)	-0.78	<b>0.001625</b>	<b>-0.59</b>
AR-GOR-2-Leach	0.716666(14)	0.512485(11)	-2.98	<b>0.006355</b>	<b>-0.76</b>
AR-HUD-3-Leach	0.715500(10)	0.512528(12)	-2.15	<b>0.005592</b>	<b>-0.25</b>
AR-BAR-4-Leach	0.719937(48)	0.512437(11)	-3.92	<b>0.008719</b>	<b>-1.15</b>
AR-LOZ-5-Leach	0.714994(12)	0.512422(14)	-4.21	<b>0.005637</b>	<b>-1.19</b>
CH7-Leach	0.710109(13)	0.512573(09)	-1.27	<b>0.001489</b>	<b>+0.41</b>
CH10-Leach	0.716000(18)	0.512353(17)	-5.56	<b>0.004194</b>	<b>-1.68</b>

Tab. 7.9 : isotopic signature of South America leached samples

### *Comparison with bibliographic data*

There are a number of data about Sr-Nd isotopic composition of Argentine loess (Gallett et al., 1998), from different areas of Patagonia (Grousset et al., 1992), from the Andes, and the Quaternary volcanic centres of the Southern Andes (Hawkesworth et al., 1979, and Futa and Stern, 1988), and from the Argentine continental shelf (Basile et al., 1997).

However, all these measurements have been performed on the bulk samples (all size included) and are not suitable for direct comparison with the ice core dust.

For the fine (<5 µm) fraction of South American samples, a set of 8 samples has been measured by Gemmiti (2000) and another sample in the same size fraction is reported in Grousset et al. (1992). They are reported all in Fig. 7.9 along with the data obtained in this work.

It can be observed that most of the samples (shaded area in Fig. 7.9) span the  $0.704 < {}^{87}\text{Sr}/{}^{86}\text{Sr} < 0.720$  and  $+3 < \epsilon_{\text{Nd}}(0) < -6$  isotopic interval.

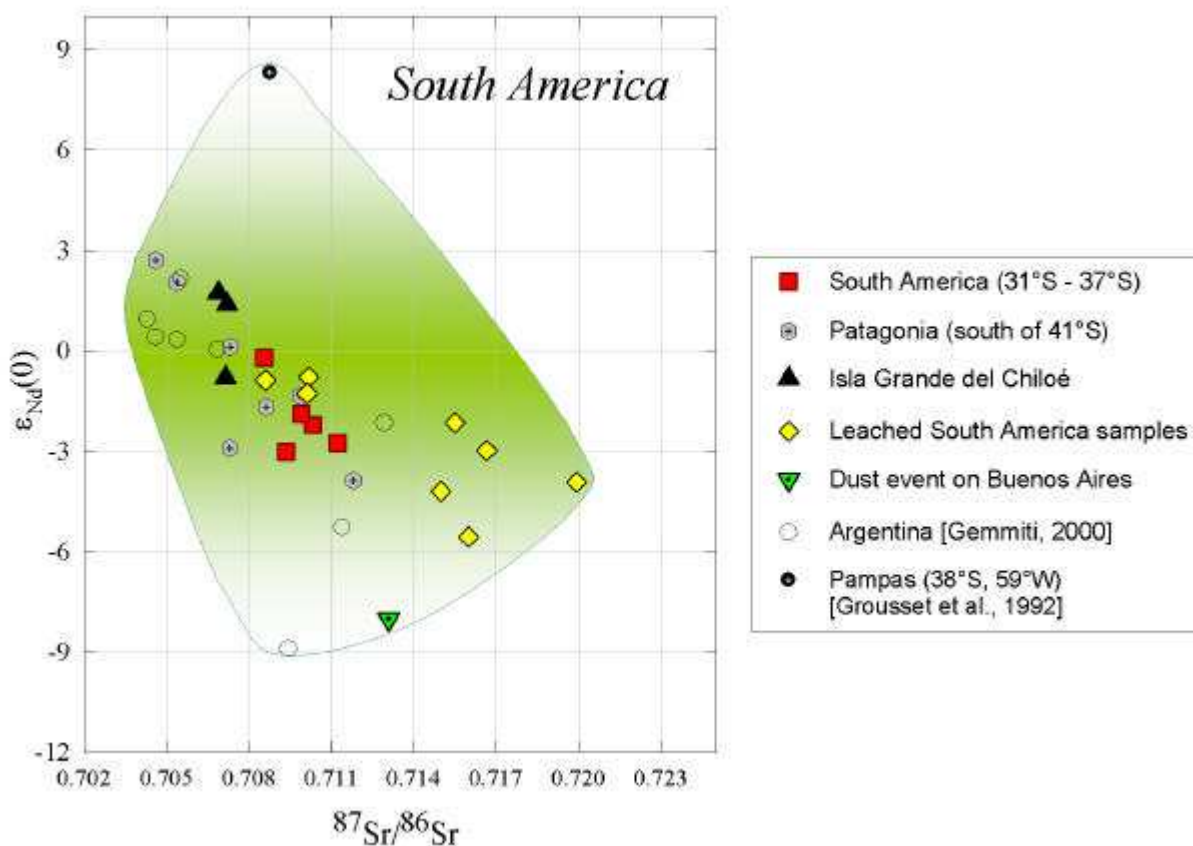


Fig. 7.9: Isotopic field for South America traced from all data available on the < 5 µm fraction, both on leached and unleached samples. [Data from Grousset(1992), Gemmiti(2000), and this work]. The shaded area represents the field including the majority of samples.

## 7.2.2 New Zealand

The Sr-Nd isotopic ratios for the <5  $\mu\text{m}$  fraction of the New Zealand (South Island) samples analyzed in this work are reported in Tab. 7.10 and Fig. 7.10.

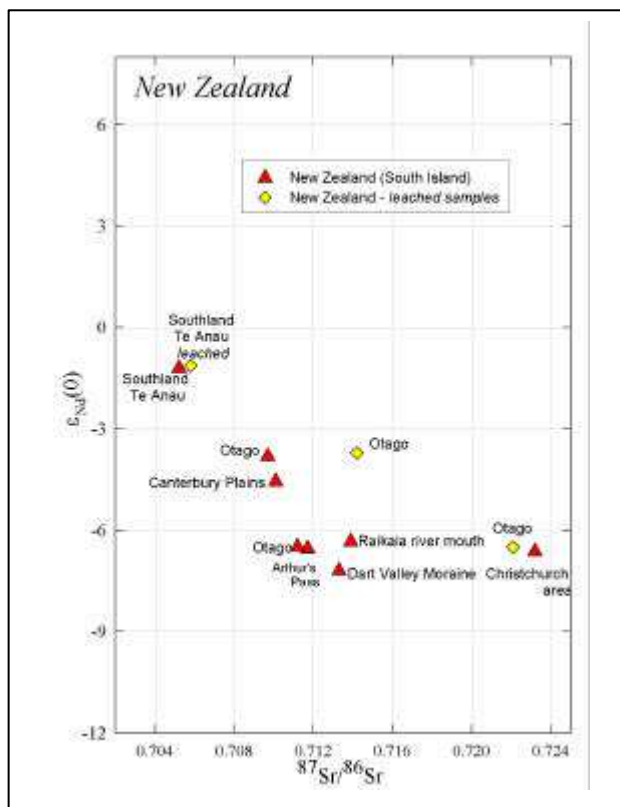
Tab. 7.10: New Zealand samples analyzed in this study

Original code	$^{87}\text{Sr}/^{86}\text{Sr}$ ( $\pm 2\sigma \times 10^6$ )	$^{143}\text{Nd}/^{144}\text{Nd}$ ( $\pm 2\sigma \times 10^6$ )	$\epsilon_{\text{Nd}}(0)$
NZ12	0.705183 (24)	0.512576 (11)	-1.21
NZ 22	0.709683(19)	0.512442 (20)	-3.82
NZ136	0.713883 (21)	0.512313 (10)	-6.34
NZ143	0.723239 (24)	0.512298 (20)	-6.63
NZ 37	0.711657 (17)	0.512302 (12)	-6.55
NZ15	0.711190 (26)	0.512306 (17)	-6.49
NZ121	0.710064 (27)	0.512404 (75)	-4.56
NZ7B	0.713260 (21)	0.512269 (158)	-7.20

New Zealand samples span a wide Sr isotopic range ( $0.709 < ^{87}\text{Sr}/^{86}\text{Sr} < 0.723$ ) and a more restricted Nd interval ( $-3.8 < \epsilon_{\text{Nd}}(0) < -7.2$ ), with only one exception (NZ12 from Southland district).

The three leached samples (Tab. 7.11) show a higher  $^{87}\text{Sr}/^{86}\text{Sr}$  than the unleached counterpart and the  $\Delta ^{87}\text{Sr}/^{86}\text{Sr}$  is quite important for NZ15-Leach. The  $\Delta \epsilon_{\text{Nd}}(0)$  shifts, on the opposite, are close to zero for all three samples.

Fig. 7.10: New Zealand samples analyzed in this work.



Tab. 7.11: New Zealand samples leached

code	$^{87}\text{Sr}/^{86}\text{Sr}$ ( $\pm 2\sigma \times 10^6$ )	$^{143}\text{Nd}/^{144}\text{Nd}$ ( $\pm 2\sigma \times 10^6$ )	$\epsilon_{\text{Nd}}(0)$	$\Delta ^{87}\text{Sr}/^{86}\text{Sr}$	$\Delta \epsilon_{\text{Nd}}(0)$
NZ 12- Leach	0.705820(29)	0.512580(22)	-1.13	<b>0.000637</b>	<b>0.08</b>
NZ 22- Leach	0.714248(15)	0.512448(17)	-3.71	<b>0.004565</b>	<b>0.12</b>
NZ15- Leach	0.722100(18)	0.512305(14)	-6.50	<b>0.010910</b>	<b>-0.01</b>



**New Zealand : comparison with bibliographic data**

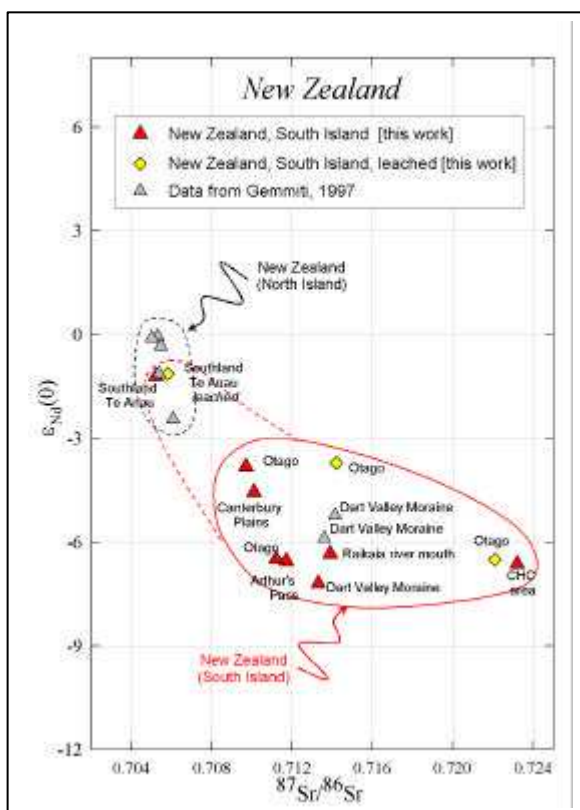
The only bibliographic data on the <5 µm fraction of samples from New Zealand are those from Gemmiti (2000) on five samples from the North Island and two samples from the Dart Valley (South Island). The results are reported in the table here below.

Tab. 7.12 New Zealand samples analyzed by Gemmiti (2000) for the <5 µm fraction.

code	Geographical area	Geographical coordinates	$^{87}\text{Sr}/^{86}\text{Sr}$ ( $\pm 2\sigma \times 10^6$ )	$^{143}\text{Nd}/^{144}\text{Nd}$ ( $\pm 2\sigma \times 10^6$ )	$\epsilon_{\text{Nd}}(0)$
NZ1	North Crater Rotopaunga	39° S, 175° E North Island	0.705305 (11)	0.512635 (05)	-0.06
NZ2	South Crater Mt. Tongariro	39° S, 175° E North Island	0.705449 (10)	0.512621 (04)	-0.33
NZ3	Wellington district	39° S, 175° E North Island	0.706065 (07)	0.512513 (24)	-2.44
NZ4	Red Crater	39° S, 175° E North Island	0.705012 (13)	0.512633 (11)	-0.10
NZ6	Tongarino Park	39° S, 175° E North Island	0.705354 (07)	0.512580 (24)	-1.13
NZ5	Dart Valley Moraine Bottom valley	44° S, 168° E South Island	0.713591 (04)	0.512336 (05)	-5.89
NZ7	Dart Valley Moraine High valley	44° S, 168° E South Island	0.714148 (06)	0.512370 (03)	-5.23

The two samples NZ5 and NZ7 are moraine sediments from the Dart Valley of South Island (District of Otago). They have been collected respectively in the bottom and in the highest part of the valley. Sample NZ7 is composed of the finer sediments of the moraine, while the coarser ones constitute the NZ7b sample analyzed in this work (see Tab. 7.10)<sup>2</sup>.

Fig. 7.11: Bibliographic data from New Zealand.



<sup>2</sup> From both moraine samples (fine and coarse) only the <5 µm fraction has been extracted and measured.

### 7.2.3 The non-glaciated areas of Antarctica

One sample from the Northern Victoria Land (NVL) and three samples from the McMurdo Dry Valleys region have been analysed in this work. From this latter area some measurements were performed in year 2000 by Gemmiti. To check for the precision of the measurements two samples (A1 and A4) have been re-selected for their fine fraction and re-measured. The results are reported in Tab. 7.13 and Tab. 7.14.

<i>Original code</i>	$^{87}\text{Sr}/^{86}\text{Sr}$ ( $\pm 2\sigma \times 10^6$ )	$^{143}\text{Nd}/^{144}\text{Nd}$ ( $\pm 2\sigma \times 10^6$ )	$\epsilon_{\text{Nd}}(0)$
A1	0.712440 (09)	N.M.	N.M.
A4	0.710040 (23)	0.512582 (11)	-1.03
A9	0.715600 (14)	0.512129 (19)	-9.93
NVL	0.748814 (16)	0.511919 (09)	-14.03

Tab. 7.13 : Antarctic samples analyzed in this work

<i>Original code</i>	$^{87}\text{Sr}/^{86}\text{Sr}$ ( $\pm 2\sigma \times 10^6$ )	$^{143}\text{Nd}/^{144}\text{Nd}$ ( $\pm 2\sigma \times 10^6$ )	$\epsilon_{\text{Nd}}(0)$
A1[*]	0.713913 (10)	0.511997 (08)	-12.50
A2[*]	0.703194 (15)	0.512929 (07)	5.68
A4[*]	0.709797 (41)	0.512492 (08)	-2.85
A5[*]	0.703357 (09)	0.512818 (08)	3.51
A6[*]	0.705804 (07)	0.512687 (02)	0.96
A7[*]	0.711757 (31)	0.512306 (10)	-6.48
A8[*]	0.708914 (11)	0.512376 (12)	-5.11

Tab. 7.14 : Antarctic samples analyzed by Gemmiti (2000)

The difference between our measurements and Gemmiti's is very low ( $\Delta ^{87}\text{Sr}/^{86}\text{Sr} = 0.001475$  for sample A1 and 0.000241 for A4;  $\Delta \epsilon_{\text{Nd}}(0) = -1.25$ ). Five samples have been leached and the results show a small shift for Sr and almost no variations for Nd, with the exception of sample A5. Sample A4 has been subjected two times to the leaching procedure and the repetition of the Sr measurement allows to appreciate the good repeatability of the measurements.

<i>Original code</i>	$^{87}\text{Sr}/^{86}\text{Sr}$ ( $\pm 2\sigma \times 10^6$ )	$^{143}\text{Nd}/^{144}\text{Nd}$ ( $\pm 2\sigma \times 10^6$ )	$\epsilon_{\text{Nd}}(0)$	$\Delta ^{87}\text{Sr}/^{86}\text{Sr}$	$\Delta \epsilon_{\text{Nd}}(0)$
A2-Leach	0.703399(17)	0.512928(11)	5.66	<b>0.000205</b>	<b>-0.02</b>
A4-Leach	0.713281(16)	0.512521(09)	-2.28	<b>0.003243</b>	<b>-1.25</b>
A4-Leach-repeated	0.713259(23)	N.M.	N.M.		
A5-Leach	0.708833(14)	0.512678(08)	0.78	<b>0.005476</b>	<b>-2.73</b>
A9-Leached	0.717688(16)	0.512156(18)	-9.40	<b>0.002088</b>	<b>+0.53</b>
A10-Leached	0.722897(16)	0.512067(07)	-11.14		

Tab. 7.15: Leached samples from the McMurdo Dry Valleys region

The isotopic field for all the available data is reported in Fig. 7.12, along with one other data for the fine fraction of a moraine sample from Terre Adélie (67°S, 140°E) from Grousset et al. (1992).

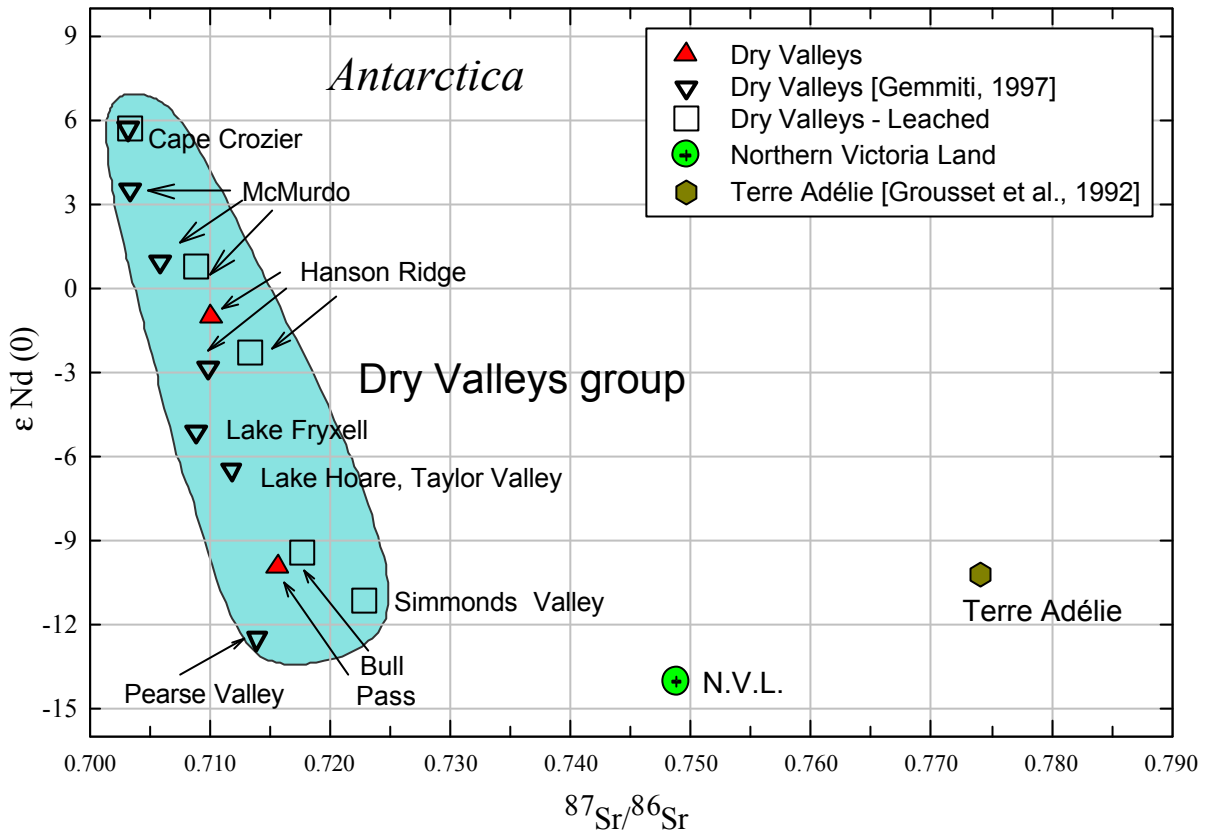


Fig. 7.12: Isotopic signature for the non-glaciated areas of Antarctica.

Samples from the exposed areas of coastal East Antarctica (Terre Adélie and Northern Victoria Land) show low radiogenic Nd values ( $\epsilon_{Nd}(0) < -7$ ) and highly radiogenic Sr ( $^{87}Sr/^{86}Sr > 0.717$ ), a signature that is typical of old continental crust and coherent at first approximation with the geological history of the East Antarctic.

Samples from the McMurdo Dry Valleys area, on the other hand, include glacial sediments that are mixture of crustal and volcanic rocks. The imprint of the recent (Late Miocene to present day) volcanism can justify the wide  $\epsilon_{Nd}(0)$  interval ( $-12.5 < \epsilon_{Nd}(0) < +5.7$ ). The interval for Strontium isotopes instead is relatively more restricted ( $0.703 < ^{87}Sr/^{86}Sr < 0.722$ ). The volcanic imprint is particularly evident in samples from Mc Murdo (Erebus volcano area) and Cape Crozier.

Because of such isotopic differences the two categories of samples will be considered as separate groups (“Coastal East Antarctica” and “Dry Valleys” group respectively).

### 7.2.4 South Africa

Five samples from South Africa have been analyzed in this work. The results are reported in Tab. 7.16 and in Fig. 7.13 , together with a sample from Grousset et al. (1992) from the Kalahari desert (<5  $\mu\text{m}$  fraction).

Original code	$^{87}\text{Sr}/^{86}\text{Sr}$ ( $\pm 2\sigma \times 10^6$ )	$^{143}\text{Nd}/^{144}\text{Nd}$ ( $\pm 2\sigma \times 10^6$ )	$\epsilon_{\text{Nd}}(0)$
NA1	0.721330 (117)	0.512098 (27)	-10.53
NA2	0.721042 (21)	0.512083 (09)	-10.83
NA3	0.722849 (19)	0.512104 (19)	-10.42
NA4	0.719708 (23)	0.512207 (20)	-8.41
S.AF.	0.747157 (33)	0.511382 (22)	-24.50

Tab. 7.16 : South African samples analyzed in this work

The five samples analyzed do not pretend to be exhaustive for whole South Africa. As for coastal East Antarctica, the signature of south Africa samples is typical for old crustal rocks and coherent with the first-order geological history of this region.

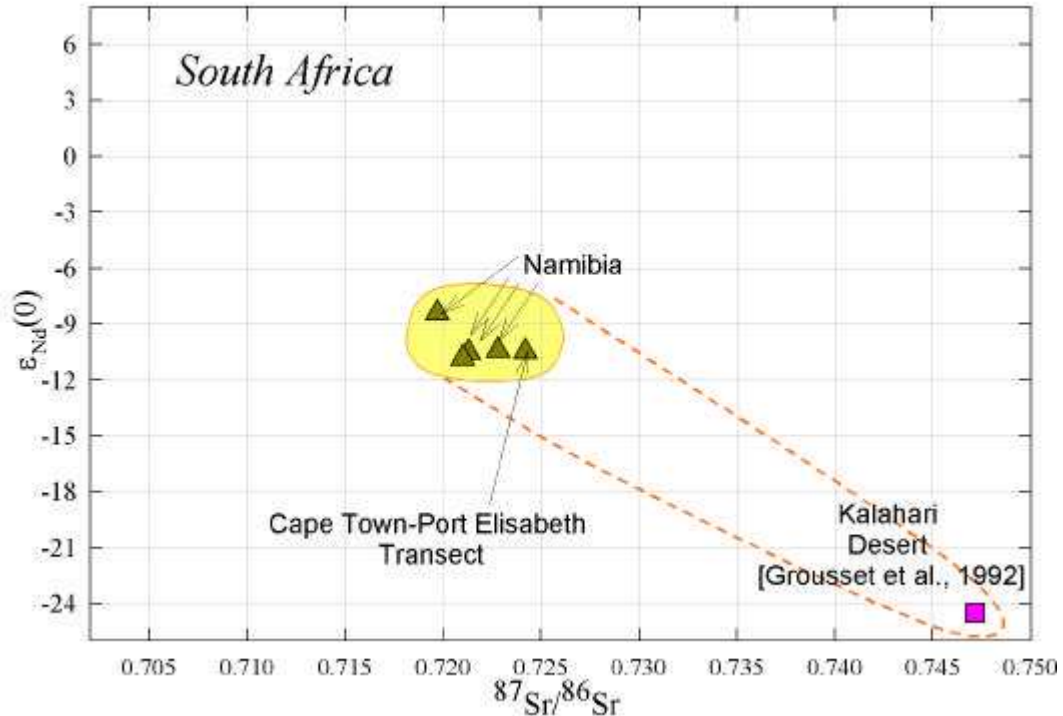


Fig. 7.13 : South African samples (fine fraction) analyzed in this work and in Grousset et al., 1992.

## 7.3 Discussion

### 7.3.1 The dust provenance in glacial periods

In § 7.1.1 it has been pointed out that the Sr-Nd isotopic ratios for EDC, Vostok, Dome B and KMS glacial samples are very similar among the sites and for all the climatic periods investigated. The reproducibility of a single measurement proved to be very good and no significant difference has arisen between the centrifuged dust samples and the isotopic signature of particles remaining in the supernate. This gives confidence to the dust extraction method used and to the analytical procedures.

Overall, the data are coherent with previous results from Basile (1997), Basile et al. (1997) and Grousset et al. (1992) on the Vostok (Stage 4, 6, 8, 10, 12) and on the old Dome C (Stage 2) ice cores.

The homogeneity in space and in time arising from the ICD isotopic signature suggests a common dominant source of dust for all glacial periods and over a large portion of the East Antarctic plateau.

In Fig. 7.14 the isotopic fields for all the candidate sources (<5  $\mu\text{m}$  fraction, unleached samples only) and the ICD are reported.

As already remarked, South Africa, Australia and the exposed rocks of coastal East Antarctica show the typical signature of old continental crust (low radiogenic Nd and highly radiogenic Sr) that is coherent at first approximation with the geological history of these continents, that originally constituted portions of Gondwanaland. On the other hand, the signatures of New Zealand, the Dry Valleys of Antarctica and southern South America partly overlap. This could be anticipated by their similar tectonic context, since all three are young orogenic environments marked by andesitic volcanic activity.

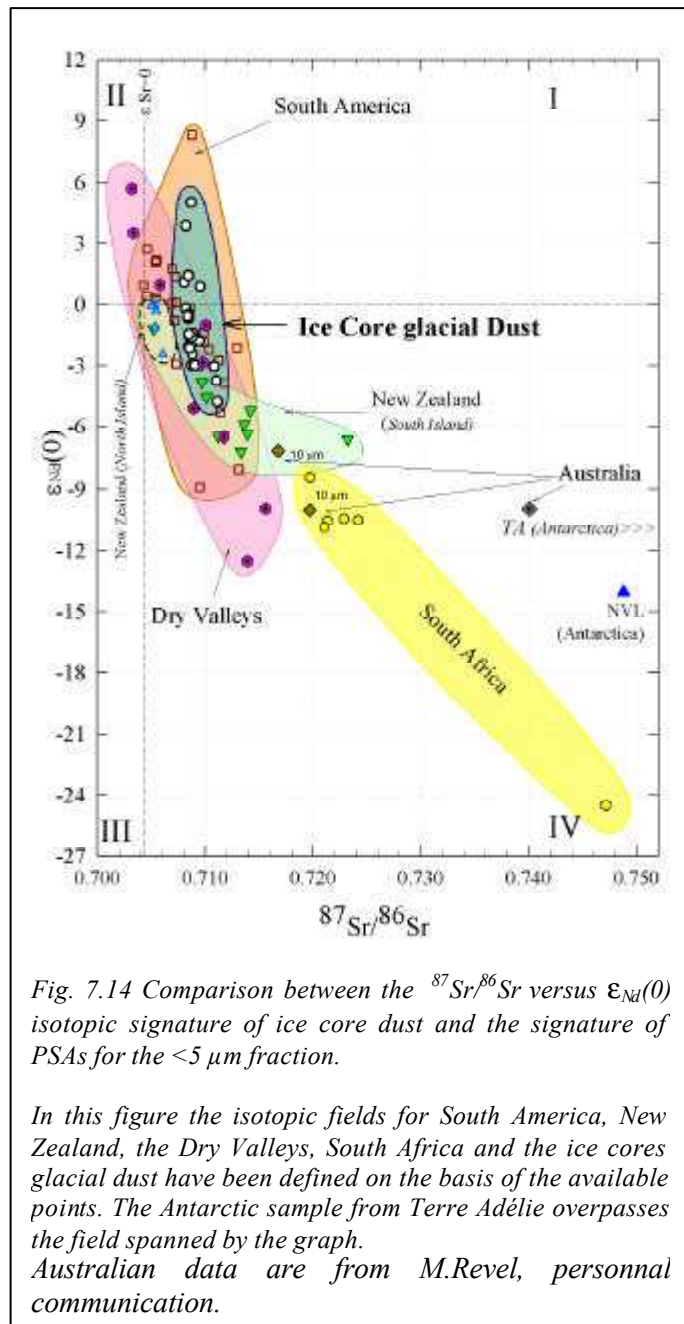


Fig. 7.14 Comparison between the  $^{87}\text{Sr}/^{86}\text{Sr}$  versus  $\epsilon_{\text{Nd}}(0)$  isotopic signature of ice core dust and the signature of PSAs for the <5  $\mu\text{m}$  fraction.

In this figure the isotopic fields for South America, New Zealand, the Dry Valleys, South Africa and the ice cores glacial dust have been defined on the basis of the available points. The Antarctic sample from Terre Adélie overpasses the field spanned by the graph. Australian data are from M.Revel, personal communication.

The isotopic fields for PSAs traced in this figure are based on a very limited number of samples, but nevertheless they are globally similar to the fields previously traced by Grousset (1992) and Basile (1997) and on the basis of bulk (all sizes) samples.

The Antarctic glacial dust appears very different from South Africa, Australia<sup>3</sup> and coastal East Antarctica and therefore these regions can be excluded as dominant sources in cold periods. On the opposite, the ice core dust signature is situated in the overlap region between New Zealand (South Island), the Dry Valleys and southern South America. If a possible contribution from all these three sources cannot be excluded from isotopic measurements only, many complementary arguments help in the interpretation.

### *The McMurdo Dry Valleys ?*

The samples from the McMurdo Dry Valleys consist of glacial sediments derived from the old East Antarctic continental shield<sup>4</sup> and mixed with young volcanic rocks (Late Tertiary and Quaternary).

The volcanic imprint is particularly evident in samples from Mc Murdo (Erebus volcano area) and Cape Crozier (see Fig. 7.12). Overall, the Strontium isotopes are restricted into the range  $0.703 < ^{87}\text{Sr}/^{86}\text{Sr} < 0.716$  while  $\epsilon_{\text{Nd}}(0)$  spans a relatively wider interval (+6 to -13).

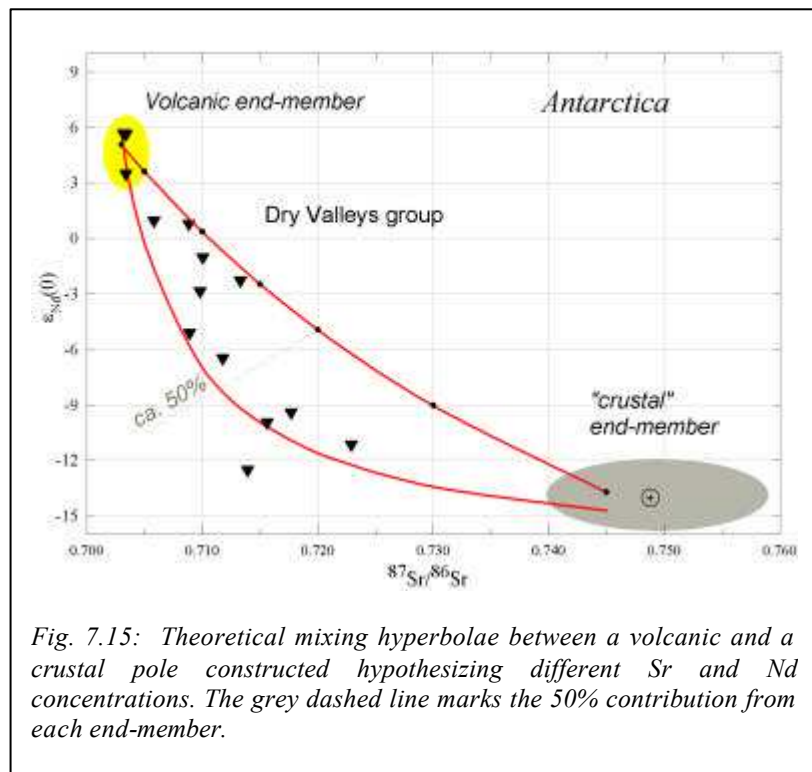


Fig. 7.15: Theoretical mixing hyperbolae between a volcanic and a crustal pole constructed hypothesizing different Sr and Nd concentrations. The grey dashed line marks the 50% contribution from each end-member.

<sup>3</sup> The two Australian samples reported in Fig. 7.14 have been analysed in Canberra by Dr. M.Revel-Rolland in the framework of a Franco-Australian collaboration that is in course. Samples were sorted around a modal value of 10  $\mu\text{m}$ .

<sup>4</sup> East Antarctica was part of the ancient continent of Gondwanaland and has many similarities with continents that were adjacent, such as Australia, South Africa, India and Brazil. It consists of a Precambrian to lower Paleozoic basement with a complex history and structure, intruded by granite and peneplained by weathering and glacial processes, underlying a large sequence of sediments of the Upper Paleozoic. Basic igneous rocks were intruded in Jurassic times within the basement rocks, and these rocks erupted in some places to form basalt flows and tuffs. No younger rocks are known in East Antarctica except for the volcanics that may range in age from 10 Ma to the present, erupted after the onset of glaciation in East Antarctica (Campbell and Claridge, 1987).

Hypothesizing two endmembers (volcanic and crustal) as in Fig. 7.15, it can be observed that almost all data are included within the mixing field.

Dust archived in the ice cores from East Antarctica shows a geochemical similarity with the Dry Valleys of Antarctica (Fig. 7.16). Therefore, a possible contribution from this region cannot be excluded. However, several complementary arguments suggest that this region was unlikely the principal dust source during cold stages.

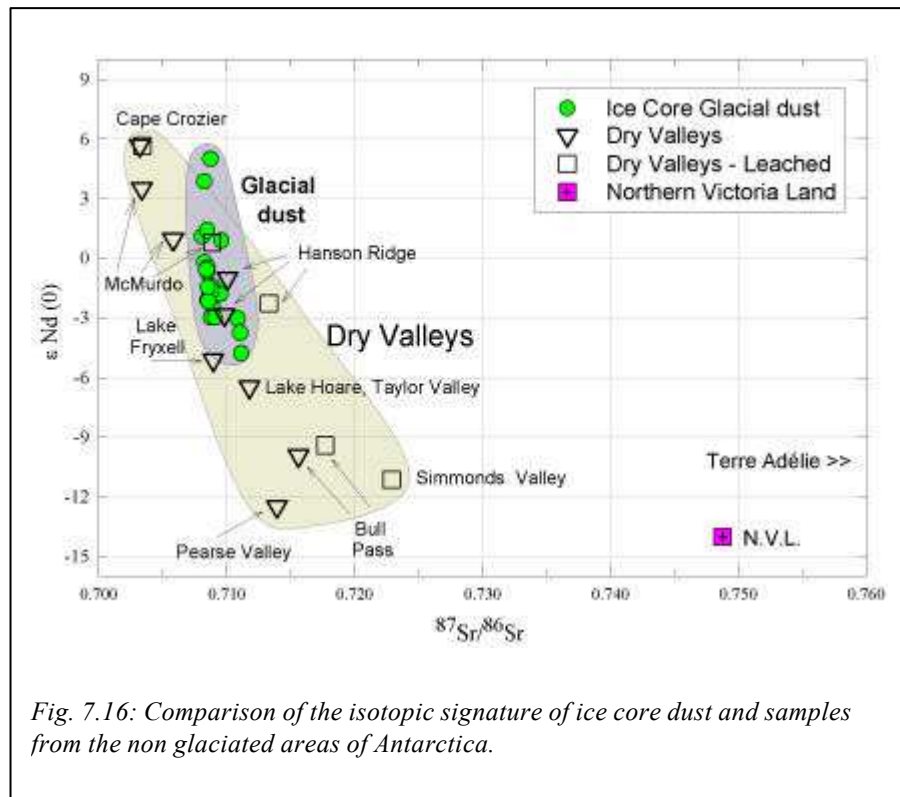


Fig. 7.16: Comparison of the isotopic signature of ice core dust and samples from the non glaciated areas of Antarctica.

First, in glacial times the ice-free areas were less extended than today, and the glacier's fronts were closer to the coast (Denton, 1991).

Second, the strong catabatic winds blow off the East Antarctic Plateau and carry the mineral aerosol towards the ocean (Schwerdtfeger, 1970). In order to be transported back to the high Plateau, the particles must be uplifted into the middle-high troposphere and finally advected into the Continent; this kind of transport is very unlikely.

A further argument suggesting the atmospheric transport from West to East Antarctica is not usual is the presence of only one volcanic tephra layer from Marie Byrd Land volcanoes in the Vostok ice core during the last 420 kyrs (Basile et al., 2001) and one in the Dome C core (Kyle et al., 1981). This volcanic province of West Antarctica has been very active in the late Pleistocene, as evidenced by the ~2000 visible ash layers of the Byrd ice core (Gow and Williamson, 1971), but the transport to the inner Plateau seems not favoured.

Finally, a dust advection from the Dry Valleys would carry considerable amounts of salts into the polar Plateau, in particular carbonates and gypsum (e.g. Campbell and Claridge, 1987) that have not been found in Antarctic ice (De Angelis et al. 1992).

**New Zealand ?**

New Zealand is a long and narrow twin island lying south of 35°S and characterised by latitudinal and longitudinal climatic and environmental differences. Southern regions are primarily under the influence of the westerly winds, while the northern regions extend into the subtropical ridge of high pressures. The South Island is traversed southwest-northeast by the Southern Alps and contrasting temperature and precipitation regimes exist in function of longitude. During LGM windiness increased in the South Island, where ice cover was extended to the coastal lowlands of the central west coast and some loess deposits were formed (McGlone et al., 1993).

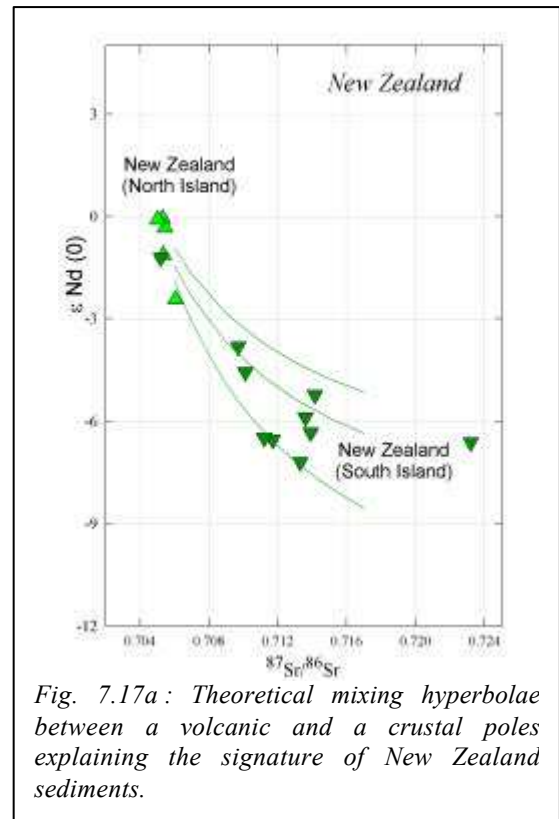


Fig. 7.17a : Theoretical mixing hyperbolae between a volcanic and a crustal poles explaining the signature of New Zealand sediments.

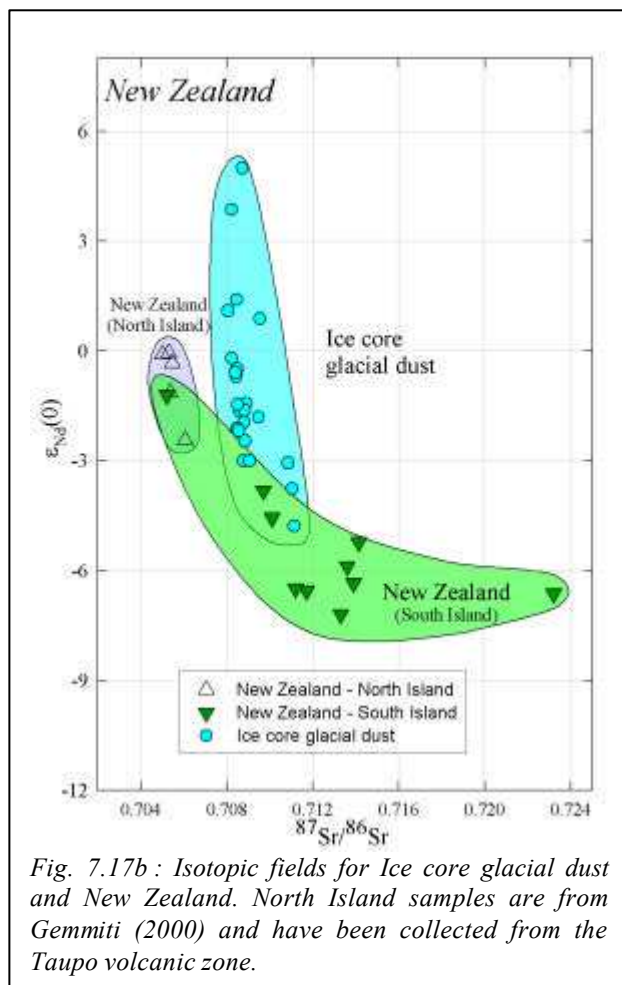


Fig. 7.17b : Isotopic fields for Ice core glacial dust and New Zealand. North Island samples are from Gemmiti (2000) and have been collected from the Taupo volcanic zone.

The samples from the North Island keep the imprint of recent volcanic activity<sup>5</sup> within this region.

Also in the Canterbury and Otago districts of the South Island there are volcanic rocks (tholeiitic to alkaline basaltic rocks, heritage of Miocene and Pliocene intraplate volcanism), but overall the sediments from the South Island (samples NZ1 to NZ10) appear slightly less radiogenic in Nd than in the North. Most of them span the isotopic field  $0.709 < ^{87}\text{Sr}/^{86}\text{Sr} < 0.723$  and  $-3.8 < \epsilon_{\text{Nd}}(0) < -7.2$ , with only one exception.

The whole set of samples obtained from New Zealand seems aligned along a mixing hyperbola between a volcanic and a crustal pole (Fig. 7.17a).

<sup>5</sup> Volcanic activity within the Northland Volcanic Arc until 15 Myrs ago, the Hauraki region in the late Pleistocene, and the Taupo Volcanic Zone for present time.

Rhyolites, andesites and dacites are common rocks in the North Island



The ice core dust glacial field partially overlaps that of the South island of New Zealand, as shown in Fig. 7.17b. However, this region has very limited surface extent and therefore seems unlikely the main responsible for the high dust flux in glacial periods. Moreover, if the atmospheric circulation was favourable to such a transport it would be surprising that no contribution from the nearby large deserts of Australia is detected. Finally, the absence of tephra layers from the Taupo Volcanic Zone in the Vostok ice core for the last 420,000 years (Basile et al., 2001) also suggests an atmospheric path quite unfavourable from this region.

### ***Southern South America: the dominant source***

The southern part of South America is under the continuous flux of Westerly winds. Moisture is largely removed from the air masses as they pass over the Andes, and the eastern side of the mountain chain in an extensive rain-shadow zone with very low annual rainfall. This region has geomorphologic and environmental conditions favourable for primary production, mobilization and transport of fine grained dust (Clapperton, 1993). As described in § 1.4.1, several aeolian deposits characterize southern South America both in the Chaco-Pampa plains - where in Quaternary times the Pampean Aeolian system was formed - and further south in Patagonia (Iriondo, 1999).

During cold periods the primary production of particles was enhanced. Continental glaciers favoured the alteration of primary rocks, providing sandy and silty particles. These can be either *primary* sources for long-range dust transport or they can be mobilized and transported (in liquid or aeolian phase) to another site topographically suitable for concentration of sediments. In this latter case they can become *secondary* sources for mineral aerosol. A good example are the plains east of the Andean Cordillera, where fluvio-glacial deposits, alluvial fans and widespread loess and loess-like deposits have been generated.

Sediments from the andesites and the volcanic rocks of the Cordillera keep the typical signature of their parent rock; such particular signature distinguishes Patagonian loess from all other loess deposits around the world, in particular from those of the Northern Hemisphere (Gallett et al., 1998).

In this work South America has been detailed at high degree through samples from the Pampas, Patagonia and Chilean Andes, but no sample from the Antarctic Peninsula has been analysed. This latter region was formed within the Andean orogeny and constitutes a prolongation of the Andes of South America. Therefore, a first order geochemical similarity with southern South America should be expected.

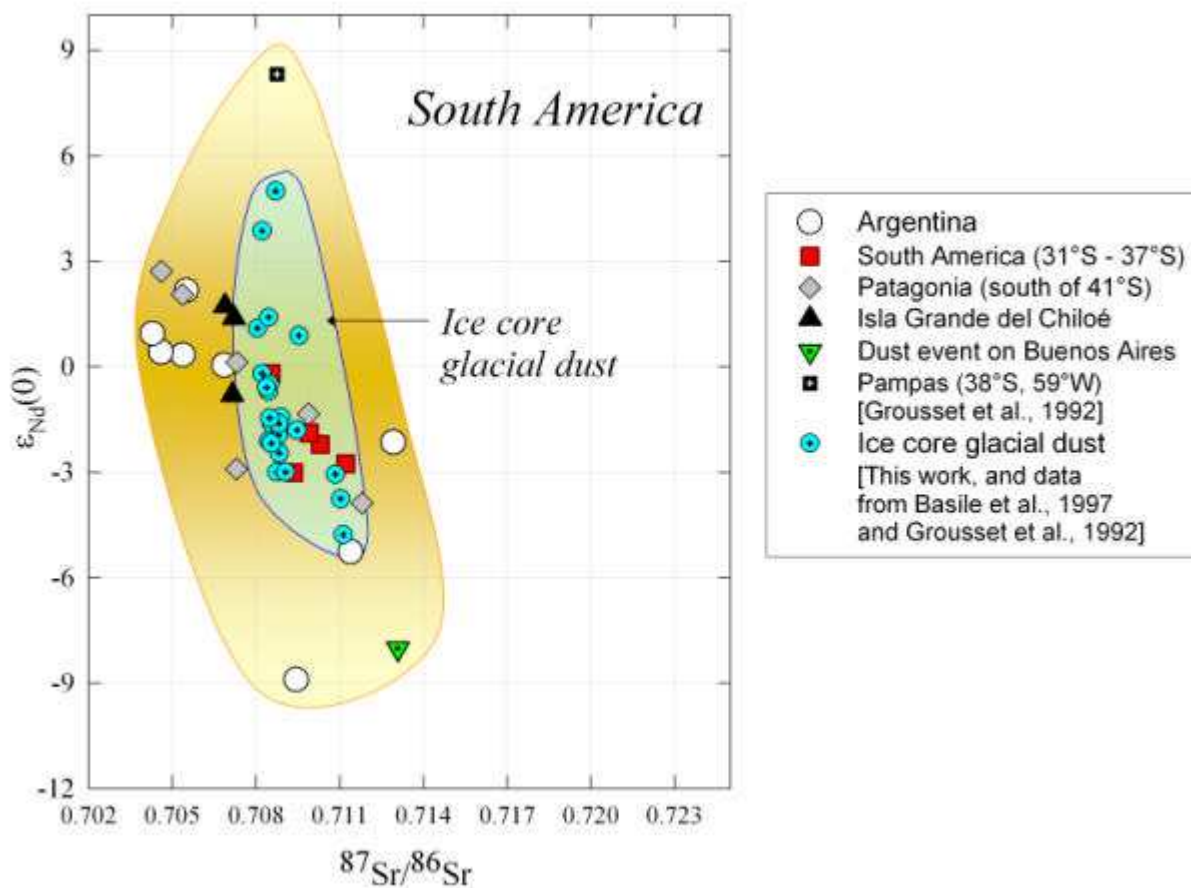


Fig. 7.18 : Comparison between ice core dust signature and fine (<5  $\mu\text{m}$ ) fraction of South America samples.

The isotopic field of the <5  $\mu\text{m}$  fraction of south American samples (Grousset et al., 1992; Gemmiti, 2000; this work) is reported in Fig. 7.18. Results shows that it is difficult to distinguish sub-fields for the different sub-regions (Pampas, Patagonia, Argentina, etc.), and therefore -at this step- southern South America can be considered homogeneous from the isotopic point of view.

In figure 7.19 are plotted only the samples analysed in this work (see Tab. 6.4 for their geographic origin); it can be noticed that the values appear aligned along a mixing hyperbola between two end-members, one more radiogenic in Nd and less radiogenic in Sr (e.g. volcanic) and another one with opposite characteristics.

Southern South America was probably the dominant source for East Antarctic dust in glacial times, as already evidenced by Basile (1997) and Grousset (1992) on the basis of its geochemical signature, and by Gaudichet et al. (1986) on the basis of mineralogical data.

A favourable atmospheric pathway from southern South America seems suggested also by the South Atlantic origin (South Sandwich Island and the Antarctic Peninsula) of the volcanic tephra layers of the Vostok ice core (Basile et al., 2001).

Moreover, recent Atmospheric circulation models for LGM (Lunt and Valdes, 2002) also support this hypothesis and the authors estimate the Patagonian source (31°S-50°S) as about 620% stronger than today, when the decreased soil moisture and vegetation and the increase in land area due to sea level fall are considered. Dust transport simulations for the LGM (Andersen, 1998) evidenced from spring to fall a preferential advection from South America.

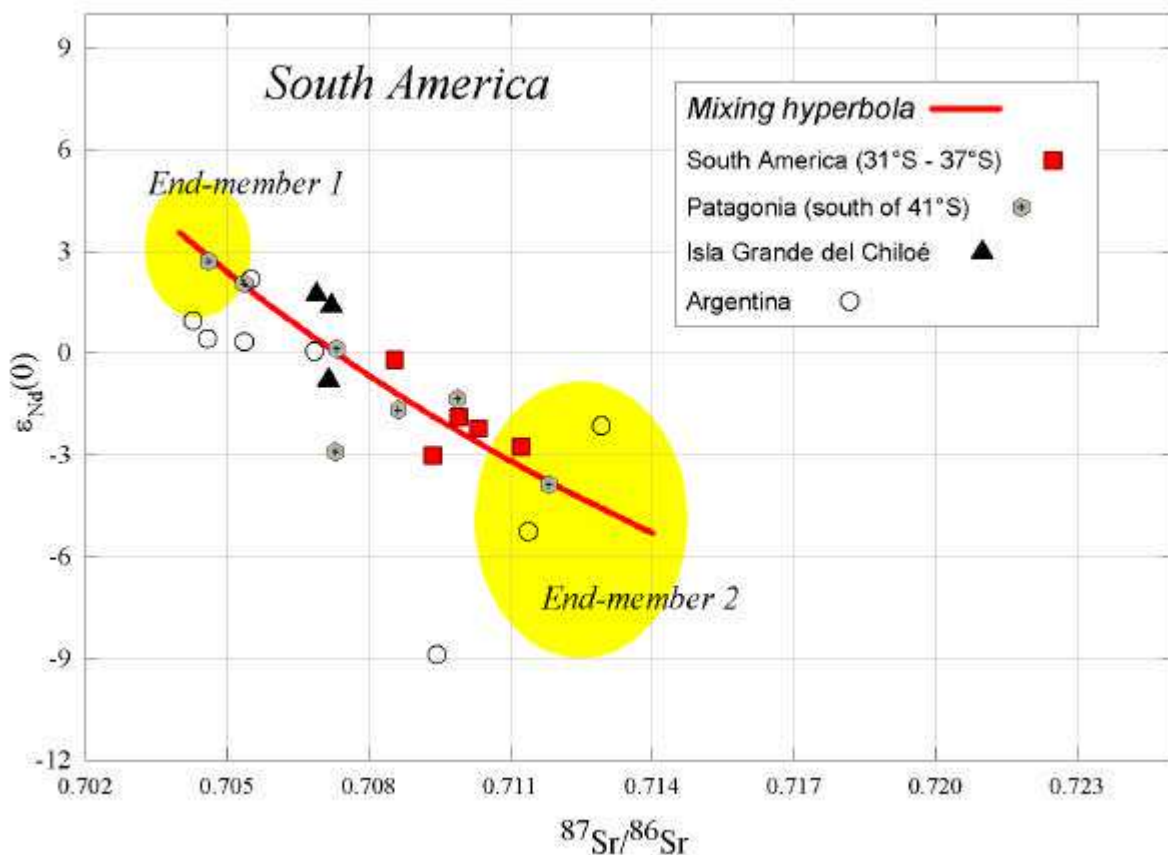


Fig. 7.19: South America samples analysed in this work and theoretical mixing hyperbola traced on the basis of two end members, one volcanic and the other with more crustal character.

Bibliographic data exist on *bulk* (all sizes) samples from Patagonian loesses (from Gallett et al. 1998, and Grousset et al., 1992), the Argentine continental shelf (from Basile et al., 1997), the Andean lavas and Andesites (from Hawkesworth et al, 1979; Francis et al., 1977; Futa and Stern, 1988), and they are reported in Fig. 7.20.

Andesites and lavas are very low radiogenic in Sr and span a wide range of  $\epsilon_{Nd}(0)$ . The Argentine continental shelf keeps almost the same signature of the loess (Gallett et al., 1998, Fig. 7.19) since

the primary material is the same. In glacial periods, when the sea level was lower, the shelf was exposed and constituted a possible source for dust.

As expected, the fine fraction of sediments brings on average a  $^{87}\text{Sr}/^{86}\text{Sr}$  signature more radiogenic than the bulk.

With such grain-size effect, the ICD isotopic field is completely surrounded by the South American samples, while it was not the case when bulk samples were considered (Basile et al., 1997).

The slight offset towards more radiogenic  $^{87}\text{Sr}/^{86}\text{Sr}$  values of the Antarctic ICD samples with respect to bulk sediments was attributed by Basile et al. (1997) either to a possible contribution of another source, like Australia or South Africa (10-15% maximum) or to a grain-size effect (see § 4.4.1). The new data favor this latter hypothesis (Fig. 7.20).

\*\*\*\*\*

### Glacial dust: conclusions

Dust reaching East Antarctica shows the same isotopic signature at the different sites and for all the glacial periods investigated, suggesting a common and unvarying provenance.

A strict geochemical similarity arises between ice core glacial dust and the signature of Southern south

America, the Antarctic Dry Valleys and New Zealand, these two latter documented for the first time.

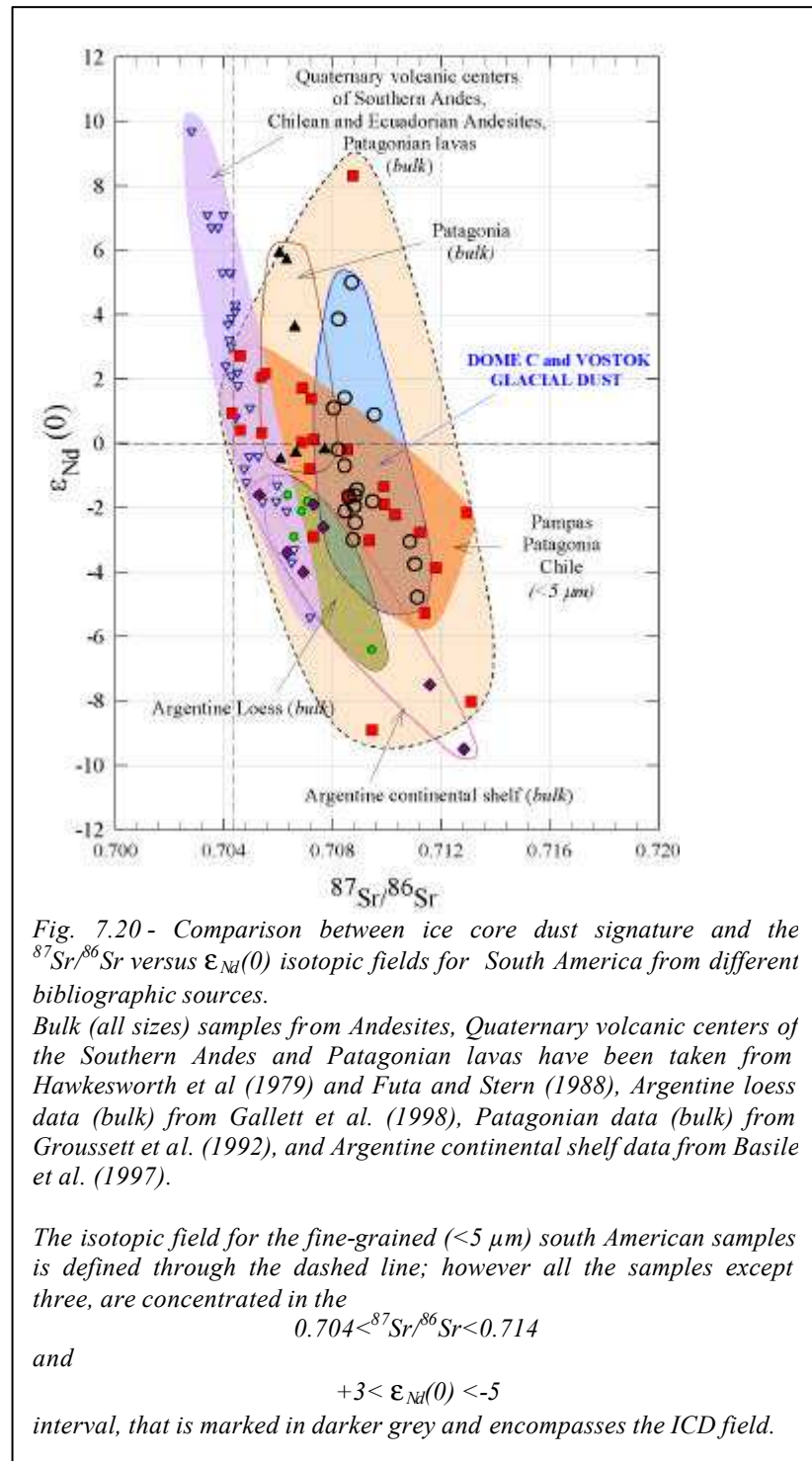


Fig. 7.20 - Comparison between ice core dust signature and the  $^{87}\text{Sr}/^{86}\text{Sr}$  versus  $\epsilon_{\text{Nd}}(0)$  isotopic fields for South America from different bibliographic sources.

Bulk (all sizes) samples from Andesites, Quaternary volcanic centers of the Southern Andes and Patagonian lavas have been taken from Hawkesworth et al (1979) and Futa and Stern (1988), Argentine loess data (bulk) from Gallett et al. (1998), Patagonian data (bulk) from Grousset et al. (1992), and Argentine continental shelf data from Basile et al. (1997).

The isotopic field for the fine-grained (<5  $\mu\text{m}$ ) south American samples is defined through the dashed line; however all the samples except three, are concentrated in the

$$0.704 < ^{87}\text{Sr}/^{86}\text{Sr} < 0.714$$

and

$$+3 < \epsilon_{\text{Nd}}(0) < -5$$

interval, that is marked in darker grey and encompasses the ICD field.

If a possible contribution from all of them cannot be excluded from isotopic measurements alone, several complementary arguments suggest southern South America as the most probable source area in glacial times.

### 7.3.2 The Interglacials

The Quaternary climatic and environmental changes occurred between glacial and interglacial stages modified sensibly the conditions in continental areas; for example, vegetation cover and pedogenesis developed, sea level rose, hydrological conditions changed as well as the atmospheric circulation.

The EDC ice core has shown unequivocal changes in dust size between glacial and interglacials (§7.1.2), suggesting variations in the atmospheric circulation. In front of these observations a basic question arises: is the dust geographic provenance the same in warm and in cold periods?

Despite the limited number of samples (four Holocene samples, one sample from interglacial stage 5.5 in EDC core and one  $^{143}\text{Nd}/^{144}\text{Nd}$  value for stage 5.5 in Vostok core), the isotopic signature of interglacial samples appears clearly less radiogenic in Nd with respect to glacial dust (Fig. 7.7 and 7.21).

This suggests a possible contribution from an additional source during warm periods. In §7.3.2 some hypothesis are made.

An interesting point to underline is that the glacial/interglacial isotopic difference is unlikely due to environmental changes occurring at the source through environmental processes like pedogenesis.

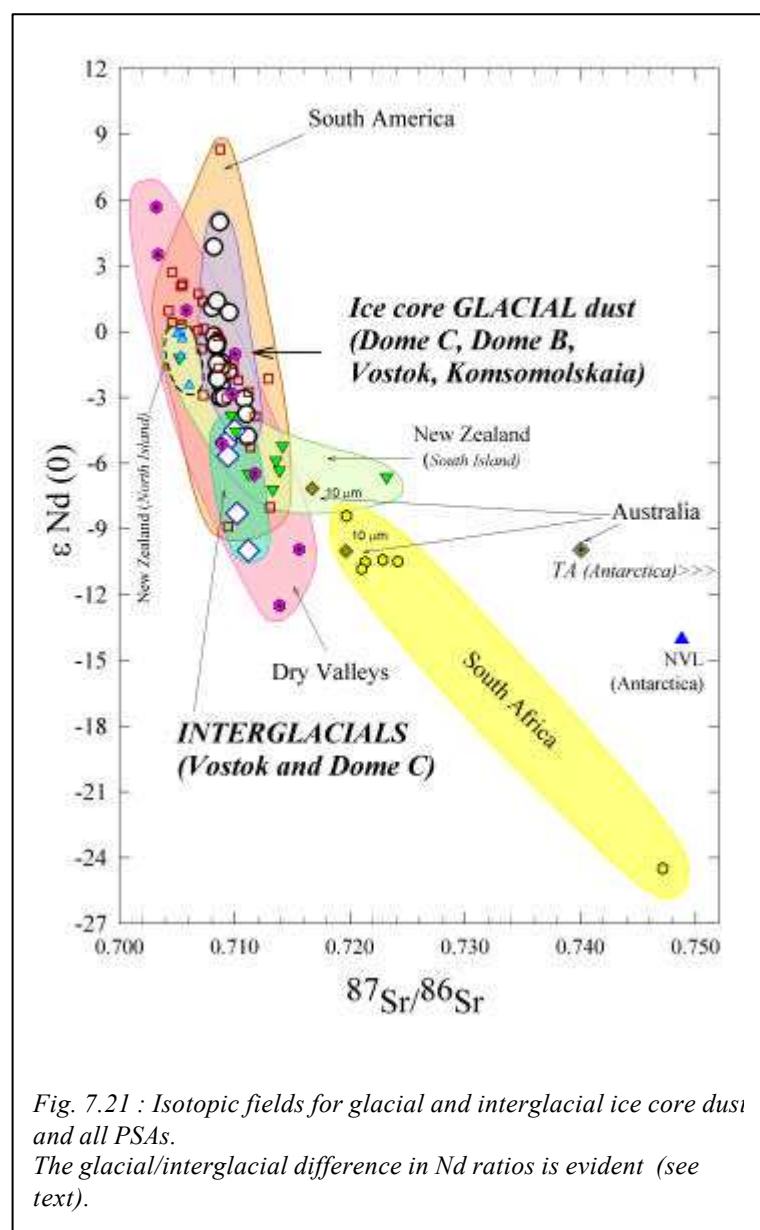


Fig. 7.21 : Isotopic fields for glacial and interglacial ice core dust and all PSAs. The glacial/interglacial difference in Nd ratios is evident (see text).

In fact, the chemical alteration of primary rocks can induce a fractionation between Rb and Sr<sup>6</sup> but not between Sm and Nd, both characterized by very low solubility in water. Chemical weathering linked to soil development therefore could be expected to induce eventually a shift in Sr rather than Nd.

### Dust sources during interglacials: some hypothesis

#### *South America?*

The overall isotopic field that can be deduced from the available fine-grained south America samples shows the highest frequency into an interval of  $\epsilon\text{Nd}(0)$  more radiogenic with respect to interglacial dust.

The interglacial isotopic signature therefore could be hardly explained solely by a South America dust provenance.

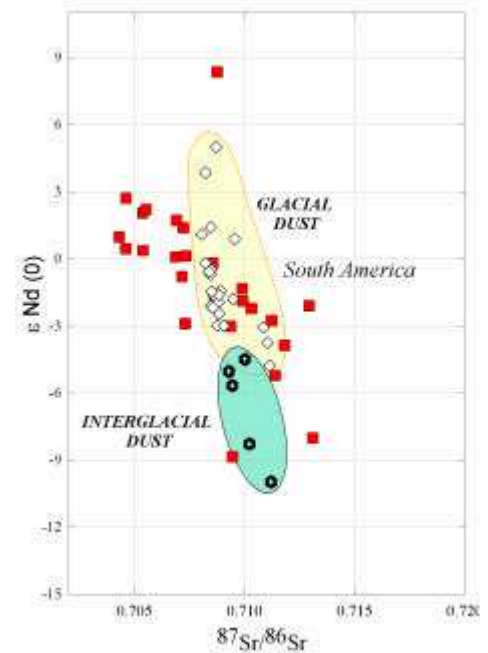
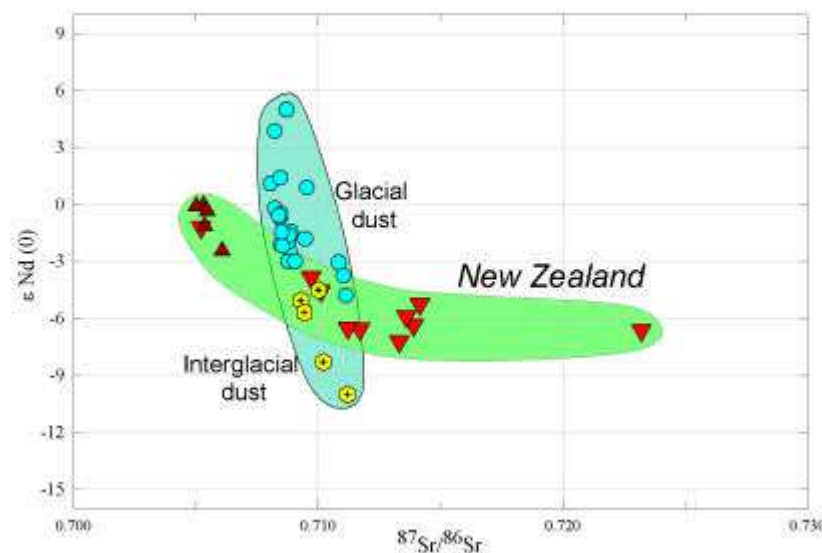


Fig. 7.22 : Isotopic fields for glacial and interglacial dust and South America.



#### *New Zealand?*

The isotopic field for New Zealand defined by the samples analysed in this work varies largely in Sr, and crosses the ice core dust one. However, New Zealand Nd values seem not sufficiently negative to account for the variability of interglacial dust isotopic signature.

Fig. 7.23: Isotopic fields for ice core dust and New Zealand (<5 $\mu\text{m}$ ).

<sup>6</sup> Strontium is more soluble than Rubidium. This latter has affinity for clay minerals (as K), while the former is loss to solution during weathering (with Ca). The fine-grained silicate clastic sediments have therefore a high Rb/Sr ratio and hence develop in time a high  $^{87}\text{Sr}/^{86}\text{Sr}$  (Bickle, 1994).

### **Dry Valleys?**

The signature of the fine-grained fraction (<5 µm) of the Dry Valleys samples embraces the ice core dust interglacial and glacial fields. This suggests a possible contribution from the dry Valleys region.

The clay mineral composition of dust in Antarctic ice and in the non-glaciated areas of Antarctica also does not allow to exclude this region as possible source. Illite has been identified as the most abundant clay mineral in Antarctic ice, together with minor proportions of smectite and chlorite, and rare kaolinite (see Gaudichet et al., 1992). The exposed areas of East Antarctica are also characterised by abundant illite and micas with variable degree of weathering, and minor amounts of chlorites (see Campbell and Claridge, 1987). However, calcite (and gypsum) encrustations are quite common in coastal East Antarctica, while they are absent in Antarctic ice<sup>7</sup>. The exposed areas of coastal Antarctica are also very rich in salts derived from rock weathering or having marine origin (close to the coast).

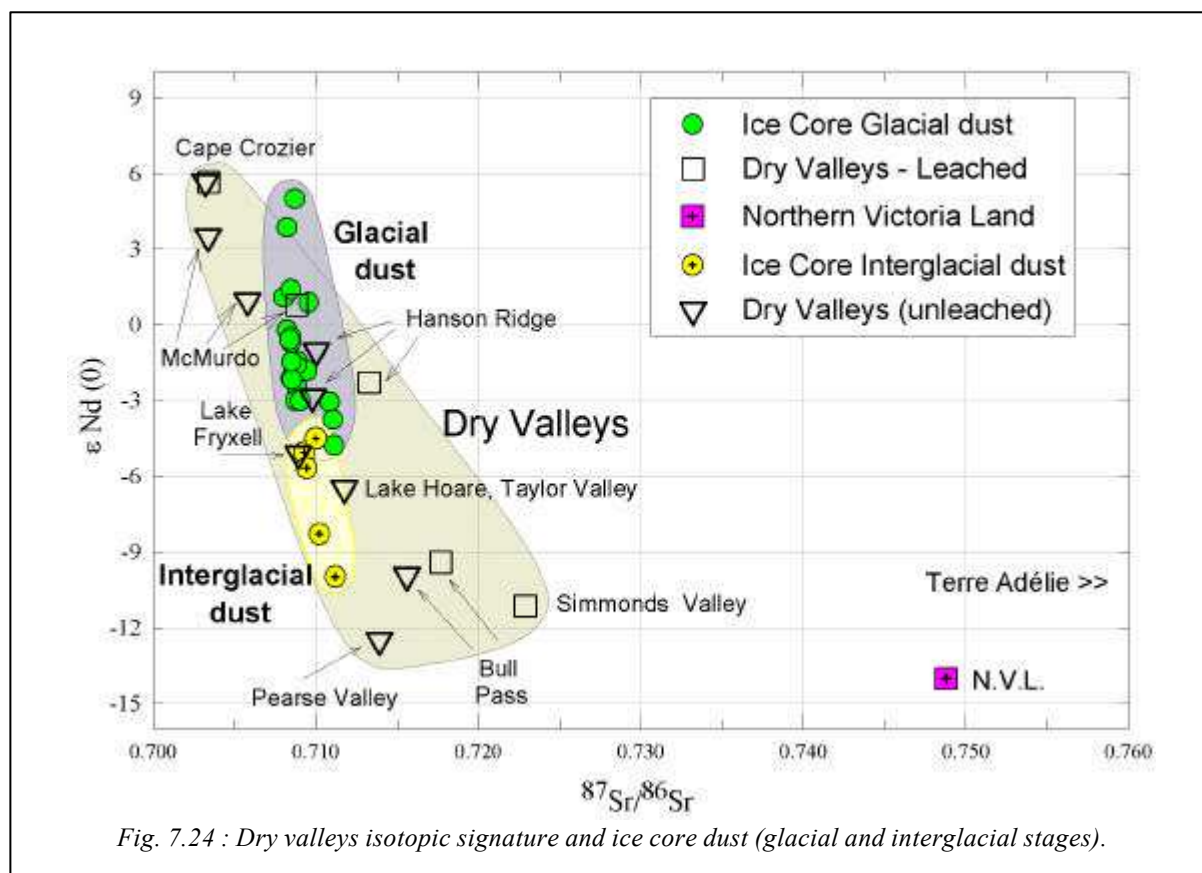


Fig. 7.24 : Dry valleys isotopic signature and ice core dust (glacial and interglacial stages).

A direct atmospheric transport of dust from the Dry Valleys to the interior of the high plateau seems not favoured by the strong catabatic winds blowing off the continent and towards the sea. Mesoscale cyclonic activity (e.g. in the Ross Sea region) can allow air uplift and advection of mild and moist

<sup>7</sup> However, calcite could be present at the source and lost en route through interaction with acid aerosol.

maritime air towards the ice-sheet interior (Gallée, 1996), but the influence of such vortices is limited to the lower tropospheric levels (Carrasco et al., 2003).

The isotopic resemblance of ice core dust with the Dry Valleys field, therefore, could be misleading and must be considered with caution.

Actually, the isotopic signature of interglacial dust could be obtained through mixing of two different end-members. Mixing hyperbolae can be defined on the basis of the Sr and Nd concentrations and isotopic composition of the end-members (see Faure, 1986).



### ***South America and Australia?***

In Fig. 7.25 three theoretical mixing lines have been traced between a south American end-member, established through the average Sr-Nd isotopic ratios for all the south America samples analysed in this work (Tab. 7.8), and an Australian end-member established through the available bulk and fine-grained samples (M. Revel, personal communication).

This exercise performed allows to observe that the isotopic field of interglacial dust can be crossed by mixing lines, and that the minimum contribution from Australia that is necessary to obtain the values observed is in the order of 20 % to 35% .

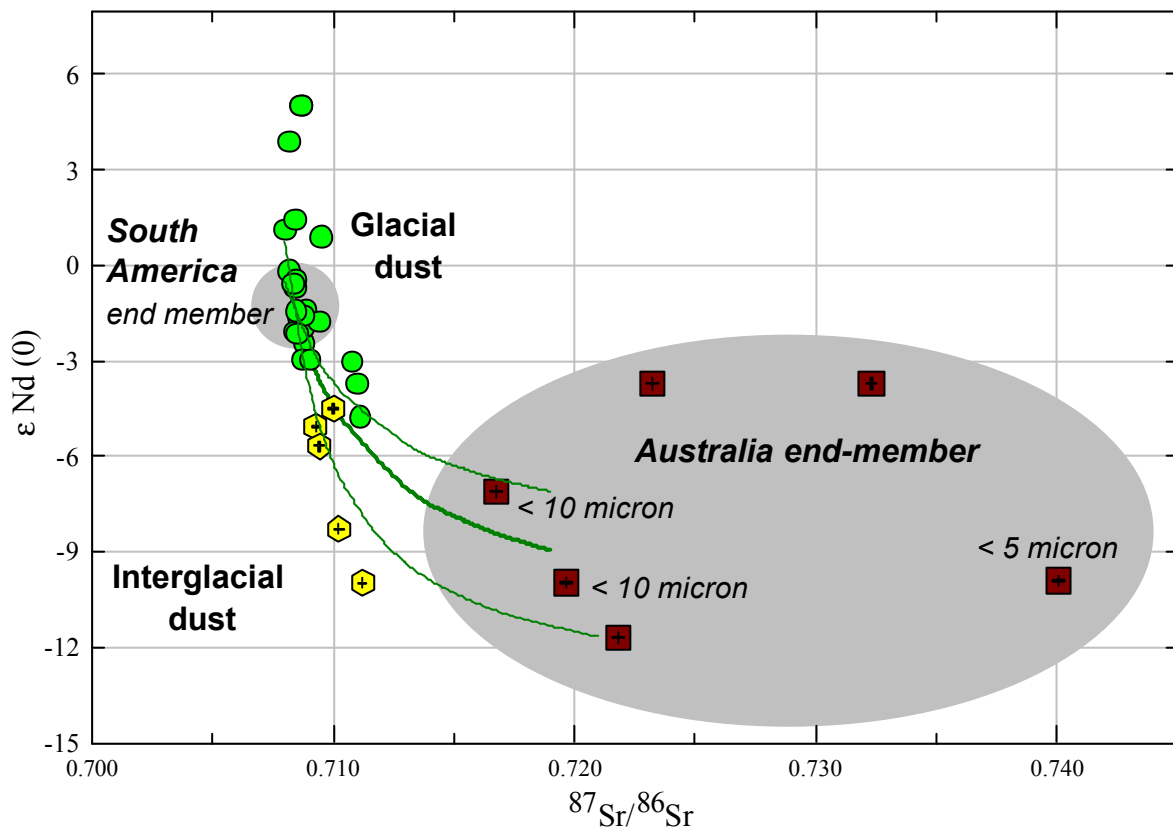


*Fig. 7.25 : Theoretical mixing hyperbolae between South America and Australia end members.*

*In this figure the south America end member is kept constant and has been characterized with average Upper Continental Crust concentrations (Taylor and McLennan, 1985) of Sr (350 ppm) and Nd (26 ppm) and  $^{87}\text{Sr}/^{86}\text{Sr} = 0.708365$  and  $\epsilon_{\text{Nd}}(0) = -1.3$ . The Australian end member is defined on the basis of a limited number of samples. The three lines represent different hyperbolae constructed on the basis of slightly different isotopic values and crustal abundances for both elements.*

The hyperbolae that can be traced are different according to the characterisation of the end-members. The fine-grained samples available for Australia are not representative for such large continent, and therefore a more accurate estimation of the possible Australian contribution to interglacial dust can be evaluated more precisely only after a more complete documentation of this potential source.

### *South America and South Africa?*

The theoretical mixing hyperbolae traced between a South American pole (defined on the basis of the average values of South America samples) and two possible end-members from southern Africa (Namibia and southern Cape, and the Kalahari Desert) do not cross the interglacial dust field (Fig. 7.26). Despite the number of south Africa samples is very limited, this pole seems unlikely a candidate contributor for interglacial dust in Antarctica.

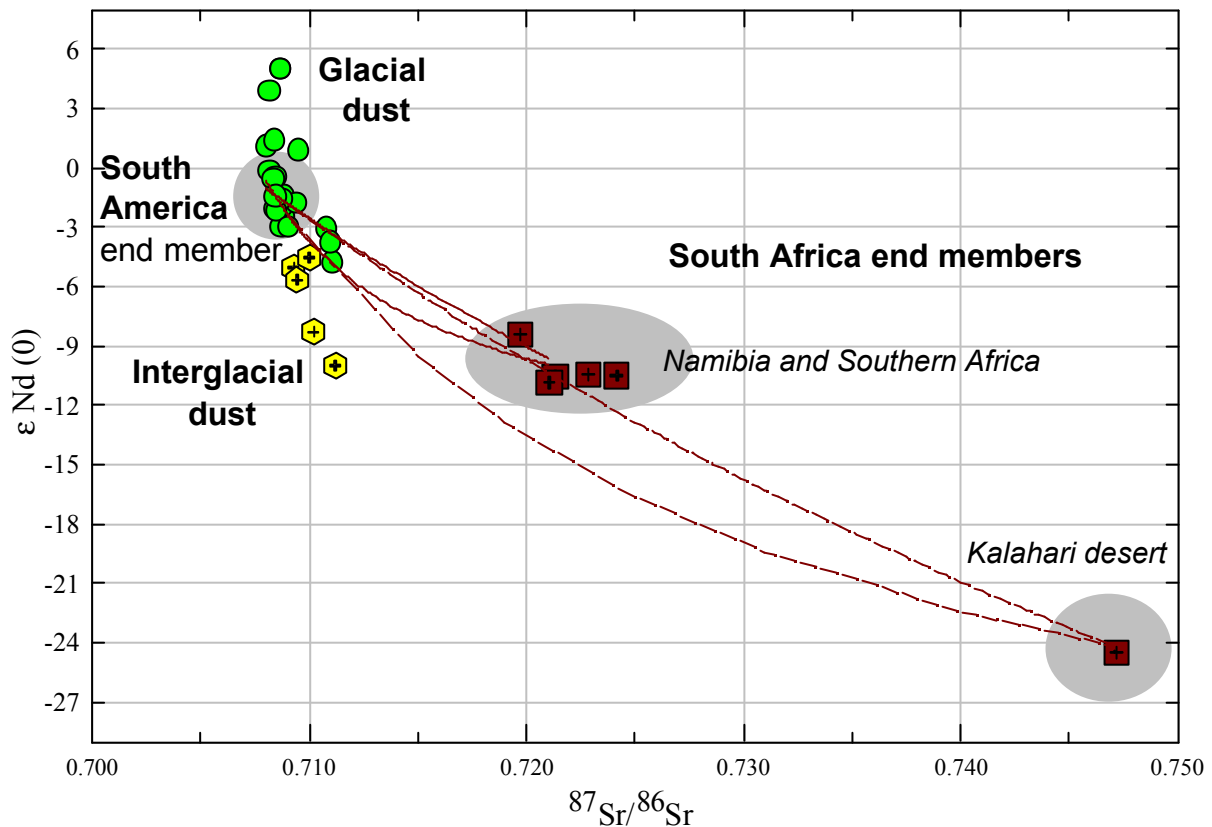


*Fig 7.26: Theoretical mixing hyperbolae between South America and a south Africa end-members. The Sr-Nd isotopic ratios for the different poles represent the average value of the samples analysed in this work (<5 micron fraction). The Kalahari sample has been taken from Grousset et al. (1992). Two hyperbolae per each couple of end-members have been traced assuming varying abundances of Sr and Nd.*

### *South America and Antarctica?*

The exposed rocks of coastal East Antarctica can be reasonably discarded as possible source. The high radiogenic Sr values of the samples from these regions, as for South Africa, impedes every realistic mixing hyperbola to cross the interglacial dust field (Fig. 7.27).

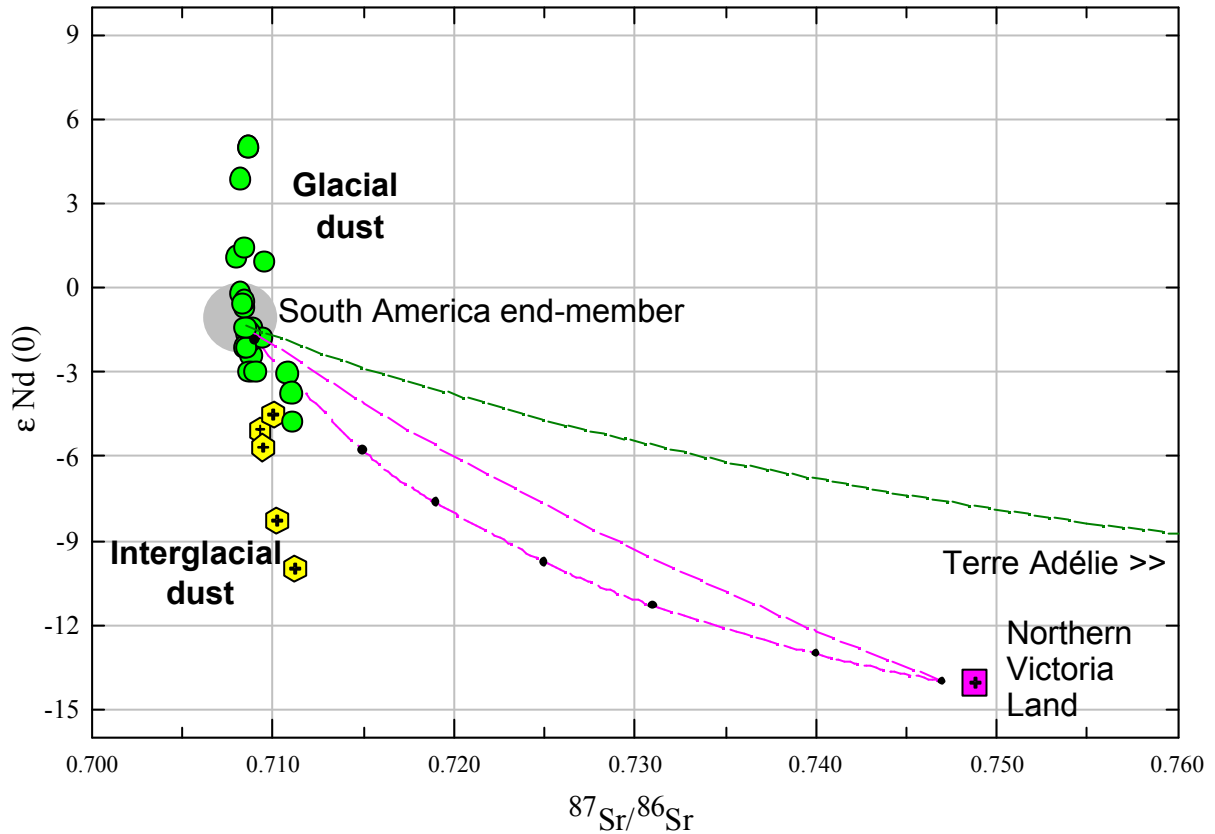


*Fig. 7.27: Theoretical mixing hyperbolae between South America and the non glaciated areas of East Antarctica (Northern Victoria Land and Terre Adélie).*

*The Sr-Nd isotopic ratios of the different poles represent the average value of the fine-grained (<5  $\mu m$ ) samples analysed in this work. The Kalahari sample has been taken from Grousset et al. (1992). Two hyperbolae per each couple of end-members have been traced assuming varying abundances of Sr and Nd.*

\*\*\*\*\*

### **Interglacial dust: conclusions**

Five interglacial samples show an isotopic signature significantly different in Nd from glacial dust, and the Southern south America isotopic field seems not sufficient to account for the differences observed. Data suggest the possibility of an additional source for dust during warm periods.

The similarity arising between the ice core interglacial dust and the Dry Valleys isotopic field suggests a possible contribution from these areas, but such apparent match could be fictitious and seems not confirmed by complementary arguments.

A contribution from rock outcrops of coastal East Antarctica and from south Africa can reasonably be discarded from isotopic arguments; on the other hand, a mixture of Australia and south America dust seems quite probable, but further measurements on PSA samples from Australia are needed to document this latter end-member at higher detail.

### 7.3.3 The Sr contribution from carbonates

For the PSA samples, the results have shown that the leaching procedure induced shifts in the isotopic composition of Sr isotopes systematically towards more radiogenic values.

For the ice core dust, the single leaching experiment performed on one Dome B glacial (stage 2) sample has shown no changes in Sr isotopic composition, confirming observations of different authors (e.g. Legrand and Mayewski, 1987; De Angelis et al., 1992 and Anklin et al., 1995) that there are no carbonates in East Antarctic ice. This is coherent also with the ice pH slightly acid (about 5.5). Moreover, the absence of carbonates in particles extracted from the ice is proved by some analysis made on filtered dust ( $>0.4 \mu\text{m}$ ) from the Old Dome C core, that evidenced a Ca/Al ratio impoverished respect to the Upper Continental Crust (De Angelis, personal communication).

The lack of carbonates in Antarctic ice could be due to:

(1) absence of such compounds at the source

and/or

(2) loss *en route*: in this case the calcite originally present in the dust at the source is weathered during atmospheric transport through reactions with acid aerosol (De Angelis et al., 1992). From the PSA to the Plateau in fact, dust encounters acidifying species in the atmosphere that can partially weather compounds en route.

Anyway the question about the comparison between the ICD signature and the PSA (see § 4.4.1) remains opened.

Previous authors (Basile et al., 1997) adopted an “*unleached-unleached*” strategy for Antarctic ice. In the present study we followed basically this latter approach, but have also performed several leaching tests to enlarge the PSA fields of the unleached samples for the maximum “ $\Delta \text{}^{87}\text{Sr}/\text{}^{86}\text{Sr}$ ” due to eventual carbonate contribution. *If the carbonate contribution is taken into consideration, the PSA fields result enlarged but the general conclusions drawn for dust provenance do not change.*

An important point to note is that the leaching procedure is supposed to remove exclusively carbonates from the samples; however, it cannot be excluded a possible *bias* on other phases. The labile volcanic glasses or the clay minerals, for instance, where strontium resides adsorbed on mineral surfaces and in interlayer sites could have been influenced by the leaching procedure. Such a possible isotopic *bias* (if it does exist) is difficult to quantify, and the measure of both leached and unleached fine-grained samples would be recommended to estimate the maximum  $\Delta \text{}^{87}\text{Sr}/\text{}^{86}\text{Sr}$  for carbonate contribution.

\*\*\*\*\*                   \*\*\*\*\*                   \*\*\*\*\*

### Summary

*EDC, Dome B, KMS and Vostok ice cores show identical Sr-Nd isotopic imprint for glacial dust, suggesting a common geographical provenance at all sites and for all cold stages. Comparison with samples from PSA selected in the equivalent size range, in association with complementary arguments, suggests southern South America as the most probable contributor.*

*Interglacial dust signature from EDC and Vostok differs significantly from glacial dust, and a mixture between South America and Australia is possible.*

*The isotopic fingerprint of dust is often insufficient alone to distinguish between different sources and has to be associated to complementary arguments of various nature.*

## **Chapter 8 - RESULTS AND DISCUSSION ABOUT DUST VARIABILITY**

This chapter shows the results about dust variability obtained in the framework of this Thesis.

Some results have made object of papers already published or in review. For them, the integral text of the manuscript is reported.

Chapter 8 is composed of four thematic parts.

First, results about the dust variability within the LGM/Holocene transition are shown and commented (8A). Then, results about dust variability within the Holocene at the different sites are presented, discussed and compared (8B). A scenario is proposed for the observed dust changes (8C). Finally, the EDC dust record is extended to 3138 m depth, back to the early to middle Pleistocene.

## 8A – THE LAST CLIMATIC TRANSITION

### 8A.1 The first dust record from EPICA-Dome C ice core

Here is reported the integral text of a manuscript appeared in *Climate Dynamics* **18**(8), 647-660, 2002 under the title:

**“GLACIAL TO HOLOCENE IMPLICATIONS OF THE NEW 27,000-YEAR DUST RECORD FROM THE EPICA DOME C (East Antarctica) ICE CORE”.**

#### ***Abstract***

*Insoluble dust concentrations and volume-size distributions have been measured for the new 581 m deep EPICA Dome C ice core (Antarctica). Over the 27,000 years spanned by the record, microparticle measurements from 169 levels, to date, confirm evidence of the drastic decrease in bulk concentration from the Last Glacial Maximum (LGM) to the Holocene (interglacial) by a factor of more than 50 in absolute value and of about 26 in flux.*

*Unique new features revealed by the EDC profile include a higher dust concentration during the Antarctic Cold Reversal phase (ACR) by a factor of 2 with respect to the Holocene average. This event is followed by a well-marked minimum that appears to be concomitant to the methane peak that marks the end of the Younger Dryas in the Northern Hemisphere.*

*Particle volume-size distributions show a mode close to 2  $\mu\text{m}$  in diameter, with a slight increase from the LGM to the Holocene; the LGM/Holocene concentration ratio appears to be dependent on particle size and for diameters from 2 to 5  $\mu\text{m}$  it changes from 50 to 6.*

*Glacial samples are characterised by well-sorted particles and very uniform distributions, while the interglacial samples display a high degree of variability and dispersion. This suggests that different modes of transport prevailed during the two climatic periods with easier penetration of air masses into Antarctica in the Holocene than during Glacial times. Assuming that southern South America remained the main dust source for East Antarctica over the time period studied, the higher dust content recorded during the ACR which preceded the Younger Dryas period, represents evidence of a change in South America environmental conditions at this time. A wet period and likely mild climate in South America is suggested at circa 11.5-11.7 kyr B.P. corresponding to the end of the Younger Dryas. The Holocene part of the profile also shows a slight general decrease in concentration, but with increasingly large particles that may reflect gradual changes at the source.*

#### **8A.1.1 Introduction**

Records of insoluble microparticles (dust) in ice cores provide one of the most detailed and best preserved sources of paleoclimatic information, in particular in terms of past storminess and dustiness as well as the location, extent and conditions of source areas (Svensson, 1998). Dust data are useful for the reconstruction of past circulation patterns and environmental conditions using General Climate Models (GCM). The role of mineral aerosol in the climate dynamics is quite complex and not yet fully understood, but exerts a radiative forcing effect on the climatic system (Sokolik and Toon, 1996). Dust may also contribute to biogeochemical cycles (Kumar and Anderson, 1995; De Baar et al., 1995) and therefore participate in atmospheric CO<sub>2</sub> regulation.



There is considerable evidence in paleoenvironmental archives from polar and low-latitude ice cores (e.g. De Angelis et al., 1987; Hansson, 1994, Thompson et al., 1995; Steffensen 1997, Petit et al., 1981, 1999; Briat et al., 1982) and from marine (e.g. Rea, 1994) and terrestrial deposits (e.g. Kukla, 1989) that the atmospheric dust load, and consequently deposition in oceans and on continents, was greater during glacial periods. A recent estimate suggests a 2.5 fold increase of the mean value on a global scale (Mahowald et al., 1999) during the last glacial maximum (LGM). However, the increase is much greater for polar latitudes and Antarctic ice cores from Dome C and Vostok have revealed an LGM flux 10 to 20 times greater than that of the Holocene (Petit et al., 1981, 1990; De Angelis et al., 1984). Similarly, for the GRIP ice core (Summit, Greenland), the ratio between the highest peaks of the LGM and those of the current climatic stage yields an extreme value of about 68 (Steffensen, 1997).

The high glacial dust input in East Antarctica can be explained by the synergetic action of many factors involving the atmosphere, biosphere, hydrosphere and lithosphere. There are three basic conditions to consider: (1) the increased aridity on the continents due to changes in soil moisture and/or vegetation cover coupled with an enlargement of the dust-source areas caused by sea-level lowering (Petit et al., 1981; Joussaume, 1990); (2) the more vigorous atmospheric circulation enhanced by the steeper southern temperature gradient generated by the northward extension of sea ice (COHMAP Members, 1988) and (3) the reduction in the intensity of the hydrological cycle leading to less efficient scavenging by precipitation and consequently more efficient transport of dust (Joussaume, 1989; Hansson, 1994; Yung et al. 1996). Even when taking into account most of these factors, initial GCM simulations failed to reproduce the LGM dust increase for polar areas. Mahowald et al. (1999), however, recently obtained a 20-fold increase for high latitudes sites by adding a simulation of vegetation changes to a GCM. Vegetation traps dust and this effect is drastically reduced under glacial conditions.

Here we present the record of continental insoluble microparticles from the upper 581 m of a new ice core recovered during the 1997/98 and 1998/99 field seasons in the East Antarctic plateau at the Dome C site (75° 06' S, 123° 21' E). This ice core was drilled within the framework of the European Project for Ice Coring in Antarctica (EPICA). The elevation (3233 m) and the geographical location of the site make it suitable for paleoclimatic studies. Given the high altitude of the interior of the East Antarctic plateau, the site makes it possible to record the atmospheric aerosol background. For the dust emitted by the continental regions of the Southern Hemisphere, the small-sized component is transported over long distances to the polar area. This reflects a large-scale phenomenon including environmental changes in the source area associated with climate. Since the dust deposited in the East Antarctic ice cores during the glacial climate likely originated from Patagonia and South America (Grousset et al.,

1992, Basile et al., 1997), the EDC dust record can potentially provide information on the dynamics of the climate and environmental change of this area.

The EDC core climatic record is deduced from the isotopic composition of the ice and the profile has been described in Jouzel et al. (2001). The chronology of the core (Schwander et al., 2001) has been established through an ice flow model coupled with temporal markers. These include the depths marked by volcanic events from the Vostok core dated over the last 7,000 years (indirectly through comparison of  $^{10}\text{Be}$  and  $^{14}\text{C}$  production), the end of the Younger Dryas at 11.5 kyr BP taken from Greenland ice layer counting and matched to the EDC core with the

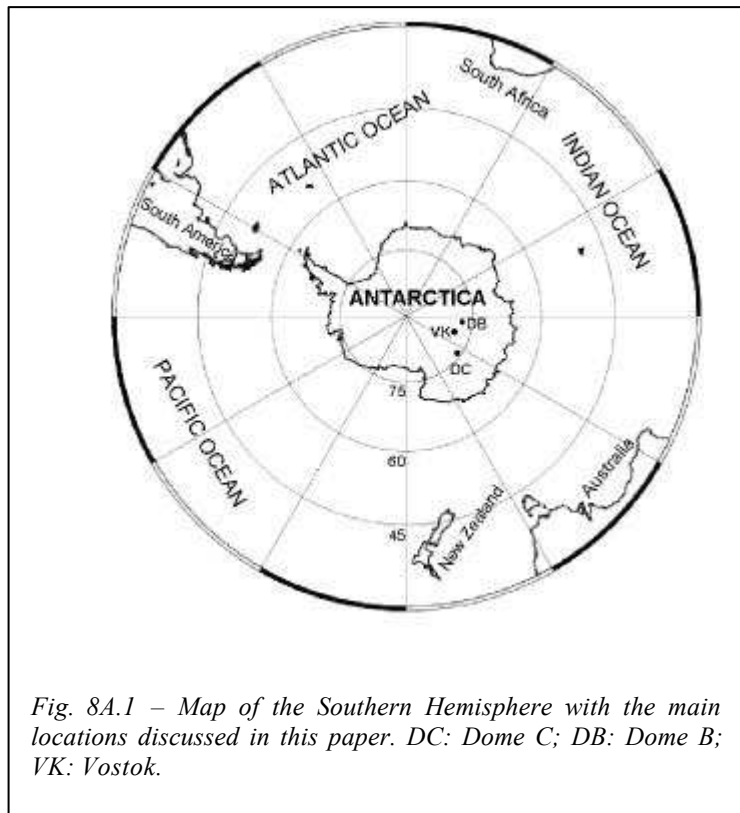


*Fig. 8A.1 – Map of the Southern Hemisphere with the main locations discussed in this paper. DC: Dome C; DB: Dome B; VK: Vostok.*

global  $\text{CH}_4$  event, and the estimated depth of the  $^{10}\text{Be}$  peak at 41 kyr BP. The time period covered by the core spans about 27,000 years with an error of 0.25 kyr at 11.5 kyr BP and 1 kyr at 41 kyr BP (Schwander et al., 2001).

The climatic record shows three main periods: the Holocene, characterized by high deuterium values, the isotopic transition, and the stage with minimum deuterium values corresponding to the Last Glacial Maximum and the end of the last glacial period. Taking the EDC record as a climatic reference, Jouzel et al. (2001) compared and synchronized other isotopic records from Vostok, Dome B, Komsomolskaya and old Dome C cores. This provides a remarkable overview of the climate history of the East Antarctic plateau back to the LGM period. Interestingly, all the records clearly confirm the evidence of a two-step pattern of the last deglaciation. After an initial warming, a well-marked phase of cooling followed, referred to as the Antarctic Cold Reversal (ACR). The ACR preceded the cooling phase of Younger Dryas from the Northern Hemisphere by about 1 kyr (Jouzel et al. 1995). The Younger Dryas was characterized by a return to almost glacial climatic conditions with high dust content in Greenland ice, while the dust content from Antarctic record looks different during the ACR, reaching a level close to the Holocene value (Jouzel et al. 1995).

Taking advantage of the good quality of the EDC ice core and some improvements in laboratory dust measurements, we will document this mid-deglaciation and the other periods. We will also characterize the size distributions of the dust particles over the entire length of the record and discuss the variations in terms of changes in transport and/or environmental changes over the sources. We will finally compare this Antarctic record with Greenland dust records.

### **8A.1.2 Analytical procedure**

A total of 169 ice increments taken from depths of 10 m to 581 m were analysed. Each 5-cm long sample represents about 2 years for the Holocene and 4 to 5 years for the LGM period, because of some thinning of the ice, as well as the halving of snow accumulation rate between the two periods (Jouzel et al., 1987, and 2001). The mean resolution is one sample per 3 to 4 meters of ice (i.e. one sample per about 135 years) for the Holocene period and one sample per 2 to 3 m (about 230 years) for the LGM.

Ice samples were decontaminated by three repeated washings in ultra-pure water (MilliQ®). For the porous firn, the outer part of the samples was scraped away over about 2 mm of thickness using a lathe. For the firn part down to 100 m depth, we selected one ice core increment every 5 m and analysed several 5 cm long adjacent sub-samples to check our decontamination procedure.

Data for the uppermost 40 meters of the core (spanning the last 700 yrs) are not reported in this paper since the use of the lathe, the very high porosity of the firn and the low number of available measurements do not allow us to exclude the possibility of contamination of these samples.

The measurements of dust concentration and size distribution were performed using a Multisizer IIe® Coulter Counter set up in a class 100 clean room. The instrument works on the basis of the detection of the electric signal generated by the particles that are forced to flow through a small aperture tube (50 µm in diameter). The water sample is made conductive by adding a pre-filtered 20% NaCl electrolyte solution giving a 1% concentration to the final solution. Melted samples were mechanically stirred continuously before the analysis in order to prevent sedimentation in the container. At least three consecutive counts were performed on each volume of 500 ml. The reproducibility of the measurements is good for highly concentrated samples (better than 2% for 50,000 particles per g), while some scattering may occur for samples with low concentrations (up to 20% for 1,000 particles per g). The particle size is expressed by the diameter of a sphere with an equivalent volume. The mass was calculated from the measured volume assuming a particle density of 2.5 g/cm<sup>3</sup>. The instrument was set for measurements of particles with diameters from 0.7 to 20 µm in 256 channels on a logarithmic scale. Similar techniques and procedures were used by Steffensen (1997) to perform measurements on the GRIP ice core.

Statistical analyses were performed on the volume-size distributions of particles along the core. All distributions were considered from 0.7  $\mu\text{m}$  to the uppermost limit of the continuous distribution curve that is about 5  $\mu\text{m}$  for the EDC core. This makes it possible to separate spurious counts caused by electric noise and/or big particles due to possible contamination of the samples. This effect is significant for the Holocene samples with low concentrations. For example, more than 99% of the total counts are included in the interval from 0.7 to 5  $\mu\text{m}$  for both LGM and Holocene samples, but the contribution of particles greater than 5  $\mu\text{m}$  to the total volume may represent up to 2% and 40%, respectively.

The volume-size distributions of samples were fitted with a lognormal function, as suggested by several authors (Patterson and Gillette, 1977; Royer et al., 1983, Steffensen, 1997).

$$dV/d \ln D = a * \exp [-0.5*(\ln (D/D_v)/(\sigma_g))^2] \quad (1)$$

where

$$a = V/ [(2\pi)^{1/2} * \sigma_g] \quad (2)$$

The distribution is defined by three parameters: the total volume  $V$ , the modal diameter  $D_v$ , where the derivative is null, and  $(\sigma_g)$  the Geometric Standard Deviation which describes how closely the particle volume is distributed around the mean. This function is quite useful since the  $n^{\text{th}}$  moment of a lognormal function is also a lognormal function with the same  $\sigma_g$  but with a mean diameter  $D_m$  (Royer et al., 1983):

$$D_m = D_v * \exp [n*(\ln \sigma_g)^2] \quad (3)$$

Therefore, the modal diameter of the volume distribution ( $D_v$ ) can be easily transformed to the corresponding number mean diameter  $D_n$ , while the geometric standard deviation  $\sigma_g$  is common to all the distributions.

The lognormal regressions provide a reasonable initial estimate of the dust distributions. However with our high-resolution measurements (256 channels) and for highly concentrated samples, some differences occur: the mode of the distribution is slightly shifted and the volume distribution appears slightly left-skewed (Fig. 8A.3a). A better fit could be obtained using a four-parameter Weibull function (Fig. 8A.3b).

$$dV/d \ln D = a * ((c-1)/c)^{((1-c)/c)} * (g^{(c-1)}) * \exp (-g^c) + ((c-1)/c) \quad (4)$$

Where

$$g = \text{abs} ((D-D_v)/b + ((c-1)/c)^{1/c}) \quad (5)$$

This function provides a slightly improved correlation coefficient (Tab. 8A.1).

### 8A.1.3 Results

The profile of dust concentration in the EDC core versus depth is shown in Fig. 8A.2a, along with the deuterium record. The number of particles/ml and mass content (ppb) have been plotted on a logarithmic scale since it is assumed that dust concentration in snow is the end result of a series of phenomena and factors having a synergetic (multiplicative) effect. The average number and mass concentrations every 20 metres are also reported in Tab. 8A.1.

The EDC dust record indicates a drastic decrease in continental windblown dust from the LGM (195,000 particles/ml,  $790 \cdot 10^9 \text{ g} \cdot \text{g}^{-1}$  or 790 ppb for depth interval 480–580 m) to the warm Holocene period (3,900 particles/ml, 15 ppb for depth interval 40–360 m). The ratio between mean LGM and Holocene concentrations is greater than 50 for both particle number and mass. As the snow accumulation rate changes by a factor of 2 between the two periods (Jouzel et al., 1987, in press), a dust flux ratio of about 26 is inferred.

The same general behaviour can be found in the dust records of the other East Antarctic ice cores (Vostok, Dome B and old Dome C, Fig. 8A.2) along with their respective isotopic profiles. For the three ice cores, the LGM to Holocene ratio is respectively 24, 35 and 28 (Table 8A.2), which is lower than the ratios for our EDC

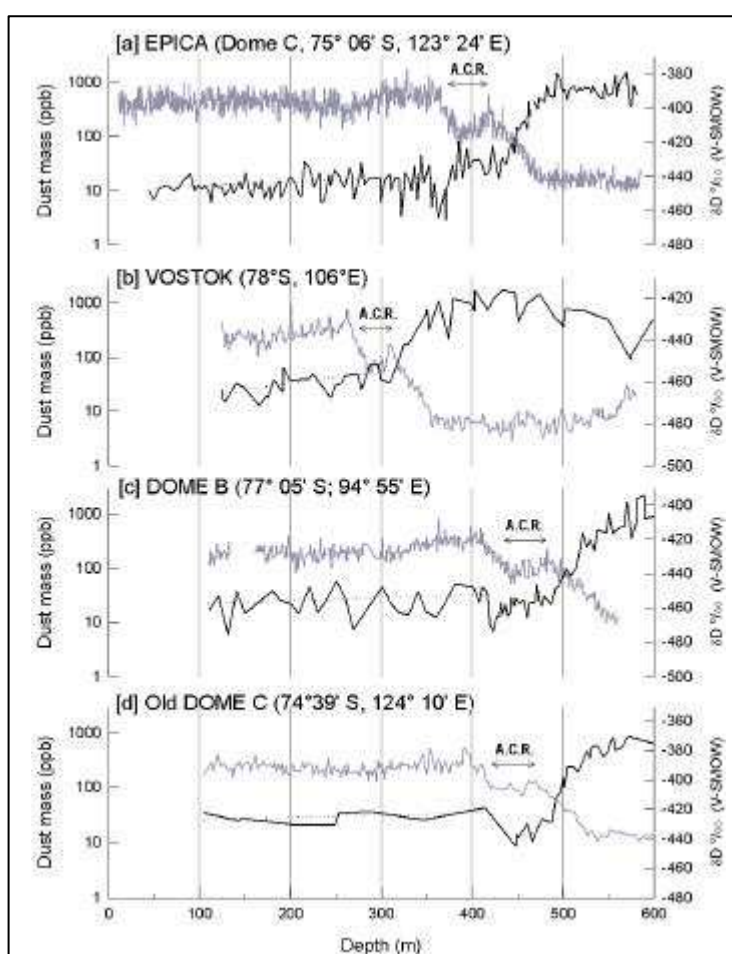
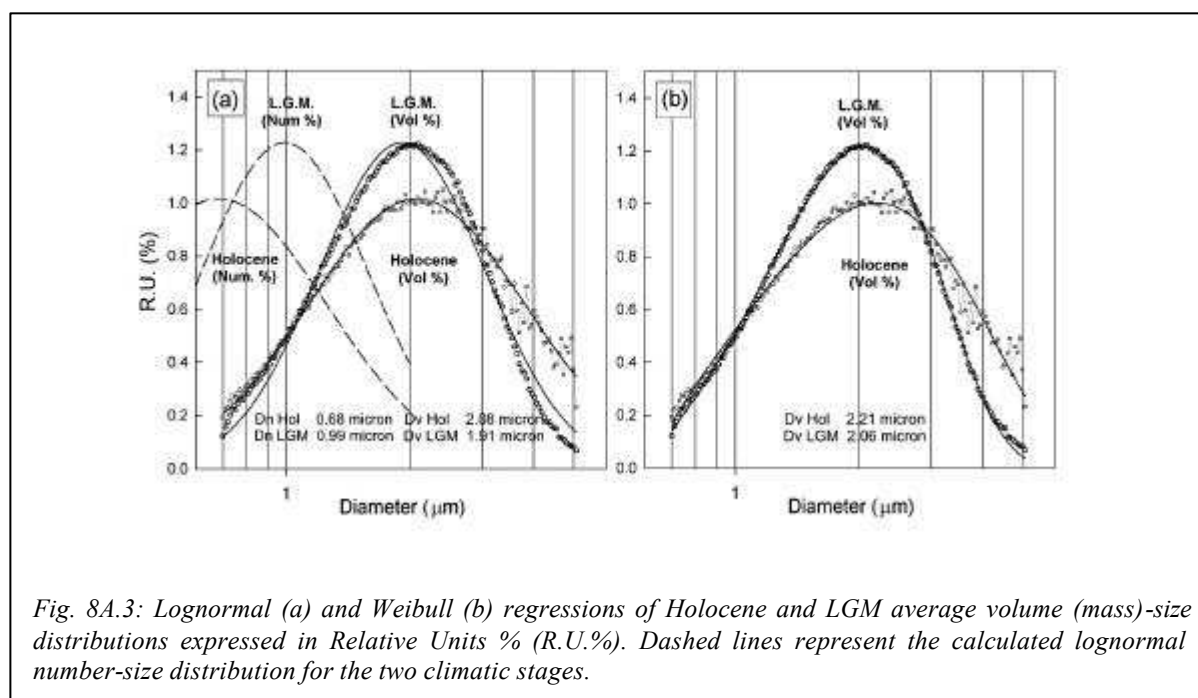


Fig. 8A.2 – Record of insoluble dust mass (black line) and Deuterium (gray line) versus depth (Jouzel et al., in press) for East Antarctica ice cores. From top to bottom: EPICA- Dome C (this work), Vostok (Petit et al., 1990), Dome B (Jouzel et al., 1995) and old Dome C (Royer et al., 1983). For the four cores, the Antarctic Cold Reversal phase of the isotope (A.C.R.) is reported. The Holocene is on the left side of the profile while the glacial period is on the right. A slight decreasing trend for the particle mass during the Holocene is suggested in all profiles by the dotted line.

data. However, while the LGM concentrations are almost the same between the cores, their Holocene values are higher than the values for EDC. Since the number of measurements was rather low for the above cores and the analytical procedure less reliable than the one we used for EDC, we cannot exclude the possibility of contamination in their Holocene concentrations.

Based on the stable isotope content, the deglaciation occurs in two steps and a cold phase appears in the middle of deglaciation, corresponding to the ACR (420-375 m depth in the EDC core, Fig.8A.2a). In this depth interval, the microparticle mass concentration is about 30 ppb and therefore two times greater than the mean Holocene concentration. Moreover, between 360 and 373 m depth, the dust record shows a well-marked period of extremely low dust concentrations, with a mean particle mass of 7 ppb and an absolute minimum of 2.9 ppb observed at 371 m depth.

From the onset of the Holocene to the uppermost part of the core, the EDC dust profile suggests, over and above the natural variability of the data, a slight but significant general decrease with a rate of about 0.9 ppb per 1000 yrs in mass and 200 particles/ml per 1000 yrs in number. This tendency seems to be common to all records and particularly evident for the Vostok data (Fig. 8A.2b), but however this may be simply a coincidence.



In Fig. 8A.3 we report the average volume-size distributions of all Holocene and LGM samples, normalised to 100% in the interval between 0.7 and 5 μm. A slight increase in the mode of the distribution (D<sub>v</sub>) can be observed from LGM (1.91 ± 0.02 μm) to Holocene (2.08 ± 0.12 μm) samples, and simultaneously the values of σ<sub>g</sub> increase. These two parameters were averaged every 20 m of depth and are reported in Tab. 8A.1 along with the calculated values for D<sub>n</sub>. Note that the mean

diameter of the size-number distributions is smaller for Holocene than for LGM particles, because of a greater value for  $\sigma_g$  (Fig. 8A.3a). Sub-micron particles are, therefore, proportionally more numerous during the Holocene, but obviously this has little influence on the total mass.

From the mode and the geometric standard deviation of the lognormal distribution, we deduce that 68% of the total volume (mass) is included in the interval of size expressed by  $[\exp(\ln D_v - \ln \sigma_g); \exp(\ln D_v + \ln \sigma_g)]$ . This gives an interval from 1.11 to 3.81  $\mu\text{m}$  for Holocene samples and from 1.20 to 3.05  $\mu\text{m}$  for LGM samples, respectively. The narrower interval of glacial samples relative to the Holocene suggests LGM dust particles more closely distributed around the mean diameter or better sorted.

The mean value for  $D_v$  calculated with the Weibull function is  $2.14 \pm 0.18 \mu\text{m}$  along the whole core and it shifts from  $2.06 \pm 0.03 \mu\text{m}$  in the LGM to  $2.21 \pm 0.14 \mu\text{m}$  during the Holocene. While the absolute value of  $D_v$  is slightly different from the lognormal fit, the LGM-Holocene shift by  $\sim 0.15 \mu\text{m}$  is confirmed.

The records of the number and mass concentration along with the two parameters of the lognormal fit are reported in Fig. 8A.4 against age. Number and mass concentrations (Fig. 8A.4b and 4c) show a very similar pattern and two concentration peaks of 1470 and 1525 ppb occur in the glacial period at 19 and 26 kyr B.P., respectively. Along the core, the data appears to be less scattered during the LGM than during the Holocene, even taking into account the smoothing effect that may be induced by the longer periods covered by each sample for the LGM than for the Holocene.

The large deglacial fall of both dust number and mass concentration starts at about 18 kyr B.P. (Fig. 8A.4b and 8A.4c) almost in concomitance with the beginning of the isotope rise and climate warming. The Holocene dust value reaches a first minimum at about 14.6 kyr B.P., while the isotope rise instead continues until about 14 kyr. Then, the temperature decreases during the ACR phase and dust slightly re-increases reaching concentrations two times higher the mean Holocene level both in number and mass. After this, a second deglaciation step occurs and the dust concentration drastically drops to very low levels with a well-marked minimum at around 11.5-11.7 kyr B.P. (371 m depth) before reaching Holocene value. Then, the Holocene is characterised by a general decrease in mineral aerosol as already noted.

The modal values ( $D_v$ ) and  $\sigma_g$  of the volume-size distributions are reported in Fig. 8A.4d and 8A.4e along with average values over 20 metres. The mean values along the entire core are  $2.00 \pm 0.13 \mu\text{m}$  and  $1.78 \mu\text{m}$  respectively, but both parameters clearly show an increase from the LGM to the Holocene. Particles from the glacial period are characterized by low values for mode ( $1.91 \pm 0.02 \mu\text{m}$ )

and  $\sigma_g$  ( $1.6 \pm 0.01$ ), indicating fine and very well-sorted particles. Both parameters are almost constant over this climatic period. Note that at the start of the deglaciation, the onset of the dust decrease is concomitant with the uppermost limit of the narrow and well-sorted distributions of the glacial period. During the deglaciation, while  $\sigma_g$  increases regularly, the particle mode reaches a minimum at mid-deglaciation with average values of  $1.7 \mu\text{m}$  or even lower for individual samples. The Holocene particles display a highly variable character and coarser modes ( $2.08 \pm 0.12 \mu\text{m}$ ) and  $\sigma_g$  ( $1.8 \pm 0.11$ ). For both the parameters, the value progressively increases during the Holocene, and maximum values occur between 2 and 7 kyr B.P. The change of the modal diameter along the EDC core is independent on the type of regression chosen and same trend is confirmed when the Weibull fit is applied to the whole set of distribution data (Tab. 8A.1). Only the absolute value of the mode is systematically shifted.



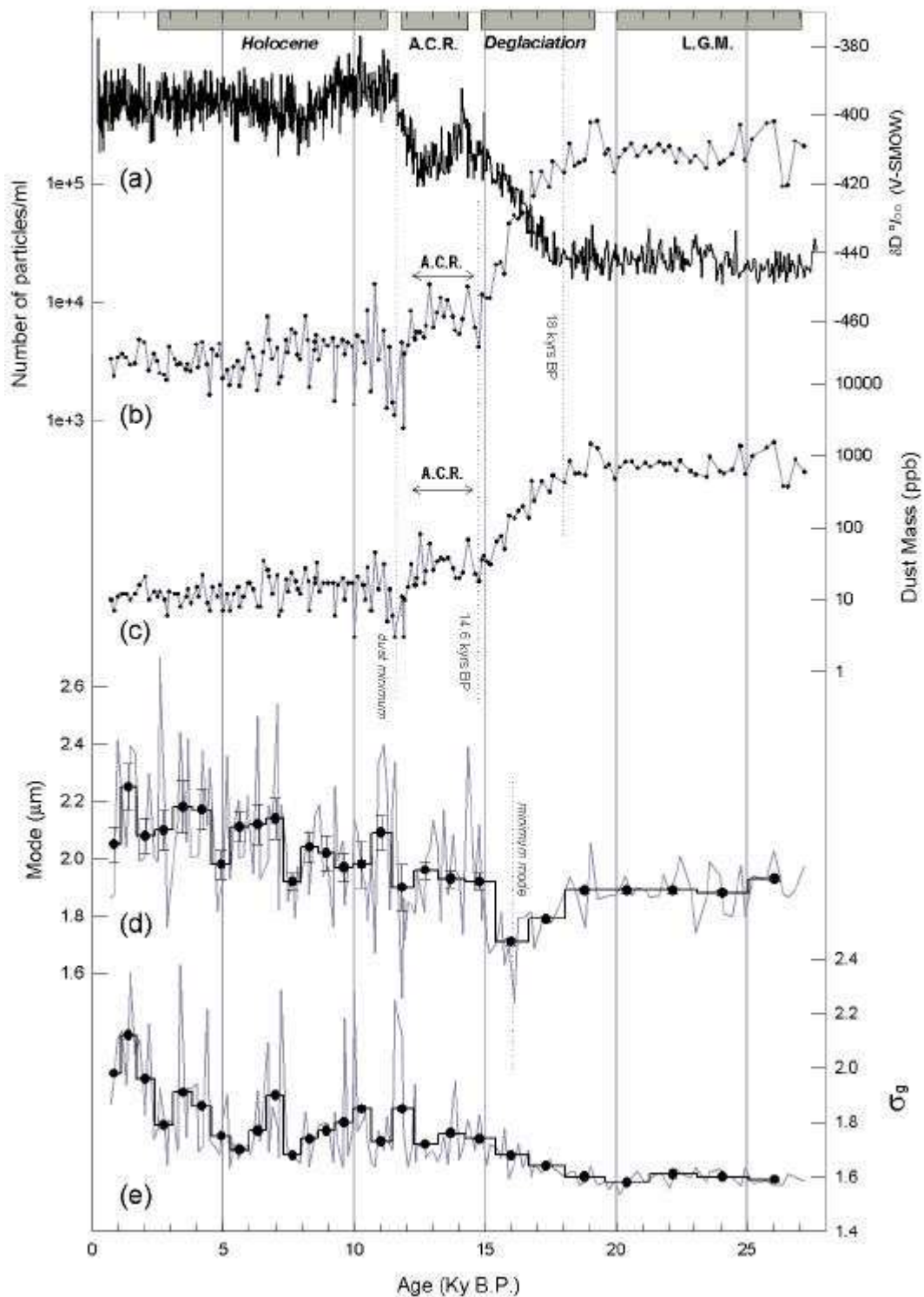


Fig. 8A.4 – EDC dust number content (b), mass concentration (c), modal diameter (d) and geometric standard deviation (e) along with the deuterium profile (a) taken from Jouzel et al. (2001) and plotted versus age (from Schwander et al., in press). The average values over 20 metres are also plotted both for modal diameter (black points with error bars in fig.4-d) and the geometric standard deviation (black points in fig.4-e). The gray areas on the top represent, for each climatic period, the interval taken for characterization of the insoluble particle distribution and reported in Tab. 8A.3.

#### 8A.1.4 Discussion

##### *Regional to inter-hemispheric significance of the EDC dust record*

The EDC dust record shows an LGM/Holocene flux ratio of about 26. This change appears slightly higher than a previous estimate of 15 from the Vostok and old Dome C cores (Petit et al., 1990), likely because of our lower EDC concentration for the Holocene sample, while glacial concentrations remain similar to previous values. It also confirms that the drastic drop in dust concentration from glacial to Holocene levels occurs at about 14.6 kyr B.P., according to the EDC chronology. This level is an interesting temporal marker for Antarctic ice core records, assuming the dust source is the same for the different sites or governed by the same processes. Interestingly, Jouzel et al. (1995) assigned 14.6 kyr B.P. to the onset of Holocene dust levels in Antarctic cores based on several arguments such as the cross-check between Greenland and Antarctica methane and isotope composition from atmospheric oxygen entrapped in air bubbles, as well as the comparison with deep ocean core records. However before drawing conclusions on the representativity of the dust records from East Antarctica, the question of the geographical origin of the source needs to be addressed.

Dust in Antarctic ice is mainly of continental origin (Briat et al., 1982; Gaudichet et al., 1988), as shown by the presence of various detritic minerals such as illite, crystalline silica, feldspar and smectite as well as volcanic glass shards (Gaudichet et al., 1986 1988, 1992). Mineral dust reaching the interior of Antarctica is advected through the troposphere at levels higher than 4 km, the elevation of the East Antarctic plateau, after transport over very long distances. A contribution from nearby ice-free areas of Antarctica seems unlikely since it would be impeded by the katabatic winds blowing off the continent. Moreover, the surrounding cold ocean provides unfavourable conditions for atmospheric convection and the vertical ascent of particles. Isotopic fingerprints of glacial dust from Vostok and Dome C cores, based on  $^{87}\text{Sr}/^{86}\text{Sr}$  and  $^{143}\text{Nd}/^{144}\text{Nd}$  (Grousset et al., 1992; Basile et al., 1997) suggest that the Patagonia region of South America is the main source. The isotopic composition of loess and soils from this region closely matches the signature of ice core dust, to a far greater extent than any other potential source area or mixture of sources. This holds also for dust in interglacial ice for which preliminary measurements of the isotopic signature is compatible with a South American origin. (Basile, 1997). The preferential atmospheric pathway for transport of dust from South America to East Antarctica is also suggested by the relative abundance of volcanic ash layers found in the Vostok core, originating from South Sandwich volcanoes in the southern South Atlantic (Basile, 1997, Basile et al., in press).

The Patagonian region was much colder and dryer during the LGM and fluvio-glacial erosion processes were intense, forming an environment favouring dust mobilisation and deflation. There is evidence of

a dry and windy climate over wide areas of South America during the late Quaternary period, including aeolian features, loess deposits, paleodunes and deflation basins (Clapperton, 1993).

Furthermore, the glacial climate of South America was greatly influenced by the large extension of sea ice in the South Atlantic Ocean (Heusser, 1989). At the LGM, the polar front was displaced northward and consequently also the Westerlies belt. Compared to present day, the spring limits of sea ice in the Southern Ocean during the last glacial period were about 3° to 5° latitude further north in the Pacific sector, 4° to 5° latitude further north in the Indian sector and at least 8° further north in the Atlantic (Burkle and Cirilli, 1987). Therefore, sea ice extent in the vicinity of South America, with the incipient closure of Drake Passage, presumably had an important influence in the climate of this region (Heusser, 1989a). Similarly on the basis of glaciological data from Patagonia, Hulton et al. (1994) proposed that the LGM precipitation belt in South America shifted northwards by about 5° latitude with respect to the Holocene, located around 50°S. He suggested an LGM reduction of precipitation at 50°S as well as a lowering of the equilibrium line of the Southern Patagonian ice cap by 360 m at 56°S with respect to that of the Holocene.

The decrease in the dust concentration by an order of magnitude at the time of deglaciation is likely the result of concomitant factors. We believe that it is primary linked to the changes in the Southern Ocean and a key role has been played by reduction of sea ice extent in the Southern Atlantic Ocean, as supported by the drastic decrease in the sea-ice related diatom *E. Antarctica* (Burckle and Cooke, 1983). This event likely occurred at the same time as the re-initiation of North Atlantic Deep Water formation (Charles and Fairbanks, 1992). Given that the extent of sea ice and the intensity of the Westerlies are closely correlated (Simmonds, 1981), the decrease of the polar front activity contributed to a reduction in the dust deflation at the source and the harsh environment over South America. The source area was also reduced by the melt water pulse (MWP1a, Fairbanks, 1989), which likely submersed more than a half of the previously exposed continental shelf of Argentina (Jouzel et al., 1995). The onset of warmer climate made conditions less favourable for dust mobilisation and long-range transport: the southward shift of the precipitation belt (Lamy et al., 1999) led to a damp environment favouring a greater vegetation coverage as shown by paleo-vegetation proxies (Heusser, 1989-b). Moreover, greater evaporation and precipitation enhanced the hydrological cycle and led to more efficient scavenging of the aerosol. These factors could account for the drastic reduction of dust after the glacial period.

The general decreasing trend from ~ 11 kyr B.P. to present may be the result of long-term changes to certain factors. The trend is very slight and gradual and rapidly-changing sensitive features, such as vegetation cover or atmospheric circulation, are therefore probably not the main controlling factors. More likely, the trend is a combined result of a gradual reduction in the dust reservoir available for

wind deflation by the reduction of glacier and periglacial processes, the progressive increase in biological activity and the development of pedogenesis.

The change in the paleoenvironment of the source regions is important as far as the dust cycle is concerned. The absolute minimum of the dust concentration is of particular interest in this respect. The EDC profile shows a slight dust increase during the ACR phase and a well-marked minimum centred around 11.5-11.7 kyr B.P. The latter corresponds to the end of the Younger Dryas in the Northern Hemisphere (11.5±0.2 kyr B.P.), marked by a peak in methane concentration (Chappellaz et al., 1993). The methane event was associated with a sudden warming and an increase in biological (microbial) activity linked to the extension of wetlands in the Northern Hemisphere. East Antarctic records suggest that South American dust sources were also reduced likely because of a period of increased humidity. In this respect, McCulloch et al. (2000) suggest, on the basis of pollen records, a very wet phase in southern South America at the time of the last termination. Beside the higher precipitation linked to climatic changes, this region received an additional input of water derived from local sources such as Andean glaciers, snowcaps and permafrost, in response to probable local warmer conditions. This event may be therefore of a inter-hemispheric to global extent.

### ***The Antarctic Cold Reversal***

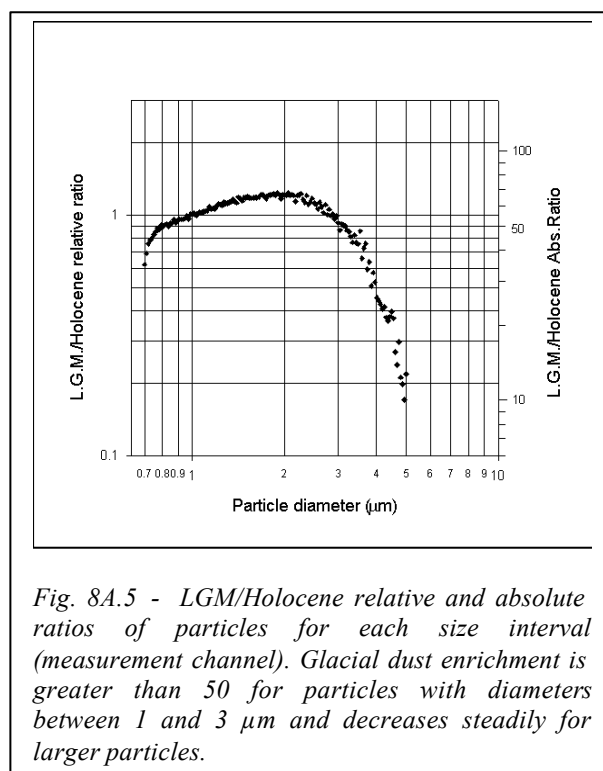
The climate and environmental changes that occurred during deglaciation and the ACR phase are today of great interest. This mid-deglaciation cold episode is clearly evident in the isotopic record of deep Antarctic ice cores. On the other hand, the development of an event similar to the Younger Dryas (YD) at high-latitudes on Southern Hemisphere continents, especially South America, is a matter of debate.

Wenzens (1999) reports a list of nine glacier advances which may have occurred in southern Patagonia (from 48°S to 51°S) at the time of the European YD. McCulloch and Bentley (1998) describe a glacial advance along the Strait of Magellan that they believe took place ca. 1 kyr earlier than the onset of the YD. Jouzel et al. (1995) has also concluded that the coldest part of the ACR preceded the YD by about 1 kyr. Evidence of a late-glacial re-advance has also been detected by Clapperton et al. (1995) for the central Magellan Strait, by Marden and Clapperton (1995) for Grey and Tyndall glaciers (51°08' and 51°15'S), and by Denton et al. (1999) for the southern Chilean lake district and from a proglacial lake in the nearby Argentine Andes. They suggested that re-advances were probably restricted to sites in the southern Andes where precipitation increased during the interval because of the southward shift of the Westerlies. Moreover, sites where the change in climate was insufficient to overcome the main deglaciation trend probably show no record of the event. In opposition, Lumey and Switsur (1993) and Asworth and Hoganson (1993) do not share this view. Note also that Heusser and Rambassa (1987),

Heusser (1989-b, 1993) and Clapperton et al. (1989) report an ACR imprint in pollen spectra while Markgraf (1991, 1993) suggests that the observed changes may be a response to local rather than global factors.

This short overview indicates that the onset of a mid-deglaciation cold phase in the Southern Hemisphere is not unequivocally documented. In this context, the slight increase in dust concentration during the ACR revealed in the EDC ice core is of particular importance for paleoclimatic reconstruction. It is however difficult to attribute this change to one or more specific parameters. This feature does not resemble a return to glacial conditions, but reflects some slight climatic change in the source area at this time.

### *Glacial and interglacial dust transport*



The size distribution of aeolian dust deposited at remote polar sites is essentially influenced by the dynamics of the atmosphere, such as the wind velocity and distance from the sources (Pye, 1987). Moreover, other factors could be important such as the environmental conditions at the source affecting soil and vegetation typologies as well as the efficiency of scavenging by precipitation during transport. Two main questions arise from the profile of EDC dust distribution parameters. First, what is the cause of the difference between the well-sorted and slightly finer glacial particles and the heterogeneous interglacial particles? Second, what is the reason for the increase in the mode of the particles over the Holocene period?

Our data for EDC indicates that the mass distribution of dust is centered around a modal diameter of approximately 2 µm with a geometric mean standard deviation of 1.6-1.8 along the core. For old Dome C and Vostok cores, Royer et al. (1983) and De Angelis et al. (1984) obtained values similar to ours for modal diameter, while their  $\sigma_g$  was only slightly higher ( $2.2 \pm 0.2$ ). For Holocene samples, Petit et al. (1981) and De Angelis et al. (1984) suggested a shift toward smaller particles in comparison with LGM samples. In opposition, our results from EDC indicate an increase toward larger modes. In the light of these new high size-resolution measurements, we believe that the previous data, obtained using a 16 channel counter instead of a 256-channel counter, may be highly inaccurate.

During the LGM period, the parameters of the dust distribution from EDC are very similar for all samples while those for the Holocene period display a variability between samples. Generally speaking, the LGM distributions have an almost constant mode and the lowest  $\sigma_g$  values. This fact cannot be related to the longer time intervals covered by the LGM samples with respect to the Holocene samples. Averaging consecutive Holocene distributions will lead to a mean distribution with greater  $\sigma_g$  values. During the Holocene, there is a general gradual increase in the mode and in  $\sigma_g$ . The highest values of the mode are observed in the late Holocene, from about 2 to 7 kyr B.P. (Fig. 8A.4d).

Fig. 8A.5 shows the LGM/Holocene relative and absolute ratios of the fraction of particles in each size interval. This ratio changes with particle size from values greater than 50 (for particles from 0.7 to 3  $\mu\text{m}$ ) to less than 10 for particle of 5  $\mu\text{m}$ . For particles from 2 to 5  $\mu\text{m}$ , the ratio decreases approximately as a function of the 3<sup>rd</sup> power of the diameter. This means that the LGM size distribution does not represent a simple homothetic amplification of the Holocene distribution and vice versa. Holocene samples display a large-particle enrichment with respect to the LGM. Conversely, LGM show a large-particle depletion, suggesting that gravitational settling has occurred. Therefore, our data suggest that LGM dust remained in the atmosphere longer to allow the settling of large particles. Small-sized particles remain because of their longer residence time. This in turn can be linked to different mechanisms of transport between the two climatic periods<sup>1</sup>.

Significant change in ice core dust size distribution have been also observed in the Northern Hemisphere for the Penny Ice Cap (Zdanowicz et al., 2000). The mode was close to 1  $\mu\text{m}$  during the glacial period and at the time of the large Laurentide ice sheet. Then, after deglaciation, the mode shifts to very large particles (up to 6  $\mu\text{m}$ ) for the Holocene period because the dust source was closer. For EDC the change in particle size could be due to the possible contribution of an additional source of dust, absent during the LGM period. This remains possible since to date, the dust sources for the Holocene period are not as well-defined by isotopic finger printing as the LGM dust samples. This is because of technical problems associated with the very low dust content. However, preliminary measurements tend to confirm that the isotopic signature for the Holocene has the same geographical origin, i.e. South America (Basile, 1997, and personal communication). So, we believe that the dust source for the Antarctic dust record remained the same (South America) over the entire period.

We therefore have to consider the change in transport mode. During the glacial period, Antarctica was surrounded by widespread sea-ice cover both in winter and summer (Denton et al., 1991) and the polar front was displaced further north. The strengthening of the polar vortex by the sharp latitudinal thermal gradient may have favoured higher geostrophic winds and well-marked zonal circulation.

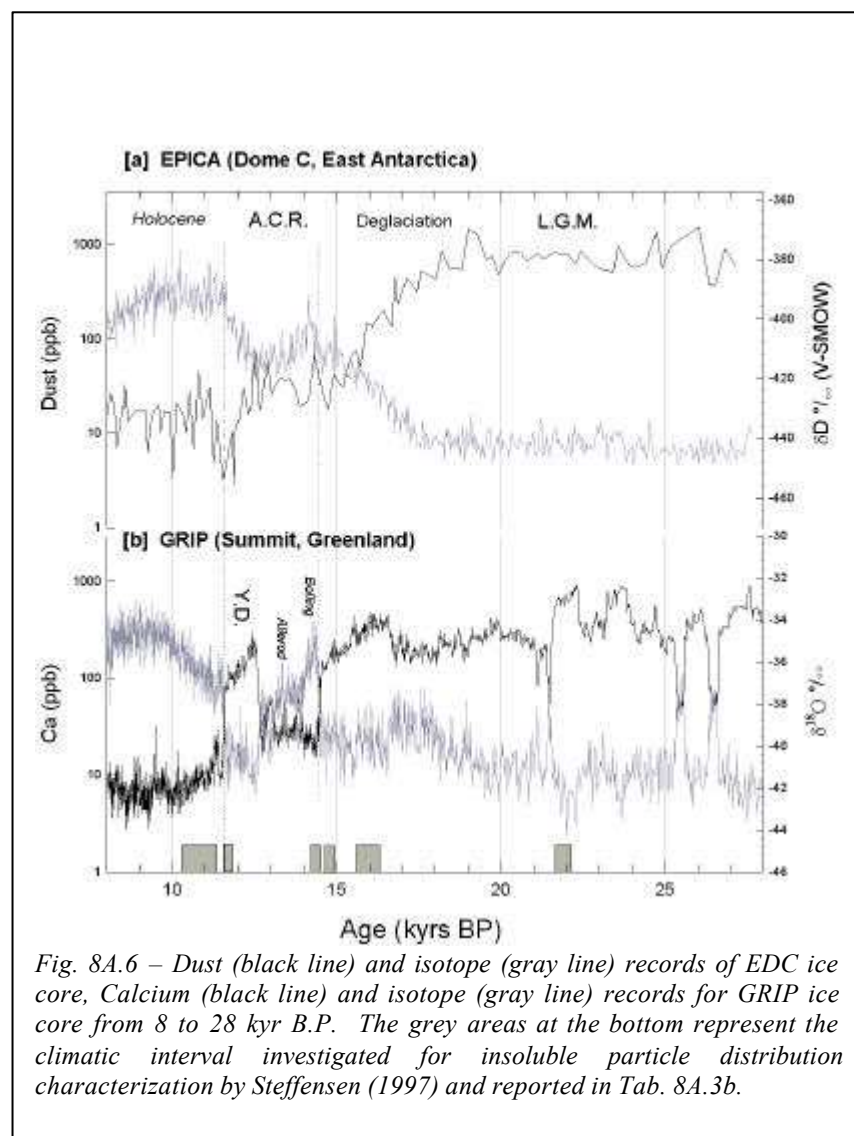
---

<sup>1</sup> This will be discussed in detail in § 8A.3

These conditions caused the interior of the Antarctic East plateau to be more isolated from storm tracks or from the direct penetration of middle latitude air masses. In opposition, during the Holocene period, the drastic reduction of sea ice and the progressive warming of the Southern Ocean weakened the southward polar front allowing air masses and aerosol to penetrate more easily into Antarctica. This suggests that a more effective meridional circulation prevailed.

With such a scenario, longer dust trajectories are expected for the LGM. The continental deflation was intense and the atmospheric dust load for mid-latitudes was likely high. The reduction in the intensity of the hydrological cycle and the decreasing aerosol scavenging efficiency led to a longer residence time in the atmosphere. This may account also for the effective sorting of the particles and the low variability in the size distribution parameters of LGM dust. In opposition, for Holocene dust, sources were weaker, and the reduced residence time of the dust in the atmosphere with a shorter time for transport to Antarctica led to less effective sorting of particle size (i.e. high  $\sigma_g$ ) as well as the possibility for larger particles or distributions with high modes to be transported over the Antarctic plateau. This may also account for the higher variability in dust concentration and in particle size parameters.

Such a scenario, linking the glacial/interglacial particle characteristics and mode of transport, seems consistent with the interpretation of Zielinski and Mershon (1997) concerning the dust distribution parameters found in GISP2 Greenland ice. The authors stated that the Mass Mean Diameter of



particles could be considered as a proxy for paleo-storminess, while Mean Number Diameter could be related to increased Westerlies intensity that in turn is dependent on latitudinal temperature and pressure gradients.

Concerning the gradual increase of the mode of Holocene dust (Fig.8A.4d and 8A.4e), several factors may again be involved. One is environmental changes at the source. The first five millennia of the Holocene have been characterised in southern South America by high temperatures, relatively high precipitation and vegetation patterns of the forest-steppe type. The second part of the interglacial instead seems to be cooler and wetter with a diminishing of open vegetation and with woodland converted to closed forest (Heusser, 1989b). Paleovegetation data also suggest increased storminess and cloud cover in the second part of the Holocene. These changes may directly affect the biological activity in soils as well as the pedogenetic processes. This could affect dust particles characteristics by agglomerating or flocculating fine particles. Mineralogical studies of Holocene samples focussed on clay minerals, which are mainly derived from physical and chemical rock weathering and represent the final product of soil genesis, would be useful in this matter (Maggi, 1997).

#### ***Comparison with the Greenland GRIP dust record***

The parameters of the size distribution of dust from different climatic periods in the Greenland GRIP core (Steffensen, 1997) are compared with EDC data in Table 8A.3. The mode of the distribution of GRIP dust fitted by a log normal distribution ranges from 1.5 to 2  $\mu\text{m}$ , which is slightly smaller than for EDC. No clear trend in mode of distribution is observed between the Glacial and Holocene period and the finest values have been observed for the Pre-Boreal (warm) period. The geometric standard deviation ( $\sigma_g$ ) is also in the same range as EDC values and the lowest values and the best-sorted distributions are also suggested for the LGM period.

In Fig. 8A.6 the dust and isotope profiles of EDC and GRIP cores are compared for the time interval between 8 and 27 kyr B.P. The calcium record is taken as a proxy for continental dust for GRIP (Steffensen, 1997), calcium representing mostly the contribution of soluble carbonates from soils of the sources. Despite the different time resolution, the most significant difference between the two profiles concerns the timing and amplitude of the oscillations. The transitions from cold to mild periods and vice-versa are marked in the Greenland record by very rapid shifts in calcium content (a few decades) that are closely correlated with  $\delta^{18}\text{O}$  (Fuhrer et al., 1999). This has been attributed mainly to changes in circulation patterns at the highest latitudes of the Northern Hemisphere, coupled with increased dust mobilisation at the Asian source (Fuhrer et al., 1999). On the other hand, the dust oscillations in the EDC core are less accented and appear to be smoothed. Moreover, dust changes are less correlated with temperature fluctuations than in the GRIP record. The ACR period and the absolute minimum of dust at circa 11.5 kyr BP clearly demonstrate the differences between the dust



and temperature signals. This different behaviour has been confirmed by additional dust measurements (not shown) with an enhanced resolution as well as in the non-sea-salt Calcium from continuous flow line analysis (Rothlisberger et al., 2000).

During deglaciation, Greenland and EDC profiles differ significantly. During the warm Bolling phase and through the Alleröd period, dust would appear to have been present at relatively lower levels than for the glacial stage. At this time, the ACR occurred in Antarctica and dust remained at a substantial level (twice the Holocene value). At the onset of the cold Younger Dryas (12.7 kyr B.P.), dust rose steadily to glacial levels in Greenland until the end at 11.5 kyr B.P., where it drops to the low Holocene value. In opposition, dust decreases in Antarctica from 12.5 kyr B.P. and this trend continues to the lowest concentration reached at 11.7-11.5 kyr B.P. Finally, EDC and Greenland records both display low dust content at 11.5 kyr B.P., corresponding to a steady warming in both records as well as a wet period likely of global extent.

#### **8A.1.5 Conclusions**

The new set of measurements of the concentration and size distribution of insoluble microparticles obtained using a high-resolution counter has made it possible to document the LGM/Holocene period spanning the last 27,000 years. The EDC dust record introduces new considerations on the dynamics of the past climate in the Southern Hemisphere. During the last glacial period, the dust flux in East Antarctica was 26 times the Holocene level, an increase which is slightly higher than the previous estimate. For the ACR, a slight but significant dust concentration has been observed for the first time in Antarctica, indicating a substantial depression of climate and environment in South America during the same period, but not synchronous with the Younger Dryas. Also, a well-marked minimum in dust concentration occurred at 11.5-11.7 kyr that corresponds to the steady warming which immediately followed the end of the cold phase of the Younger Dryas in the Northern Hemisphere. This minimum dust concentration is interpreted as corresponding to a wet period. Indeed such a wet period, probably associated with a milder climate, would not have been restricted to the Northern Hemisphere and may have strongly affected the source region for dust in Antarctica.

The parameters of the size distribution of the particles indicate that the mode of dust for the LGM is smaller and the particles better sorted than for dust deposited during the warm Holocene period. We suggest that different long-range transport modes are involved for the continental dust. During the glacial period, a combination of factors such as sea ice extension and the northward shift of the polar front formed a more efficient barrier to the penetration of air masses into Antarctica. In spite of the increase of the polar vortex and zonal circulation, dust particles remained longer in the atmosphere thanks to a lower efficiency of dust scavenging by precipitation. This is in opposition with the

Holocene pattern for which the penetration of air masses in Antarctica is likely easier and atmospheric circulation more meridional. The drastic change in the environment of the dust source (likely southern South America) as well as the reduced residence time of particles related to an enhanced hydrologic cycle, steadily contributed to the reduction in the dust transported to Antarctica.

Comparison of EDC and Greenland dust records shows significant differences in timing and magnitude. The rapid dust changes observed in the Greenland core are sharp and closely correlated to temperature variations. In Antarctica, this relation is not as direct as is demonstrated by the modest increase of dust during the cold phase of the ACR.

Finally, the Holocene part of the record shows a general decrease of aerosol concentration that could point out a gradual reduction of primary production and/or mobilisation of dust at the source. The distribution parameters show higher modes with the highest values in the second part, possibly reflecting a gradual change at the source such as the evolution of soil characteristics.

## Tables

				Log-normal						Weibull					
Particle concentration (Average every 20 m of depth)				$dV/dLn D = a \cdot \exp(-0.5 \cdot (\ln(D/Dv)/\sigma_g)^2)$ $a = V / [(2\pi)^{1/2} \cdot \sigma_g]$						$dV/d LnD = a \cdot ((c-1)/c)^{(1-c)/c} \cdot (g^{(c-1)})^c \cdot \exp(-g^c) + ((c-1)/c)$ $g = \text{abs}((D-Dv)/b + ((c-1)/c)^{1-c})$					
Depth (m)	N.samples	Number/mi	Mass (p.p.b.)	correlation	a	Dv (um)	St.err. of Dv	Geom.st.dev.	Dn** (um)	correlation	Dv (um)	St.error of Dv	a	b	c
40-60	3	3027	9.5	0.87	0.95	2.03	0.03	1.98	0.50	0.87	2.14	0.05	0.94	2.85	1.59
60-80	4	3252	11.6	0.82	0.91	2.28	0.05	2.16	0.38	0.87	2.30	0.05	0.91	3.21	1.56
80-100	4	3929	14.9	0.88	0.97	2.04	0.03	1.92	0.57	0.87	2.15	0.04	0.96	2.76	1.62
100-120	5	2893	10.6	0.85	0.99	2.15	0.04	1.91	0.61	0.84	2.25	0.05	0.97	2.88	1.62
120-140	6	2923	10.8	0.91	1.01	2.15	0.03	1.85	0.69	0.92	2.33	0.04	1.01	2.74	1.84
140-160	5	3276	12.8	0.88	1.04	2.18	0.03	1.81	0.76	0.89	2.43	0.05	1.06	2.81	2.15
160-180	6	3151	11.3	0.88	0.97	2.14	0.03	1.94	0.57	0.87	2.24	0.05	0.95	2.98	1.57
180-200	5	3035	12.6	0.93	1.11	2.14	0.02	1.71	0.90	0.94	2.33	0.03	1.11	2.52	2.05
200-220	5	3071	16.5	0.90	1.10	2.05	0.03	1.72	0.85	0.92	2.24	0.04	1.11	2.41	2.02
220-240	6	4004	15.6	0.88	0.97	2.27	0.04	1.97	0.57	0.87	2.40	0.05	0.95	3.15	1.62
240-260	6	4456	16.8	0.96	1.12	1.92	0.01	1.69	0.84	0.96	2.05	0.02	1.10	2.19	1.85
260-280	5	4689	20.4	0.90	1.07	2.05	0.03	1.75	0.80	0.90	2.16	0.04	1.05	2.44	1.75
280-300	5	3737	14.1	0.91	1.03	2.00	0.02	1.82	0.68	0.90	2.08	0.04	1.00	2.52	1.63
300-320	5	4276	16.0	0.94	1.07	2.00	0.09	1.75	0.78	0.94	2.16	0.03	1.06	2.40	1.86
320-340	6	4071	14.2	0.95	1.06	1.91	0.02	1.76	0.73	0.96	2.07	0.02	1.05	2.33	1.84
340-360	5	5684	21.7	0.95	1.05	1.98	0.02	1.78	0.73	0.94	2.07	0.03	1.03	2.41	1.68
360-380	7	3478	11.3	0.91	1.03	1.86	0.02	1.81	0.65	0.91	1.93	0.04	1.01	2.31	1.62
380-400	8	6922	34.8	0.97	1.09	1.99	0.01	1.72	0.83	0.97	2.14	0.02	1.08	2.32	1.87
400-420	7	7762	29.0	0.97	1.08	1.91	0.01	1.74	0.76	0.97	2.01	0.02	1.06	2.25	1.72
420-440	7	9751	35.7	0.97	1.06	1.94	0.01	1.77	0.74	0.98	2.07	0.02	1.05	2.34	1.77
440-460	7	37958	120.8	0.99	1.15	1.71	0.01	1.67	0.78	1.00	1.79	0.01	1.12	1.89	1.75
460-480	7	105007	361.9	0.99	1.19	1.80	0.01	1.63	0.88	1.00	1.93	0.00	1.17	1.96	1.94
480-500	7	214440	850.7	0.99	1.21	1.90	0.01	1.61	0.97	1.00	2.06	0.00	1.20	2.06	2.06
500-520	7	180006	724.3	0.99	1.25	1.89	0.01	1.58	1.01	1.00	2.03	0.00	1.23	1.98	2.07
520-540	8	181232	716.3	0.98	1.21	1.90	0.01	1.61	0.97	1.00	2.05	0.00	1.20	2.05	2.04
540-560	7	185890	743.0	0.99	1.21	1.91	0.01	1.60	0.98	1.00	2.05	0.00	1.20	2.04	2.04
560-580	7	216022	862.4	0.98	1.24	1.95	0.01	1.59	1.03	1.00	2.11	0.00	1.23	2.08	2.12

Table 8A.1 – EDC dust concentration (Number and mass) along with the parameters for the Lognormal (normalised volume parameter, mode diameter and geometric standard deviation) and Weibull regressions (normalised volume parameter, a, b, c) of volume-size distributions, averaged over every 20 meters of depth.  $D_n$  represents the calculated mode of the number-size distribution (see text).

ICE CORE	Average Holocene dust mass (ppb)	Sampling Frequency Holocene (yrs)	Average LGM dust mass (ppb)	Sampling Frequency L.G.M. (yrs)	LGM/Holocene Abs. concentration
EDC	15±7	135	790 ± 290	230	53
VOSTOK	35 ±18	~600	849 ± 471	~600	24
DOME B	25 ± 12	~300	875 ± 541	~500	35
Old Dome C	23 ± 10	~900	640 ±169	~450	28

Table 8A.2 – Average dust mass concentration for the Holocene and LGM in four East Antarctic ice cores and the approximate time frequency of sampling for the two climatic periods. The number of samples analysed for the Holocene is 81 for the EDC core (this work), 24 for Vostok (Petit et al., 1990), 51 for Dome B (Jouzel et al., 1995), and 17 for old Dome C (Royer et al., 1983).

[a] <u>EPICA</u>				
	Log-normal modal Diameter (Dv)	$\sigma$	Number of samples averaged	Time interval (yrs B.P.)
Holocene	2.06 ± 0.21	1.80 ± 0.10	70	2,400-11,300
A.C.R.	1.94 ± 0.17	1.73 ± 0.09	19	11,900-14,300
Deglaciation	1.79 ± 0.11	1.65 ± 0.06	25	14,700-19,200
L.G.M.	1.91 ± 0.02	1.60 ± 0.01	30	20,000-27,000

[b] <u>GRIP</u>				
	Log-normal modal Diameter (Dv)	$\sigma$	Number of samples	Time interval (yrs B.P.)
Holocene	1.60 – 1.80	1.71	350	(38-2,023)-(3,029-3,045)
Pre-Boreal	1.50	1.74	75	10,181-11,450
Younger Dryas	1.68	1.57	49	11,612-11,714
Bølling	1.54	1.75	99	14,320-14,410
Pre- Bølling	1.66	1.71	21	14,493-14,601
Glacial	1.76	1.65	66	15,839-16,362
L.G.M.	1.94 – 2.02	1.61-1.68	154	21,644-22,143

Table 8A.3 - Comparison between Lognormal fit parameters from selected samples representing different climatic periods in EDC (a) and GRIP (b, from Steffensen, 1997) ice cores.

References
Ashworth AC, Hoganson J (1993) The magnitude and rapidity of the climate change marking the end of the Pleistocene in the mid-latitudes of South America. <i>Palaeogeogr Palaeoclimato Palaeoecol</i> 101: 263-270.
Basile I , Grousset FE, Revel M, Petit JR, Biscaye PE, Barkov NI (1997) Patagonian origin of glacial dust deposited in East Antarctica (Vostok and Dome C) during glacial stages 2, 4 and 6. <i>Earth Planet Sci Lett</i> 146: 573-589.
Basile I (1997) Origine des aérosols volcaniques et continentaux de la carotte de glace de Vostok (Antarctique). PhD thesis, LGGE-Université Joseph Fourier - Grenoble I Grenoble, pp 58-254.
Briat M, Royer A, Petit JR, Lorius C (1982) Late glacial input of eolian continental dust in the Dome C ice core: additional evidence from individual microparticle analysis. <i>Ann Glaciol</i> , vol 3, 27-30,1982.
Burkle LH, Cooke DW (1983) Late Pleistocene <i>Eucampia antarctica</i> abundance stratigraphy in the Atlantic sector of the Southern Ocean. <i>Micropaleontology</i> 29: 6-10
Burkle LH, Cirilli J (1987) Origin of Diatom ooze belt in the Southern Ocean: implications for late Quaternary paleoceanography. <i>Micropaleontology</i> 33: 86
Chappellaz JA, Blunier T, Reynaud D, Barnola JM, Schwand J, Stauffer B (1993) Synchronous changes in atmospheric CH <sub>4</sub> and Greenland climate between 40 and 8 kyr BP <i>Nature</i> 366: 443-445.
Charles CD, Fairbanks RG (1992) Evidence from Southern Ocean sediments for the effect of North Atlantic deep-water flux on climate. <i>Nature</i> 355: 416-419.
Clapperton CM, Sugden DE, Birnie J, Wilson M (1989) Late-glacial and Holocene glacier fluctuations and environmental change in South Georgia, southern ocean. <i>Quat Res</i> 31: 210-228.
Clapperton CM (1993) Nature of environmental changes in South America at the Last Glacial Maximum <i>Palaeogeogr Palaeoclimato Palaeoecol</i> 101: 189-208.
Clapperton CM, Sugden DE, Kaufman DS, McCulloch R (1995) The last glaciation in the central Magellan

- strait, southernmost Chile. *Quat Res* 44: 133-148.
- COHMAP Project Members (1988) Climatic changes of the last 18000 years: observations and model simulations. *Science* 241: 1043-1052.
- De Angelis M, Legrand M, Petit JR, Barkov NI, Korotkevitch YS, Kotlyakov VM (1984) Soluble and insoluble impurities along the 950 m deep Vostok ice core (Antarctica) - Climatic implications. *Journal of Atmospheric chemistry* 1: 215-239.
- De Angelis M, Barkov NI, Petrov VN (1987) Aerosol concentrations over the last climatic cycle (160 kyr) from an Antarctic ice core. *Nature* 325: 318-321.
- De Baar HJW, Jong JTMD, Bakker DCE, Loscher BM, Veth C, Bathmann U, Smetacek V (1995) Importance of iron for plankton blooms and carbon dioxide drawdown in the Southern Ocean. *Nature* 373: 412-415.
- Denton GH, Prentice ML, Burkle LH (1991) Cainozoic history of the Antarctic ice sheet. Tingey RJ, *Geology of Antarctica*, 17, Oxford Science Publications, Oxford, pp.363-433.
- Denton GH, Heusser CJ, Lowell TV, Moreno PI, Andersen BG, Heusser LE, Schluchter C, Marchant DR (1999) Interhemispheric linkage of paleoclimate during the Last Glaciation. *Geografiska Annaler* 81A(2): 107-153.
- Fairbanks RG (1989) A 17,000-year glacio-eustatic sea level record: influence of glacial melting rates on the Younger Dryas event and deep-ocean circulation. *Nature* 342: 637-642.
- Fuhrer K, Wolff EW, Johnsen SJ (1999) Timescales for dust variability in the Greenland Ice Core Project (GRIP) ice core in the last 100000 years. *Journal of Geophysical Research* 104: 31043-31052.
- Gaudichet A, Petit JR, Lefevre R, Lorius C (1986) An investigation by analytical transmission electron microscopy of individual insoluble microparticles from Antarctic (Dome C) ice core samples. *Tellus* 38B: 250-261.
- Gaudichet A, De Angelis M, Lefevre R, Petit JR, Korotkevitch YS, Petrov VN (1988) Mineralogy of insoluble particles in the Vostok Antarctic ice core over the last climatic cycle (150 Kyr). *Geophys Res Lett* 15: 1471-1474.
- Gaudichet A, De Angelis M, Joussaume S, Petit JR, Korotkevitch YS, Petrov VN (1992) Comments on the origin of dust in East Antarctica for present and ice age conditions. *Journal of Atmospheric chemistry* 14: 129-142.
- Grousset FE, Biscaye PE, Revel M, Petit JR, Pye K, Joussaume S, Jouzel J (1992) Antarctic (Dome C) ice-core dust at 18 k.y. BP: isotopic constraints and origins. *Earth Planet Sci Lett* 111: 175-182.
- Hansson ME (1994) The Renland ice core. A northern hemisphere record of aerosol composition over 120000 years. *Tellus* 46B: 390-418.
- Heusser CJ, Rambassa J (1987) Cold climatic episode of Younger Dryas age in Tierra del Fuego. *Nature* 328: 609-611.
- Heusser C (1989) Polar perspective of Late-Quaternary climates in the Southern Hemisphere. *Quat Res* 32: 60-71.
- Heusser CJ (a)(1989) Late quaternary vegetation and climate of southern Tierra del Fuego. *Quat Res* 31: 396-406.
- Heusser CJ (b)(1993) Late-Glacial of Southern South America. *Quat Sci Rev* 12: 345-350.
- Hulton N, Sugden D, Payne A, Clapperton C (1994) Glacier modeling and the climate of Patagonia during the last glacial maximum. *Quat Res* 42: 1-19.
- Joussaume S (1989) Desert dust and climate: an investigation using an atmospheric general circulation model. Leinen M and Sarnthein M Ed., *Paleoclimatology and Paleometeorology: Modern and Past Patterns of Global Atmospheric Transport*. NATO Workshop. pp 253-263.
- Joussaume S (1990) Three-dimensional simulation of the atmospheric cycle of desert dust particles using a general circulation model. *Journal of Geophysical Research* 95: 1909-1941.
- Jouzel J, Lorius C, Petit JR, Genthon C, Barkov NI, Kotlyakov VM, Petrov VM (1987) A continuous isotope temperature record over the last climatic cycle (160,000 years). *Nature* 329: 403-408.
- Jouzel J, Vaikmae R, Petit JR, Martin M, Duclos Y, Stievenard M, Lorius C, Toots M, Melières MA, Burckle LH, Barkov NI, Kotlyakov VM (1995) The two-step shape and timing of the last deglaciation in Antarctica. *Clim Dyn* 11: 151-161.
- Jouzel J, Masson V, Cattani O, Falourd S, Stievenard M, Stenni B, Longinelli A, Johnsen SJ, Steffensen JP, Petit JR, Schwander J, Souchez R (in press) A new 27 ky high resolution East Antarctic climate record. *Geophys. Res. Lett.*
- Kukla G (1989) Long continental records of climate - an introduction. *Palaeogeogr Palaeoclimato Palaeoecol* 72: 1-9.
- Kumar N, Anderson RF, Mortlock RA, Froelich PN, Kubik P, Ditrich-Hannen B, Suter M (1995) Increased biological productivity and export production in the glacial Southern Ocean. *Nature* 378: 675-680.
- Lamy F, Hebbeln D, Wefer G (1999) High-resolution marine record of climatic change in mid-latitude Chile during the last 28000 years based on terrigenous sediment parameters. *Quat Res* 51: 83-93.

- Lumey SH, Switsur R (1993) Late Quaternary chronology of the Titao Peninsula, southern Chile. *J Quat Sci* 8: 161-165.
- Maggi V (1997) Mineralogy of atmospheric microparticles deposited along the GRIP ice core. *Journal of Geophysical Research* 102: 26,725-26,734.
- Mahowald N, Kohfeld K, Hansson M, Balkanski Y, Harrison SP, Prentice IC, Schulz M, Rodhe H (1999) Dust sources and deposition during the Last Glacial Maximum and current climate: a comparison of model results with paleodata from ice cores and marine sediments. *Journal of Geophysical Research* 104: 15,895-15,916.
- Marden CJ, Clapperton CM (1995) Fluctuations of the South Patagonia Icefield during the last glaciation and the Holocene. *J Quat Sci* 10: 197-210.
- Markgraf V (1991) Younger Dryas in South America? *Boreas* 20: 63-69.
- Markgraf V (1993) Younger Dryas in southernmost South America - An update. *Quat Sci Rev* 12: 351-355.
- McCulloch RD, Bentley MJ (1998) Late glacial advances in the strait of Magellan, southern Chile. *Quat Sci Rev* 17: 775-787.
- McCulloch RD, Bentley MJ, Purves RS, Hulton NRJ, Sugden DE, Clapperton CM (2000) Climatic inferences from glacial and palaeoecological evidence at the last glacial termination, southern South America. *J Quat Sci* 15: 407-417.
- Patterson EM, Gillette DA (1977) Commonalities in measured size distribution for aerosol having a soil-derived component. *Journal of Geophysical Research* 82: 2,074-2,082.
- Petit JR, Briat M, Royer A (1981) Ice Age aerosol content from East Antarctic ice core samples and past wind strength. *Nature* 293: 391-394.
- Petit JR, Mounier L, Jouzel J, Korotkevich YS (1990) Paleoclimatological and chronological implications of the Vostok core dust record. *Nature* 343: 56-58.
- Petit JR, Jouzel J, Raynaud D, Barkov NI, Barnola JM, Basile I, Bender M, Chappellaz J, Davis M, Delaygue G, Delmotte M, Kotlyakov VM, Legrand M, Lipenkov VY, Lorius C, Pépin L, Ritz C, Saltzman E, Stievenard M (1999) Climate and atmospheric history of the past 420000 years from the Vostok ice core, Antarctica. *Nature* 399: 429-436.
- Pye K (1987) Aeolian dust and dust deposits. Academic Press, San Diego, pp 334.
- Rea DK (1994) The paleoclimatic record provided by eolian deposition in the deep sea: the geologic history of wind. *Rev. Geophys* 32: 159-195.
- Rothlisberger R, Hutterli MA, Sommer S, Wolff EW, Mulvaney R (2000) Factors controlling nitrate in ice cores: Evidence from the Dome C deep ice core. *J Geophys Res* 105 (D16): 20,565-20,572.
- Royer A, De Angelis M, Petit JR (1983) A 30000 year record of physical and optical properties of microparticles from an East Antarctic ice core and implications for paleoclimate reconstruction models. *Clim Change* 5: 381-412.
- Schwander J, Jouzel J, Hammer CU, Petit JR, Udisti R, Wolff E (in press) A tentative chronology for the EDC Dome Concordia ice core. *Geophys Res Lett*
- Simmonds I (1981) The effect of sea ice on a general circulation model of the Southern Hemisphere. *International Association of Hydrological Sciences Publication* 131: 193-206.
- Sokolik IN, Toon OB (1996) Direct radiative forcing by anthropogenic airborne mineral aerosols. *Nature* 381: 681-683.
- Steffensen JP (1997) The size distribution of microparticles from selected segments of the GRIP ice core representing different climatic periods. *J Geophys Res* 102 (C12): 26,755-26,763.
- Svensson A (1998) Characterization of continental dust in the Greenland GRIP ice core back to 44 kyr BP. PhD thesis, University of Copenhagen, pp84.
- Thompson LG, Mosley-Thompson E, Davis ME, Lin PN, Henderson KA, Cole-Dai J, Bolzan JF, Liu KB (1995) Late glacial stage and Holocene tropical ice core records from Huascaràn, Peru. *Science* 269: 46-50.
- Wenzens G (1999) Fluctuations of outlet and valley glaciers in the Southern Andes (Argentina) during the Past 13000 Years. *Quat Res* 51: 238-247.
- Yung YL, Lee T, Wang CH, Shieh YT (1996) Dust: a diagnostic of the hydrologic cycle during the Last Glacial Maximum. *Science* 271: 962-963.
- Zielinski GA, Mershon GR (1997) Paleoenvironmental implications of the insoluble microparticle record in the GISP2 (Greenland) ice core during the rapidly changing climate of the Pleistocene-Holocene transition. *Geol. Soc. Am. Bull.* 109: 547-559.
- Zdanowicz CM, Zielinski GA, Wake CP, Fisher DA, Koerner RM (2000) A Holocene record of atmospheric dust deposition on the Penny Ice Cap, Baffin Island, Canada. *Quaternary Research* 53: 62-69.

## **8A.2 High resolution EDC dust record for the last deglaciation and the Holocene**

The new features arising from the first EDC ice core record (§8A.1), have been documented in detail at high temporal resolution. The results have been published in *Annals of Glaciology*, Vol.35, 2002, in a manuscript appeared under the title:

### **“LGM-HOLOCENE CHANGES AND HOLOCENE MILLENNIAL-SCALE OSCILLATIONS OF DUST PARTICLES IN THE EPICA-DOME C ICE CORE (EAST ANTARCTICA)”**

#### ***Abstract***

*Measurements of the concentration and size distribution of dust particles found in the EPICA (European Project for Ice Coring in Antarctica) – Dome C (EDC) ice core provide records covering the last 27,000 years. The total concentration decreased drastically by a factor of 55 from the Last Glacial Maximum (LGM, 800 ppb) to the Holocene (15 ppb), with a well-marked absolute minimum around 11,500-11,600 years ago. This later almost corresponds to the end of the Younger Dryas in Greenland, which was marked by a methane peak related to the expansion of tropical wetlands. Assuming that the source region for Antarctic dust is the southern part of South America, the Antarctic dust minimum suggests a larger geographical extent for this wet period.*

*The volume(mass)-size distribution of the particles displays a mode which is close to 2  $\mu\text{m}$  in diameter, shifting from 1.9  $\mu\text{m}$  in the glacial period to 2.07  $\mu\text{m}$  in the Holocene. As opposed to previous results from old Dome C, EPICA suggests a greater proportion of large particles in Holocene samples than in LGM samples. In addition, for the period between 13,000 and 2,000 BP, structured millennial-scale oscillations of the dust mode appear. These are especially well-marked before 5,000 years ago, with higher frequencies also present.*

*The difference between LGM and Holocene particle distributions may be related to changes in the pattern of dust transport to East Antarctica. At Dome C the greater proportion of coarse particles observed during the Holocene suggests greater direct meridional transport. During the LGM, atmospheric circulation was likely more zonal, leading to removal of a higher portion of large dust particles from the atmosphere before reaching Antarctica. Changes in atmospheric circulation could also be the cause of the millennial-scale dust mode oscillations during the Holocene.*

#### **8A.2.1 Introduction**

There is clear evidence of climate system variability at millennial-scale frequencies during the last glacial period. The most striking records are those from Greenland ice cores (e.g. Dansgaard et al., 1984, 1993) and North Atlantic marine sediments (e.g. Oppo and Lehman, 1995; Bond et al., 1993), but other evidence from both land and sea, even outside the high latitude regions of the Northern Hemisphere (e.g. Charles et al., 1996; Behl and Kennett, 1996; Clark and Bartlein, 1995; Porter and An, 1995), suggest that this variability may have had a wider extent. Such variations may have existed in Antarctica, even if the warm interstadials recorded in Greenland between 20,000 and 40,000 years ago are small or even absent (e.g. Sowers and Bender, 1995; Mazaud et al, 2000).

Recently, millennial-scale variability of the climate system has been demonstrated for the Holocene, particularly the unambiguous evidence arising from North Atlantic marine sediments (Bond et al.,

1997; Bianchi and McCave, 1999; Giraudeau et al., 2000; Marchitto et al., 1998). Similar oscillations were also suggested in ice core records from Greenland (Mayewski et al., 1997) as well as in marine sediments from the Indian Ocean (Sarkar et al., 2000). The Southern Hemisphere lacks documentation on this matter, though a record from a marine sediment core off the Chilean coast contains similar millennial-scale fluctuations (Lamy et al, 2001).

In this context, we have analysed the insoluble dust in the new Antarctic ice record from EPICA-Dome C (EDC, 75°06' S, 123°21' E) which spans the last 27,000 years (Jouzel et al., 2001). Our study focuses on the LGM-Holocene changes in dust particle concentration and size distribution and reveals evidence of millennial-scale oscillations in Antarctica over the period between 13,000 and 2,000 years ago.

### **8A.2.2 Analytical procedure**

A total of 360 levels within the new 580 m deep EDC ice core were analysed for insoluble dust concentration and size distribution. For the period from 2,000 to 13,000 years ago, which includes most of the Holocene, we processed 265 samples, representing a temporal resolution of one sample every 40 years. Each sample (5 cm) integrates at least 2-3 years of accumulation.

The decontamination procedure, the preparation of the samples for analysis and the analytical instrument (Coulter Counter Multisizer IIe©, 256-channels) were the same as those used for preliminary studies and are described in Delmonte et al. (2002). Due to the very low concentrations involved, rigorous decontamination and calibration procedures have been applied. Our counter allows detection of particles with diameters larger than 0.7  $\mu\text{m}$ . The number of particles with diameters larger than 5  $\mu\text{m}$  is close to zero in EDC ice. The upper limit of the continuous distribution is given by the first channel preceding the channel with zero particles on three successive measurements. This allows us to separate spurious counts caused by electric noise and/or very big particles introduced by possible contamination of the samples. More than 99% of the total number of particles both for LGM and Holocene samples are in the 0.7-5  $\mu\text{m}$  interval. The number of channels in this interval is  $\sim 140$ , and between two adjacent channels, particle size increases geometrically by a factor of 1.014.

A mass-size distribution was calculated from the volume-size distribution for each sample assuming a particle density of 2.5  $\text{g}/\text{cm}^3$  and fitted using a lognormal function. As described in previous studies (e.g. Royer et al., 1983; Steffensen, 1997), this function defines distributions using three parameters: the total mass ( $M_t$ ), the modal diameter ( $D_v$ ), where the derivative is null, and the geometric standard deviation ( $\sigma_g$ ), which describes how closely the particle size is distributed around the mode.



### 8A.2.3 Results

The Deuterium record (Jouzel et al., 2001) is taken as the climatic reference in Fig. 8A.7-A. It exhibits low values for the glacial LGM period (before 18,000 years ago), a transition phase showing a two-step pattern during the Antarctic Cold Reversal (ACR) phase, then higher values for the Holocene starting at about 11,500 years ago.

The total dust particle number concentration per gram ( $\text{g}^{-1}$ ) and total mass ( $\text{mg kg}^{-1}$  or  $10^{-9} \text{ g g}^{-1}$  or ppb) of the EDC ice core are shown in Fig. 8A.7-B and 8A.7-C along with the non-sea-salt Calcium (nss-Ca) concentration from continuous flow line analysis, taken as a proxy for continental windblown dust (Rothlisberger et al., 2000 and references therein).

The dust concentrations are higher

in number and mass during the LGM ( $197,000 \pm 63,000 \text{ g}^{-1}$ ,  $790 \pm 300 \text{ ppb}$  for the period from 27,000 to 18,000 years ago) compared to those of the warmer Holocene period ( $3,900 \pm 2,000 \text{ g}^{-1}$ ,  $15 \pm 9 \text{ ppb}$  from 11,400 to 2,000 years ago). During deglaciation, the drastic decrease in dust concentration (1.5 orders of magnitude) starts at  $\gg 18,000$  years ago, roughly at the same time as the isotope change, and ends at about 14,600 years ago. The ratio between mean LGM and Holocene dust concentrations is about 55 for both number and mass. Given that the snow accumulation rate during the glacial period was about one half that of Holocene, the change in dust flux is actually a factor of 27.

The three-parameter lognormal distribution suitably depicts the main differences between glacial and Holocene particles. The fitted distributions show correlation coefficients of up to 0.98 for highly concentrated LGM samples but only 0.75 for the very low concentrations of Holocene samples. We made sure this had no consequences on our results by checking that the change in the calculated mode of the distribution correctly followed the observations and did not bias the data. For example, a change

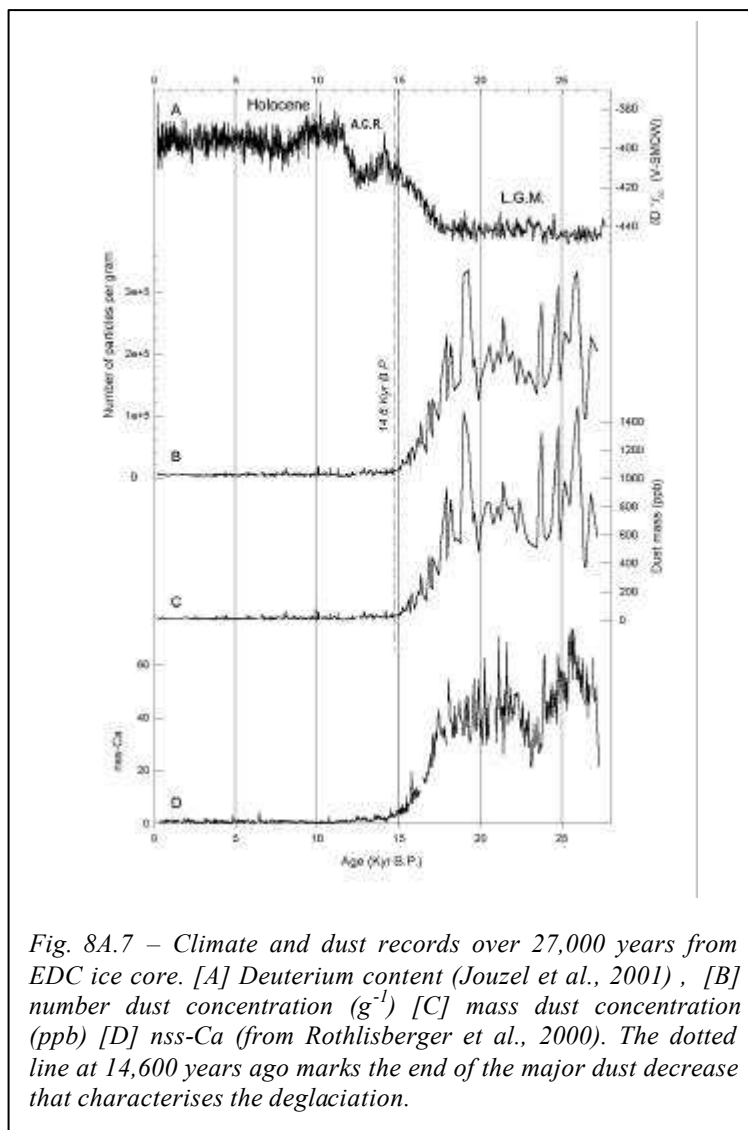


Fig. 8A.7 – Climate and dust records over 27,000 years from EDC ice core. [A] Deuterium content (Jouzel et al., 2001) , [B] number dust concentration ( $\text{g}^{-1}$ ) [C] mass dust concentration (ppb) [D] nss-Ca (from Rothlisberger et al., 2000 and references therein). The dotted line at 14,600 years ago marks the end of the major dust decrease that characterises the deglaciation.

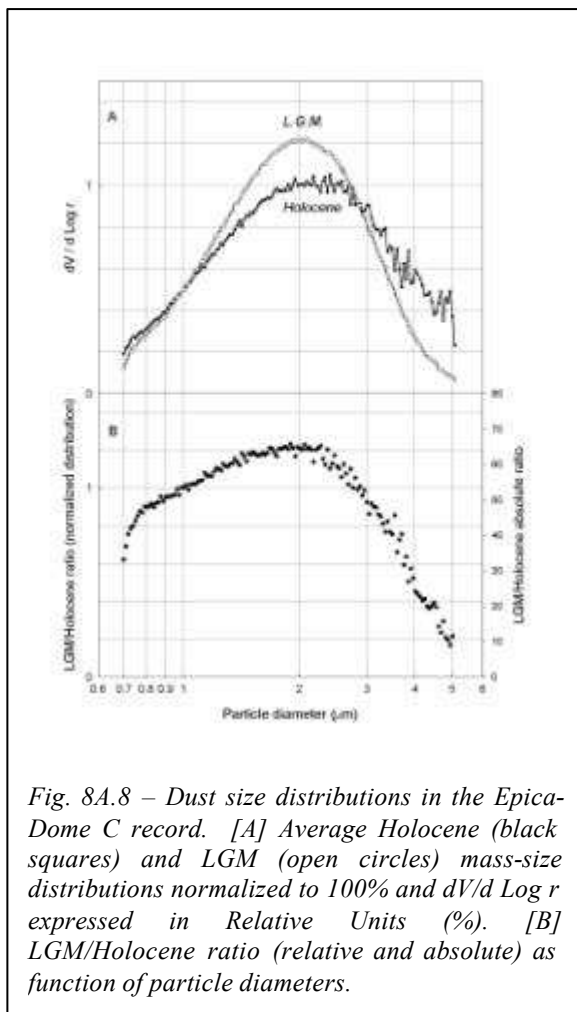


Fig. 8A.8 – Dust size distributions in the Epica-Dome C record. [A] Average Holocene (black squares) and LGM (open circles) mass-size distributions normalized to 100% and  $dV/d \log r$  expressed in Relative Units (%). [B] LGM/Holocene ratio (relative and absolute) as function of particle diameters.

particles might be due to an apparent gravitational settling during transport. In addition, glacial samples display very similar modal diameters (mean  $D_v$  is  $1.9 \pm 0.07 \mu\text{m}$ ) and  $\sigma_g$  values ( $1.6 \pm 0.03$ ). For Holocene samples, both parameters are higher and display a larger variability: mean  $D_v$  of  $2.07 \pm 0.24 \mu\text{m}$  and  $\sigma_g$  equal to  $1.8 \pm 0.15$ .

Fig. 8A.9 displays the number and mass concentration, the mode of the mass-size distribution of dust for the period 13,000-2,000 years ago along with Greenland  $\text{CH}_4$  record from the GRIP ice core. During deglaciation, dust decreases sharply to 14,600 years ago and then remains at a level of ca. 30 ppb and  $6000 \text{ g}^{-1}$  during the Antarctic Cold Reversal (ACR, Fig. 8A.9-B and 8A.9-C). This event is followed immediately by a further decrease to value of  $6 \pm 3 \text{ ppb}$  ( $1900 \pm 1300 \text{ g}^{-1}$ ) that marks the absolute minimum for the whole profile. This phase is well depicted in the profile and spans about 200 years, centred around 11,500-11,600 years ago; it seems to correspond to the end of the Younger Dryas in Greenland (Fig. 8A.9-E) that was marked by the methane rise and was taken as stratigraphic marker (Schwander et al., 2001; Jouzel et al., 2001) to link GRIP and EDC ice core chronologies. Actually, the expected dating uncertainty of  $\pm 250$  years at 11,500 does not allow us to depict the exact phasing of these two events, as will be discussed later in the text.

of  $0.12 \mu\text{m}$  in the mode of the lognormal fit reflects a mean increase in mass concentration represented by coarse particles ( $>3 \mu\text{m}$ ) of 3-4 %. The observed oscillations of  $D_v$  from  $1.9 \mu\text{m}$  to  $2.4 \mu\text{m}$  during the Holocene (see after) would therefore be representative of a change of 15% in large particle mass contribution. In Fig. 8A.8-A, the normalized distribution for the Holocene clearly displays a larger mode and a greater proportion of large particles than for the LGM.

Fig. 8A.8-B shows that the LGM/Holocene ratio varies with size, in particular being much smaller for large particles. Compared to the Holocene size distributions, LGM distributions display more small ( $1-3 \mu\text{m}$ ) and fewer coarse ( $3-4 \mu\text{m}$ ) particles. The ratio of particles with diameters between 2 and  $5 \mu\text{m}$  decreases approximately as a function of the 3<sup>rd</sup> power of the diameter (i.e. it is proportional to the mass), suggesting that depletion of large

From 11,500 to 2,000 years ago the number and mass concentration display a gradual decrease from ca. 4,000 to 2,000  $g^{-1}$  and from 30 to 15 ppb respectively.

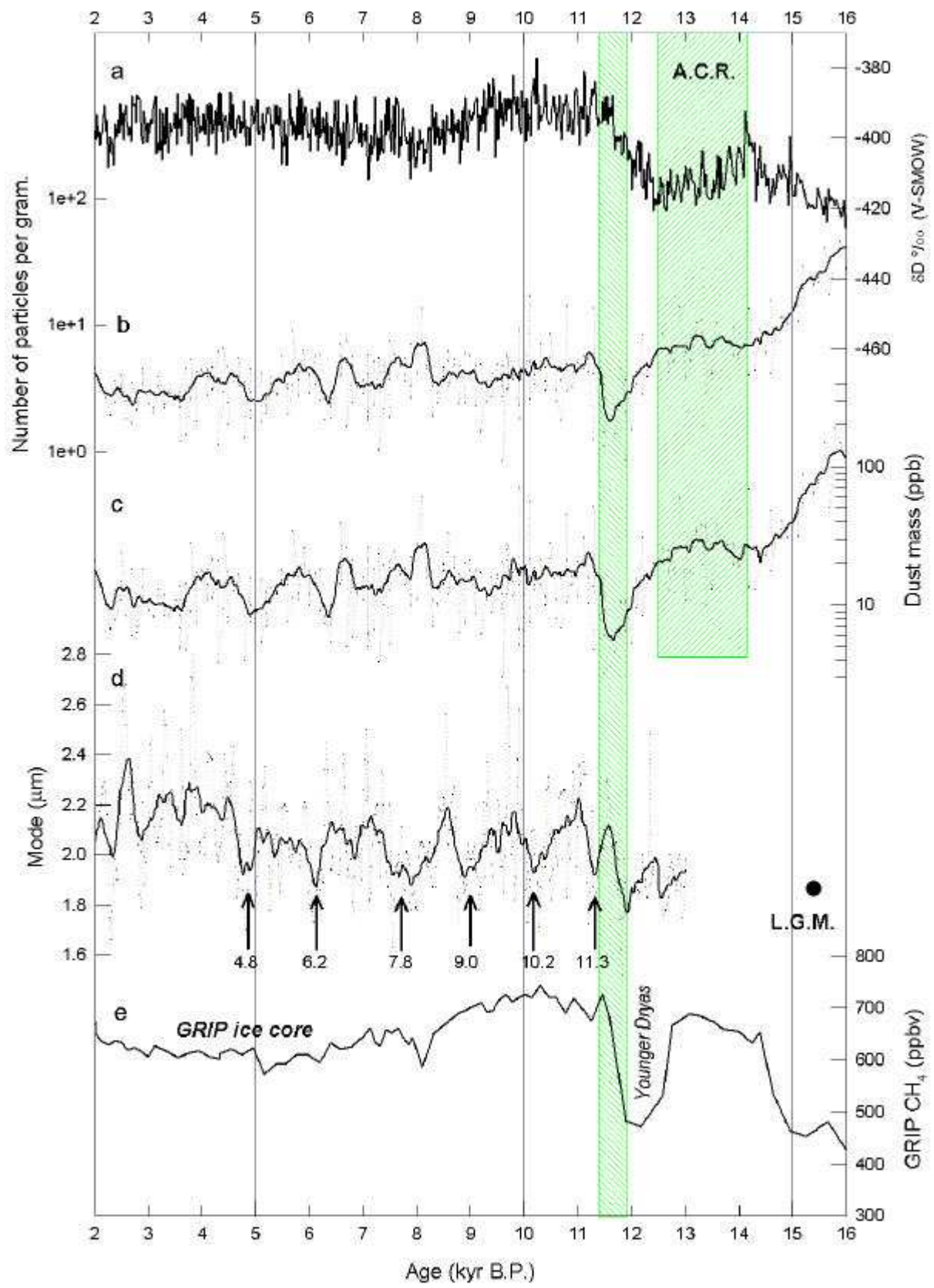
Fig. 8A.9-D shows the  $D_v$  profile. First, except for a value at 12,000 years ago, all Holocene  $D_v$  values are higher than the mean LGM value. Secondly, the profile shows structured fluctuations suggesting some cycles with a millennial-scale periodicity. These are more evident before 5,000 years ago, and five cycles can be observed in the profile between 11,300 and 4,800 years ago. The minimums are separated by 1,100-1,600 years. Spectral analysis of the data (not shown) reveals several bands and one of them peaks at 1,300 years (with F-test confidence levels >95%, using the Multitaper method). There appear to be other significant higher frequency oscillations corresponding to multi-century periods, but they need to be further studied before drawing conclusions. From 11,300 to 4,800 years ago,  $D_v$  oscillates around  $2.03 \pm 0.2 \mu m$ . Then, a step increase is observed, followed by oscillations around  $2.15 \pm 0.2 \mu m$ . Moreover, the millennial oscillations become less clear or are dampened by higher-frequency oscillations.

Each millennial-scale oscillation in the Holocene part of the EDC ice core includes on average of 30 samples. As evidenced by Benoist et al. (1982), there is the possibility that even structured fluctuations might have no climatic significance. Up to now there are no data on other cores about fluctuations in dust size distribution with such detail and even for the Old Dome C core this kind of data does not exist. So this feature needs to be confirmed with replication on other records.

*Fig. 8A.9 (pag. 157) – Climate and dust records and  $CH_4$  record over the last 16,000 years. [A] Deuterium taken from Jouzel et al. (2001), [B] dust number concentration ( $g^{-1}$ ), [C] dust mass concentration (ppb) [D] mode ( $D_v$ ) of the lognormal fit of the mass-size distribution. [E]  $CH_4$  from GRIP is also reported (Chappellaz et al., 1993).*

*The smoothed dust records (black lines) represent the unweighted running averages over 280 years (7 samples) of individual measurements (dots). Arrows in [D] refer to the periods during which minimum modal values occur. The LGM value represents the mean  $D_v$  for the period from 20,000 to 27,000 years ago.*

*The grey box on the right includes the ACR; the one on the left the period with the minimum dust concentration. For this latter, the width of the box represents the location of absolute minimum concentrations with shift of  $\pm 250$  years that represents the expected uncertainty in the timescale at 11,500 years ago.*



#### **8A.2.4 Discussion**

##### ***LGM to Holocene changes***

There is widespread evidence in polar and low-latitude ice cores (e.g. Hansson, 1994, Steffensen 1997, Petit et al., 1981, 1999; Briat et al., 1982), as well as in marine (e.g. Rea, 1994) and terrestrial deposits (e.g. Kukla, 1989), that the atmospheric dust load was greater during glacial periods. The nature of insoluble microparticles of continental origin deposited in polar areas is the end result of a series of factors including the source areas, long range transport mechanisms and mode of deposition (Basile et al., 1997). The environmental conditions at the source area primarily affect dust production, with wind strength determining mobilisation and aeolian deflation. Deserts, arid regions with scarce vegetation, are good candidates for aeolian erosion. The regional meteorological conditions must also be favourable for dust ascension and injection into the upper troposphere. Subsequently, atmospheric circulation needs to be of sufficient strength to transport dust over distances of up to 10,000 kilometres, taking several days or weeks. Dust is removed from the atmosphere by both gravitational settling and scavenging processes that are mostly linked to the hydrological cycle and the presence of water. Different atmospheric circulation patterns can yield longer or shorter paths and therefore different dust transport times from the source to the ice sheet. Deposition in central polar area occurs mostly by dry deposition (De Angelis et al. 1997). Finally, the dust concentration in the ice will also depend on the snow accumulation rate which in turn depends on the local climate (Alley et al., 1995).

The high dust concentration in polar ice cores during the LGM can therefore be interpreted as the result of both regional and large scale factors as well as several concomitant conditions. There is considerable evidence indicating that the LGM was windy and that the continents were arid with reduced vegetation (Mahowald et al., 1993). In parallel to the extension of glaciers in mountainous areas, periglacial processes such as erosion from frost action were more widespread. This may have produced fine sediments in rivers and outwash plains. Loess deposits and other aeolian features characterise the late Quaternary period (Charlesworth, 1957). Under colder climate, the reduction in the intensity of the hydrological cycle affects vegetation and also reduces scavenging of dust in the atmosphere. It is generally thought that the steeper latitudinal temperature gradient during the LGM led to an intensification of the Westerlies (Climap, 1976). However the effect on the dust concentration in Antarctica is not obvious since General Circulation Model simulations do not predict drastic changes (e.g. Joussaume, 1993).

Previous ice cores studies (Petit et al., 1981; De Angelis et al., 1984) evidenced values similar to ours. However, they suggested the presence of slightly coarser particles during the LGM than in the Holocene, and interpreted this as evidence of more efficient transport. Our new measurements from

EDC make the old Dome C data inaccurate<sup>2</sup>. Thanks to the high quality of the new core and improvements in analytical measurement techniques (a 256-channel counter instead of a 16-channels counter) we now have a consistent set of high quality data comprising ca. 360 measurements of particle concentrations and size distributions. For particles with diameter of 2  $\mu\text{m}$  the difference between two channels is about 0.029  $\mu\text{m}$  while for the old instrument it was about 0.5  $\mu\text{m}$ . The analytical precision thus has increased by a factor of 16. Moreover, for the old Dome C data the total number of samples was only 50 for the last 27,000 years, and only 10 of these were from the Holocene.

Our new results clearly indicate differences between LGM and Holocene dust both in terms of absolute concentration and size distribution. The LGM/Holocene ratio is about 55 in absolute concentration and 27 in flux. This is higher than the previous value of 10-30 (Petit et al., 1981), likely due to the lower Holocene concentrations found for EDC. By comparison, EDC Nss-Ca (Fig.1), taken as a proxy for continental dust, changes from  $\sim 50$  ppb (LGM) to  $\sim 2$  ppb (Holocene), representing a factor of  $\sim 25$  in concentration and  $\sim 12$  in flux. This difference from our values in the LGM/Holocene ratio may be due to either a change in the Ca content of the dust (e.g. Ca content would be about 7% and 14% for Holocene and LGM dust respectively) or a higher Ca content in the large particles than in the smaller particles. Further work is needed to clarify this point.

Dust is transported to high altitudes in the troposphere to reach inland sites of the East Antarctic plateau at 4,000 m a.s.l. Dust mainly has a continental origin (Briat et al., 1982; Gaudichet et al., 1988). Its isotopic signature for Vostok and Dome C cores, based on  $^{87}\text{Sr}/^{86}\text{Sr}$  and  $^{143}\text{Nd}/^{144}\text{Nd}$  (Grousset et al., 1992; Basile et al., 1997), suggests that the Patagonian region in southern South America is likely the main source for the LGM period. For the Holocene, preliminary measurements suggest an isotopic signature compatible with a southern South American origin (Basile, 1997). In addition, the preferential atmospheric pathway for transport of dust from South America to East Antarctica is suggested by the relative abundance of volcanic ash layers found in the Vostok core, most originating from South Sandwich volcanoes located in the southern South Atlantic (Basile, 1997, Basile et al., 2001). Moreover, back trajectory analysis using the UKMO Unified Model applied to present-day and LGM conditions suggests that 80% of air masses arriving at Dome C have passed over South America and almost 20% over Australia. This ratio is almost unchanged during the course of the year and for each season (Lunt and Valdes, 2001). We assume therefore that dust in EDC (and

---

<sup>2</sup> The difference in LGM/Holocene trend of dust size between EDC ice core and previous results was attributed to the improvements in the analytical technique used. However, in the light of the results presented in §8A.3, the possibility of a different trend in the LGM/Holocene dust size from one site to another could be attributed to the regional pattern of variability of the atmospheric circulation inside the East Antarctic plateau during the last climatic transition.

likely for East Antarctica) originated mainly from southern South America both during the LGM and the Holocene.

During the glacial period, southern South America was colder and dryer than during the Holocene. The equilibrium line of Patagonian glaciers was considerably lower (Hulton et al., 1994), periglacial erosion processes were intense, and the environment was favourable for dust mobilisation and deflation (Clapperton, 1993). The ~120 m drop in sea level caused an increase in the emerged area by a factor of about 2 in this region. Sea ice extended further Northward, especially in the South Atlantic (Burkle and Cirilli, 1987). The polar front as well as the Westerlies belt moved Northward and this considerably affected southern South American climate (Heusser, 1989).

We believe therefore that the drastic change in the dust concentration between the LGM and the Holocene (Fig. 8A.7) is the result of a number of concomitant factors including changes in the climate and environment at the source, the transport mechanism and conditions in the Southern Ocean. The decrease of dust is also the result of a milder and wetter climate at the source as well as an increased intensity of the hydrological cycle, enhancing evaporation and precipitation to produce more efficient scavenging of aerosol.

The change in the size distribution provides certain indications concerning the long-range transport of the continental aerosol. At first glance, a closer source such as the ice-free areas of Antarctica could be used to explain the greater proportion of large particles during the Holocene; however, preliminary Sr-Nd measurements indicate southern South America as the source. In addition, ice-free areas in Antarctica likely increased in the course of the Holocene. Therefore, the dust concentration in ice should increase whereas the observed concentration decreases at the same time as the particle size increases. Therefore, Antarctica is likely not be a significant source<sup>3</sup>.

With respect to the LGM distributions, the Holocene in EDC ice core displays a relatively higher content of large particles (>3  $\mu\text{m}$ ) as well as less-sorted distributions. Interestingly, the proportion of coarse particles (>2  $\mu\text{m}$ ) was also greater in Greenland ice cores during the Holocene (6.4% - 11.9%) than during the LGM (3.9% - 6.1%) (Steffensen, 1997). The changes in EDC could be interpreted by an apparent shorter time of transport towards this site. Indeed, during the LGM, we believe that the polar front was located farther north, the very cold temperatures forming a strong thermal Antarctic anticyclone and an efficient barrier against direct penetration of warm subantarctic air masses. On the other hand, during the Holocene, Antarctica was warmer and the barrier effect became less efficient as the polar front moved southward.

---

<sup>3</sup> This paper has been written before Sr-Nd measurements reported in Chap. 7 were performed. The conclusions reported here basically do not change but the reader is recommended to take into account what reported in § 7.3.

We also speculate that the decrease in the efficiency of the polar front as a barrier is also linked to the change of sea ice extent around Antarctica, as suggested by marine records (Burckle and Cooke, 1983).

### ***Holocene dust changes***

There are certain features of particular interest in the record such as the plateau in dust concentration during the ACR phase, the development of a 200-year phase of very low concentrations reaching a minimum value around 11,500 years ago, as well as a general decrease during the Holocene.

For the ACR period, the slightly greater values of dust concentration with respect to the average Holocene values do not represent a return to glacial conditions as is the case for the Younger Dryas in the Northern Hemisphere. They may be the result of slight changes in the environmental conditions in southern South America at that time. However, the evidence in this region is not obvious and still subject to debate. Some glaciological (e.g. Wenzens, 1999; McCulloch and Bentley, 1998) and palynological proxies (e.g. Heusser and Rambassa, 1987; Heusser, 1993) indicate a cooling phase which likely enhanced periglacial processes and therefore dust sources, while others (Lumey and Switsur, 1993; Asworth and Hoganson, 1993; Markgraf, 1993) do not show this signature.

The well-marked period of minimum dust concentrations starts around 12,000 years ago and reaches its lowest values at 11,500-11,600 years ago. The EDC record suggests that southern South American dust sources were also less active at this time, which could correspond to a period of increased humidity at this time in this area and simultaneously could also correspond to higher precipitation rates at the EDC site. This event seems to correspond to the methane rise in the Northern Hemisphere (Fig. 8A.9-E) which marks the end of the Younger Dryas cold phase (Chappellaz et al, 1993) and is used as stratigraphic marker for the EDC chronology. However, the uncertainty of the EDC timescale is estimated  $\pm 200$  years at 10,000 years ago and  $\pm 2,000$  years for the glacial period (Schwander et al., 2001), and this does not allow us to state if the absolute minimum of dust concentration coincides with the beginning of the methane rise or with the culmination of the methane peak at the end of the Younger Dryas (see shaded area in Fig. 8A.9).

Since this methane increase at 11,500 years ago was associated with a sudden warming and extension of wetlands in the Northern Hemisphere, we speculate that it also corresponds to significant rapid climatic changes in southern South America and Antarctica, and therefore could have been of an inter-hemispheric to global extent.

Dust concentration displays a gradual decreasing trend from 11,600 to 2,000 years ago. We speculate that this represents a progressive reduction in primary dust production and mobilisation at the source. This is probably related to several factors including a decrease in periglacial processes, an increase in



biological activity, the pedogenesis of soils as well as the expansion of the vegetation cover leading to an enhanced dust trapping effect.

In addition, changes in the mode of the volume-size distribution of the particles (Fig. 8A.9-D) indicate some organised fluctuations with an apparent millennial-scale periodicity (on average 1,200-1,600 years), well marked between 11,500 and 4,800 years ago. Other significant oscillations at higher frequency are also present in the record, but they need to be studied in further detail. A step-like change occurs around 4,800 years ago, and the average mode increases by about  $\sim 0.12 \mu\text{m}$  (Fig. 8A.9).

Evidence of millennial-scale variability of the climate system has already been found for the last glaciation (e.g. Adams, 1999). Recently, several records have also suggested millennial periodicity for the Holocene, such as marine sediments from the North Atlantic Ocean (Bond et al., 1997; Bianchi and Cave, 1999; Giraudeau et al., 2000; Marchitto et al., 1998) showing an apparent periodicity of 1,400-1,500 years but with large band widths ( $\pm 500$  years). Such band widths make direct correlation with events from our Antarctic record difficult. Note also that a similar periodicity has been suggested in the ice chemistry of the GISP2 ice core (Mayewski et al., 1997) but it did not appear in the Holocene  $\delta^{18}\text{O}$  record (Grootes and Stuiver, 1997). In addition to the low amplitude of these periodicities, the chronological uncertainties between records as well as the often inadequate temporal resolution of marine records make it difficult to accurately determine the pacing of millennial and centennial variations.

The origin of the observed millennial scale variations in the climate system is still not understood. Broecker (1999, 2000) suggests an internal ocean-atmosphere variability, while Van Geel (1999) and Stuiver (1993) support the hypothesis of a forcing on the climate system induced by changes in solar activity. Harmonics of orbital frequencies have been studied by Pestiaux et al. (1988) and Loutre (1992), but these have longer periods.

To date, such events are poorly documented in the Southern Hemisphere for the Holocene. Interestingly, a high resolution marine record covering the last 7,000 years on the continental slope off southern Chile (Lamy et al., 2001) has been obtained at a site with high sedimentation rates. This record is sensitive to changes in rainfall and in turn linked to latitudinal shifts of the Westerlies. Millennial periodicity similar to that from Northern Atlantic sediments has been observed; however, the link between the two records is not well understood.

The changes in the sorting and mode size of dust during the Holocene, using the same interpretation as for the LGM/Holocene changes, could be the result of differences in the atmospheric circulation efficiency affecting the duration of aeolian transport of dust. We thus believe that the increase of large particles relative to small ones reflects an easier penetration of air masses towards the interior of

Antarctica and vice versa. Observed periodicities could be interpreted as the oscillation between a situation of more meridional transport and a situation of more zonal circulation in the South Atlantic. In other words, these fluctuations are likely representative of changes in the efficiency of the polar front as a meteorological barrier in South Atlantic. They are therefore probably linked to sea ice extent in the South Atlantic that in turn is a response to conditions of ocean and atmospheric circulation in the Southern Ocean.

### 8A.2.5 Conclusions

The EDC ice core dust record has allowed documentation of changes in the concentration, flux and size distribution of insoluble particles transported to East Antarctica (Dome C) over the last 27,000 years. Between the LGM and the Holocene, drastic changes in dust concentration were accompanied by significant differences in particle size. As an explanation, we suggest more zonal atmospheric circulation around Antarctica during the LGM and a more meridional pattern during the Holocene, allowing easier penetration of air masses.

The record shows a gradual decrease of the total concentration over the last 13,000 years as well as a period with very low dust concentration near the end of the Younger Dryas. Significant millennial-scale fluctuations in the mode of particle size are observed, especially before 5,000 years ago. Higher frequency fluctuations are superimposed on this signal.

Holocene Antarctic records therefore reflect oscillations similar to those found in North Atlantic marine records. This suggests that millennial-scale variability of the Holocene climate is an inter-hemispheric phenomenon; however, further work will be required to determine whether or not this variability is caused by a common primary forcing.

#### References

- Adams, J., M. Maslin and E. Thomas. 1999. Sudden climate transition during the Quaternary. *Prog. Phys. Geogr.*, 23 (1), 1-36.
- Alley, R.B., Finkel R.C., Nishizumi, K., Anandakrishnan, C.A., Shuman, C.A., Mershon, G., Zielinski, G.A., and P.A. Mayewski. 1995. Changes in continental and sea-salt atmospheric loadings in central Greenland during the most recent deglaciation: model-based estimates, *J. Glaciol.*, 41, 503-514.
- Ashworth, A.C. and J. Hoganson. 1993. The magnitude and rapidity of the climate change marking the end of the Pleistocene in the mid-latitudes of South America. *Palaeogeogr., Palaeoclimatol., Palaeoecol.*, Ser., 101, 263-270.
- Basile, I. 1997. *Origine des aérosols volcaniques et continentaux de la carotte de glace de Vostok (Antarctique)*. (These de Doctorat, Université Joseph-Fourier--Grenoble I)
- Basile, I., F.E. Grousset, M. Revel, J.R. Petit, P.E. Biscaye and N.I. Barkov. 1997. Patagonian origin of glacial dust deposited in East Antarctica (Vostok and Dome C) during glacial stages 2, 4 and 6. *Earth Planet. Sci. Lett.* 146 (3-4), 573-589.
- Basile, I., J.R. Petit, S. Touron, F.E. Grousset and N.I. Barkov. 2001. Volcanic tephra in Antarctic (Vostok) ice-cores: source identification and atmospheric implications. *J. Geophys. Res.* 106 (D23), 31915-31931.
- Behl, R.J. and J.P. Kennett. 1996. Brief interstadial events in the Santa Barbara Basin, NE Pacific, during the last 60 kyr. *Nature* 379, 243-246.
- Benoist, J.P., Jouzel, J., Lorius, C., Merlivat, L. and M. Pourchet. 1982. Isotope climatic record over the last 2.5 ka from Dome C, Antarctica, ice cores. *Ann Glaciol* 3, 17-22.

- Bianchi, G.G. and I.N. McCave. 1999. Holocene periodicity in North Atlantic climate and deep-ocean flow south of Iceland. *Nature* 397, 515-517.
- Bond, G., W.S. Broecker, S.J. Johnsen, J. McManus, L. Labeyrie, J. Jouzel and G. Bonani. 1993. Correlation between climate records from North Atlantic sediments and Greenland ice. *Nature* 365(6442), 143-147.
- Bond, G., W. Showers, M. Cheseby, R. Lotti, P. Almasi, P. DeMenocal, P. Priore, H. Cullen, I. Hajadas and G. Bonani. 1997. A pervasive millennial scale cycle in the North Atlantic Holocene and glacial climates. *Science* 278(5341), 1257-1266.
- Briat, M., A. Royer, J.R. Petit and C. Lorius. 1982. Late glacial input of eolian continental dust in the Dome C ice core: additional evidence from individual microparticle analysis. *Ann. Glaciol.*, 3, 27-31.
- Broecker, W.S. 2000. Abrupt climate changes: causal constraints provided by the paleoclimate record. *Earth Sci. Rev.* 51(1-4), 137-154.
- Broecker, W.S., S. Sutherland and T-H. Peng. 1999. A possible 20-th century slowdown of Southern Ocean deep water formation. *Science* 286(5442), 1132-1135.
- Burkle, L.H. and J. Cirilli. 1987. Origin of Diatom ooze belt in the Southern Ocean: implications for late Quaternary paleoceanography. *Micropaleontology* 33, 82-86.
- Burkle, L.H. and D.W. Cooke. 1983. Late Pleistocene *Eucampia antarctica* abundance stratigraphy in the Atlantic sector of the Southern Ocean. *Micropaleontology* 29, 6-10.
- Chappellaz, J.A., T. Blunier, D. Reynaud, J.M. Barnola, J. Schwand and B. Stauffer. 1993. Synchronous changes in atmospheric CH<sub>4</sub> and Greenland climate between 40 and 8 kyr B.P. *Nature* 366(6454), 443-445.
- Charles, C.D., J. Lynch-Stieglitz, U.S. Ninnemann and R. Fairbanks. 1996. Climate connections between the hemisphere revealed by deep sea sediment core/ice core correlation. *Earth Planet. Sci. Lett.*, 142(1-2), 19-27.
- Charlesworth, J.K. 1957. *The Quaternary era*. Arnold Ed. 1700 pages.
- Clapperton, C.M. 1993. Nature of environmental changes in South America at the Last Glacial Maximum. *Palaeogeogr., Palaeoclimatol., Palaeoecol., Ser.*, 101, 189-208.
- Clark, P.U. and P.J. Bartlein. 1995. Correlation of the late-Pleistocene glaciation in the western United States with North Atlantic Heinrich events. *Geology* 23, 483-486.
- Climap Project Members 1976. The surface of ice age earth. *Science* 191(4232) 1131-1137.
- Dansgaard, W., S.J. Johnsen, H.B. Clausen, D. Dahl-Jensen, N.S. Gundestrup, C.U. Hammer and H. Oeschger. 1984. North Atlantic climate oscillations revealed by deep Greenland ice cores. In Hansen, J.E. and T. Takahashi, eds. *Climate processes and climate sensitivity*. Washington, DC, American Geophysical Union, 288-298 (Geophysical Monograph 29, Maurice Ewing Series 5.)
- Dansgaard, W., S.J. Johnsen, H.B. Clausen, D. Dahl-Jensen, N.S. Gundestrup, C.U. Hammer, C.S. Hvidberg, J.P. Steffensen, A.E. Sveinbjomsdottir, J. Jouzel and G. Bond. 1993. Evidence for general instability of past climate from a 250-kyr ice core record. *Nature* 364(6434), 218-220.
- DeAngelis, M., M. Legrand, J.R. Petit, N.I. Barkov, Y.S. Korotkevitch and V.M. Kotlyakov. 1984. Soluble and insoluble impurities along the 950 m deep Vostok ice core (Antarctica) - Climatic implications. *J. Atmos. Chem.* 1, 215-239.
- DeAngelis, M., J.-P. Steffensen, M. Legrand, H. Clausen, and C.U. Hammer. 1997. Primary aerosol (sea salt and soil dust) deposited in Greenland ice during the last climatic cycle: comparison with east Antarctic records. *J. Geophys. Res.*, 102(C12), 26,681-26,698.
- Delmonte, B., J.-R. Petit and V. Maggi. 2002. Glacial to Holocene implications of the new 27,000 year dust record from the EPICA Dome C (East Antarctica) ice core. *Climate Dyn.* 18(8), 647-660.
- Gaudichet, A., M. De Angelis, R. Lefevre, J.R. Petit, Y.S. Korotkevitch and V.N. Petrov. 1988. Mineralogy of insoluble particles in the Vostok Antarctic ice core over the last climatic cycle (150 Kyr). *Geophys. Res. Lett.* 15 (13), 1471-1474.
- Giraudeau, J., M. Cremer, S. Manthé, L. Labeyrie and G. Bond. 2000. Coccolith evidence for instabilities in surface circulation south of Iceland during Holocene times. *Earth Planet. Sci. Lett.* 179(2), 257-268.
- Grootes, P. and M. Stuiver. 1997. 18O/16O variability in Greenland snow and ice with 10-3 to 105 year time resolution. *J. Geophys. Res.* 102 (C12), 26,455-26,470.
- Grousset, F.E., P.E. Biscaye, M. Revel, J.R. Petit, K. Pye, S. Joussaume and J. Jouze l. 1992. Antarctic (Dome C) ice-core dust at 18 ky BP: isotopic constraints and origins. *Earth. Planet. Sci. Lett.* 111(1), 175-182.
- Hansson, M.E. 1994. The Renland ice core: a Northern hemisphere record of aerosol composition over 120 000 years. *Tellus* 46B(5), 390-418.
- Heusser, C.J., Rabassa, J. 1987. Cold climatic episode of Younger Dryas age in Tierra del Fuego. *Nature* 328, 609-611.
- Heusser, C.J. 1989. Climate and chronology of Antarctica and adjacent South America over the last 30,000 years. *Palaeogeogr., Palaeoclimatol., Palaeoecol., Ser.* 76, 31-37.
- Heusser, C. J. 1993. Late-glacial of southern South America. *Quat. Sci. Rev.*, 12, 345-350.
- Hulton, N., D. Sugden, A. Payne and C. Clapperton. 1994. Glacier modeling and the climate of Patagonia during

- the last glacial maximum. *Quat. Res.* 42(1), 1-19.
- Joussaume, S. 1993. Paleoclimatic tracers: An investigation using an atmospheric general circulation model under ice age conditions. 1: Desert dust. *J. Geophys. Res.* 98 (D2), 2767-2805.
- Jouzel, J., V. Masson, O. Cattani, S. Falourd, M. Stievenard, B. Stenni, A. Longinelli, S.J. Johnsen, J.P. Steffensen, J.R. Petit, J. Schwander and R. Souchez. 2001. A new 27 kyr high resolution East Antarctic climate record. *Geophys. Res. Lett.*, 28(16).
- Kukla, G. 1989. Long continental records of climate -- an introduction. *Palaeogeogr., Palaeoclimatol., Palaeoecol.*, 72, 1-9.
- Lamy, F., D. Hebbeln, U. Rohl and G. Wefer. 2001. Holocene rainfall variability in southern Chile: a marine record of latitudinal shifts of the Southern Westerlies. *Earth Planet. Sci. Lett.* 185(3-4), 369-382.
- Loutre, M.F., A. Berger, P. Bretagnon and P.-L. Blanc. 1992. Astronomical frequencies for climate research at the decadal to century time scale. *Climate Dyn.* 7, 181-194.
- Lumey, S.H. and R. Switsur. 1993. Late Quaternary chronology of the Titao Peninsula, southern Chile. *J. Quat. Sci.* 8, 161-165.
- Lunt, D.J. and P.J. Valdes. 2001. Dust transport to Dome C, Antarctica, at the Last Glacial Maximum and present day. *Geophys. Res. Lett.* 28 (2), 295-298.
- Mahowald N, Kohfeld K, Hansson M, Balkanski Y, Harrison SP, Prentice IC, Schulz M, Rodhe H. 1999. Dust sources and deposition during the Last Glacial Maximum and current climate: a comparison of model results with paleodata from ice cores and marine sediments. *J. Geophys. Res.* 104, 15,895-15,916.
- Marchitto, T.M., W.B. Curry and D.W. Oppo. 1998. Millennial-scale changes in the North Atlantic circulation since the last glaciation. *Nature* 393, 557-561.
- Markgraf, V. 1993. Paleoenvironments and paleoclimates in Tierra del Fuego and southernmost Patagonia, South America. *Palaeogeogr., Palaeoclimatol., Palaeoecol.*, 102, 53-68.
- Markgraf, V. 1998. Past climates of South America. In Hobbs, J.E., J.A. Lendesay and H.A. Bridgman, eds. *Climates of the southern continents: present, past and future.*
- Mayewski, P., L.D. Meeker, M.S. Twickler, S. Whitlow, Q. Yang, W.B. Lyons and M. Prentice. 1997. Major features and forcing of high-latitude northern hemisphere atmospheric circulation using a 110,000 year-long glaciochemical series. *J. Geophys. Res.* 102 (C12), 26,345-26,366.
- Mazaud, A., F. Vimeux and J. Jouzel. 2000. Short fluctuations in Antarctic isotope records: a link with cold events in the North Atlantic? *Earth Planet. Sci. Lett.* 177(3-4), 219-225.
- McCulloch, R.D. and M.J. Bentley. 1998. Late-glacial advances in the strait of Magellan, southern Chile. *Quat. Sci. Rev.* 17(8), 775-787.
- McCulloch, R.D., M.J. Bentley, R.S. Purves, N.R. J. Hulton, D.E. Sugden and C.M. Clapperton. 2000. Climatic inferences from glacial and palaeoecological evidence at the last glacial termination, southern South America. *J. Quat. Sci.* 15(4), 407-417.
- Oppo, D.W. and S.J. Lehman. 1995. Suborbital timescale variability of North Atlantic Deep Water during the past 200,000 years. *Paleoceanography* 10, 901-910.
- Pestiaux, P., I. Van Der Mersch and A. Berger. 1988. Paleoclimatic variability at frequencies ranging from 1 cycle per 10,000 years: evidence for nonlinear behaviour of the climate system. *Climatic Change* 12, 9-37.
- Petit, J.R., M. Briat and A. Royer. 1981. Ice Age aerosol content from East Antarctic ice core samples and past wind strength. *Nature* 293(5831), 391-394.
- Petit, J.R., J. Jouzel, D. Raynaud, N.I. Barkov, J.M. Barnola, I. Basile, M. Bender, J. Chappellaz, M. Davis, G. Delaygue, M. Delmotte, V.M. Kotlyakov, M. Legrand, V.Y. Lipenkov, C. Lorius, L. Pépin, C. Ritz, E. Saltzman and M. Stievenard, 1999. Climate and atmospheric history of the past 420,000 years from the Vostok ice core, Antarctica. *Nature* 399(6735), 429-436.
- Porter, S.C. and Z. An. 1995. Correlation between climate events in the North Atlantic and China during the last glaciation. *Nature*, 375, 305-308.
- Rea, D.K. 1994. The paleoclimatic record provided by eolian deposition in the deep sea: the geologic history of wind. *Rev. Geophys.* 32 (2), 159-195.
- Rothlisberger, R., M.A. Hutterli, S. Sommer, E.W. Wolff and R. Mulvaney. 2000. Factors controlling nitrate in ice cores: evidence from the Dome C deep ice core. *J. Geophys. Res.*, 105 (D16), 20,565-20,572.
- Royer, A., M. de Angelis and J.-R. Petit. 1983. A 30,000 year record of physical and optical properties of microparticles from an East Antarctic ice core and implications for paleoclimate reconstruction models. *Climatic Change* 5(4), 381-412.
- Sarkar, A., R. Ramesh, B.L.K. Somayajulu, R. Agnihotri, A.J.T. Jull and G.S. Burr. 2000. High resolution Holocene monsoon record from the eastern Arabian Sea. *Earth Planet. Sci. Lett.* 177(3-4), 209-218.
- Schwander J, Jouzel J, Hammer CU, Petit JR, Udisti R, Wolff E. 2001. A tentative chronology for the EPICA Dome Concordia ice core. *Geophys Res Lett* 28, 4243-4246.
- Sowers, T. and M. Bender. 1995. Climate records covering the last deglaciation. *Science* 269(5221), 210-214.
- Steffensen, J.P. 1997. The size distribution of microparticles from selected segments of the GRIP ice core

representing different climatic periods. *J. Geophys. Res.* 102 (C12), 26,755-26,763.

Stuiver, M. and T.F. Braziunas. 1989. Atmospheric  $^{14}\text{C}$  and century-scale oscillations. *Nature* 338, 405-408.

Stuiver, M. and T.F. Braziunas. 1993. Sun, ocean, climate and atmospheric  $^{14}\text{CO}_2$ : an evaluation of causal and spectral relationships. *Holocene* 3(4), 289-305.

Van Geel, B., O.M. Raspopov, H. Renssen, J. Van der Plicht, V.A. Dergachev and H.A. J. Meijer. 1999. The role of solar forcing upon climate change. *Quat. Sci. Rev.* 18, 331-338.

Wenzens, G. 1999. Fluctuations of outlet and valley glaciers in the Southern Andes (Argentina) during the Past 13,000 years. *Quat. Res.* 51(3), 238-247.

### **8A.3 The LGM-Holocene dust records from Dome B, Komsomolskaya and EPICA-Dome C ice cores.**

The last climatic transition has been documented at high resolution in three East Antarctic ice cores; surprisingly, the coherency of the dust concentration changes nests opposite regional evolutions of the transport mode. A paper has been submitted to *Climate Dynamics* (18<sup>th</sup> September 2003) under the title:

**“OPPOSITE REGIONAL CHANGES AND QUASI-MILLENNIAL OSCILLATIONS IN ATMOSPHERIC CIRCULATION OVER EAST ANTARCTICA DURING THE LAST CLIMATIC TRANSITION.”**

#### ***Abstract***

*Three dust profiles from Dome B (DB), EPICA-Dome C (EDC) and Komsomolskaya (KMS) ice cores (East Antarctica) show the same evolution of the dust input to the polar plateau during the last climatic transition. Moreover, the dust isotopic ( $^{87}\text{Sr}/^{86}\text{Sr}$  versus  $^{143}\text{Nd}/^{144}\text{Nd}$ ) signature identifies a common southern South American origin during the Last Glacial Maximum (LGM) and the deglaciation.*

*However, the particle size distribution reveals significant differences inside East Antarctica during tglacial period and unequivocally opposite evolutions during the climatic transition: at EDC and KMS the small glacial particles gradually increase to coarser dimensions while at Dome B the evolution is clearly contrary. At this latter site, moreover, dust size and concentration changes are almost synchronous.*

*All size distribution records show century to millennial-scale fluctuations superposed on the main trend of changes.*

*We hypothesize the grading of the dust is associated to the altitude of its pathway within the troposphere, and we link the finer particles to the upper air layers over the Antarctic ice sheet because of a probable longer time of flight and residence time.*

*At the end of the glacial period (20 kyr B.P.) the data suggests the subsidence from upper levels was the highest over the Dome C-KMS region, while Dome B area was under influence of air masses from mid tropospheric levels. Then, preferential subsidence progressively moved or expanded southward and at 10 kyr B.P. it was localized over the Dome B region, while the Dome C- KMS region received relatively more dust from lower troposphere pathway.*

*Among other factors, the synoptic situation around Antarctica, the ocean properties and the eastward displacement of ocean-atmosphere anomalies modulate the inflow of air to Antarctica. Their influence is likely reflected in the asynchronous records and in the sub millennial oscillations of dust size.*

### 8A.3.1 Introduction

The paleo-dust cycle is today documented by many terrestrial, marine and polar proxies, especially for the Quaternary period (see Mahowald et al., 1999, and Kohfeld et al., 2001, and references therein). Among the cold periods of the Pleistocene, the last climatic cycle has become a major focus for dust cycle modelling, largely because of the considerable amount of evidence documenting deposition rates and transport paths of aeolian lithogenic material, that are necessary for the evaluation of General Circulations Models (GCM) results.

The ca. 13 million km<sup>2</sup> wide Antarctic continent is a large repository of climatic archives but still rather poorly documented with respect to dust studies: the Byrd ice core (80°S, 120°W) provides the only West Antarctic dust record (Thompson and Mosley Thompson, 1981), while for East Antarctica dust concentration changes since the Last Glacial Maximum (LGM) are documented at low resolution by the first Dome C ice core (*old* Dome C, 74°39'S, 124°10'E, Royer et al., 1983), the Vostok (78°28'S, 106°48'E) ice core (Petit et al., 1999), and the Dome B (77° 05' S, 94° 55'E) ice core (Jouzel et al., 1995). Recently, Delmonte et al. (2002a and 2002b) provided a new highly resolved dust record spanning the last 27 kyr from the new EPICA-Dome C ice core (75° 06'S, 123° 21'E) drilled in the framework of the European Project for Ice Coring in Antarctica.

Dust archived in East Antarctic ice is exclusively of aeolian origin and originates from deflation of the Southern Hemisphere continents. Its short and long-term variability in concentration and size distribution reflects several climatic and environmental intricate-factors such as meteorological conditions, ground surface properties at the source regions, hydrological cycle, removal processes, atmospheric circulation characters, snow accumulation at the site.

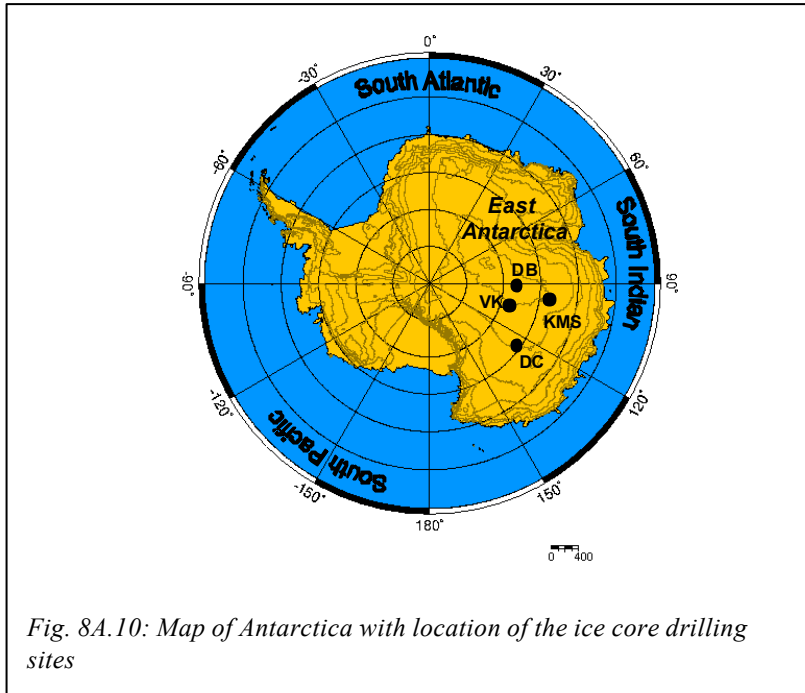
During the last glacial period, all Antarctic ice cores indicate that the atmosphere was dusty in response to increased aridity and more vigorous atmospheric circulation (Petit et al., 1999). A recent correlation between the dust concentration profiles from Vostok and EPICA-Dome C over the last 220,000 years<sup>1</sup> (Delmonte et al., submitted) makes each ice core record representative of the entire East Antarctica in this respect.

Such a covariance between ice records suggests an apparent first-order uniformity in the dust input over East Antarctica and therefore in parameters influencing dust flux such as source strength, scavenging processes en route and transport conditions. Since these parameters are closely linked, difficulties arise to isolate each of the processes. However, in this respect, the change in the dust size distribution is mostly linked to the transport conditions and characteristic, and this makes it an interesting tool for investigation and assessment of the paleo-circulation dynamics (e.g. Ruth et al.,

---

<sup>1</sup> See Chapter 8D.

2003). Recently, variation of the dust size evolution during the last 27 kyr and a part of the Holocene in the EPICA-DomeC ice core revealed some new aspects (Delmonte et al., 2002a, 2002b). As example, the dust from the last glacial maximum (LGM) evidenced finer particles than dust from the Holocene (Delmonte et al., 2002a) while prior studies for other sites concluded the opposite (e.g. Briat et al. 1982, for the Vostok site). For the EDC site, it was suggested that patterns of dust transport to the site changed with climate and that an easier incursion of air masses operated during the Holocene with respect to the LGM. Moreover, millennial and secular scale oscillations in the dust size distributions have been also observed for the last 13 kyr in this core by Delmonte et al. (2002b); the authors suggested that these atmospheric circulation changes were linked to Southern Ocean and global thermohaline circulation (Delmonte et al., 2002b and submitted).



Similarly, secular-scale oscillations in dust size have been detected in a Vostok ice core for a large part of the Holocene period. Because of a tight chronological link with the EPICA dust record through stratigraphic markers (volcanic events), Delmonte et al. (submitted)<sup>2</sup> evidenced the variations in size distribution are in opposite phase with EPICA, thus suggesting regional variability within the East Antarctic plateau.

In this study the dust concentration and size distribution changes over East Antarctica have been investigated for the last climatic transition (from 10 to 20 kyr B.P.) from three ice cores (Fig. 8A.10) : Dome B, Komsomolskaia and EPICA-Dome C (EDC) ice cores, all situated within 1000 km from each other.

Stable isotope analysis of these cores (Jouzel et al., 2001) indicate that the studied period encompasses a major change in the earth climate and environment with the last glacial period (or Marine Isotopic stage 2) and last glacial maximum (LGM), the deglaciation (or termination 1) until the beginning of the Holocene period, this latter being fairly similar to our present day climate.

<sup>2</sup> See § 8B.1



The pattern of the temperature changes deduced from stable isotope for the last climatic transition, thoroughly documented for East Antarctica (see Jouzel et al., 2001), consists in a two-step process with two warming trends interrupted by the Antarctic cold reversal (ACR). Adopting the respective original chronologies for several ice cores in East Antarctica, Jouzel et al. (2001) found a considerable match among the records and a quasi synchronicity of the changes.

Since major changes have occurred over continents in the Southern hemisphere, which may affect the relative contribution to the Antarctic dust and possibly the variability of the dust size distribution, we also investigated for each ice core the dust provenance to constrain the geographical location of the source. This was done by using the well established geochemical technique of  $^{87}\text{Sr}/^{86}\text{Sr}$  versus  $^{143}\text{Nd}/^{144}\text{Nd}$  isotopic tracers (Biscaye et al., 1997; Basile et al., 1997).

### **8A.3.2. Analytical techniques**

#### ***The ice cores***

The 780m deep Dome B ice core (DB, 77° 05' S, 94° 55'E, 3650 m a.s.l) has been obtained during the 1987-1988 austral season by the 33<sup>rd</sup> Soviet Antarctic expedition. The site is located about 870 km from Dome C, and has a similar ( $\sim 3 \text{ g cm}^{-2} \text{ a}^{-1}$ ) accumulation rate (Jouzel et al., 1995). The climatic record and the chronology were published by Jouzel et al. (1995) along with a preliminary profile for dust concentration. The record covers the last 30 kyr.

The 885 m deep Komosmolskaia ice core (KMS, 74° 05' S, 97° 29' E, 3500 m a.s.l) was extracted in 1983 by the 28<sup>th</sup> Soviet Antarctic Expedition. Accumulation rate for the Holocene is about  $5 \text{ g cm}^{-2} \text{ a}^{-1}$ , the timescale established by Ciais et al. (1992) and the climatic record is from Jouzel et al. (2001). The record covers only the last 16 kyr that corresponds to middle deglaciation.

The 788 m EPICA Dome C (EDC, 75° 06'S, 123° 21'E, 3233 m a.s.l.) core has been described Jouzel et al. (2001) for the climate record over the last 27 kyr; the ice core chronology established by Schwander et al. (2001), and a first dust profile by produced by Delmonte et al (2002a), which is here now documented at higher resolution.

#### ***Samples for dust concentration and size distribution measurements***

Ice samples have been selected from the three ice cores for the period from 10 to 20 kyr B.P.; the number of samples for each core, the relative sampling depth and resolution are reported in Tab.8A.4. The procedure of sample preparation and decontamination is described in detail in Delmonte et al. (2002a). All samples (5-6 cm in length) are representative of ca. 3 years. Measurements have been performed in random order using a particle counter (Coulter Counter Multisizer IIe©, 256-channels)

set up in the class 100 clean room of LGGE-CNRS laboratory (Grenoble, France), and calibrated with a 2.07  $\mu\text{m}$  latex.

The instrument was set to detect particles with equivalent spherical diameter from 0.7 to 20  $\mu\text{m}$ . Each concentration and size distribution data is the average of at least three independent measurements. The total mass of particles has been calculated from the volume-size distribution assuming an average density of 2.5  $\text{g}/\text{cm}^3$ . Laboratory blanks were checked after each sample analysis and the average value was  $\sim 1$  ppb of dust.

The mass-size distribution of particles in East Antarctic ice is usually well sorted around a mean mass diameter of about 2  $\mu\text{m}$  and it can be fitted with Lognormal or Weibull functions (Delmonte et al., 2002a). The regressions properly smooth the data and their modal value can be used as a proxy for particle dimensions. However, the fitting partially reduces the variability of the signal, especially when dealing with low concentration samples with high data scattering (see for example Fig.8A.12d-e-f).

Therefore, we introduce the relative contribution to the total mass represented by the fine particles (FPP) or by the coarse particles (CPP) within arbitrary size intervals and computed from the raw data of the counter. Here we choose for the fine particle percentage (FPP) the interval from 1 and 2  $\mu\text{m}$ .

### ***Samples for Sr-Nd isotopic measurements***

Two samples for each site have been selected for  $^{87}\text{Sr}/^{86}\text{Sr}$  and  $^{143}\text{Nd}/^{144}\text{Nd}$  isotopic analysis. They were taken from the LGM period on DB and EDC ice cores, and from the deglaciation on KMS. Sample preparation consists of decontamination through three repeated washings in ultra-pure water (MilliQ), in a class 100 clean room (LGGE-CNRS, Grenoble). The mineral fraction was extracted by centrifugation as in Basile (1997). The evaporation method used in previous studies (Grousset et al., 1992; Basile et al., 1997) was not used in order to avoid possible Sr contribution from marine aerosols.

After centrifugation, the supernatant of the sample was removed using a syringe and bottom samples gathered for a next centrifugation. The final bottom liquid ( $\sim 20$ -30 ml from about 300-900 g initial sample) was evaporated. The amount of dust collected was estimated from final sample by Coulter Counter. The total mass was very low and varied by a factor of  $\sim 10$  among the samples, from  $\sim 10$   $\mu\text{g}$  to  $\sim 100$   $\mu\text{g}$  (Tab. 8A.5).

Coulter Counter measurements of the supernatant gave evidence for residual (very diluted) particles with a size distribution identical to the whole initial sample. This suggests an overall lack of differentiation in the size during centrifugation, and probable absence of mineralogical (hence isotopic) differentiation. However, a test was made by analysing isotopic composition of particles

from the supernatant of a DB sample, collected by filtration. This test gave no evidence for isotopic differentiation with dust (bottom sample) from centrifugation<sup>3</sup>.

The chemical procedures for Sr and Nd separation and the isotopic measurements have been performed at the Department of Cosmochemistry of the Max Plank Institute of Mainz (Germany). The laboratory procedure for sample preparation and analysis is detailed in Bogdanovski (1997). Separation of Sr and Nd has been done using ionic exchange columns, through two repeated passages in order to improve sample purification. The total amount of Sr and Nd collected has been calculated assuming an average Upper Continental Crust (UCC) concentration for both elements (350 ppm and 26 ppm respectively, Taylor and Mc Lennan, 1985), and a ~95% efficiency for each passage through the columns. Laboratory blanks are lower than 20 pg for both elements.

The total amounts of Sr and Nd (reported in Tab. 8A.5) are extremely low, and they span from ~3 ng to ~40 ng for Sr and from ~0.2 to 3 ng of Nd. With such low amount, isotopic analysis require a highly-sensitive Thermo-Ionization Mass Spectrometer (TIMS) especially built for small terrestrial and extraterrestrial samples (Bogdanovski, 1997). Before the measurements the samples transferred on the filament were let at ~800°C for 10-12 hours to enhance the sample purification and improve the signal. Then they were slowly heated to 1200-1300 °C for measurements. Each sample measurement was done over a duration of ~17-24 hours for each sample, and the Sr and Nd ratio represents the average of ~600 individual ratios (Tab. 8A.6).

Neodymium ratios  $\epsilon_{Nd}(0)$  are expressed as :

$$\epsilon_{Nd}(0) = \left( \frac{{}^{143}\text{Nd}}{{}^{144}\text{Nd}} \right)_{\text{meas}} / \left( \frac{{}^{143}\text{Nd}}{{}^{144}\text{Nd}} \right)_{\text{CHUR}} - 1 \times 10^4$$

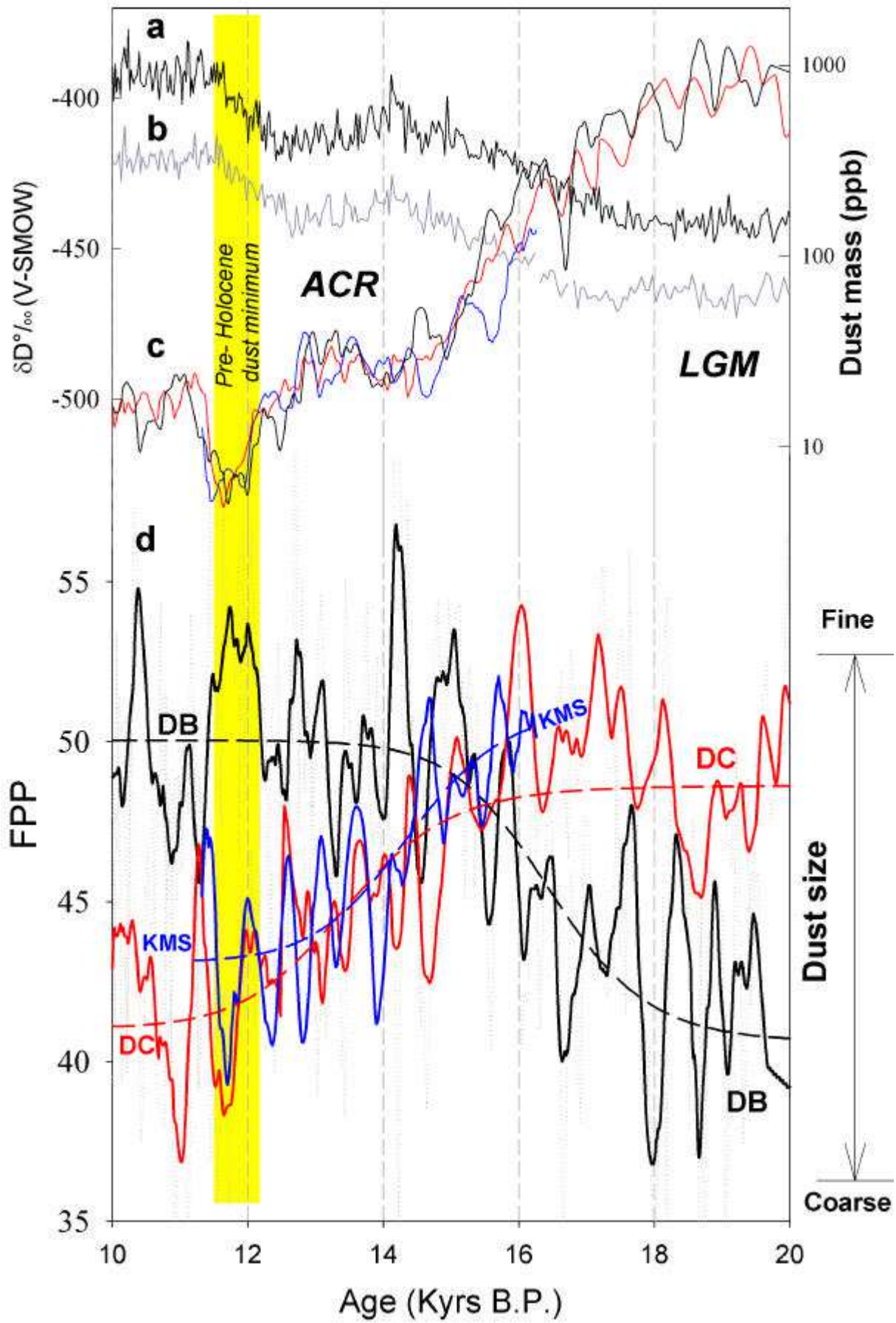
where the  ${}^{143}\text{Nd}/{}^{144}\text{Nd}$  ratio for the CHUR (Chondritic Uniform Reservoir) is 0.512638 (Jacobsen and Wasserbrug, 1980). The measured  ${}^{143}\text{Nd}/{}^{144}\text{Nd}$  ratios have been corrected for mass fractionation by normalizing to  ${}^{146}\text{Nd}/{}^{144}\text{Nd} = 0.7219$ .

\*\*\*\*\*

*Fig. 8A.11(Pag. 173): Climate and dust records for the deglaciation*  
*[a] and [b]: Stable isotopic profiles of Dome B (from Jouzel et al., 1995) and EDC (from Jouzel et al., 2001) ice cores.*  
*[c]: Dust concentration records from Dome B (black line) EDC96 (red line) and KMS (blue line) smoothed with a 200-yr running average.*  
*[d]: Dust FPP records (Fine Particle Percent, see text) from Dome B (black line) EPICA Dome C (red line) and Komsomolskaya (blue line).*  
*The dotted grey lines correspond to raw data, the solid lines to a 200-yr running average and the dashed lines to the mean trend of each series. The squares on the right hand side of fig. 2d indicate the average LGM FPP for Dome B and Dome C.*

---

<sup>3</sup> See Chapter 7.



### 8A.3.3 Results

#### *The dust concentration profiles*

The dust concentration profiles for the three ice cores are shown in Fig. 8A.11c (running average over ca. 200 yrs) along with the isotopic profiles from DB and EDC. The investigated time period spans the end of the LGM and the climatic transition until the beginning of the Holocene (10 to 20 kyr B.P.). The KMS record is shorter and covers the deglaciation from ca. 16.4 B.P. to ca. 11.2 kyr B.P.

The three dust concentration profiles are remarkably similar, and the general trend covariate almost synchronously without timescale adjustment. The average dust concentrations for each climatic period are reported in Tab. 8A.4. Very high concentrations characterize the Last Glacial Maximum (850 ppb at DB and 730 ppb at EDC respectively), and start to decrease rapidly at ca. 18 kyr B.P., and reach a minimum value with typical Holocene levels at ~14.5 kyr B.P. Follows a shallow re-increase of dust in concomitance to the Antarctic cold reversal (ACR) from 14.5 to 12.2 kyr B.P. where concentration are up to about two times the Holocene levels are seen on the three sites. After a decrease following this event, a well marked pre-Holocene dust minimum is also seen in the three records. This event, during which dust concentrations decrease to ca. 7-9 ppb, spans 800-1000 yrs from 11.3 to 12.1 kyr BP and represents a good stratigraphic marker.

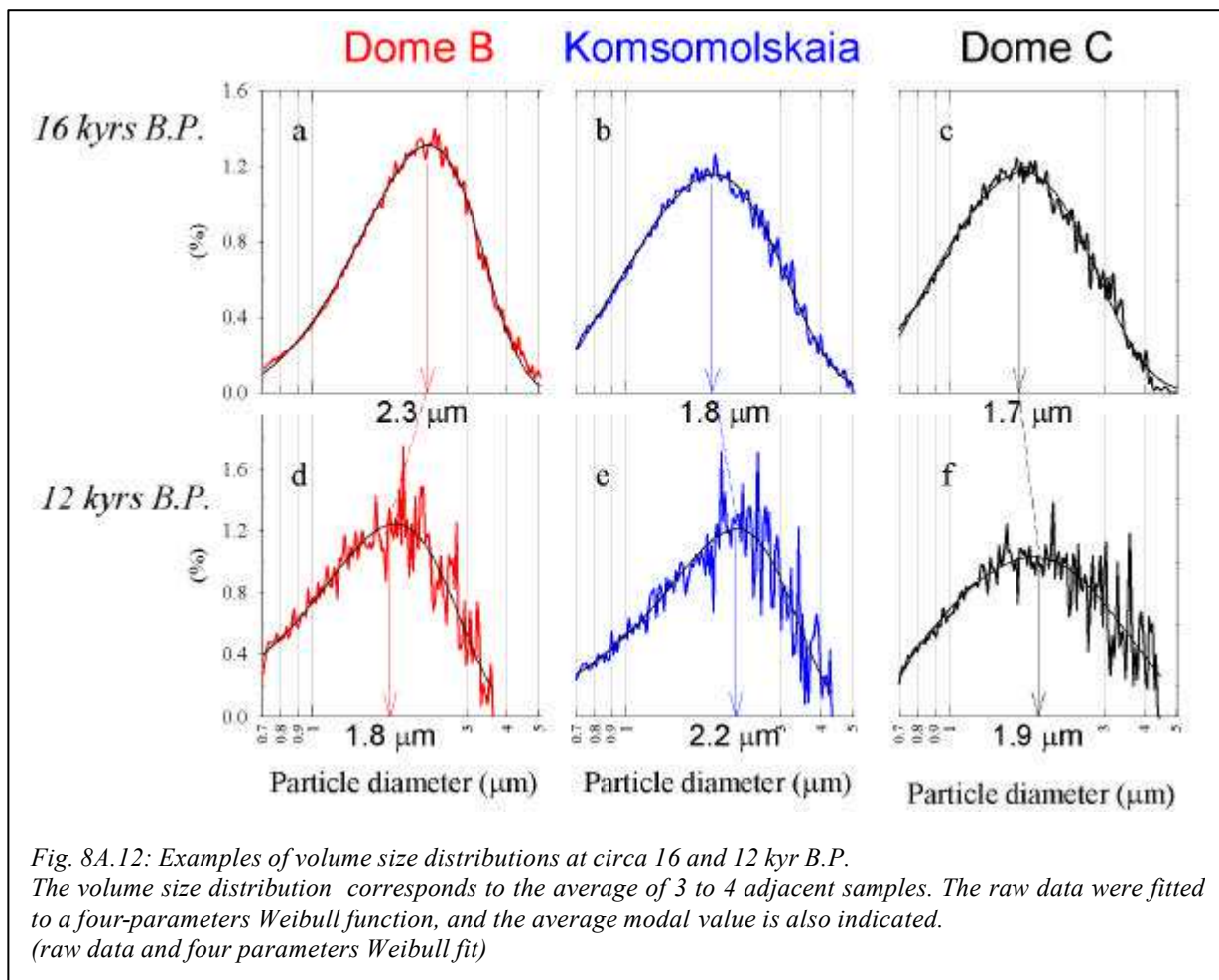
#### *The dust size distribution records*

The sequence of the main trends in FPP (dashed lines on Fig 8A.11d) during climatic transition highlights two important phenomena: first the opposite evolution of the dust size distributions between DB on a hand and EDC and KMS on an other hand; second, a different timing and duration of the changes.

The FPP records for the three cores (running average over ca. 200 years) are shown in Fig 8A.11d along with the long-term trend of the changes (dashed line in Fig. 8A.11d). For the studied period, evolution of dust size displays a large variability with structured oscillations around a mean trend. The overall tendency is of interest and this latter shows clear opposite behaviors between the sites. This clearly contrasts with the general covariance observed for the particle mass concentration.

The size distribution is clearly different from site to site. As example, the average distributions of 3-4 adjacent samples selected from each core around 16 kyr B.P. and 12 kyr B.P. are reported in Fig. 8A.12. Between 16 and 12 kyr BP, the average mode of DB decreases from ~2.3  $\mu\text{m}$  to ~1.8  $\mu\text{m}$  (Fig. 8A.12a and 8A.12d), while at the same time the dust mode increases from ~1.8  $\mu\text{m}$  to ~2.2  $\mu\text{m}$  for KMS (Fig. 8A.12b and 8A.12e) and from ~1.7  $\mu\text{m}$  to ~1.9  $\mu\text{m}$  (Fig. 8A.12c and 8A.12f) for EDC respectively.

Over the studied period, the trend is also different between sites. During the late LGM, from 18 to 20 kyr B.P., the DB dust is characterized by higher proportions of relatively large particles with a modal value of  $\sim 2.4 \mu\text{m}$  and conversely by lower contribution of fine particles, FPP  $\sim 41\%$ . At the same time, the EDC dust is marked by higher contribution of relatively finer graded dust with modal value  $\sim 1.9 \mu\text{m}$  on average, as already noted by Delmonte et al.(2002a), and a FPP value of  $\sim 48\%$ . Indeed this difference between the two sites already existed during the preceding millennia (since  $\sim 26$  kyr B.P.) as documented by a set of 12 additional samples from DB giving a low value for FPP ( $\sim 41.5\%$  on average), and for EDC a FPP value of  $\sim 47.3\%$  (average of 45 samples).



At DB, the change from coarse LGM size to finer, starts at circa 18 kyr B.P. and steadily operates over a  $\sim 3\text{-}4$  kyr duration, i.e. almost synchronously with the fall of the total dust concentration, until reaching the average Holocene size (FPP  $\sim 50\%$ ) at about 14.5 kyr B.P. For EDC, the dust size change evolves in the opposite, with a change from FPP 48% starting at 16 kyr B.P., spanning over a longer time period (ca. 5-6 kyr) and reaching the average Holocene values (FPP  $\sim 41\%$ ) at  $\sim 10.5$  kyr B.P. Interestingly, the KMS particle size profile follows the EDC dynamic of the change from finer to coarser dust particles within the deglaciation.

Also, at 15 kyr B.P. the trends intersect and the FPP for the three dust records are comparable.

The main trends of the FPP is overlaid by multi-centennial to millennial-scale fluctuations, for the three records. The sampling resolution is almost constant in depth for the three ice cores, but as accumulation rate significantly changed during the deglaciation, the time resolution gradually decreases with depth, this making an obstacle for accurate spectral analysis. However, for the purpose of this paper we retain that a visual inspection suggests that minimum values of the multicentennial to millennial-scale fluctuations are separated by 600-700 year periods.

Such short term oscillations do not appear to be in phase between the sites, that is not surprising since dating is not well constrained over the entire period. However, it is worth noting that at the time of the pre-Holocene dust concentration minimum, considered as a stratigraphic marker, FPP profiles show again a different behavior between sites with a relative maximum on DB and a relative minimum for both EDC and KMS.

### ***The dust isotopic composition***

The  $^{87}\text{Sr}/^{86}\text{Sr}$  versus  $^{143}\text{Nd}/^{144}\text{Nd}$  isotopic ratios are reported in Fig. 8A.13-a and 8A.13-b and Tab. 8A.6. The signature of all the samples is almost identical and spans a very narrow interval between  $0.708316 < ^{87}\text{Sr}/^{86}\text{Sr} < 0.709058$  and  $-3 < \epsilon_{\text{Nd}}(0) < -0.58$ . Fig. 8A.13-a and the zoom in Fig. 8A.13-b show that the ice core dust (ICD) isotopic field for LGM is extremely restricted even considering the error bars. The isotopic ratio of dust from the *old* Dome C ice core, analyzed by Basile (1997) using the same technique for dust extraction, is reported in Fig. 8A.13-b. It matches very closely our data.

The isotopic signature of the DB sample obtained by filtering the supernatant (# DB-a-filtered) is almost identical to that of particles from centrifugation ( $\Delta ^{87}\text{Sr}/^{86}\text{Sr} \sim 0.000096$  and  $\Delta \epsilon_{\text{Nd}}(0) \sim 0.097$ ). This confirms that the extraction procedure used does not generate mineralogical and isotopic fractionation into the samples.

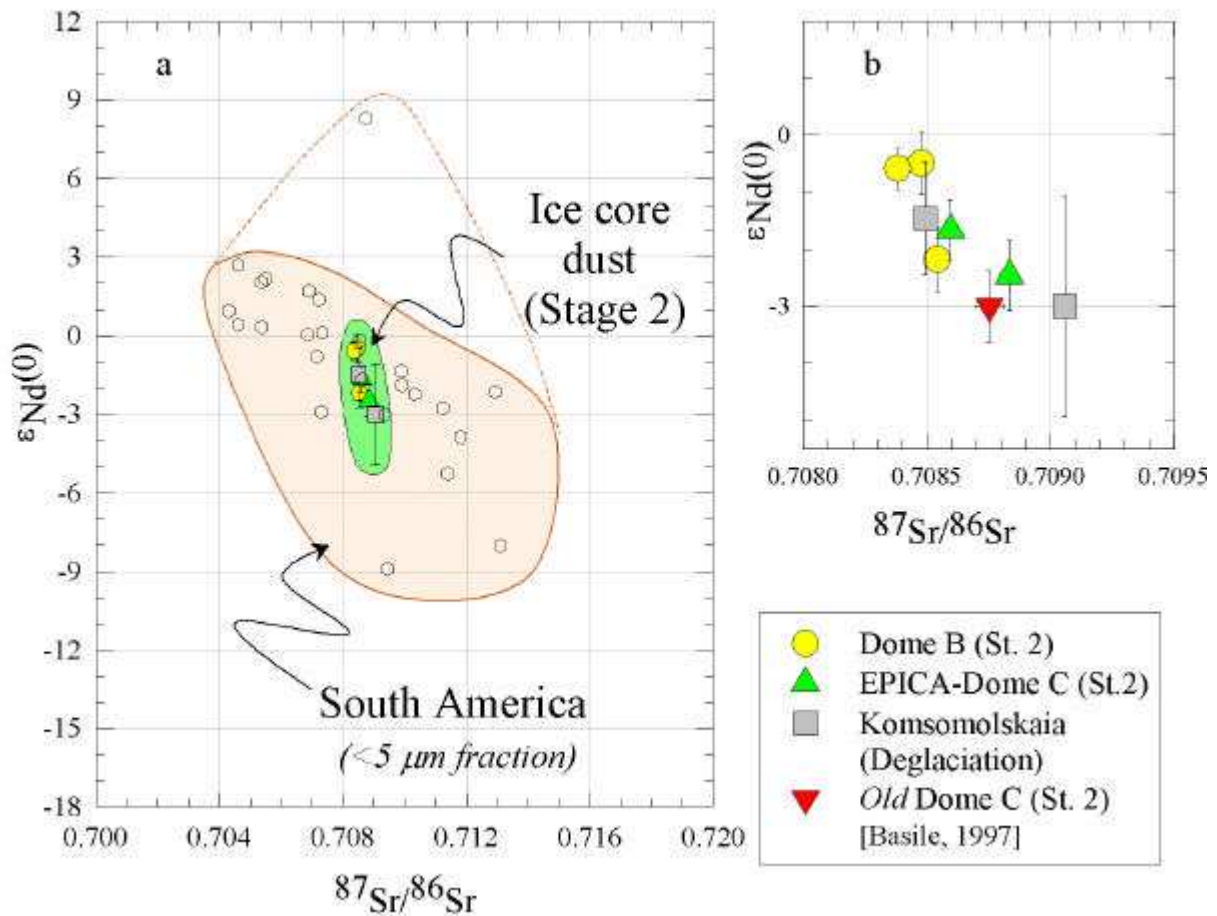


Fig. 8A.13: Sr and Nd isotope results for the ice and potential source area

[a] Comparison between the isotopic field of ice core dust to Southern South American samples (from Delmonte et al., submitted) selected with an equivalent size (<5 $\mu m$ ).

[b] Zoom on the ice core isotopic signature for LGM and Deglaciation samples from Dome B, Dome C and KMS analyzed in this work with error bars.

#### 8A.3.4. Discussion

The dust input (flux) to Antarctica depends on many factors, which can be classified in three main categories. First, the *source strength*, including soil properties, vegetation cover and factors influencing the amount of particles available for deflation (Tegen et al., 2002); second, the processes occurring *en route*, linked to the hydrological cycle; third, the transport. Process *en route* are mainly the wet and dry deposition processes (Tegen and Fung, 1994) affecting the mean residence time of the particles in the air. At polar latitudes and in East Antarctica, deposition processes are dominated by the dry deposition (Legrand et al., 1997). The residence time of aerosol is also size-dependent. For particles with diameters between 1.6 and 3  $\mu m$  it has been estimated to ca. 180-220 hours (Tegen and Fung, 1994). Finally, the *transport* also plays a key role, both in terms of time of transit between the



source and the sink, and transport pathway for aerosol through the troposphere. Interestingly, the dust size distribution depends mainly only on transport conditions.

### ***The geographical sources for dust***

The isotopic signature at the three sites appears almost identical (Fig. 8A.13a and 8A.13b), and gives evidence for a common dust origin at the three sites and likely for the whole East Antarctic plateau during the LGM.

An analog isotopic investigation (Delmonte et al., submitted) obtained a common geographical provenance for Dome C and Vostok dust during cold stages 2, 4 and 6. In this latter study, the isotopic signature of ice core dust have been compared to the signature of potential source areas (PSAs) from the continents of the Southern Hemisphere. The Sr-Nd signature of the PSAs was measured on the grain size fraction equivalent to the long range transported dust, i.e. on the  $<5 \mu\text{m}$  fraction, in order to prevent isotopic differences due to grain size effects. Southern South America ( $>31^\circ \text{S}$  of latitude) was confirmed to be the dominant dust source for Dome C and Vostok during cold periods, as previously proposed by Grousset et al. (1992) and Basile et al. (1997).

For comparison, the isotopic ratios of the  $<5 \mu\text{m}$  fraction of loesses and aeolian samples from the Pampas, Patagonia and Chile are reported in Fig. 8A.13a (details about the PSAs will be reported elsewhere). The excellent match between the isotopic signature of the LGM dust analyzed in this study with the southern South American one (Fig. 8A.13a) nicely confirms the same conclusion also for Dome B and KMS sites.

### ***The dust concentration records***

The dust concentration changes from the late LGM to the beginning of the Holocene period (20 to 10 kyr B.P.) show a parallel evolution at Dome B, EDC and KMS sites, giving evidence for a uniformity in the dust input to the East Antarctic plateau. Since the accumulation rate at Dome B and EDC sites is almost the same (Jouzel et al., 1995) the dust fluxes are also comparable.

The features of the dust changes during the last deglaciation, initially depicted in a first study of EDC dust record at low resolution (Delmonte et al., 2002a), are now characterized in better detail. Complementary documentation comes from the Dome B and KMS records. In particular, all profiles show a shallow re-increase in dust concentration in concomitance with the ACR phase and a well marked pre-Holocene dust minimum. Both of these events have been interpreted as possible changes in the environmental conditions at the dust source regions (Delmonte et al., 2002a). The ACR dust event could be the signal of a possible return to cooler conditions during the last termination, despite controversial evidences for a cold phase on the Southern Hemisphere continents at that time (e.g. Markgraf, 1991). The pre-Holocene dust minimum on the other side, is thought to be primarily related

to the hydrological cycle, either in terms of increased humidity at the source (e.g. a humid period in South America) and hence a weakening of its strength, or to an increased scavenging *en route* through wet deposition (Delmonte et al., 2002b). As the dominant source of dust is likely unique (South America), the pre Holocene dust minimum is probably a climatic event affecting the dust input over the entire East Antarctica and therefore confidently as a stratigraphic marker.

### ***The regional differences of the dust transport during LGM.***

From previous study, the fine dust size on EDC during the LGM was attributed to the enhanced isolation of the site from meridional penetration of air masses (Delmonte et al. 2002b). The new data from DB and KMS allows to complete the picture for central East Antarctica, suggesting that regional variability and the enhanced isolation for some sites during the glacial period occurred in tandem with preferential incursions of air masses carrying dust towards other sites of the plateau. For the drilling site of Vostok, which is ~300 km from DB, we have only reliable data for the Holocene period (see Chap. 8B) and some from the LGM (Briat et al, 1982), but the deglaciation is not documented. Nevertheless, the grade of the Holocene dust at Vostok is finer than EDC dust (Delmonte al. 2003), and lower than the Vostok LGM dust. The total change in the Vostok dust grade after the climatic transition appears therefore in similar to DB.

The LGM dust is characterized by significant differences in particle size between the DB and EDC ice cores, and from 20 to 18 kyr BP the  $\Delta FPP$  is about ~ 7% (corresponding to difference in mode  $\Delta\mu$  ~0.5  $\mu\text{m}$ ). The KMS core is does not cover this climatic period. However, because its evolution during the deglaciation is remarkably similar to that of EDC, we may expect this similarity holds for the LGM.

Dry deposition processes dominate the dust fallout over East Antarctica, and the particle size differences may be the result of different transport times ( $t$ ). This in turn, could reflect either (1) a contribution from two or more independent sources at different distance and leading to different transit time for aerosols, or (2) different wind speeds of the dust-carrying air masses from the source(s) to the sites, or (3) different dust trajectories from a common source.

Since it has been observed the geographical origin of mineral aerosol is common for the three sites and the processes occurring “*en route*” such as dry/wet deposition processes are likely the same, the hypothesis 1 and 2 can be reasonably discarded. Therefore aerosol trajectories in the troposphere have to be considered.

According to Ruth et al. (2003), when all parameters of transport are identical (dry deposition mechanisms and velocity, mixing heights, and comparable size distributions), the transit time ( $t$ ) from the source to the sink may be deduced directly from the dust mode. Longer or shorter  $t$ , in turn, can be related to different pathways. Our data gives for the LGM, a DB to EDC ratio for the dust mode :

$$(\mu_{DB}/\mu_{DC})_{LGM} \sim 1.26$$

and a transit time ratio  $(t_{DB}/t_{DC})_{LGM}$  of  $\sim 0.6-0.8$  can be derived from Ruth et al. (2003), depending on the different scenarios of modes for the reference size distribution. In other words, the time of dust transport from South America to EDC can be estimated to be  $\sim 1.25$  to  $\sim 1.7$  times longer than that to DB, assuming wind speeds are the same. A similar proportion is deduced for the length of the respective atmospheric trajectories.

Now, with respect to the long range transport from southern South America, the  $\sim 870$  km distance between Dome B and EDC sites can hardly explain the grading difference we observed in dust. Therefore, air masses should have followed very different pathways to reach the sites.

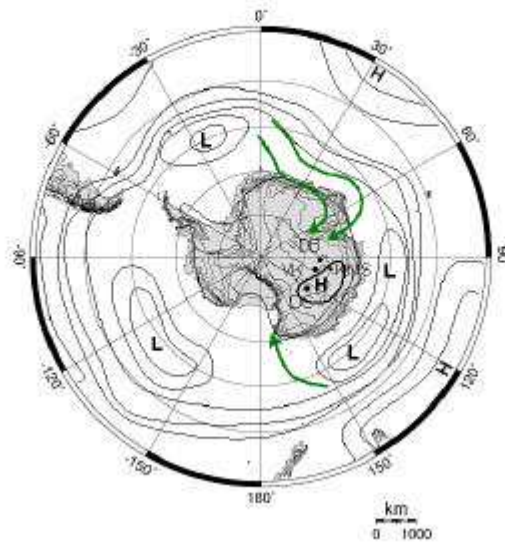
GCM simulations for dust during the LGM suggest a preferential pathway for dust for reaching Antarctica. Changes in horizontal dust fluxes are suggested by the modeled seasonal dust flux in the Southern Hemisphere during the LGM (Andersen, 1998), showing for the austral spring (September to November) a possible dust advection from Patagonia to the East Antarctic either through short-cut trajectories around the Weddel sea and onto the Queen Maud Land (as indicated in Fig. 8A.14a), or through longer and more zonal circumpolar paths. The author evidenced that dust flux lines from Patagonia enter the Antarctic from about  $45^\circ$  E during LGM and about  $80^\circ$  E during the present day, a conclusion which may account for LGM dust at Dome B site. Indeed, difficulties arise for interpreting the Holocene period for which EDC has to be on a short cut trajectory with respect to DB, while EDC is located at the east of DB and more downwind with respect to the general atmospheric circulation.

#### ***A scenario for the dust grading : effect of the altitude of the pathway to Antarctica***

A possible explication for the different dust sizes would be different pathways for dust, but these have to be considered in a three dimensional space. Indeed, the size of the mineral aerosol in the atmosphere decreases with height (Tegen and Lacis, 1996). In general, the higher the altitude reached by the dust, the longer the residence time because atmospheric water content drastically decreases with temperature and is very low over Antarctica.

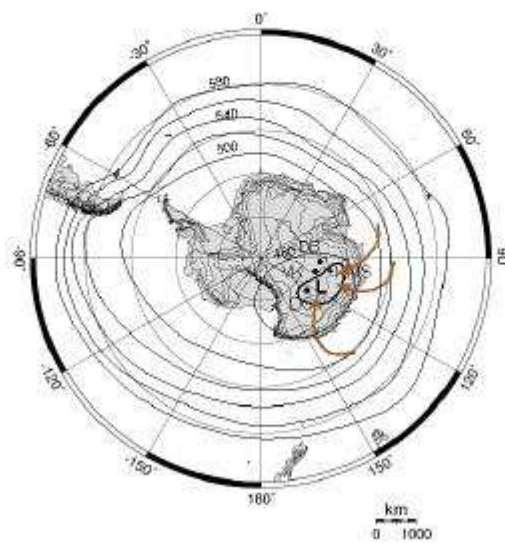
Due to its cold surface, Antarctic acts as a thermal anticyclone with divergent surface wind fields over the plateau. In altitude, Antarctica acts as a large Low and upper air convergence is generated with consequent sinking (subsidence, see James, 1989). Advection from layers above the inversion over Antarctica leads to the shallow temperature rise during winter time generating the so called “coreless winters”(Schwerdtfeger, 1984). The local advection of mid to high tropospheric air masses (higher than 4000 m a.s.l and likely up to tropopause) is therefore possible by deep lows in altitude, and air subsidence from different tropospheric levels may lead to variable grade in the dust in the Antarctic precipitations. Finally the higher graded dust would be associated to a preferential subsidence from upper air level.

LGM.  
surface



**a**

LGM.  
500 hPa



**b**

Figure 8A.14.: Sketch of a scenario for LGM pressure fields.

[a]: Hypothesized average Sea Level Pressure fields and possible inflow from mid troposphere air masses. The short-cut path (arrows) from the South Atlantic to Dome B inferred by Andersen (1998) is shown.

[b]: Tentative reconstruction of pressure fields above the boundary layer. The sketch chart reports the mean 500 hPa isobar height for the LGM (arbitrary scale), and indicates the zone of higher troposphere air convergence and sinking suggested by the data.

### *A sketch for evolution of the subsidence strength during the last climatic transition*

The climatic changes associated with the LGM-Holocene transition, such as the weakening of the polar front and the reduction of the sea ice extent (e.g. Jouzel et al., 1995), implied a general reorganization of the atmospheric circulation in the circum-antarctic.

The main trend of dust size distributions at DB, EDC and KMS shows a see-saw regional evolutions during the deglaciation as well as asynchronous timing and duration of the changes. At the beginning of the Holocene (ca. 10 kyr B.P.) the differences between the sites are opposite in sign with respect to the LGM situation with fine particles (instead coarser) being on average slightly more abundant at DB (and likely Vostok) than at EDC and KMS.

Beside the different horizontal (meridional) air mass advection, a contribution to the dust pathway variability may come from the altitude of transport. The fine dust with longer residence time in the atmosphere is carried by upper tropospheric air masses, that may preferentially subside in certain areas. The low temperatures during LGM made the subsidence more pronounced than in the Holocene everywhere in Antarctica. Our data suggests the preferential upper air subsidence would have encompassed the EDC-KMS region during LGM period. In the meantime, DB (and likely Vostok) was under influence of air from lower level with possible short cut trajectories. Figure 8A.14a and 8A.14b report a sketch for tentative reconstruction of the mean pressure field for the 60° E-120° E sector of central East Antarctica during the LGM at sea level and at in the middle troposphere (altitude of 500 hPa isobar, arbitrary scale). Arrows in the former chart indicate the LGM trajectories of mid-tropospheric air masses from Andersen (1998, modified), while in the latter chart they indicate the paths of convergence and sinking of high tropospheric air, carrying finer dust to the drilling sites.

In the line of this interpretation, the changes during the climatic transition are likely to reflect atmospheric circulation arrangements from a glacial state (20 kyr B.P.) with a relative higher subsidence over the Dome C and KMS areas (Fig. 8A.14b and 8A.15e), and air masses carrying finer dust, to an interglacial state (10 kyr B.P.) with a higher relative subsidence over Dome B and Vostok area (Fig. 8A.15b). This would correspond, in other terms, to a southward displacement of the vortex (highest subsidence).

According to the scenario proposed, after the LGM at ~18 kyr B.P. (Fig. 8A.15e) the vortex over EDC and KMS probably started to expand or to shift southward towards the Dome B and Vostok (Fig. 8A.15d). This time period corresponds also to the start of the decreasing of the total dust concentration. At around 15 kyr B.P. all the sites were likely under the same subsidence and circulation regime (Fig. 8A.15c) and this corresponds to the end of LGM dust decrease. Then, the southward migration of the vortex continued (Fig. 8A.15b) by a probable reduction of the relative subsidence over EDC and KMS until the beginning of the Holocene. At this time it was centered over

Dome B and Vostok region and the Dome C-KMS sites were more influenced by direct incursions of mid troposphere air masses carrying slightly coarser dust. In other terms, the main trend of LGM-Holocene dust size changes could be attributed to a change in the eccentricity of the polar vortex.

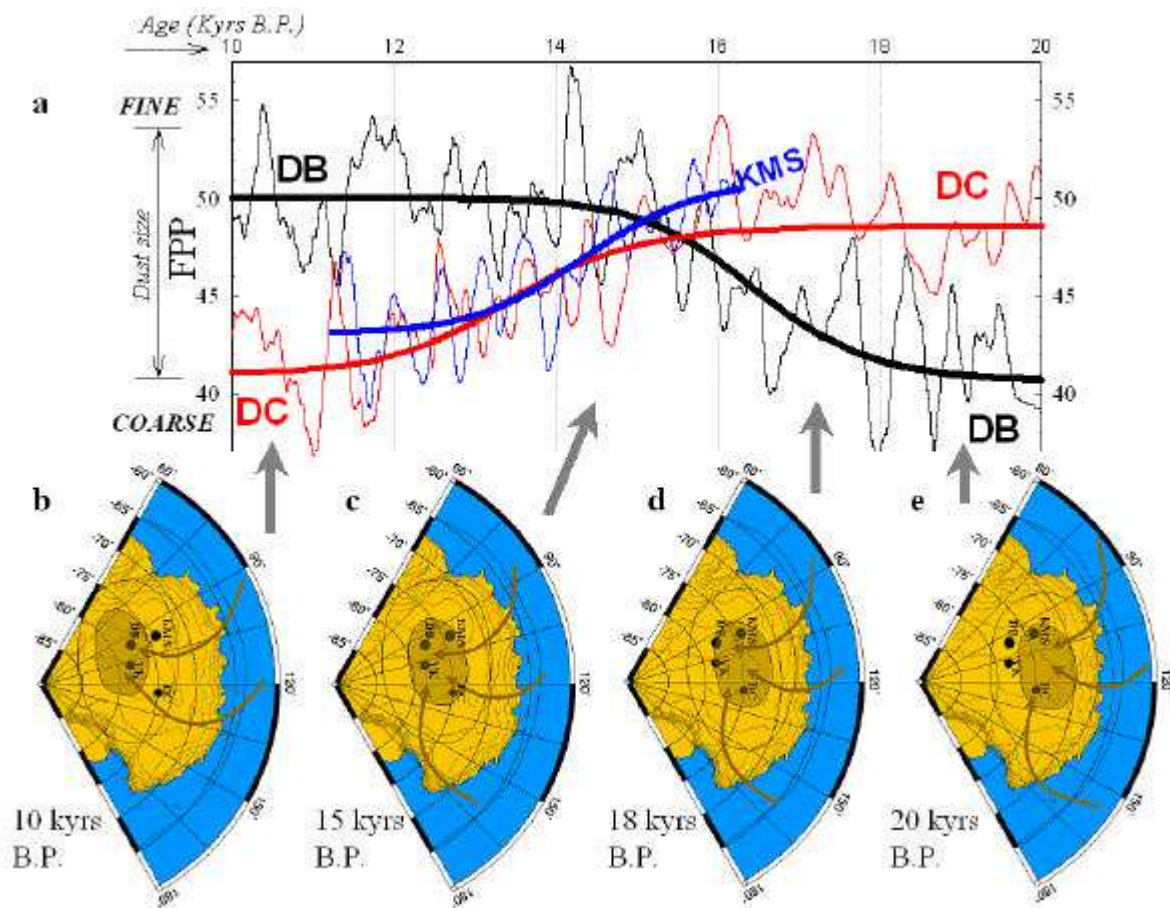


Figure 8A.15: Sketch of the vortex migration during the deglaciation

[a] Dust size evolution at the three sites (same as fig. 2d)

[b] to [e] : Average position of the preferential areas of upper air convergence and subsidence over central East Antarctica suggested by the data. After the LGM, at 18 kyr B.P. the vortex expanded or shifted southwards towards the Dome B region. At about 15 kyr B.P. all sites were likely under the same circulation regime. The displacement continued until 10kyr B.P. the beginning of the Holocene.

### *The sub-millennial oscillations*

Superposed on this main trend and vortex migration, the short-term oscillations of dust size are present with a periodicity of about ~600-700 year periods (Fig. 8A.11d). Millennial and centennial-scale periodicities of dust size variability have been evidenced already from the Late glacial and Holocene records from EDC and Vostok ice cores from 13 to 2 kyr B.P. (Delmonte et al., 2002b and submitted). The authors suggested that multi-century periodicities are probably harmonics of the fundamental millennial pacing (~1200 yrs) for the dust advection to the Plateau and the atmospheric circulation, as the possible expression of changes in the circum-antarctic ocean-atmospheric system derived from the global dissipation of the Thermohaline circulation (Delmonte et al., submitted). The atmospheric circulation in the circum-antarctic is dominated by the zonal (West to East) component and at any time perturbed by atmospheric waves. Wavenumbers 1 to 3 (wavenumber 1 corresponding to the eccentricity of the polar vortex) explain most of the variance of the 500 hPa isobar (Tyson, 1986). They are defined by more or less stationary waves associated with structures distorting the mean zonal circulation (winter continental Highs and summer Lows), and responsible for the meridional exchanges of air masses. Moreover, more or less intense transient cyclonic centers, stationary or migrating around Antarctica between 65° S-62° S, also contribute to the perturbation of the zonal circulation (Jones and Simmonds, 1993). The sea ice margin responds to atmospheric forcing and in turn can affect the cyclogenesis in the circum-antarctic and the synoptic low pressure systems (e.g. Carleton, 1989).

Because the atmospheric centres of influence in the circum Antarctic may be variable in position and strength, they can modulate the meridional penetration of (mid) troposphere air masses onto the polar plateau (see Andersen, 1998), and their eastward displacement around the continent can favor the horizontal displacements alternatively towards one sector or the other.

A wavering effect of this type, discussed in detail elsewhere (Chap. 8B.1), could also account for the different phasing and asynchronous multi-centennial dust variations that can be observed among the sites and for the opposite phase in correspondence to the pre-Holocene dust minimum.

#### **8A.3.4 Conclusions**

The uniformity of the mineral dust provenance and fluxes to East Antarctica during the last climatic transition veils significant differences in the dust transport pathways. These latter, monitored through its size distribution, show two poles apart inside East Antarctica during the deglaciation (20 to 10 kyr B.P.).

It is hypothesized that during the last glacial period upper air convergence and sinking dominated in the Dome C-KMS area, while more direct meridional advection of air masses penetrated towards Dome B (and likely Vostok). The gradual changes occurring between 20 and 10 kyr B.P. lead to an opposite situation at the beginning of the Holocene, suggesting a southward displacement of the vortex.

The dust advection is also sensitive to the variable position of the atmospheric Highs and Lows in the circum-antarctic, in turn related to the Southern ocean and sea ice extent. The variable displacement of these centers of influence is probably at the origin of the short-term (sub millennial) oscillations and their asynchronous occurrence observed in the records and superposed on the main trend of the changes.

At this step, further GCM simulations need to be developed to check our scenario, either for snapshot simulation for given period (e.g. LGM, 15 kyr B.P. , 10 kyr B.P.) as well as for the scenario we suggest by sensitivity tests for the air subsidence over Antarctica to variable boundaries conditions.



**TABLES**

ICE CORE	N. of samples	Sampling depth (m)	Sampling resolution (samples/years)	DUST CONCENTRATION (ppb)			
				Late LGM (18-20 kyr B.P.)	ACR (14.5-12.2 kyr B.P.)	Pre-Holocene dust minimum (11.3-12.1 kyr B.P.)	Holocene Beginning (10-11.3 kyr B.P.)
<i>Dome B</i>	186	360-609	1/52	854	46	7	18
<i>KMS</i>	102	662-870	1/50	nm	25	9	nm
<i>EDC</i>	138	322-500	1/53 from 10 to 14.5 kyr B.P. 1/100 from 14.5 to 20 B.P.	730	25	8	18

*Tab.8A.4.*

*Ice core sampling for dust concentration measurements: number of samples and relative depth interval, sampling resolution; the last four columns report the average dust concentration for each climatic period (LGM, ACR, pre-Holocene dust minimum and Holocene beginning)*

\*\*\* \*\*

Sample	Depth (m)	Climatic period	Mode of mass-size distribution (µm)	Sample Weight (grams)	Dust (µg)	Sr recover (ng)	Nd recover (ng)
<i>EDC-a</i>	518.10-518.65 520.3-520.85	Stage 2	~1.9-2	690	~65-70	22,30	1,66
<i>EDC-b</i>	569.8-570.35	Stage 2	~2.0	280	~100	34,30	2,55
<i>DB-a</i>	581	Stage 2	~2.7-2.8		110	37,73	2,80
<i>DB-b</i>	641	Stage 2	~2.4-2.5	860	100	34,30	2,55
<i>KMS-a</i>	850.08-851.23	End of Deglaciation (about 15 kyr B.P.)	~2.2	800	10	3,43	0,25
<i>KMS-b</i>			~2.0	870	30	10,29	0,76

*Tab.8A.5*

*Samples for isotopic composition measurements: sample code, ice core sections selected and relative climatic period. The modal value of the mass size distribution of each sample is also reported, along with the net ice weight (after decontamination) and total dust recover estimated by Coulter Counter after centrifugation procedures. The amount of Sr and Nd are also estimated and reported in the last two columns.*

Sample	$^{87}\text{Sr}/^{86}\text{Sr}$	$^{145}\text{Nd}/^{144}\text{Nd}$	$\epsilon\text{Nd}(0)$	Number of Sr ratios	Number of Nd ratios
<i>EDC-a</i>	0.708595 (21)	0.512553 (27)	-1.658 (0.53)	600	570
<i>EDC -b</i>	0.708834(37)	0.512512 (32)	-2.458 (0.62)	385	604
<i>EDC -b repeated</i>	0.709033 (81)			980	
<i>DB -a</i>	0.708383 (32)	0.512608 (18)	-0.585 (0.35)	675	213
<i>DB -a repeated</i>	0.708316 (39)			760	
<i>DB -a-Filtered</i>	0.708479 (18)	0.512613 (28)	-0.488 (0.55)	600	733
<i>DB -b</i>	0.708544 (28)	0.512526 (29)	-2.185 (0.57)	540	715
<i>KMS-a</i>	0.708493 (22)	0.512563 (51)	-1.463 (0.99)	245	680
<i>KMS-b</i>	0.709058 (38)	0.512484 (99)	-3.004 (1.93)	165	680

Tab.8A.6

Measured isotopic composition of the samples:  $^{87}\text{Sr}/^{86}\text{Sr}$ ,  $^{145}\text{Nd}/^{144}\text{Nd}$  and  $\epsilon\text{Nd}(0)$ . Each value represents the weighted average of a number of ratios for each element indicated in the last two columns.

## References

- Andersen KK (1998) Simulations of atmospheric dust in the glacial and interglacial climate. PhD. Thesis, Niels Bohr Institute of Astronomy, Physics and Geophysics, University of Copenhagen, Copenhagen, 136 p.
- Basile I, Grousset FE, Revel M, Petit JR, Biscaye PE, Barkov NI (1997) Patagonian origin of glacial dust deposited in East Antarctica (Vostok and Dome C) during glacial stages 2, 4 and 6. *Earth Planet Sci Lett* 146:573-589.
- Basile I (1997) Origine des aérosols volcaniques et continentaux de la carotte de glace de Vostok (Antarctique). PhD Thesis, LGGE-Université Joseph Fourier-Grenoble I, Grenoble, 254 p.
- Bogdanovski O (1997) Development of highly-sensitive techniques for Sm-Nd isotopic analysis and their application to the study of terrestrial and extraterrestrial objects. PhD Thesis, Cosmochemistry Dept. Max Plank Institute, Johannes Gutenberg Universität, Mainz.
- Briat M, Royer A, Petit JR, Lorius C (1982) Late glacial input of eolian continental dust in the Dome C ice core: additional evidence from individual microparticle analysis. *Ann Glaciol* 3:27-30.
- Carleton AM (1989) Antarctic sea-ice relationships with indices of the atmospheric circulation of the Southern Hemisphere. *Clim Dyn* 3:207-220.
- Ciais P, Petit JR, Jouzel J, Lorius C, Barkov NI, Lipenkov V, Nicolaiev V (1992) Evidence for an early Holocene climatic optimum in the Antarctic deep ice-core record. *Clim Dyn* 6:169-177.
- Delmonte B, Petit JR, Maggi V (2002a) Glacial to Holocene implications of the new 27,000-year dust record from the EPICA Dome C (East Antarctica) ice core. *Clim Dyn* 18:647-660.
- Delmonte B, Petit JR, Maggi V (2002b) LGM -Holocene changes and Holocene millennial-scale oscillations of dust particles in the EPICA Dome C ice core, East Antarctica. *Ann Glaciol* 35:306-312.
- Grousset FE, Biscaye PE, Revel M, Petit JR, Pye K, Jossaume S, Jouzel J (1992) Antarctic (Dome C) ice-core dust at 18 k.y. B.P.: isotopic constraints and origins. *Earth Planet Sci Lett* 111:175-182.
- Jacobsen SB, Wasserburg GJ (1980) Sm-Nd isotopic evolution of chondrites. *Earth Planet Sci Lett* 50:139-155.
- James IN (1989) The Antarctic drainage flow: implications for hemispheric flow on the Southern hemisphere. *Antarctic Science* 1:279-290.
- Jones DA, Simmonds I (1993) A climatology of southern hemisphere extratropical cyclones. *Clim Dyn* 9:131-

- Jouzel J, Vaikmae R, Petit JR, Martin M, Duclos Y, Stievenard M, Lorius C, Toots M, Melières MA, Burckle LH, Barkov NI, Kotlyakov VM (1995) The two-step shape and timing of the last deglaciation in Antarctica. *Clim Dyn* 11:151-161.
- Jouzel J, Masson V, Cattani O, Falourd S, Stievenard M, Stenni B, Longinelli A, Johnsen SJ, Steffensen JP, Petit JR, Schwander J, Souchez R (2001) A new 27 kyr high resolution East Antarctic climate record. *J Geophys Res* 28:3199-3202.
- Kohfeld K, Harrison SP (2001) DIRTMAP: the geological record of dust. *Earth Sci Rev* 54: 81-114.
- Legrand M, Mayewski P (1997) Glaciochemistry of polar ice cores: a review. *Rev. Geophys.* 35:219-243.
- Mahowald N, Kohfeld K, Hansson M, Balkanski Y, Harrison SP, Prentice IC, Schulz M, Rodhe H (1999) Dust sources and deposition during the Last Glacial Maximum and current climate: a comparison of model results with paleodata from ice cores and marine sediments. *J Geophys Res* 104:15895-15916.
- Markgraf V (1991) Younger Dryas in South America? *Boreas* 20:63-69.
- Petit JR (1999) Climate and atmospheric history of the past 420,000 years from the Vostok ice core, Antarctica. *Nature* 399: 429-436.
- Royer A, Angelis MD, Petit JR (1983) A 30,000 year record of physical and optical properties of microparticles from an East Antarctic ice core and implications for paleoclimate reconstruction models. *Clim Change* 5: 381-412.
- Ruth U, Wagenbach D, Steffensen JP, Biggler M (2003) Continuous record of microparticle concentration and size distribution in the central Greenland NGRIP ice core during the last glacial period. *J Geophys Res* 108: 4098-4110.
- Schwander J, Jouzel J, Hammer CU, Petit JR, Udisti R, Wolff E (2001) A tentative chronology for the EPICA Dome Concordia ice core. *Geophys Res Lett* 28: 4243-4246.
- Schwerdtfeger W (1984) *Weather and climate in the Antarctic*, Vol 15. Elsevier Science, Amsterdam, 261 p.
- Taylor SR, McLennan SM (1985) *The Continental crust: its composition and evolution*, Blackwell Scientific Publications, 312 p.
- Tegen I, Fung I (1994) Modeling of mineral dust in the atmosphere: sources, transport, and optical thickness. *J Geophys Res* 99: 22,897-22,914.
- Tegen I, Lacis AA (1996) Modeling of particle size distribution and its influence on the radiative properties of mineral dust aerosol. *J Geophys Res* 101: 19,237-19,244.
- Tegen I, Harrison SP, Kohfeld K, Prentice IC, Coe M (2002) The impact of vegetation and preferential source areas on global dust aerosol: Results from a model study. *J Geophys Res* 107, doi:10.1029/2001JD000963.
- Thompson LG, Mosley-Thompson E (1981) Microparticle concentration variations linked with climatic change: evidence from polar ice. *Science* 246: 812-815.
- Tyson PD (1986) *Climatic change and variability in southern Africa*, Oxford Univ. Press, Cape Town, 220 pag.

\*\*\*\*\*            \*\*\*\*\*            \*\*\*\*\*

### Summary

*The dynamics of dust changes in East Antarctica during the last climatic transition show uniform and synchronous changes in dust concentration at all sites and two clearly opposite evolutions of the dust transport patterns.*

*The geographical provenance for dust is identical at all sites within the East Plateau, and therefore the uniformity of dust flux can be considered associated principally to the conditions at the source regions and to the scavenging processes en route, while major differences in transport patterns can be hidden.*

*The dust transport time, examined through the particle size distribution, shows asynchronous and opposite changes between different regions of the Plateau. This is associated to a reorganization of the atmospheric circulation in the Antarctic and circum-antarctic realm during the climatic transition, and possibly to a shift in the eccentricity of the Polar vortex (wavenumber 1).*

*Quasi-millennial oscillations of dust size are clearly superposed to the main trend of changes at all sites, and they can reflect the propagation of ocean-sea ice-atmosphere anomalies in the Southern Ocean. In § 8B such features will be investigated in detail in for the Holocene period.*

## **8B - DUST VARIABILITY IN THE HOLOCENE**

It has been shown in Chap. 8A that the fluctuating dimensions of dust are a good proxy for atmospheric transport, and provide useful information about the atmospheric circulation changes at the high latitudes of the Southern Hemisphere.

After the first evidences for millennial-scale variability in dust transport to Dome B, KMS and Dome C (§ 8A.3) during the last climatic transition and to Dome C during the Holocene (introduced in § 8A.2), several efforts have been dedicated to the investigation at high temporal resolution (sub-centennial) of particle size variability in EDC, Vostok and Dome B ice cores during the Holocene.

The results are presented and discussed in this chapter, in the following order:

§8B.1 – Presentation of the EDC and Vostok Holocene records, comparison of the profiles and discussion of results (integral version of a paper submitted to *Earth and Planetary Science Letters*).

§8B.2 – The Holocene record from Dome B ice core.

§8B.3 – Comparison of dust size variations for the different sites, common periodicities, and variability nested in the dust concentration records.

## **8B.1 – Holocene records from EPICA Dome C and Vostok ice cores.**

A paper has been submitted to Earth and Planetary Science Letters under the title:

**“MILLENNIAL AND SECULAR PERIODICITIES IN ATMOSPHERIC CIRCULATION OVER ANTARCTICA DURING HOLOCENE FROM EDC AND VOSTOK ICE CORE DUST RECORDS”.**

### **ABSTRACT**

*The size distribution of mineral dust deflated from the continents and transported to the East Antarctic Plateau is taken as a proxy for the atmospheric transport over the Southern Hemisphere. We compare sub-centennial (~1 sample every 50 years) resolution atmospheric records of two East Antarctic ice cores from Vostok and EPICA Dome C covering a large part of the Holocene period, taking advantage of the presence of volcanic markers allowing tight stratigraphic correlations.*

*Dust size distribution or atmospheric circulation display significant periodic fluctuations at secular and millennial scales. The EDC record displays pronounced millennial-scale (~1200 yrs) periodicity until middle Holocene, and less marked afterward. The secular fluctuations in Vostok and records are apparently harmonics of the millennial one. The two filtered dust series in the 200-yr frequency band appear coupled for almost ~7 kyrs period of the Holocene, and they suggest a puzzling opposite phase and a regional variability in the atmospheric circulation around Antarctica. Moreover, such secular frequencies in the 200-yr band, representing 20-30% of the total variance, are also present in a <sup>10</sup>Be profile, proxy of solar activity, from a adjacent ice core at Vostok. This <sup>10</sup>Be record, linked to the two dust records by stratigraphic markers, is correlated with a composite of the two dust records, peaking at ~200 yrs (C.I. 90%) giving hint of a possible solar-climate relationship.*

*Atmospheric circulation around Antarctica is linked to the surrounding ocean and we hypothesize that the South Atlantic ocean would have a key role in connecting oceans, interplaying with the global thermohaline circulation and the sea ice around Antarctica.*

*We therefore speculate the millennial frequency of the EDC record to be the Southern expression of a mode of oscillation of the Earth system. According to the scenario proposed by Broecker et al.[20], such an oscillation may be driven by the salt anomaly from the North Atlantic. To this oscillation, our dust records support the South Atlantic ocean as a possible additional oscillator but with internal oscillation at secular periodicities as suggested by a modelling experiment from Mikolajewicz and Meier-Reimer [43]. Finally, those secular modes of oscillations of the South Atlantic Ocean would overlap the secular solar frequency bands, opening the possibility of a sun-climate relationship through amplification and frequency combination.*

### **8B.1.1 Introduction**

Climate variability at millennial and secular timescales for the recent past period is an important concern for the assessment of evolution of our present climate. In the face of a tendency for global warming, a major challenge is to decipher the anthropogenic contribution from natural occurrence [1]. The Holocene period is now documented by numerous climate proxies given by marine sediment records, but for the atmospheric variability, the ice core records are very useful in this respect.

North Atlantic ocean cores (e.g.[2-4]) have clearly shown a prominent millennial-scale mode of variability of the ocean circulation for the present interglacial period. Evidences for a similar climatic

variability have been observed in the Indian Ocean (e.g. [5]), in a South-East Pacific core drilled off the Chilean coast [6] and also in atmospheric proxies from tropical latitudes (El Nino) [7] and from polar areas of the northern hemisphere (e.g. [8]).

High resolution records from North Atlantic deep-sea sediments [9] have shown that the long ocean cycles of millennial duration contain shorter century-scale (~200 to 500 year) oscillations. The authors suggested a link with the solar activity (as observed in  $^{10}\text{Be}$  and  $^{14}\text{C}$  records), thus invoking the still unsolved solar-climate relationship. Recently, secular to decadal solar cycles component have been depicted in Icelandic marine records hinting atmospheric and thermohaline circulation link [10].

Analysis of present-day atmospheric data showed a statistical relationship between the 11-year sunspot cycle and geopotential heights [11] with the highest correlation for the subtropics. On the other hand, a model experiment for modern climate [12] also suggested that an external forcing factor such as solar activity may induce significant changes in the intensity of the Westerlies. While several Holocene climatic records also display analogous periodicities to those of the solar cycle activity [13, 14], especially at tropical latitudes [15-17], the mechanisms linking the weak solar forcing to climate at millennial and secular periodicities are not yet understood. Indeed, an amplification is required and amongst scenarios, Broecker et al [18, 19] suggested a possible coupling with the ocean and its internal oscillations, for which those latter are possibly induced by salinity anomalies.

At high latitude in the southern hemisphere, the 200 and 400-year frequency bands have been detected in bio-geological proxies of sediments from the Western side of the Antarctic Peninsula [13, 20-22]. These proxies cover the last 7,000 years, and have been interpreted as local changes in the upper ocean conditions such as the sea ice extent and wind stress together affecting local primary production. For Antarctica, in a previous study on dust from the EPICA Dome C ice core, covering period from 13 kyrs to about 4.5 kyrs B.P, Delmonte et al. [23] described millennial and even shorter time variability in the size distribution of dust. This latter is a proxy linked to atmospheric transport.

Ice cores provide a wealth of information on climate and solar activity simultaneously, the latter registered through the cosmogenic isotope  $^{10}\text{Be}$  [e.g. 24]. As ice cores can be dated with good confidence and the proxies analysed at high (few years to decade) resolution, ice cores are useful for documenting the solar-climate relationship.

In this paper we present two records of aeolian dust from East Antarctic ice cores [EPICA Dome C (EDC) 75°06' S, 123°21' E, and Vostok (VK) 78°28' S, 106°48' E], spanning a large part of the Holocene period. The dust deflated from the Southern Hemisphere continents and transported to the Plateau is graded en route, and the proportion of coarse particles with respect to the total mass is essentially a response to the efficiency of atmospheric transport. In parallel, these records are

compared to a  $^{10}\text{Be}$  record from an adjacent ice core at Vostok ([32] and Raisbeck et al, in preparation), with the aim to compare this solar proxy to the atmospheric circulation variability.

### **8B.1.2 Analytical methods and results**

#### ***The samples and the ice core records***

Two ice cores from East Antarctica have been studied for their dust content. Due to the very low content of dust (~15 ppb on average) and the use of a washing procedure for the decontamination of ice samples, the porous firm (i.e. the first ~100 m) and the fractured ice samples were not used. The upper 100 to 300 m of the EPICA-Dome C ice core span the Tardiglacial and Holocene periods from 13 kyr to 2 kyr B.P [25]. The 235 m Vostok-BH7 ice core, drilled in 1996, was selected because it was extracted without drilling fluid. The  $^{10}\text{Be}$  concentrations were measured on a third ice core, Vostok-BH1, drilled in 1989 and about 30 m adjacent to Vostok-BH7. This core is 170 m deep. A correlation of the centennial scale variations of  $^{10}\text{Be}$  with those observed in dendrochronologically dated tree rings has been used to date this ice core over the past 7,000 years ([32] and Raisbeck et al, in preparation). This datation has subsequently been used to date the EDC core over the same period [28].

All the three ice cores have been processed for electrical conductivity measurements (ECM), allowing an evaluation of the inventory of major  $\text{H}_2\text{SO}_4$  fallout from volcanic events. The ice samples selected for dust are 6-10 cm long and represent 2 to 3 years of accumulation. A total of 280 samples for EDC and 130 samples for Vostok have been taken each ~1 m, thus obtaining a time resolution of 1 sample per 40 years and 1 per 50 years respectively.

Dust mass concentrations (assuming density of  $2.5 \text{ g/cm}^3$ ) and size distributions have been performed using a 256-channel Coulter Counter. Decontamination of ice and analytical procedures are described elsewhere [23]. The samples were processed in random order and the calibration of the particle Counter was checked to avoid instrumental bias. For  $^{10}\text{Be}$ , 200 samples were taken as a continuous slice cut parallel to the core axis. Each sample was 0.5 meter long and represents about 25 years of accumulation ([32] and Raisbeck et al, in preparation).

#### ***Stratigraphic links and the relative dating***

The electrical conductivity measurement (ECM) permits detection of major volcanic eruptions which can be used as stratigraphic markers [26]. The ECM profile of Vostok BH7 and EDC record are shown on Fig 8B.1a. The depth-to-depth correspondence between BH7 and EDC ice cores (Fig 8B.1-b, I) was obtained for a period covering 7,000 years using 24 volcanic events, yielding 1 marker every ~300 years.



The matching was not done in a progressive order of depth, to prevent cumulative errors. Instead, a first general trend of the depth-to-depth relationship was estimated from climate events and comparison of the two deuterium profiles, using the end of climatic transition or beginning of the Holocene period. The overall average EPICA/Vostok ratio of accumulation is  $\sim 1.33$ . In Vostok-BH7 a 2 cm thick tephra layer [27] has been found at 102.1 m depth, and it lies between two major ECM peaks. The ash layer is not visible in the EDC core but the corresponding ice section with the expected ECM event [26] was continuously sampled (1 sample per 2 cm). Coulter counting and microscopic observations revealed the presence of a highly concentrated dust layer with large (10 to 20  $\mu\text{m}$ ) glass shards at 132.6 m depth and right between two ECM peaks. All the other 23 events have been identified from the EPICA/Vostok-ECM comparison, taking into consideration the general trend of the depth-to-depth relationship. The markers allow us to refine the relationship and select secondary events and then intermediate ones.

The accuracy of such matching can be estimated. First, all Vostok depths have been normalized by multiplying depth by 1.33 to take into account the accumulation ratio with EPICA. Assuming the correspondence (and dating) is correct for each marker, the relative variation of snow accumulation rate between the two sites has been calculated on the normalized depth-to-depth plot. The error is defined by the orthogonal distance of a marker from the extrapolated line passing through the previous two markers (see Fig. 8B.1-c). The mean (squared) misalignments of all markers gives the mean (squared) misalignment. For EDC and BH7 cores, the mean distance is  $\sim \pm 1$  m, and it represents about  $\pm 33$  years for any level, taking 2.9 cm/year as mean accumulation rate.

The same approach was applied for BH1 and BH7 Vostok cores. Because of the poor quality of the BH1 ECM record, those latter are linked by only 12 volcanic events (Fig. 8B.1-b, II). However, as the two ice cores are adjacent, only a systematic and gradual shift in the depth is observed. The mean misalignment ( $\pm 0.70$  m) corresponds to a relative error of about  $\pm 32$  years for any level, considering an accumulation rate of 2.2 cm/a for Vostok.

The EDC ice core chronology that we used as reference and transferred to the Vostok cores, is given elsewhere [28].

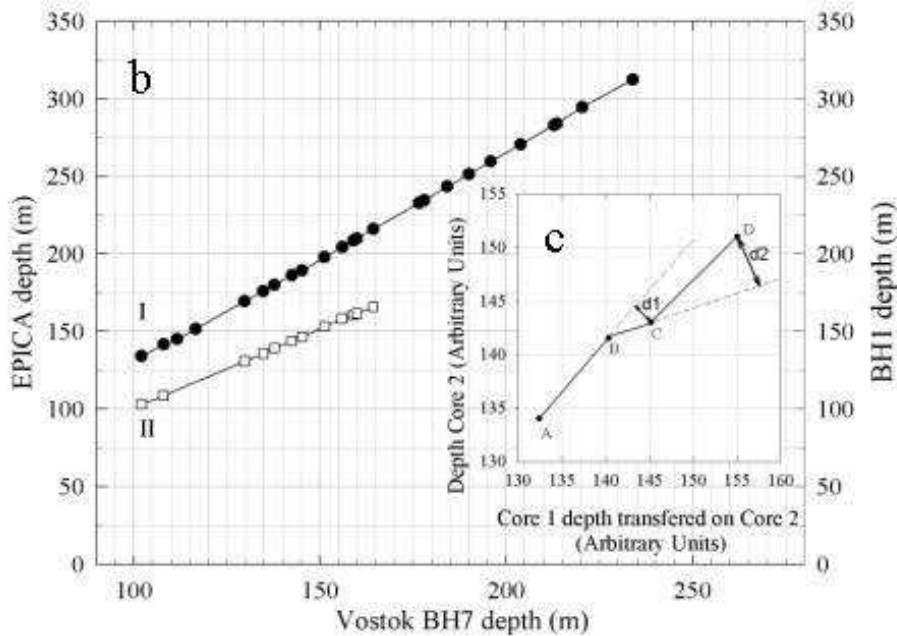
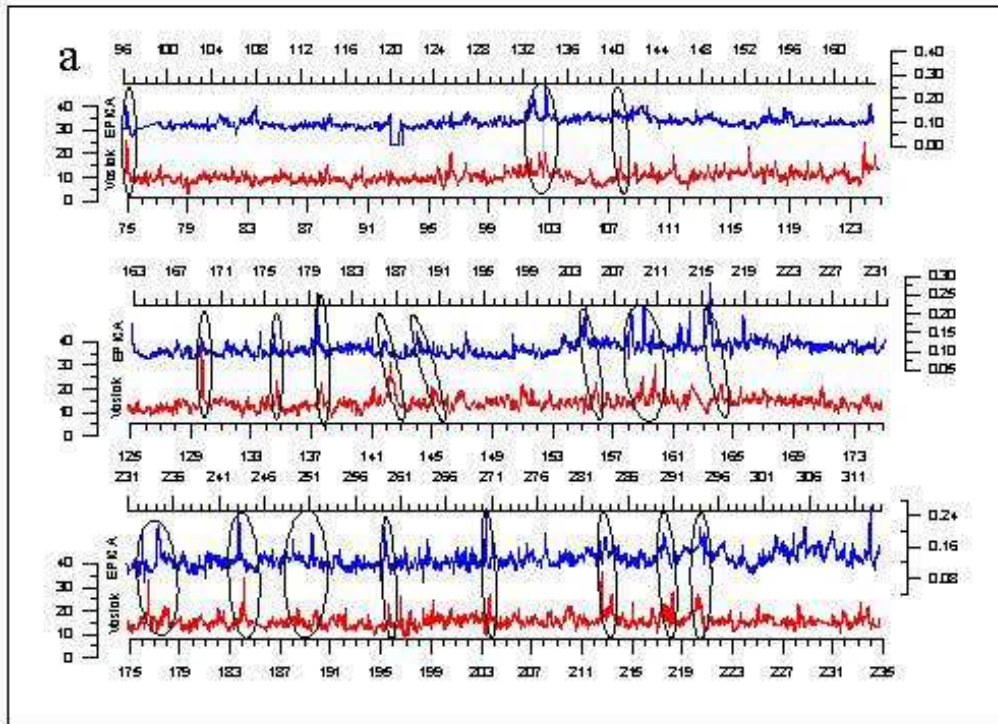


Fig. 8B.1– STRATIGRAPHIC LINK BETWEEN ICE RECORDS.

[a] ECM records (in relative units) from EPICA-Dome C and Vostok BH7. Most of events used to establish depth to depth correlation are rounded by an ellipse. An ash layer represented by a thick line link 134 m on EDC and 102.1 on Vostok.

[b] Depth to depth relationship between ice cores given by volcanic markers: I) Vostok-BH7 and EDC ice cores ; II) Vostok BH7 and Vostok BH1 ice cores.

[c] Cartoon displaying principle for the error estimation due to the variability in ice accumulation rate. Error is represented by the mean misalignment of successive markers. Distance ( $d_1$ ,  $d_2$ , ...) is calculated as the orthogonal distance to the line linking two successive markers (bold line). For clarity, the misalignments have been exaggerated.

### *EDC and Vostok dust records*

In Fig. 8B.2 we report the deuterium profile (8B.2a) of the EDC core [25] along with total dust mass concentration (8B.2b). The deuterium record displays a long term trend on which high variability is superimposed. The proportion of coarse particles (CPP, see after) for EDC and Vostok-BH7 are reported in Fig. 8B.2c and Fig. 8B.2d. As our samples represent 2 to 3 years of accumulation, we tested the significance of each point by analysing continuously seven different sections, 55 cm long, with a resolution of about one sample per year (one sample every 2 cm). For the seven sections, two of which are shown in the inserts of Fig. 8B.2c, the yearly variability (standard deviation) is 4.6%, and 2.9% when the mean over 3 years is considered. By comparison the standard deviation of CPP data for the entire record is significantly higher and is 5.2%. The difference gives us confidence in the significance of each single measurement as an indicator of real variability.

The continental dust reaching Antarctica is well sorted and the large particles with diameter greater than 5  $\mu\text{m}$  are very rare or seen only in ash layers. The size distribution generally displays a mean mass diameter around 2  $\mu\text{m}$ , and in a previous study on EDC [23] we used mathematical fit (Lognormal or Weibull functions) to characterize variations of its mode. Here instead, we use the relative proportion for a given size interval with respect to the total dust content. This simpler approach is though to be closer to the raw data, while a mathematical fit nicely smoothes distributions, but finally reduces signal variations.

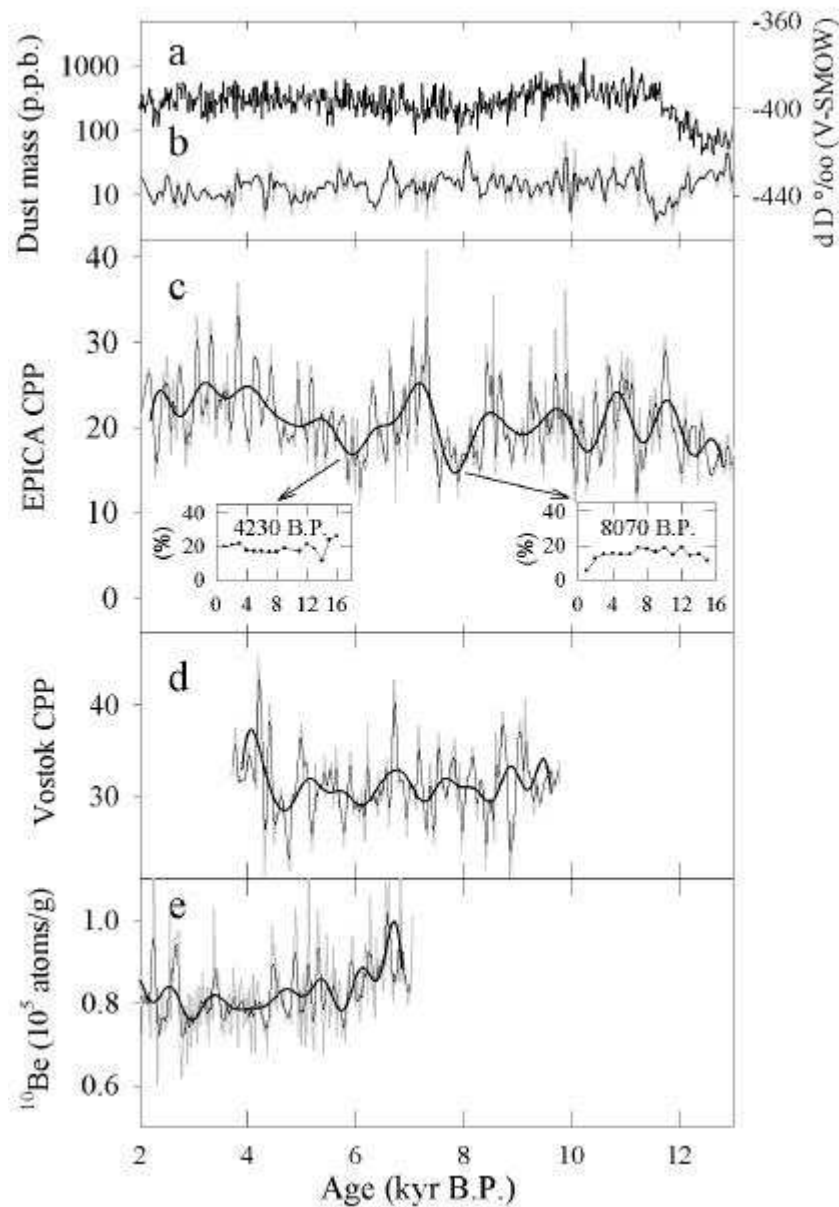


Fig. 8B.2 – EPICA AND VOSTOK HOLOCENE RECORDS . The EPICA ice chronology is taken as reference for time.

[a]-Deuterium record ( $\delta D$  expressed in ‰ with respect to SMOW) for EPICA [23] as proxy for local temperature.

[b]-Total dust mass concentration (ppb or  $10^{-9}$  g/g). Raw data and average on 70 years after re-sampling.

[c]-EPICA CPP record (%), representing the percentage of coarse particles ( $3-5 \mu\text{m}$ ) respect to the total dust mass spectrum ( $0.7-5 \mu\text{m}$ ). Raw data and average on 70 years after re-sampling.

The two inserts represent continuous 55 cm sections for 4230 B.P. and 8070 B.P. sampled at annual resolution (CPP versus time in years).

[d]-Vostok-BH7 CPP ( $2.5-5 \mu\text{m}$ ) record (%). Raw data and smoothing (200-year running average)

[e] -Vostok-BH1 RECORD of  $^{10}\text{Be}$  plotted versus age (EPICA chronology). Raw data and smoothing by a 100-yr moving average.

A low pass filter has been applied to [c], [d] and [e] to remove frequencies higher than 1 per 1000 years.

The Coarse Particle Percent (CPP) we defined corresponds to the percentage of large particles (2.5 or 3 to 5  $\mu\text{m}$  depending on site) and is thought to be most sensitive to aeolian transport. Conversely, we calculate the Fine Particle Percent (FPP, 1-2  $\mu\text{m}$ ), corresponding to particles smaller than the mode. In Fig. 8B.3, two examples of raw data for volume size distributions are shown for extremes cases. Due to the very low concentration, a scatter occurs for each channel of counting and we used the mean from at least 3 individual measurements. Between the two examples, the Lognormal fit indicates an increase in mode by about 0.50  $\mu\text{m}$  (from 1.7 to 2.2  $\mu\text{m}$ ) and this corresponds to a 15% decrease in FPP (1-2  $\mu\text{m}$ ) and a 13% increase in CPP (3-5  $\mu\text{m}$ ) respectively. The mode of distributions changes are always very tiny with respect to the whole spectrum of aerosols. Therefore the CPP parameter is believed to be more sensitive to transport and rather unlikely affected by other factors such as local snow accumulation, the source or the hydrological cycle.

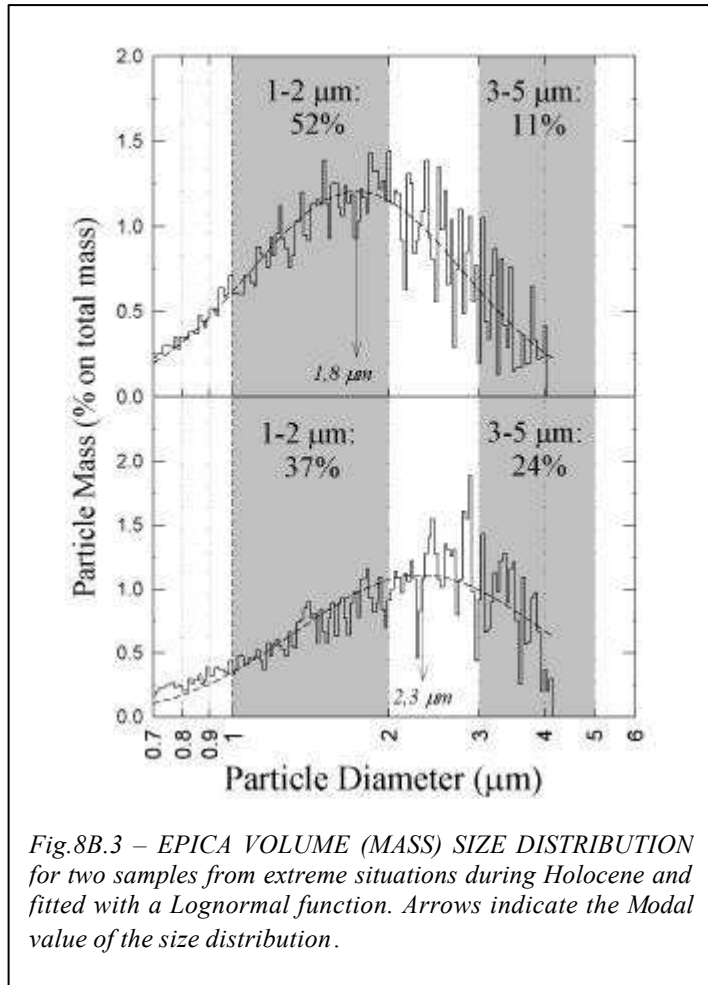


*Fig.8B.3 – EPICA VOLUME (MASS) SIZE DISTRIBUTION for two samples from extreme situations during Holocene and fitted with a Lognormal function. Arrows indicate the Modal value of the size distribution.*

The mode of distributions changes are always very tiny with respect to the whole spectrum of aerosols. Therefore the CPP parameter is believed to be more sensitive to transport and rather unlikely affected by other factors such as local snow accumulation, the source or the hydrological cycle.

A careful inspection of both EDC and Vostok size distributions indicate some clear differences. Vostok dust is slightly more graded than EPICA, and particles larger than 4  $\mu\text{m}$  are less abundant than at Dome C. For these reasons, the lower limit of CPP was chosen to start from 2.5  $\mu\text{m}$  for Vostok and from 3  $\mu\text{m}$  for EDC respectively.

In Fig 8B.4a and Fig. 8B.4b we report the FPP and CPP profiles for EDC series. Both records show similar variations but obviously of opposite sign. As previously noted for the mode of the distribution [29], Holocene values of CPP and FPP never reach the extreme value of LGM. Between 2 and 13 kyr B.P., the EDC CPP represents more than 20% of the total mass and FPP 41%, while for LGM period CPP is about 12.5% and FPP 48% respectively. A general increasing trend is observed for EDC CPP with respect to time but this trend is absent in the Vostok record. EDC smoothed data display larger amplitude variations than in Vostok. It is difficult to make a clear correlation between the maxima and minima between the two records (Fig. 8B.2).

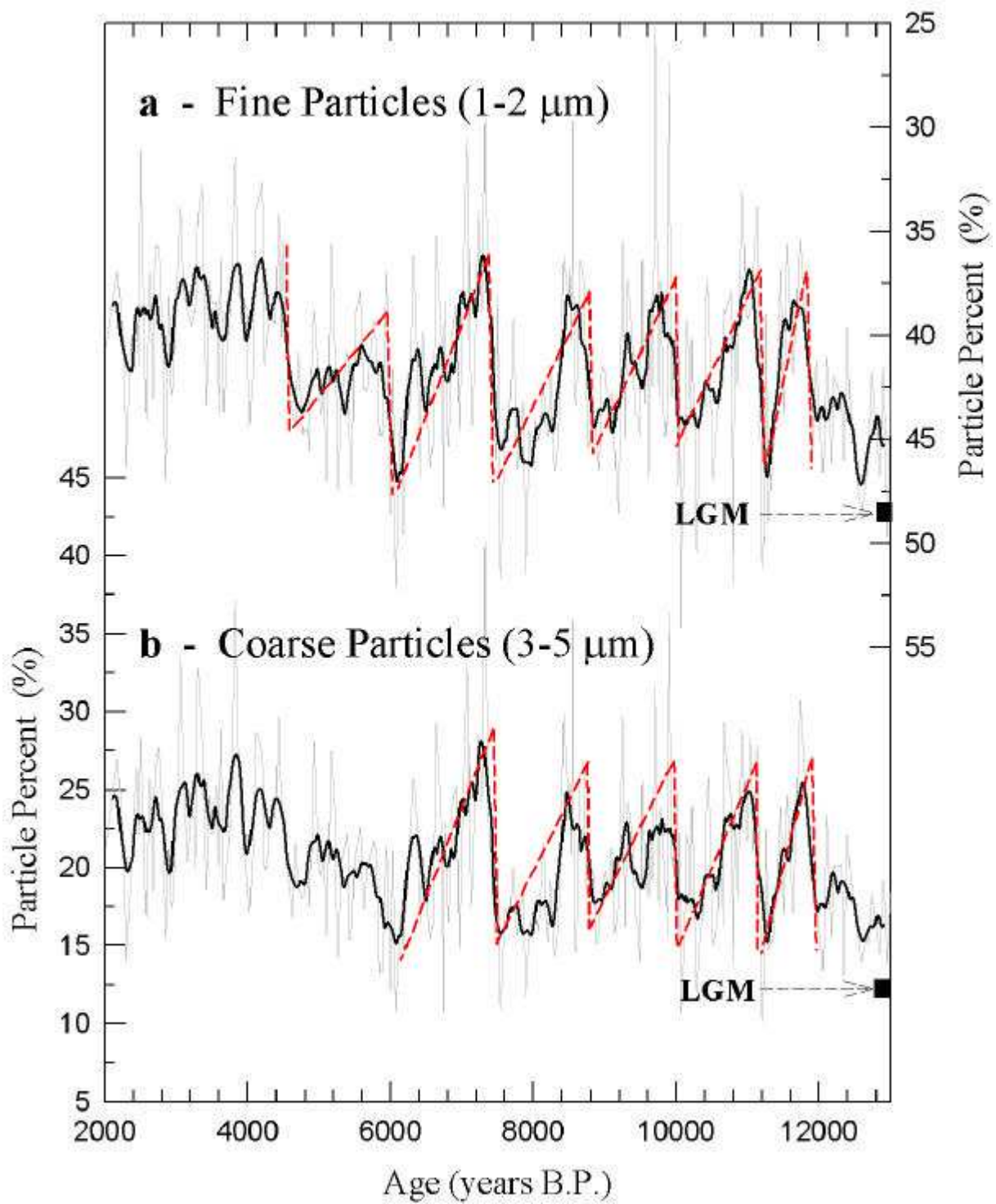


Fig. 8B.4 – EDC DUST RECORDS (2-13 kyr B.P.) :

[a] Fine (1-2  $\mu\text{m}$ ) Particle Percent (FPP, inverted scale) and running average.

[b] Coarse (3-5  $\mu\text{m}$ ) Particle Percent (CPP, the same as in Fig. 2c) and running average. The black squares indicate the average FPP and CPP value for the LGM, 48% and 12.5% respectively [23,29]. The dotted line marks the sawtooth pattern suggested by the records.

### *Spectral analysis*

The CPP profile of Vostok and EDC display clear fluctuations at centennial timescales. From ~13 kyr B.P. to 4.5-5 kyr B.P., the EDC record indicates well-structured millennial-scale rhythm (Fig. 8B.4) which seems to cease at circa 4.5-5 kyr B.P.; while afterward only the shorter term secular periodicities persist.

Spectral analysis performed with Multitaper Method (MTM, bandwidth parameter of 4 and 7 tapers, [30]), for the EDC CPP series encompassing the 5 to 13 kyr B.P. period and the 3.5 to 9.8 kyr B.P. period are reported in figure 8B.5a and 8B.5b respectively. This latter corresponds to the same period spanned by the Vostok dust record. In the former, two significant bands with high confidence level (>95%) occur at periodicities of 130-150 years and at 180-210 years. Two other bands are also significant (>90% confidence level) at about 300-320 years and at around 1200 years. When the 3.5 to 9.8 kyr B.P. time series is considered, two prominent bands at centennial periodicity arise at 130-150 years and at 180-210 years (>95% confidence level) while the 300 years band and the millennial band have lower energy.

For the Vostok CPP record (Fig. 8B.5c), MTM analysis displays a broad band (>99% confidence) at 150 to 230 years periodicities and another band at about 380 years (>95% confidence). It is

worthwhile to notice that the two independent dust series for the Holocene both contain significant centennial periodicities almost in the same frequency band. It can be noted that the secular frequencies

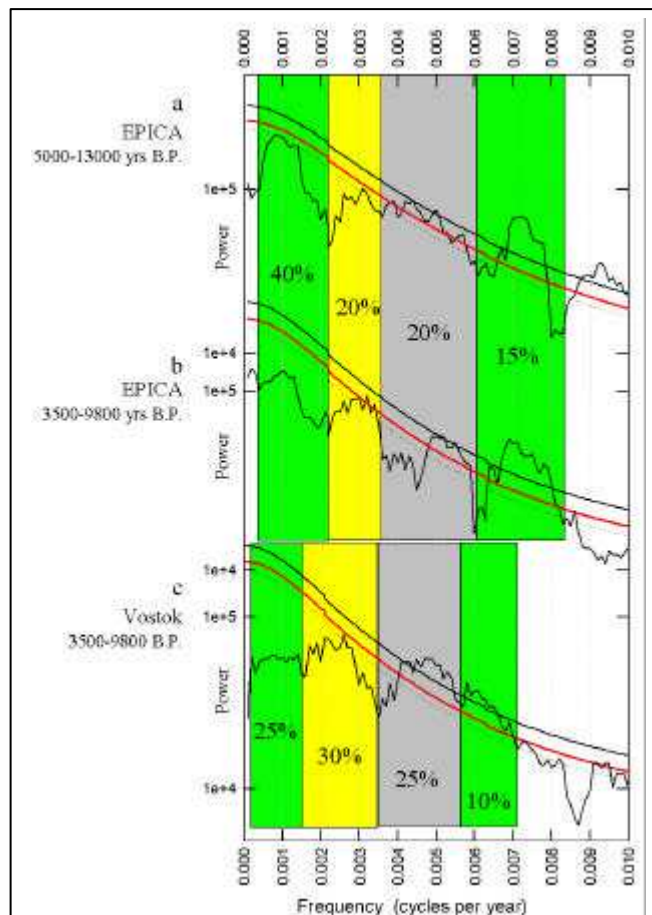


*Fig. 8B.5 –POWER SPECTRA obtained using MTM (bandwidth parameter of 4 and 7 tapers, [28])*

*[a] EPICA CPP dust record from 5 to 13 kyr B.P.*

*[b] EPICA CPP but from 3.5 to 9.8 kyrs B.P.*

*[c] Vostok-BH7 CPP dust record*

*Confidence level given by a red noise signal are shown by curves : 90% (dotted line), 95% (solid thick line) and 99% (solid thin line).*

*The percentage of the variance of the signal is indicated for each frequency band interval.*

*From left to right :*

*- 3000 to ~500-600 years*

*- ~600-500 to ~300 years*

*- ~250 to ~170 years*

*- ~170 to ~120 years)*

are approximately harmonics of the millennial one and signal variance is distributed almost equally. As an example, for EPICA, the millennial periodicity of ~1200 yrs and 600 years (i.e. its 2<sup>nd</sup> harmonics) explain about 40% of the variance, the periodicities ~400 to ~300 years (3<sup>rd</sup> and 4<sup>th</sup> harmonics) about 20%, and the band from about 250 to 150 years (5<sup>th</sup> to the 8<sup>th</sup> harmonics) also about 20%. For the Vostok, the variance of the signal is distributed for about 25 % at the millennial band, about 30% in the ~600 to ~270 years band and for 25-30% in the ~270 to ~150 years band.

### ***The 200-yr frequency band and the <sup>10</sup>Be record***

The two dust records show a 200-year frequency band which contains about ~20 to 30 % of the total signal variance. In Fig. 8B.6a and 8B.6b we report EDC and Vostok CPP profiles filtered for the band around 200 years. The two filtered series display a modulation suggesting the combination of two frequencies which are very close to 200 years. In the EDC record, the nodes reveal a millennial pacing (~1200 years) which represents the fundamental tone, assuming modulation is the result of two successive harmonics at about 200 years (e.g. 240 and 200 years or 200 and 170 years). Interestingly, for the filtered Vostok series the nodes and fundamental tones are about half duration of EDC ones (~600 years).

A visual inspection indicates the two filtered dust records are clearly in anti-phase for almost the whole 7,000 years of common period and about 29 cycles are observed. At about 4kyrs B.P. phase seems to change and three cycles (Fig. 8B.6c) are in phase. This opposite phase for most of the record is confirmed by computation of the coherence and phase analysis (not shown). Such a lead or lag by about 100 years between the EDC and Vostok records, for almost the entire records, is unlikely due to a systematic error in the depth-to-depth matching. As volcanic events are randomly distributed, the probability for an event to be located systematically at a constant distance (3 m at EDC or 2 m at Vostok) from a previous one is low.

The <sup>10</sup>Be concentration record is shown in Figure 8B.2e for the period from 2 to 7 kyr ago. MTM spectral computation (not shown) gives a significant band around 200 years (Raisbeck et al., in preparation).

The 200-years band is common for <sup>10</sup>Be record, the Vostok and EDC dust series and in all three records it is significant.



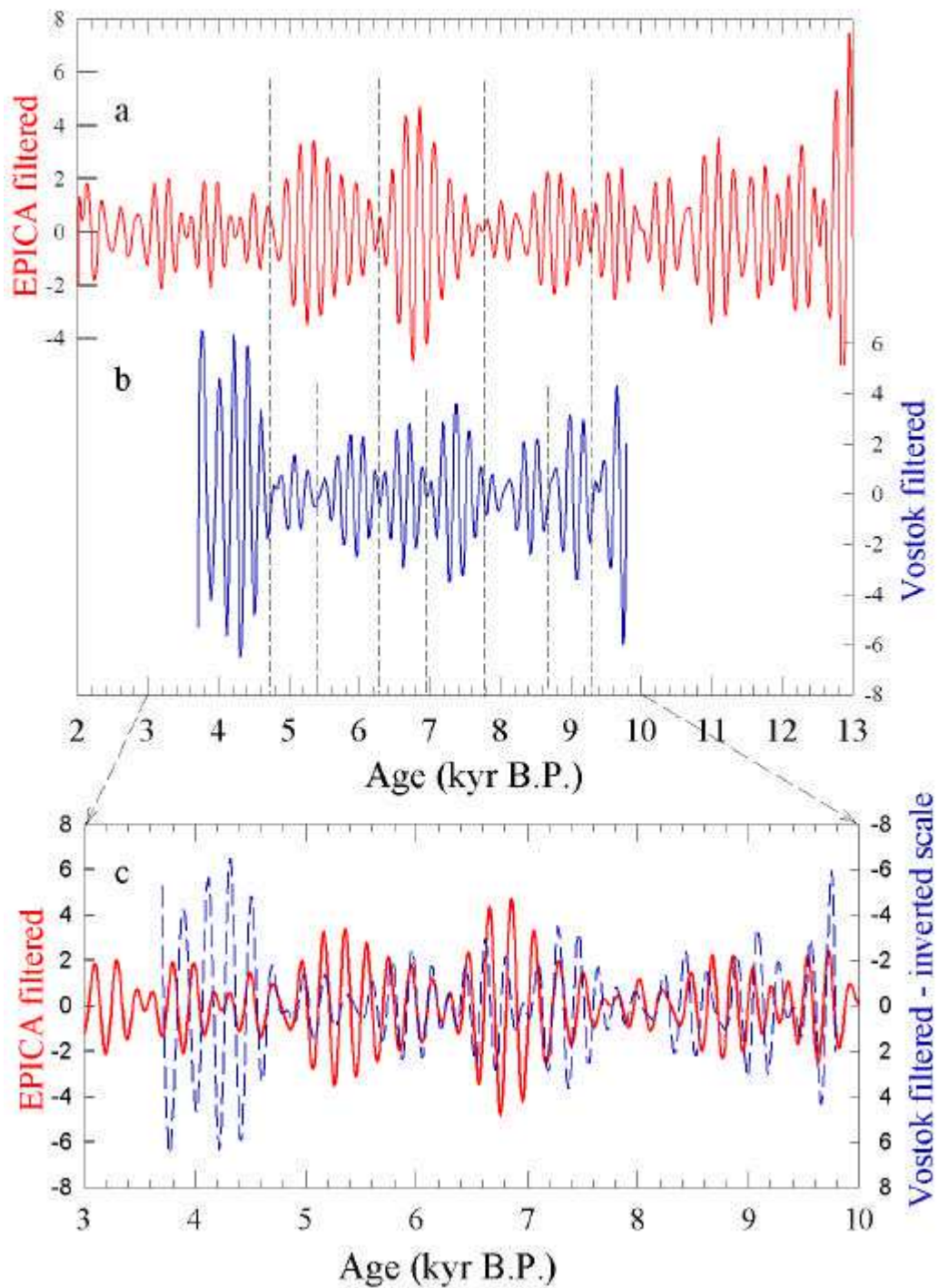


Fig. 8B.6 – **FILTERED DUST SERIES** in the 160-240 band interval: [a] EPICA [b] Vostok. In the both record modulations can be observed from ~ 9-9.5 kyrs B.P. to 4.5-5 kyrs B.P. Distance between nodes corresponds to the fundamental (millennial) tone (~1200 years for EPICA and ~600 years for Vostok). [c] Zoom for the two series from 3 to 10 kyrs B.P. interval displaying antiphase for most of the period. Vostok scale is inverted. (Continuous line: EPICA; Short dashed line: Vostok).

### **8B.1.3 Discussion: atmospheric circulation and solar activity proxies.**

The CPP value is taken as a proxy of the atmospheric circulation around Antarctica. This proxy is quite different from the total dust concentration because is quite independent of the snow accumulation rate, the conditions at the source region(s) for dust and the hydrological cycle. In a previous study of the EPICA-Dome C ice core, Delmonte et al. showed [29] that the drastic dust-concentration change from Last Glacial Maximum (LGM) to Holocene was coincident with a significant shift in particle size distribution. This was interpreted as a change in the efficiency of penetration of air masses into the polar Plateau. The observed fluctuations in particle size during the Holocene are less pronounced with respect to the LGM-Holocene ones. In this study we will use particle size proportion and CPP as proxy for fluctuations of the dust advection and therefore for the atmospheric circulation over East Antarctica.

The increasing trend seen in EDC CPP over the Holocene (Fig. 8B.2) is consistent with the trend observed for the mode [29] which was interpreted by an easier penetration of dusty air masses toward Antarctica. On the contrary, this trend is not observed in the Vostok CPP record. Such an important difference between the two sites clearly suggests that they are under different atmospheric circulation influences.

The geographical provenance of Holocene dust is not yet known, but a recent isotopic investigation suggests a common source region for the glacial dust for EDC and Vostok (Delmonte et al., submitted). If this holds true for the Holocene period, it would confirm that the differences in size are a consequence of different transport patterns.

In ice cores,  $^{10}\text{Be}$  concentration is dependent, among other parameters, on the snow accumulation rate. This was used to explain a 2-fold variation between glacial and interglacial climates [31]. However, for the rather stable Holocene interglacial period, where accumulation rates are fairly constant,  $^{10}\text{Be}$  is primarily influenced by variations in the production rate due to variable solar activity [24]. This can be shown by the good correlation between  $^{10}\text{Be}$  in ice and the  $^{14}\text{C}$  in tree rings ([32] and Raisbeck et al., in preparation].

#### ***Millennial variability***

Millennial cycles with ~1200 yrs are clear in the EDC dust record for the period from 13 to 4.5 kyrs B.P. and this band accounts for about 40 percent of the total variance. The ~1200 years periodicity are reminiscent of the pacing of events archived in North Atlantic marine records [2], and the sawtooth pattern of the CPP record (Fig 8B.3) suggests that Antarctic ice records could be the southern expression of thermohaline circulation anomalies. The CPP oscillations are more marked in the EDC dust record than in the Vostok one, and seems consistent with a more oceanic influence on Dome C and its greater sensitivity to ocean anomalies compared to Vostok.

The North Atlantic millennial fluctuations are persistent through different glacial and interglacial climatic stages, and during the last deglaciation. The average rhythm of such events is around  $1470 \pm 532$  yrs [2] in glacial periods, and while slightly shorter on average for the Holocene ( $1374 \pm 502$  years), the band is statistically the same. Closer to Antarctica, in southern Chile, millennial variability in humidity conditions was observed for the last 7700 years and interpreted as shifts in the Southern Westerlies [6]. Our evidence for millennial oscillations from Antarctic records gives them a global character. However, the origin of millennial cycles is not clearly understood. For the North Atlantic, the quasi-periodic millennial events observed during the Holocene and the glacial period are suggested to be the response to a common forcing internal to the Earth's climate system and amplified through the North Atlantic's thermohaline circulation [2]. On the other hand, Broecker et al. [18, 19] suggested millennial oscillations generated by the seesawing deepwater production between the North Atlantic and the Southern Ocean linked to the pacing of salinity anomalies. If this scenario holds true for the Holocene period and oscillations are linked to NADW formation, the anomalies may diffuse globally and the millennial periodicity would then represent the salt anomaly turnover time.

Assuming millennial frequencies are pervasive components of the Earth's climate system, we likely observe in the EDC and the Vostok Antarctic ice cores, the fundamental tones and/or their harmonics. A sawtooth pattern is indeed suggested in CPP and FPP for EDC (Fig. 8B.4) that is reminiscent of the salt anomaly pattern occurring at the time of Dansgaard-Oeschger events in North Atlantic [41].

### ***Variability at secular frequencies and the regional anomalies***

An important issue of our study is the observation of significant centennial frequencies (300, 200 and 150 years) both in EDC and Vostok, that are unlikely related to analytical biases and/or random noises. The common 200-year band of variability is particularly interesting, since it is similar to that of  $^{10}\text{Be}$  [24] and solar activity.

High-resolution marine records [9] already show oscillations at centennial timescale comparable to those of  $^{14}\text{C}$  (140, 220 and 420 years, [33]). The advantage of our ice core record is that it allows a direct comparison of atmospheric circulation and solar activity proxies from the same media. The cross correlation between CPP and  $^{10}\text{Be}$  at Vostok (not shown) indicates a maximum correlation for secular frequency and lesser degree for millennial frequency, a result already suggested from the visual inspection of all three records (Fig. 2). The absence of correlation contradicts somehow the approach suggesting a solar-climate link at millennial frequency for North Atlantic [9].

A puzzling issue is the evidence for an opposite variation in the dust size records at Dome C and Vostok for the solar (200-year) band for most of the Holocene (Fig 8B.4). A systematic 100-year lead or lag in the atmospheric circulation is observed in 25 of 29 cycles of our record. This suggests a connection between the two Antarctic locations, in other terms a phased-locked regional variability. EPICA-Dome C and Vostok are separated by ~600 km, but they share similar characteristics : altitude (3250 and 3480 m a.s.l), mean annual temperature (-54.5 and -55.4°C), mean apparent distance from

the coast (1100 and 1410 km) and probably the same dust source, at least during the glacial periods. However, in spite of the short distance with respect to the scale of the Antarctic continent, evidence of regional differences occurs.

In addition to different trend observed in EDC and Vostok CPP, the first difference is the size distribution. Dry deposition dominates the atmospheric dust removal processes over the whole very low accumulation rate area of Antarctica [34]. Therefore the short distance between the two sites with respect to the long range transport from the southern continents cannot explain the better grading of the dust reaching Vostok. This suggests that the air masses have very different pathways.

A second good example of geographical variability at the 100 km scale is given by the isotope composition of the snow collected along the 6,000 km transect of the Trans-Antarctic route [35]. The deuterium value is the lowest of the whole series at Vostok (-440 ‰) and this value is consistent with the gradual trend and the isotope-temperature relationship over more than ~2500 km from Weddell sea area through the South Pole, ending at Vostok. Sharply northward of Vostok there is a steady geographical gradient (+7 ‰ per 100km) indicating an oceanic influence, and ~ 300 km away, a second isotope-temperature relationship is obtained, shifted by 20 ‰ with respect to previous one and remain the same until the coastal area (Indian Ocean). This shift was associated with an orographic effect [35]. There are only tiny differences along the Trans Antarctica route in the Vostok area and the slope changes from plus to minus 20 m/100 km; this small effect, not yet even seen from GCM experiments [35], is sufficient however to make the site of Vostok under the deepest continental influence in Antarctica. Indeed, the isotope content of precipitation is linked to cloud history. Atmospheric pathways of entering air masses is influenced by the catabatic regime of the winds depending on the regional slope of the ice sheet surface. In central Antarctica, the general downslope cold winds induce pumping effects for the upper warm oceanic air masses which are advected [36]. The less depleted isotope content of sites off Vostok, as well as for the EDC site (-390‰), could be understood as a more oceanic influence, and/or a different air pathway from that of Vostok. In this respect, Holocene records of deuterium excess, a proxy of the sea surface temperature [37] display differences between Vostok and Dome C region, and support the variable pathway for marine air masses. With time and climate, the surface slope may change and/or the atmospheric pressure changes so that the sensitive dynamic equilibrium between air masses of two areas of influence may change and the boundary migrate. We may expect therefore a variable sensitivity of each site with respect to the ocean influence and climate changes.

Finally, present-day climate studies also give examples of regional anomalies in atmospheric and oceanic parameters. The so-called Antarctic Circumpolar Wave [38] is an eastward wave spreading around the Antarctic continent with a periodicity of about 8-10 years. Indeed, the Weddel and the Ross sea sectors are the regions contributing mostly to the variability of sea ice [39], but unfortunately the existing marine records for such areas, as well as for the East Antarctic margin (e.g. [40]) are inadequate for deciphering the centennial-scale variability as we observed from ice cores.

Since 25 of 29 cycles at 200-years on CPP records from EDC and Vostok are clearly in antiphase (Fig 8B.6c), we suggest that a regional variability in the atmospheric circulation was operating for almost 7,000 years. Hence, one could envision that the atmospheric centres of influence (Highs and Lows) modulate the penetration of air masses into the polar plateau leading the flow of dust-carrying air masses preferentially towards one site or the other. Such a wavering effect seems to be hidden at middle-late Holocene (circa 4.5 ky B.P.), and this might correspond to a changing mode of variability of the system or to a lesser sensitivity of the sites. Moreover, the common part of the dust records is not available after 3.5 ky B.P.

***Why 200 year signal so strong? Hypothesis for a mediation from the Southern Atlantic Ocean.***

Following the assumption of Broecker et al [18, 19] that the millennial frequency originates from the salt anomaly and diffuses globally through the thermohaline circulation, such an anomaly should influence the southern Atlantic and the circum antarctic ocean. However, the regional anomalies induced and their final expression in Antarctic ice cores depend on sea surface temperature, sea ice, ice sheet slope, and finally atmospheric circulation.

Mikolajewicz and Maier-Reimer (1990) performed a coupled ocean-atmosphere experiment [42] and suggested internal oscillations in the 30-500 year band for the Southern Atlantic Ocean, opening the possibility for resonance and amplification. Their model was forced by a stochastic wind

at 40°S. As a result, the flux of NADW at 30°S into the circum Antarctic current was not continuous, but pulsed and opposite to the flux of fresh water through the Drake passage, in a kind of “seesaw”

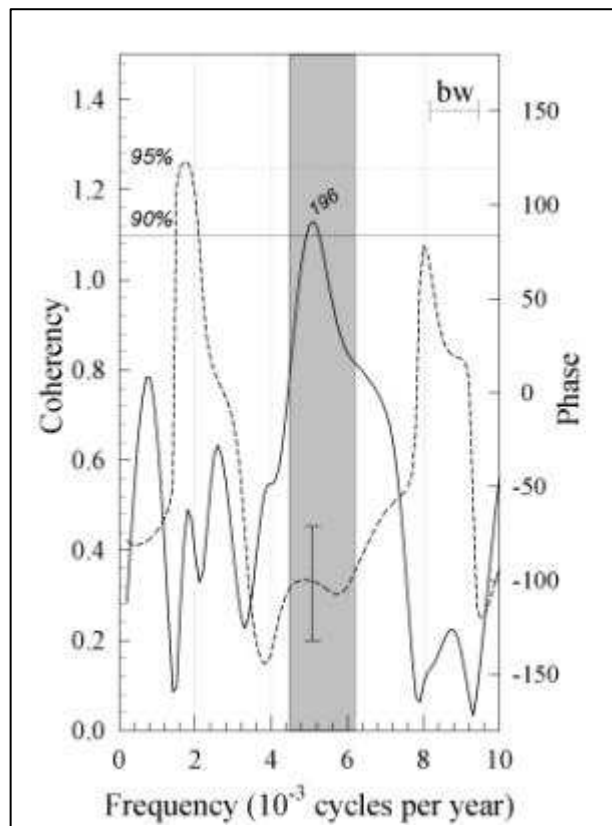


**Fig 8B.7- <sup>10</sup>Be AND DUST CORRELATION**

*Coherency and Phase between a composite signal of the dust (difference between EPICA Dome C CPP and Vostok CPP, see text) and <sup>10</sup>Be. Maximum coherency is obtained at 196 years and the shaded area represents the 200 year band. The 90% and 95% confidence levels are indicated by continuous and dotted horizontal lines.*

oscillator. From an integration over ~1500 years the model of South Atlantic Ocean indicated a mean mode of oscillation at about ~320 years.

From this model, any external forcing (e.g. atmospheric circulation at 40°S) or its harmonics may tune this system. Assuming the secular solar variability acting on atmospheric parameters (e.g. altitude of geopotential) in similar way as observed for the 11-year cycle [11] at tropical latitudes, some influence could be expected for extra tropical area in the southern latitude, and therefore a secular solar forcing on the Southern ocean system could be possible. Amongst responses, a combination of the solar frequency would result (e.g. 1/240, 1/200 years; 1/170 yr, 1/150 years) and would possibly contribute to the variance of the millennial-scale band of oscillations as well as those at 600-yr and a 300-yr bands; it is worth noticing that these latter frequencies are also clearly present in the EDC dust record.

The physical mechanisms linking solar variability at secular timescale and climate remains unknown. However, our data support such a relationship. Taking advantage of the two records of atmospheric circulation responding in opposite phase in their common secular band, we constructed a composite signal based on the difference between CPP from EDC and CPP from Vostok, which reduces the noise and strengthens the 200 year component. The cross correlation between the composite dust signal and the <sup>10</sup>Be record (Fig. 8B.7) shows high coherency in the ~200 year band (>90% confidence level) but the dust and solar signals show a phase-lag, suggesting their link is not direct.

While the millennial pacing of North Atlantic is thought to provide the major tone, the global diffusion of salt anomaly in through the south Atlantic and the circum antarctic ocean share frequency bands with the solar activity, and these factors can combine and interact through their harmonics, similarly to what is proposed for the North Atlantic [10].

### ***The Southern Ocean-Sea ice-atmosphere interactions***

The Southern Ocean can play a major role for the circum Antarctic atmospheric circulation: in particular, sea ice extent and distribution around Antarctica is a response to oceanic and atmospheric conditions, and in turn has the potential to modify the Westerlies and the cyclonic activity [38]. The consequence of a variation in the input of NADW into the South Atlantic would be a change of the heat balance of the Southern ocean, likely affecting sea ice formation [41].

In the Antarctic Peninsula, clear evidences for secular (200-300 yrs) changes in sea surface conditions (like sea surface temperature, sea ice and wind stress) are documented from bio-geochemical marine records [e.g. 13, 20, 21]. However, changes in sea surface conditions and in the pattern of sea ice cover are variable and unlikely uniform in the circumantarctic context; their local distribution and

temporal variability around the Continent may therefore induce anomalies in atmospheric circulation and air masses advection at regional scale for different sites as suggested by our two dust CPP records. At this step, modelling experiment for atmosphere-ocean-sea ice interactions will be pertinent for testing secular and millennial behaviour of the climate as well as the regional sensitivity to solar forcing.

#### **8B.1.4. Conclusions**

Two Holocene ice core records of dust size distribution from EDC and Vostok show periodical fluctuations interpreted as variations in the atmospheric circulation around Antarctica.

Significant millennial-scale oscillations (~1200 yrs) are well marked in the EDC record from 13 to ~4.5 kyrs B.P., and other secular periodicities, probably harmonics of the millennial one, are present at both sites. Among them, a significant 200-yr band is common to both records of dust and to one of cosmogenic  $^{10}\text{Be}$  from a Vostok ice core, and a composite dust record is highly coherent with the solar one within this band.

The tight relative dating between the ice cores permits detection of a regional anomaly in the atmospheric circulation around Antarctica, that appears to be favoured towards one site or the other with 200 years periodicity. This phenomenon is observed for 7,000 years during the major part of the Holocene, and is interpreted as an atmospheric connection between Vostok and Dome C sites. This requires further studies and has to be tested through modelling experiments.

The millennial-scale periodicity present in the EDC dust record is reminiscent of the pacing of oceanic and atmospheric Holocene climate records, and our data suggest this pulsation has worldwide character. Such periodicity likely represents a fundamental mode of oscillation of the earth's climatic system, that we interpret as a possible expression in Antarctica of global dissipation of the North Atlantic salt anomaly.

The Southern Ocean interacts with the atmospheric circulation around Antarctica through surface temperature and sea ice extent. Since this system can oscillate at secular frequencies we speculate that solar activity could tune the oscillation modes embedded in the Southern Hemisphere climatic system affecting ocean surface temperature, sea ice extent, and the circum-Antarctic atmospheric circulation. Our data gives new insights into climate studies but complementary modeling efforts and additional data are needed to validate this scenario.

## References

- [1] Intergovernmental Panel on Climate Change (IPCC) (2001) New York, Cambridge Univ. Press.
- [2] G. Bond, W. Showers, M. Cheseby, R. Lotti, P. Almasi, P. DeMenocal, P. Priore, H. Cullen, I. Hajadas, G. Bonani, A pervasive millennial scale cycle in the North Atlantic Holocene and glacial climates, *Science* 278 (1997) 1257-1266.
- [3] Marchitto, T.M., W.B. Curry and D.W. Oppo. 1998. Millennial-scale changes in the North Atlantic circulation since the last glaciation. *Nature* 393 (1998) 557-561.
- [4] G.G. Bianchi, I.N. McCave, Holocene periodicity in North Atlantic climate and deep-ocean flow south of Iceland, *Nature* 397 (1999) 515-517.
- [5] A. Sarkar, R. Ramesh, B.L.K. Somayajulu, R. Agnihotri, A.J.T. Jull, G.S. Burr, High resolution Holocene monsoon record from the eastern Arabian Sea. *Earth Planet. Sci. Lett.* 177(3-4) (2000) 209-218.
- [6] F. Lamy, D. Hebbeln, U. Rohl, G. Wefer, Holocene rainfall variability in southern Chile: a marine record of Southern Westerlies, *Earth Planet. Sci. Lett.* 185 (2001) 369-382.
- [7] C. Moy, G.O. Seltzer, D.T. Rodbell, D.M. Anderson, Variability of El Nino/Southern Oscillation activity at millennial timescales during the Holocene epoch, *Nature* 420, (2002) 162-165.
- [8] Mayewski, P., L.D. Meeker, M.S. Twickler, S. Whitlow, Q. Yang, W.B. Lyons and M. Prentice. 1997. Major features and forcing of high-latitude northern hemisphere atmospheric circulation using a 110,000 year-long glaciochemical series. *J. Geophys. Res.* 102 (C12) (1997) 26,345-26,366.
- [9] G. Bond, B. Kromer, J. Beer, R. Muscheler, M.N. Evans, W. Showers, S. Hoffmann, R. Lotti-Bond, I. Hajadas, G. Bonani, Persistent solar influence on North Atlantic climate during the Holocene, *Science* 294 (2001) 2130-2136.
- [10] J.T. Andrews, J. Hardadottir, J.S. Stoner, M.E. Mann, G.B. Kristjansdottir, N. Koc Decadal to millennial-scale periodicities in North Iceland shelf sediments over the last 12000 cal yr: long-term North Atlantic oceanographic variability and solar forcing, *EPSL* 210 (2003) 453-465.
- [11] K. Labitzke, H. VanLoon, The signal of the 11-year sunspot cycle in the upper troposphere-lower stratosphere, *Space Sci. Rev.* 80 (1997) 393-410.
- [12] D.T. Shindell, G.A. Schmidt, R.L. Miller, D. Rind, Northern Hemisphere winter climate response to greenhouse gas, ozone, solar, and volcanic forcing, *J. Geophys. Res.* 106 (2001) 7193-7210.
- [13] A. Leventer, E.W. Domack, S.E. Ishman, S. Brachfeld, C.E. McClennen, P. Manley, Productivity cycles of 200-300 years in the Antarctic Peninsula region: understanding linkages among the sun, atmosphere, oceans, sea ice, and biota., *GSA Bulletin* 108 (1996) 1626-1644.
- [14] L.C. Paterson, J.T. Overpeck, N.G. Kipp, J. Imbrie, A high-resolution late Quaternary upwelling record from the anoxic Cariaco Basin, Venezuela, *Paleoceanography* 6 (1991) 99-119.
- [15] U. Neff, S.J. Burns, A. Mangini, M. Mudelsee, D. Fleitmann, A. Matter, Strong coherence between solar variability and the monsoon in Oman between 9 and 6 kyr ago, *Nature* 411 (2001) 290-293.
- [16] D.A. Hodell, M. Brenner, J.H. Curtis, T. Guilderson, Solar forcing of drought frequency in the Maya lowlands, *Science* 292 (2001) 1367-1370.
- [17] P. DeMenocal, J. Ortiz, T. Guilderson, M. Sarnthein, Coherent High- and Low- latitude climate variability during the Holocene warm period, *Science* 288 (2000) 2198-2202.
- [18] W.S. Broecker, G. Bond, M. Klaus, G. Bonani, W. Wolfli, A salt oscillator in the glacial Atlantic?, *Paleoceanography* 5 (1990) 469-477.
- [19] W.S. Broecker, S. Sutherland, T.-H. Peng, A possible 20th-century slowdown of Southern Ocean deep water formation, *Science* 286 (1999) 1132-1135.
- [20] E. Domack, A. Leventer, R. Dunbar, F. Taylor, S. Brachfeld, C. Sjunneskog, O.L.S. Party, Chronology of the Palmer Deep site, Antarctic Peninsula: a Holocene palaeoenvironmental reference for the circum-Antarctic, *The Holocene* 11 (2001) 1-9.
- [21] E.W. Domack, P.A. Mayewski, Bi-polar ocean linkages: evidence from late-Holocene Antarctic marine and Greenland ice-core records, *The Holocene* 9 (1999) 247-251.
- [22] M.A. Bårçena, R. Gersonde, S. Ledesma, J. Fabr s, A.M. Calafat, M. Canals, F.J. Sierro, J.A. Flores, Record of Holocene glacial oscillations in Bransfield Basin as revealed by siliceous microfossil assemblages, *Antarctic Science* 10 (1998) 269-285.
- [23] B. Delmonte, J.R. Petit, V. Maggi, Glacial to Holocene implications of the new 27,000-year dust record from the EPICA Dome C (East Antarctica) ice core, *Clim. Dyn.* 18 (2002) 647-660.
- [24] G.M. Raisbeck, F. Yiou, J. Jouzel, J.R. Petit, <sup>10</sup>Be and <sup>8</sup>H in polar ice cores as a probe of the solar variability's influence on climate, *Phil. Trans. R. Soc. Lond.* A330 (1990) 463-470.
- [25] J. Jouzel, V. Masson, O. Cattani, S. Falourd, M. Stievenard, B. Stenni, A. Longinelli, S.J. Johnsen, J.P. Steffensen, J.R. Petit, J. Schwander, R. Souchez, A new 27 kyr high resolution East Antarctic climate



record, *J. Geophys. Res.* 28 (2001) 3199-3202.

[26] E. Wolff, I. Basile, J.-R. Petit, J. Schwander, Comparison of Holocene electrical records from Dome C and Vostok, Antarctica, *Annals of Glaciology* 29 (1999) 89-93.

[27] I. Basile I., J.-R. Petit, S. Touron, F. Grousset, N.I. Barkov, Volcanic layers in Antarctic (Vostok) ice cores : source identification and atmospheric implications, *J Geophys Res* 106(D23) (2001) 31915-31931.

[28] J. Schwander, J. Jouzel, C.U. Hammer, J.R. Petit, R. Udisti, E. Wolff, A tentative chronology for the EPICA Dome Concordia ice core, *Geophys. Res. Lett.* 28 (2001) 4243-4246.

[29] B. Delmonte, J.-R. Petit, V. Maggi, LGM-Holocene changes and Holocene millennial-scale oscillations of dust particles in the EPICA Dome C ice core (Antarctica), *Ann Glaciol* 35, in press.

[30] M.D. Dettinger, M. Ghil, C.M. Strong, W. Weibel, P. Yiou, Software expedites singular-spectrum analyses of noisy time series, *EOS trans. AGU* 76 (1995) 12.

[31] F. Yiou, G.M. Raisbeck, D. Bourlès, C. Lorius, N.I. Barkov <sup>10</sup>Be in ice at Vostok, Antarctica, during the last climatic cycle. *Nature* 316 (1985) 616-617.

[32] G.M. Raisbeck, F. Yiou, E. Bard, D. Dollfus, J. Jouzel, J.R. Petit, Absolute dating of the last 7000 years of the Vostok ice core using <sup>10</sup>Be *Mineralog. Mag.* 62A (1998) 1228.

[33] M. Stuiver, T.F. Braziunas, Atmospheric 14C and century-scale oscillations, *Nature* 338 (1989) 405-408.

[34] M. Legrand, P. Mayewski, Glaciochemistry of polar ice cores: a review, *Review of Geophysics* 35 (1997), 217-243.

[35] Q. Dahe, J.R. Petit, J. Jouzel, M. Stievenard, Distribution of stable isotopes in surface snow along the route of the 1990 international Transantarctica expedition., *Journal of Glaciology* 40(134) (1994), 107-118.

[36] H. Schwerdtfeger, The climate of the Antarctic, in *Climate of The Polar regions*, S. Orvig Eds (1970) Elsevier, New York, 253-355.

[37] F. Vimeux, V. Masson, J. Jouzel, J.R. Petit, E.J. Steig, M. Stievenard, R. Vaikmae, J.W.C. White, Holocene hydrological cycle changes in the Southern Hemisphere documented in East Antarctic deuterium excess records, *Clim Dyn* (2001) 503-513.

[38] W.B. White, R.G. Peterson, An Antarctic circumpolar wave in surface pressure, wind, temperature and sea-ice extent, *Nature* 380 (1996) 699-702.

[39] A.M. Carleton, Antarctic sea-ice relationships with indices of the atmospheric circulation of the Southern Hemisphere, *Clim. Dyn.* 3 (1989) 207-220.

[40] F. Taylor, A. McMinn, Evidence from diatoms for Holocene climate fluctuations along the East Antarctic margin, *The Holocene* 11 (2001) 455-466.

[41] W. Dansgaard, S.J. Johnsen, H.B. Clausen, D. Dahl-Jensen, N.S. Gundestrup, C.U. Hammer, C.S. Hvidberg, J.P. Steffensen, A.E. Sveinbjörnsdóttir, J. Jouzel, G. Bond, Evidence for general instability of past climate from a 250-kyr ice-core record, *Nature*, 364 (1993) 218-220.

[42] U. Mikolajewicz, E. Maier-Reimer, Internal secular variability in an ocean general circulation model, *Clim. Dyn.* 4 (1990) 145-156.

Supplementary data information:

	DEPTH INTERVAL  TIME INTERVAL	SAMPLING (cm sample/ cm core)	Number of measurements	Accumulation rate (cm ice / year)	Years Between samples	Nyquist period (years)
<b>VK-BH1</b> <sup>10</sup> Be	69-178 m 2000-7050 B.P.	50 / 50	209	2.2	25	50
<b>VK-BH7</b> Dust	104-236 m 3500-9800 B.P.	5 / 100	130	2.2	50	100
<b>EPICA</b> Dust	90-400 m 2000-13000 B.P.	5 / 110	280	2.9	40	80

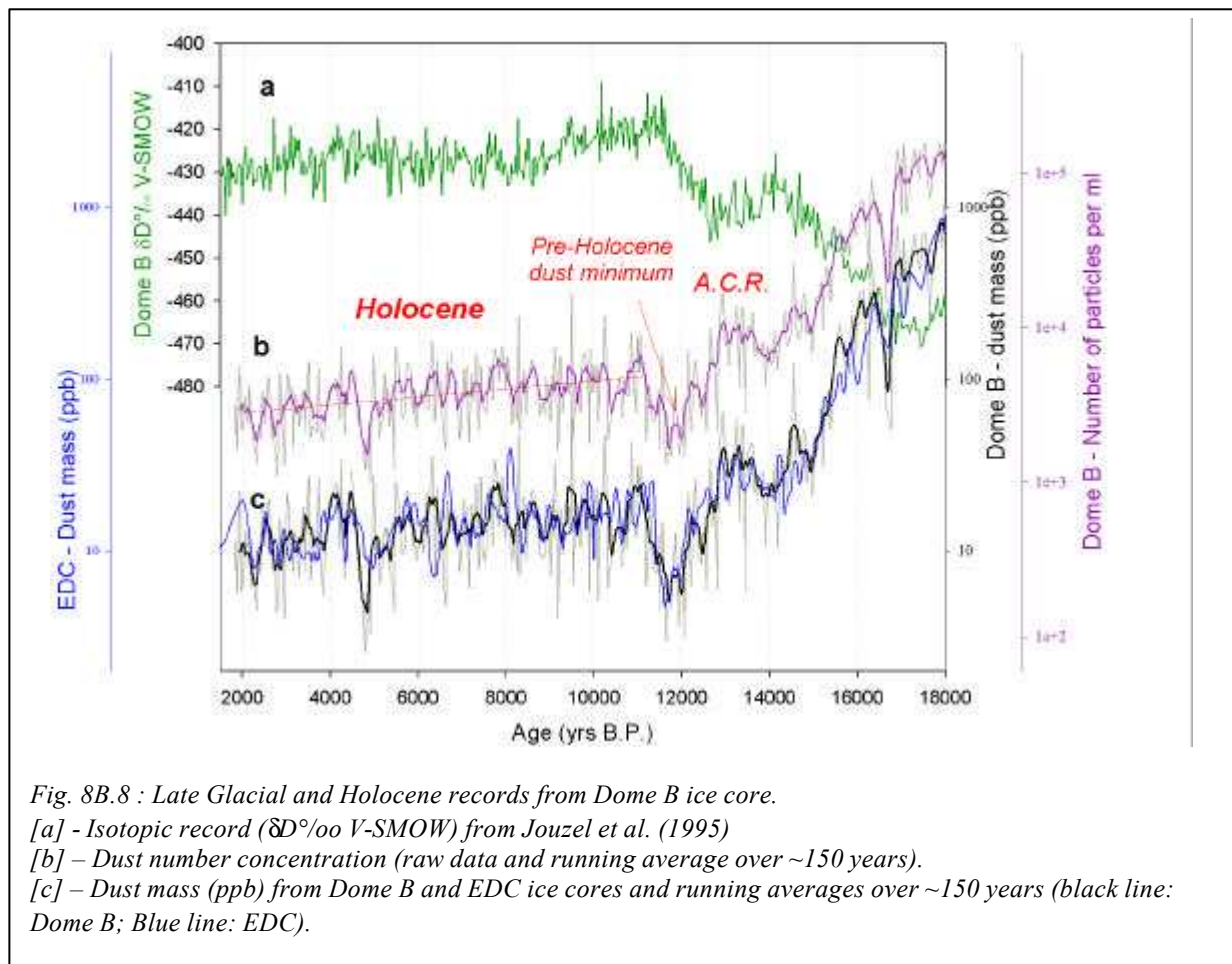
## 8B.2 Holocene variability in the Dome B ice core

### 8B.2.1 Dome B Holocene dust record

The Dome B ice core has been investigated at high temporal resolution for the Late Glacial and the Holocene periods (1 sample every 40 yrs from 1,800 to 15,000 years B.P.). The dust concentration profile is reported in Fig. 8B.8 , and we refer to § 8A.3 for a description of the deglaciation features of the record.

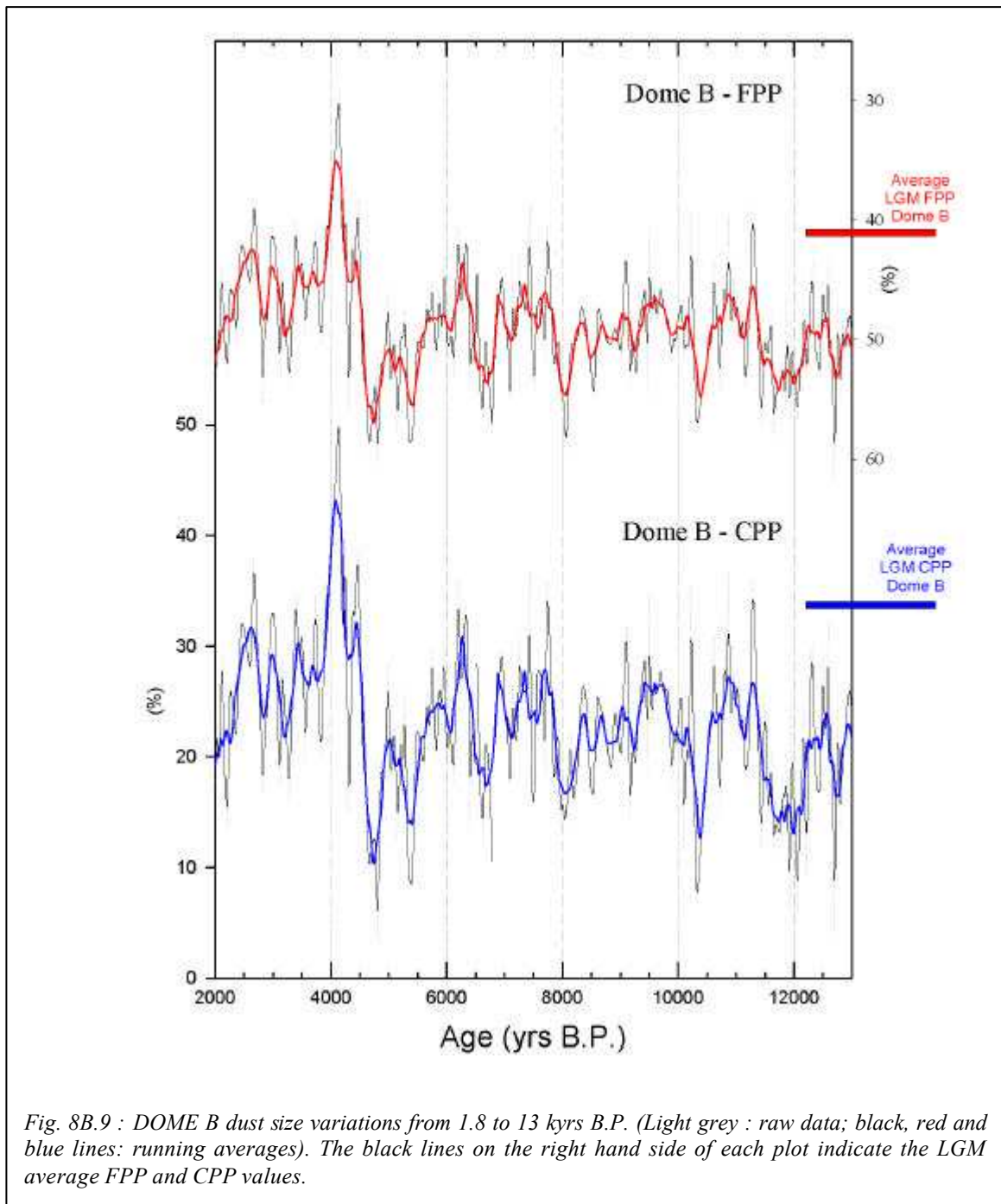
After the pre-Holocene dust minimum (situated between 411 and 430 m depth), the dust concentration profile shows fluctuating values around 4,000 Particles per ml and 15 ppb, and a general decreasing trend, already observed in the first Dome B concentration profile from Jouzel et al. (1995) as well as in the EDC and Vostok dust profiles (§ 8A.1).

As for the deglaciation (§8A.3), the Holocene part of the record confirms the tight similarity between Dome B and EDC dust concentration profiles (superposed in Fig. 8B.8). The chronology adopted for Dome B has been taken from Jouzel et al. (1995).



The dust size profile for Dome B from 2 to 13 yrs B.P. is reported in Fig. 8B.9.

The average FPP for the period investigated (1-2  $\mu\text{m}$ ) is 49%, while the CPP-calculated in the interval between 2,5 and 5  $\mu\text{m}$  particles<sup>1</sup> - is around 23%.



<sup>1</sup> For the Dome B record, as for Vostok and KMS, the Coarse Particle Percent (CPP) has been calculated in the interval 2,5-5  $\mu\text{m}$ , while for the EDC ice core, where particles are slightly coarser in the Holocene, the interval for CPP was chosen between 3 and 5  $\mu\text{m}$ . On the opposite, the Fine Particle Percent is always calculated in the 1 to 2  $\mu\text{m}$  interval, and therefore a quantitative comparison among the four ice cores is possible only for this latter.

Structured fluctuations of millennial scale duration are evident over all the Late Glacial and the Holocene, and such long term cycles appear superposed by shorter-term oscillations of secular duration.

The spectral analysis of Dome B FPP and CPP (Fig. 8B.10) points out a prominent and wide millennial scale band (>99% conf. lev.) and some multi-centennial bands. Periodicities above 99% significance can be found in the intervals between 323-370 years, 256-227 years, 167-185 years, 152-156 years and 125-118 years. The wider bands (light grey) in the figure define periodicities above 90% significance.

Differently from EDC and Vostok series, a large part of the variance of the Dome B particle size record is concentrated in the low frequency bands: periodicities >1000 years explain ~45% of the signal, and about ¾ of the total variance of the signal is explained by frequencies lower than 0.003 cycles per year (<330 years periods).

The Dome B CPP and FPP profiles filtered a band around 200 years are reported in Fig. 8B.11; the distance between the nodes, corresponding to the fundamental tone of the series, is on average 1345 years, a duration that is almost equivalent to that from EDC record of ca. 1200 years.

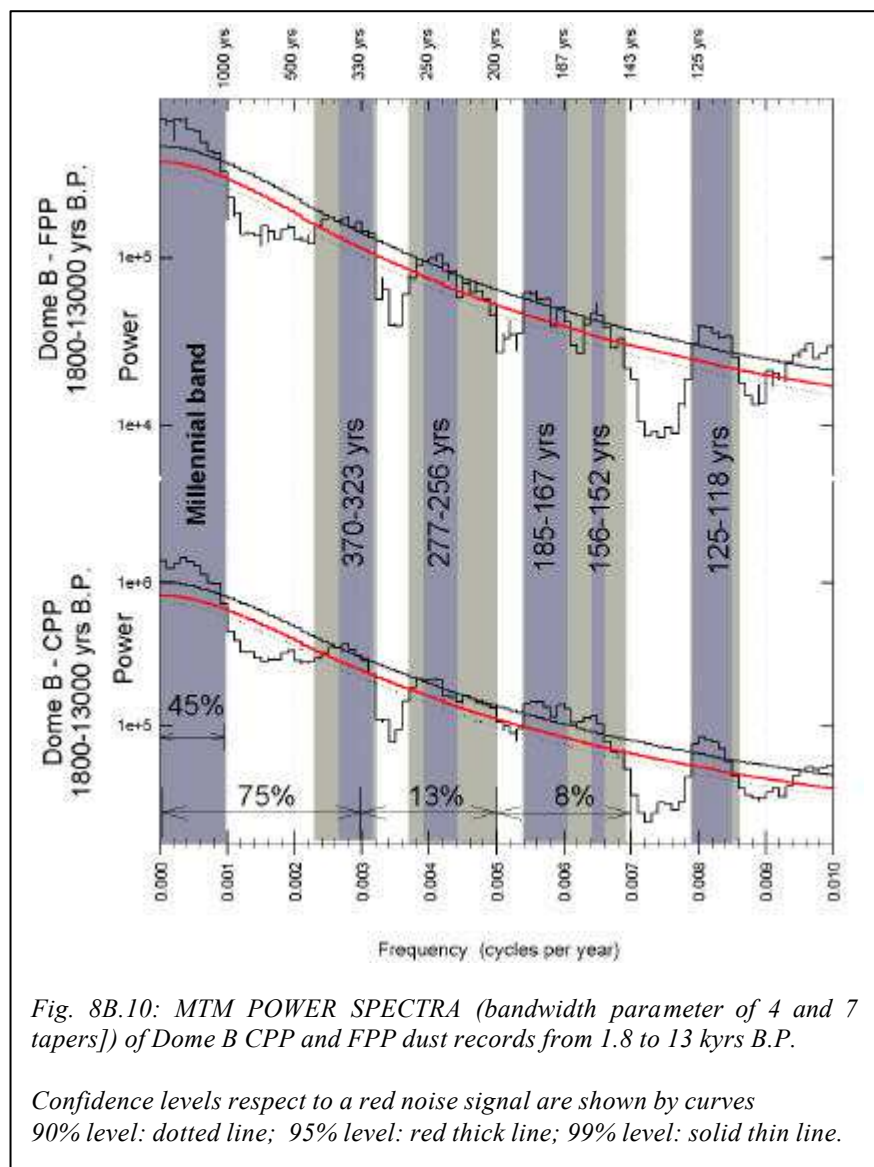
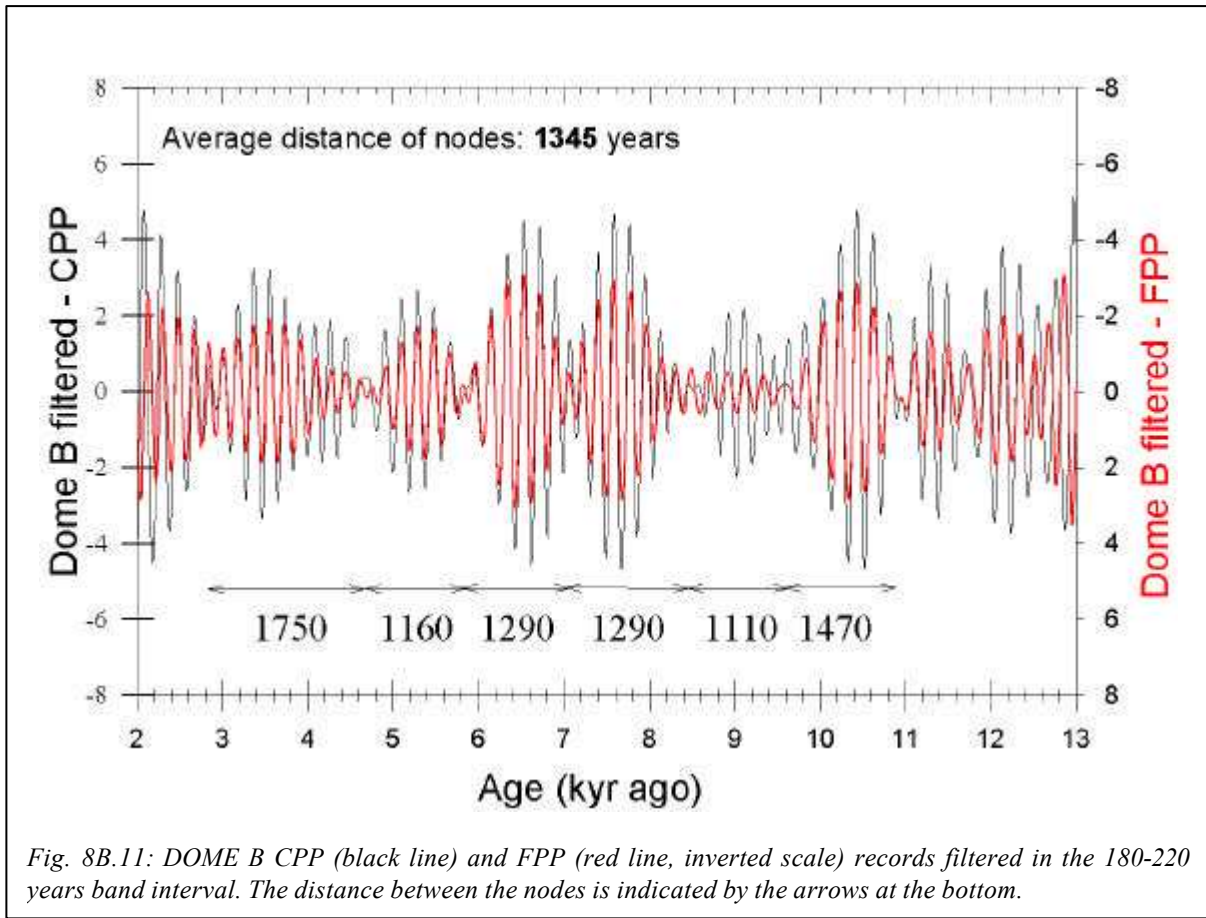


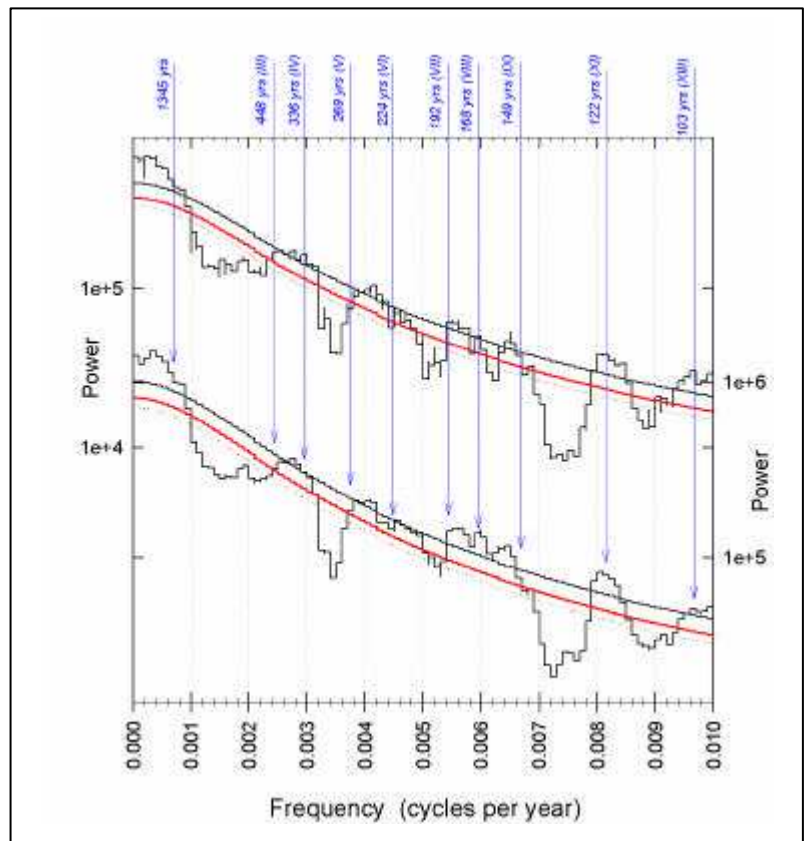
Fig. 8B.10: MTM POWER SPECTRA (bandwidth parameter of 4 and 7 tapers) of Dome B CPP and FPP dust records from 1.8 to 13 kys B.P.

Confidence levels respect to a red noise signal are shown by curves  
90% level: dotted line; 95% level: red thick line; 99% level: solid thin line.



Supposing the 1345-years periodicity as the fundamental tone, some of its harmonics actually constitute significant peaks in the MTM analysis of the CPP and FPP Dome B series.

Fig. 8B.12: MTM POWER SPECTRA of Dome B FPP (top) and CPP (bottom) dust records (same as in Fig. 8B.10), with indication of the harmonics (in brackets) of the 1345-years periodicity. Confidence levels are indicated as in Fig. 8B.10.



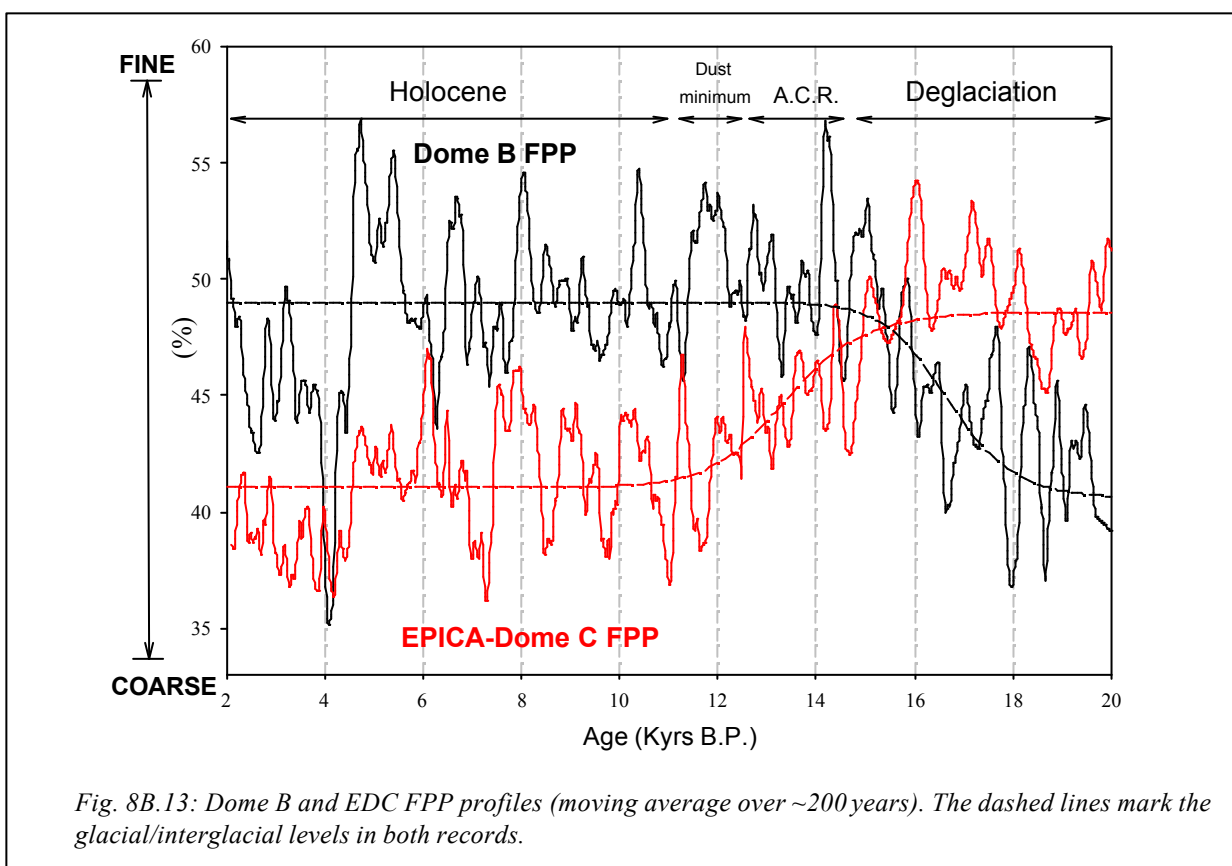
## 8B.3 Comparing the different sites

### 8B.3.1 Dome B and EDC ice core

Fig. 8B.13 compares the Dome B and the EDC FPP profiles from 2 to 20 kyrs B.P., i.e. since the LGM and until the late Holocene. A regression curve marks glacial/interglacial levels for each record, and the climatic periods are indicated by arrows at the top of the figure.

Beside a clear opposite evolution of Dome B and Dome C dust dimensional parameters during the deglaciation (§ 8A.3), this graph points out several additional information.

- 1- First, the LGM dust size pattern -characterized by coarse dust at Dome B and fine at Dome C- has no equivalent in the Holocene. Even in the late Holocene (at ca. 4 kyrs B.P.), when Dome B FPP decreases to LGM values (i.e. dust become coarser), Dome C is very different from its LGM but got similar low FPP values as Dome B.
- 2- Contrary to the LGM, the Holocene dust is finer on average at Dome B than at Dome C.
- 3- Large variations of millennial and multi-centennial scale characterize both profiles; such oscillations are clearly in antiphase in correspondence to the pre-Holocene dust minimum, but their phasing is not constant in the course of the Holocene and in the Late Holocene the main variations appear almost in phase.
- 4- Both profiles show a step-change at about 4.5 kyrs B.P. towards coarser particle dimensions.



### 8B.3.2 Dome B, EDC and Vostok dust size spectra and solar variability.

The spectral analysis of the Dome B (1.8-13 kyrs B.P.), EDC (2-13 kyrs B.P.) and Vostok (3.5-9.8 kyrs B.P.) Holocene dust size records are shown in Fig. 8B.14 and compared to the spectrum of  $^{10}\text{Be}$  from Vostok-BH1 ice core. This cosmogenic isotope is a proxy for solar variability and is supposed to be the uniform overall the East Antarctic Plateau (Raisbeck et al., 1990).

Here the comparison is performed among the power spectra of the CPP series, but the same results would be obtained if the FPP series are compared.

Two bands are common to the four spectra:

- 1- the first is the ~200 years band (190-220 years), always significant at least at >95% level.
- 2- The second is the 330-385 years band, significant at least at 90% level in the dust spectra (99% for Dome B) and present -but not significant- in the solar variability spectrum.

The prominent millennial band of Dome B (>99%) has a counterpart only in EDC, where its significance is slightly below 90% level. These two spectra share also a significant band around 245-265 years (>99% level).

Finally, the third solar band at higher frequency is found only in the EDC spectrum, but is not present in those from Dome B and Vostok .

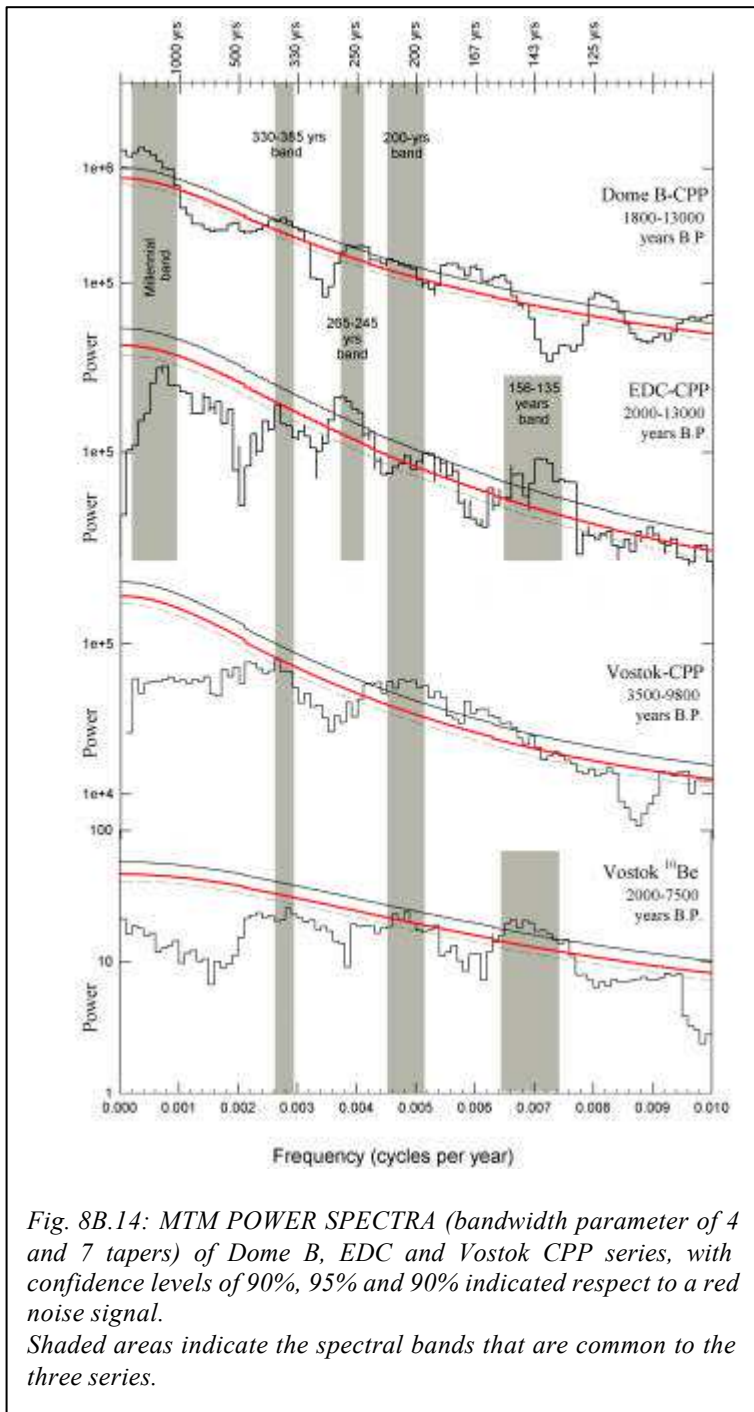
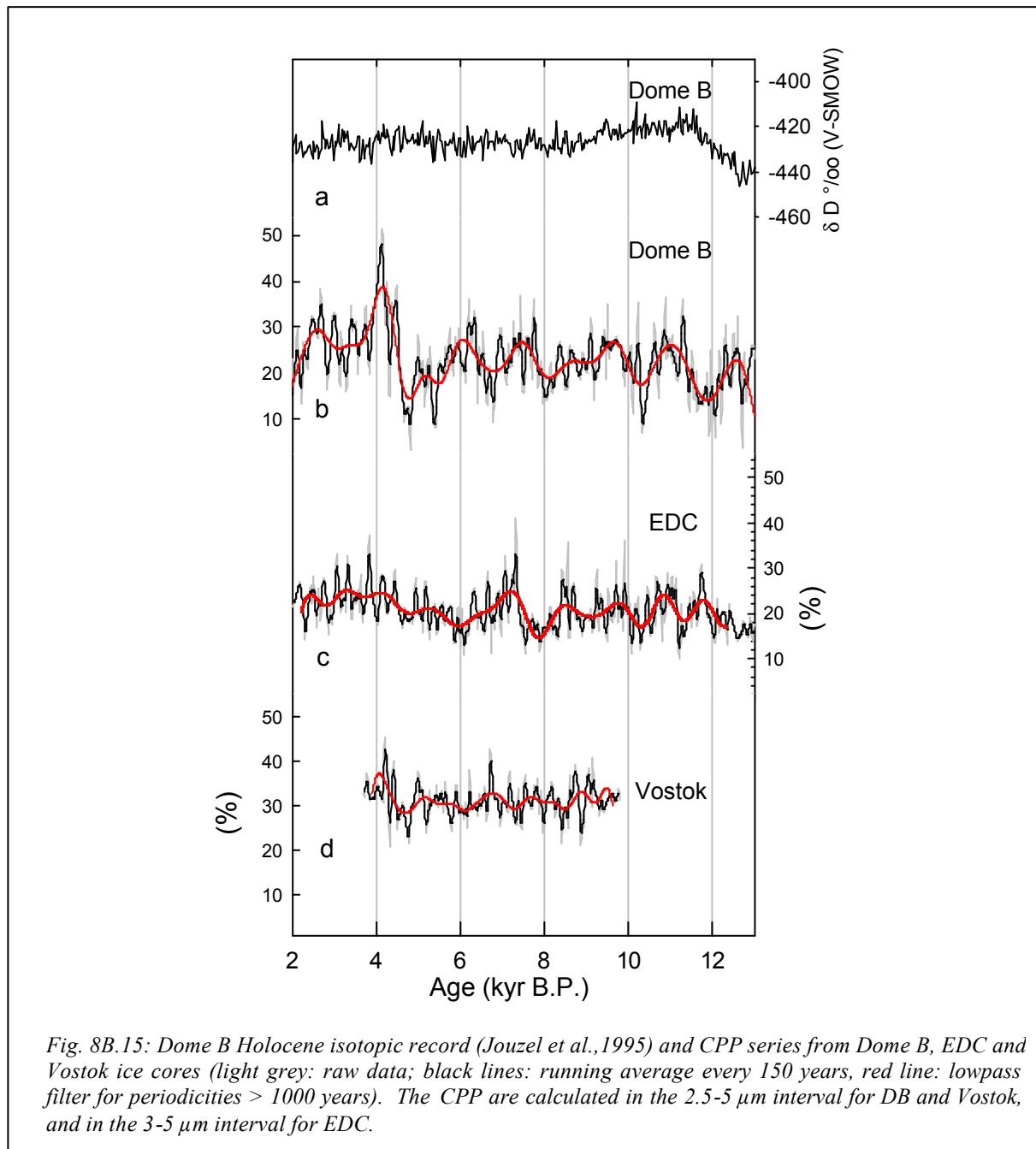


Fig. 8B.14: MTM POWER SPECTRA (bandwidth parameter of 4 and 7 tapers) of Dome B, EDC and Vostok CPP series, with confidence levels of 90%, 95% and 90% indicated respect to a red noise signal. Shaded areas indicate the spectral bands that are common to the three series.

The three CPP series are reported in Fig. 8B.15, with a lowpass filter for periodicities >1000 years., the The Dome B record shows clearly the largest amplitude of the millennial scale variations<sup>2</sup>, confirming the previous findings of a large contribution to the variance of the signal by low frequency bands.



<sup>2</sup> The calculation of the CPP in the 3-5  $\mu\text{m}$  interval for EDC makes the amplitude of the variations slightly higher with respect to the same calculation performed in the interval 2.5-5  $\mu\text{m}$ , as in the case of Vostok and Dome B. This reinforces the observation that the largest amplitude of the oscillations are present in the Dome B record.



In conclusion, the visual inspection and the spectral analysis of dust size records from three East Antarctic ice cores shows periodical changes in dust transport and likely in the atmospheric circulation around Antarctica during the Holocene.

Two bands of variability in around ~200 years and ~350 years are significant in all three dust size records and are common to the spectrum of solar variability from Vostok  $^{10}\text{Be}$  record.

EPICA-Dome C and Dome B power spectra appear very similar at low frequencies, and are characterized by a significant millennial scale band of variability and by another one around 250 years, none of which is present in the Vostok spectrum and in the solar one.

The largest amplitude of variations are found in the Dome B ice core record.

### **8B.3.3 Periodicities nested in the dust concentration records**

Assuming the dust size fluctuation are expression of a more or less favored dust advection, the imprint of such variations could be kept, at least to a certain extent, in other climatic components such as the accumulation rate in Antarctica, and/or climate conditions at the dust source regions, or in all these parameters. The spectral analysis of the dust concentration records, a parameter that depends on all these variables, can be a good indicator for this possible effect.

In this paragraph the power spectra of the dust concentration records (preliminarily de-trended through a linear regression function) are presented and compared to that of dust size and solar activity.

### EDC ice core

The spectral analysis of EDC particle size (CPP, Fig. 8B.16 a and b) and that of particle concentration (Fig. 8B.16 c) present a common periodicity (>95% and 99% significance respectively) in the 200-years band, that is common to the  $^{10}\text{Be}$  record. Also the millennial band of the dust size record is preserved in the concentration spectrum, where a 90% significant peak arises in correspondence to 1400-2500 yrs periodicities.

On the opposite, the solar bands at ~147 yrs (>99% significance) and at ~320-400 yrs (90% significance) can be observed clearly only in the dust size spectrum but are not clearly defined the concentration one.

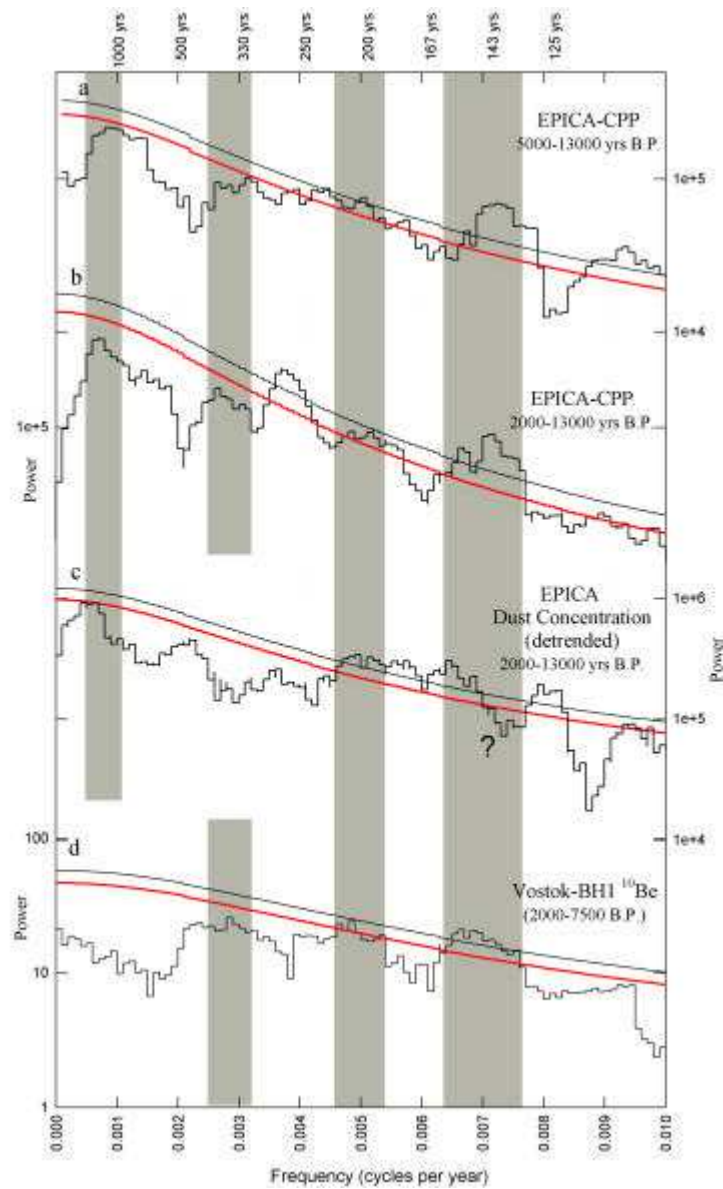


Fig. 8B.16: Power spectra of EDC CPP series (5 to 13 kyrs B.P. and 2 to 13 kyrs B.P.), dust concentration and solar activity ( $^{10}\text{Be}$  from Vostok BH1 ice core).

Confidence levels of 90% (dotted line), 95% (thick red line) and 90% (thin black line) are traced with respect to a red noise signal.

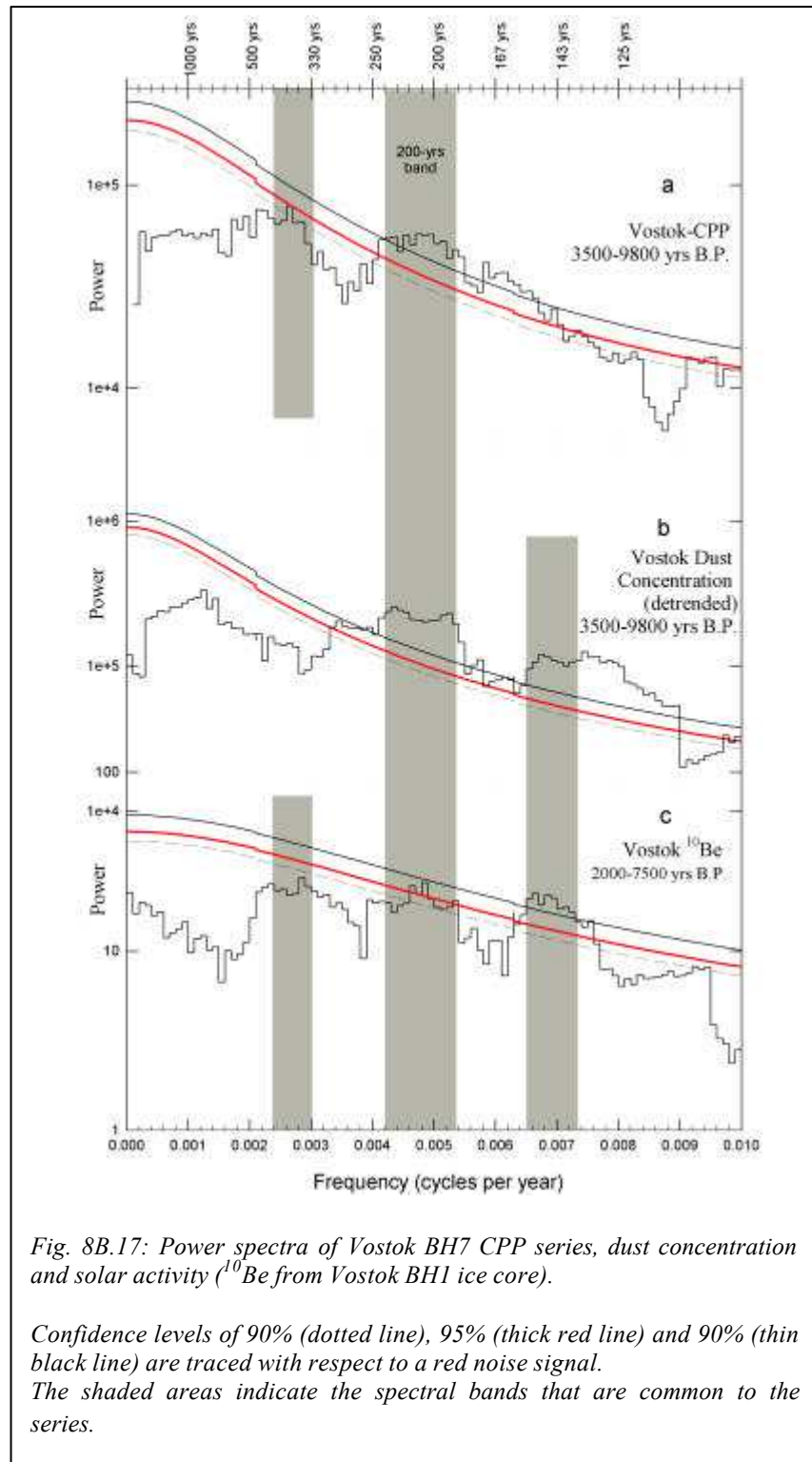
The shaded areas indicate the spectral bands that are common to the series.

### Vostok BH7 ice core

As in the case of EDC ice core, the spectral analysis of Vostok particle size (CPP, Fig. 8B.17a) and concentration (Fig. 8B.17b) shows a common 200-years band of variability (>99% significance), also common to the  $^{10}\text{Be}$  record.

The solar band around 145 yrs is significant (>99%) in the dust concentration spectrum as well as in that of size, but the peak here is not well defined.

The band around 370 yrs of  $^{10}\text{Be}$  and the size spectra is not significant in the concentration record.



***DOME B ice core***

As in EDC and in the Vostok records, the 200-yr peak is present also in the dust concentration spectrum from Dome B (90% significance). The solar band around 145 yrs, instead, is well marked only in the dust concentration spectrum, where it constitutes a well defined peak at >99% level (Fig. 8B.18).

The ~370 yrs band of <sup>10</sup>Be is significant the size spectrum (>99% level) and is present but not significant in that of dust concentration.

There are two periodicities significant both in the size and in the concentration records but absent in the solar signal: the first is the prominent millennial band (>99% level) that represents most of the variance of Dome B size variability (see § 8B.2.1); the second is the band around 250 yrs, >95% level in both spectra.

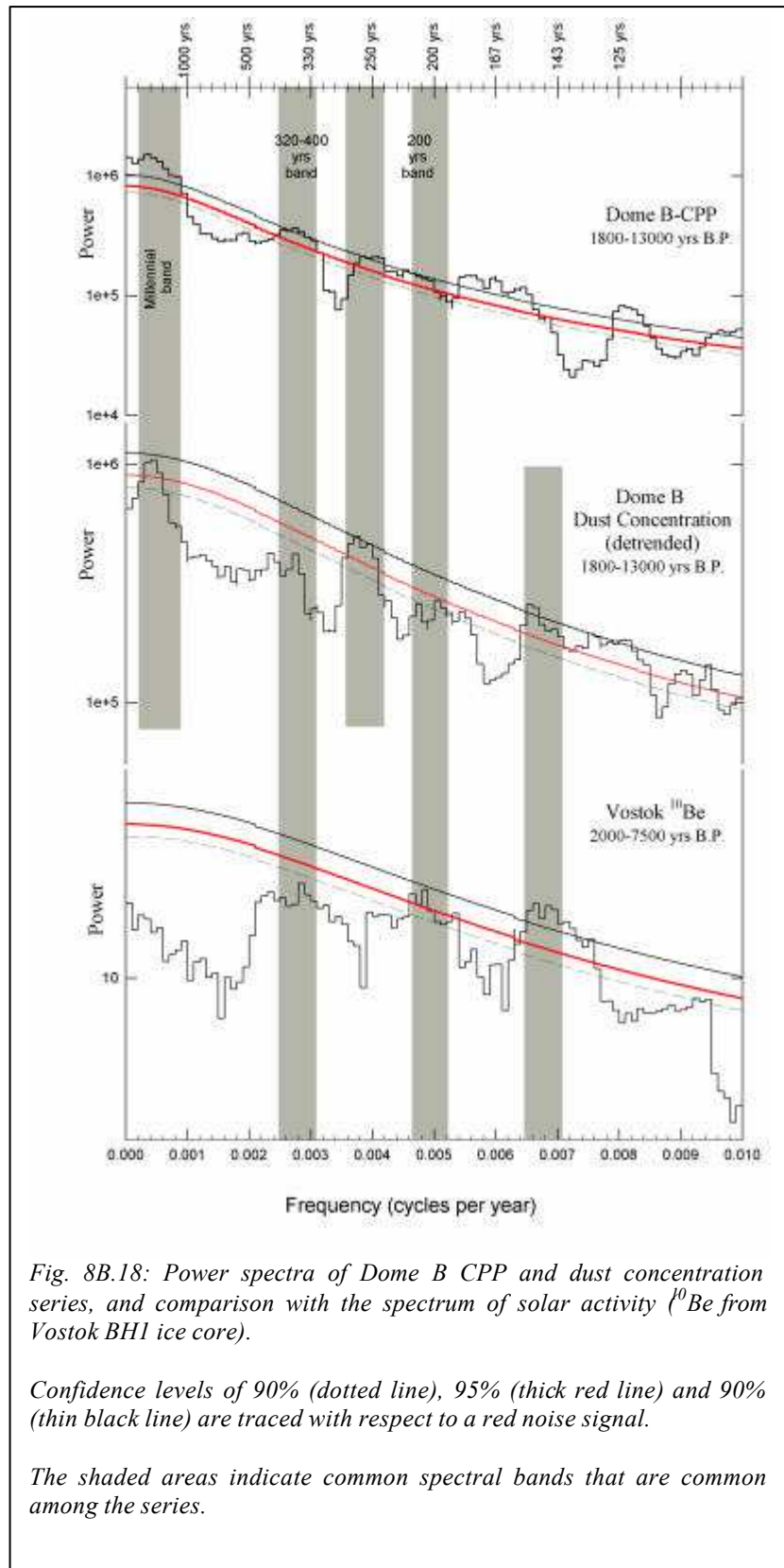


*Fig. 8B.18: Power spectra of Dome B CPP and dust concentration series, and comparison with the spectrum of solar activity (<sup>10</sup>Be from Vostok BHI ice core).*

*Confidence levels of 90% (dotted line), 95% (thick red line) and 99% (thin black line) are traced with respect to a red noise signal.*

*The shaded areas indicate common spectral bands that are common among the series.*

\*\*\* \*\*

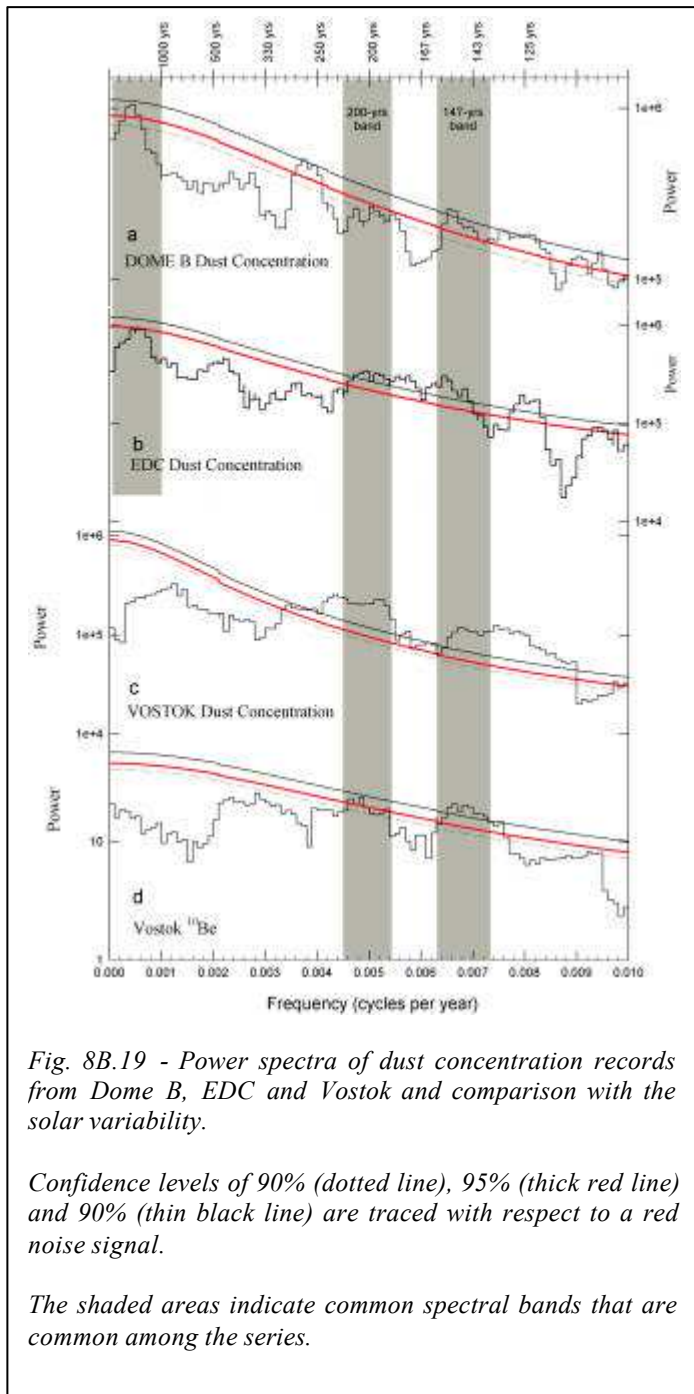


Fig. 8B.19 - Power spectra of dust concentration records from Dome B, EDC and Vostok and comparison with the solar variability.

Confidence levels of 90% (dotted line), 95% (thick red line) and 90% (thin black line) are traced with respect to a red noise signal.

The shaded areas indicate common spectral bands that are common among the series.

The spectral analysis of the dust concentration records shows some common periodicities with the dust size records and with the solar variability (200-years and 145 years bands).

The periodicities powerfully imprinted in the transport parameter and nested in the concentration records suggest that the factors responsible for the variability in particle advection probably affect also other climatic parameters like the accumulation rate in Antarctica.

This latter in turn influences the  $^{10}\text{Be}$  concentration in ice, and was used to evidence a 2 fold variation in the cosmogenic isotope between glacial and interglacial climates [Yiou et al., 1985]. Nevertheless, for the rather stable Holocene period  $^{10}\text{Be}$  is firstly influenced by cosmogenic production rate and the solar activity [Raisbeck et al., 1990].

The secular climatic variability impressed in the dust concentration records suggests that a small contribution to the  $^{10}\text{Be}$  concentration profile could derive from the periodical changes in

accumulation rate. If we accept the solar activity influences the atmospheric circulation over Antarctica ( $^{10}\text{Be}$ -dust size correlation), it should play on the accumulation rate. As the accumulation feedbacks may have a regional expression, the amplitude of  $^{10}\text{Be}$  concentration variations for a given site may be amplified or at the opposite counter balanced.

\*\*\*\*\*        \*\*\*\*\*        \*\*\*\*\*

### **Summary**

*Millennial and secular scale variability has revealed to be a characteristic feature of Holocene dust transport to the East Antarctic.*

*Dome B and EDC dust size records share a common millennial-scale band explaining a large part of the variance of both records. Moreover, a  $\approx 200$  years band and another around 330-380 years are common to Dome B, EDC and Vostok dust size records and to the  $^{10}\text{Be}$  record of solar activity from Vostok BHI ice core.*

*The same bands of variability characterizing the dust size records are also significant in the spectral analysis of dust concentration records for each core.*

*The periodical mode of variability of dust transport can be the expression of the circumpolar propagation of ocean-sea ice-atmosphere anomalies, influencing dust advection to the interior of the East Antarctic plateau.*

## Chapter 8C - A TENTATIVE SCENARIO FOR LGM AND HOLOCENE DUST TRANSPORT

### 8C.1 Factors influencing dust advection

Dust size changes are interpreted in association to different transport times (§ 8A.3; Chap. 8B), depending, in turn, on the horizontal distance and height of transport (three dimensional dust trajectories). The mean pressure fields over the Antarctic and the circum Antarctic therefore play an important role.

In the following two paragraphs the influence of (1) atmospheric conditions in the circum-antarctic (from synoptic to seasonal and interannual) and (2) the vertical structure of the atmosphere at local scale on the advection of dust-carrying air masses are taken into consideration.

Then, two possible scenarios are suggested for LGM and Holocene.

#### *The zonal and meridional circulation patterns*

The atmospheric circulation in the SH is dominated by the west-east (*zonal*) circulation, representing the geostrophic response to the latitudinal temperature and pressure gradients.

The zonal circulation, by far the largest component of the SH high latitudes atmospheric motion, is embedded at any time with perturbations taking the form of *waves*, allowing the meridional exchanges of different air masses. Continental cold air moves towards lower latitudes, warmer and moister air towards the continent.

The wavenumber 1 in the Southern Hemisphere dominates the mean pressure and height fields and contributes to the interannual variability of the westerlies; this component corresponds to the *eccentricity of the polar vortex* (Pitcock, 1980), and can be assessed through the Trans Polar Index (see Box 8C.1).

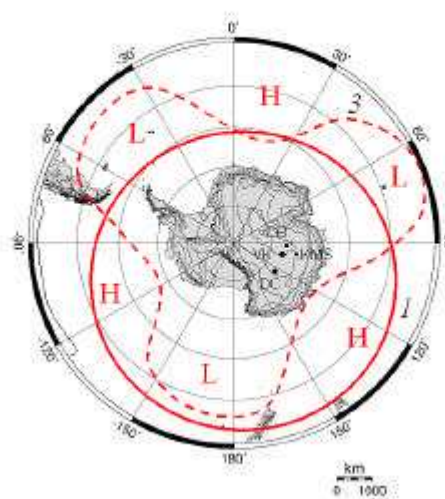


Fig. 8C.1 : Schematic illustration of standing waves 1 and 3 (after Tyson, 1986, modified).

Wavenumbers 1 to 3 define more-or-less stationary waves associated to longitudinally positioned structures (winter continental highs and summer continental lows) distorting the zonal circulation. It has been estimated that wavenumbers 1 to 3 together account for 99% of the total variance of the 500 hPa pattern (Tyson, 1986).

Such long waves propagate into the high atmosphere and can explain also part<sup>1</sup> of the variable shape and position of the polar vortex. Higher wavenumbers define baroclinic waves that are responsible for a large fraction of the horizontal transfer of energy.

Dust transport is influenced both by the average zonal circulation and by the meridional exchanges of air masses, allowing advection to the interior of the Plateau. Both of them can vary in strength at different timescales.

The cyclones, more or less intense, can be stationary or migrating, and their position oscillates around 65°S on average and around 62°S in some coastal parts of East Antarctica (Schwerdtfeger, 1984; see §1.6). The sea ice margin itself is believed to respond to the atmospheric forcing and to affect, in turn, the synoptic low pressure systems in the circum-antarctic and the cyclogenesis (Carleton, 1989).

Present-day data of circum Antarctic sea level pressure, surface winds and sea surface temperature evidence a set of climatic anomalies propagating eastward around the Southern Ocean (SO) with the Antarctic Circumpolar Current (ACC) and giving origin to the so called Antarctic Circumpolar Wave (ACW), requiring 8-10 years to encircle the globe (White and Paterson, 1996). The ACW provides the first *data evidence* that anomalies propagate with the same velocity in the ocean, the atmosphere and the cryosphere on interannual timescales and that these three media are tightly coupled.

Further evidences for periodic (3-4 years) anomalies in atmospheric and sea ice patterns linked to the passage of the ACW have been also observed in the Weddell, Ross, Amundsen and Bellingshausen Seas for the last 20 years by Venegas and Drinkwater (2001) and Venegas et al. (2001).

Through the Southern Ocean ring a *global* oceanic connection and THC are made possible, and anomalies associated to the variability of this latter - spanning from millennial (e.g. Bond et al., 1997) to secular scales (e.g. Shulz and Paul, 2002) - can be propagated.

Dust advection to Antarctica therefore, can be interpreted as the response to both oceanic and atmospheric conditions.

---

<sup>1</sup> In part, since the asymmetry of the polar vortex respect to the Antarctic is also determined by the topography of the continent.



### Box. 3 : Index related to Southern Hemisphere atmospheric circulation

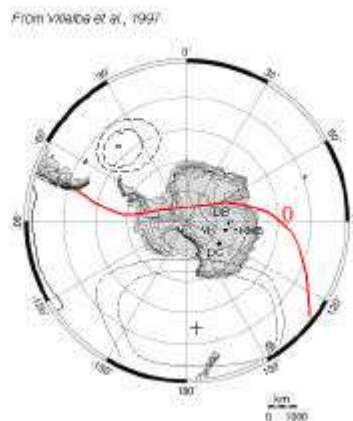
The **TPI** (Trans Polar Index) is defined as the difference in sea level pressure between Hobart (43°S, 147°E), Tasmania, and Stanley (52°S, 58°W) in the South Atlantic. It was proposed by Pittock (1980) to measure of the eccentricity of the polar vortex around the South Pole.

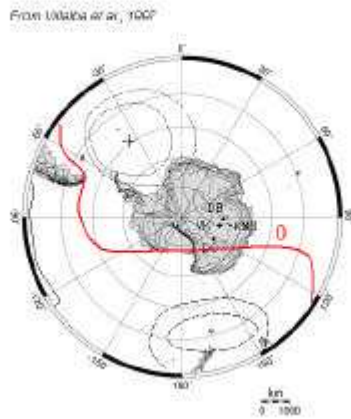
The TPI is positive or negative according to the displacement of the polar vortex towards the South America or the Australian-New Zealand sector.

The different position of the Polar Vortex influences the Westerlies flux and the position of subtropical anticyclones in an opposite sense in the two sides of Antarctica. Consequently, synoptic conditions are affected with major changes in precipitation and temperature variation.

However, it has been argued that the selection of these two sites is not optimal, and an alternative index, the Summer Trans-Polar Index (**STPI**) has been proposed (Villalba et al. 1997). STPI is defined as the difference between the normalized averages of five stations over New Zealand (Wellington, Christchurch, Hokitika and Dunedin on the South Island and Chatham Island) and three stations in the southwestern Atlantic (Grytviken on South Georgia, and Orcadas and Signy on the South Orkney Islands), and represents an index of sea level pressure (SLP) wavenumber 1 in the high latitudes of the Southern Hemisphere.

In fact, during summer the strongest connections in the mean SLP fields occurs between the southern South America-Antarctic Peninsula (SAAP) and New Zealand sectors of the Southern Hemisphere (Villalba et al. 1997). The figures here below, reproduced from Villalba et al (1997) show the spatial correlation of positive (+) and negative (-) anomalies in mean summer (December to February) SLP deduced from 50 stations in the SH, with respect to Christchurch (44°S, 177°E, a) and Orcadas (61°S, 45°W, b) from 1911-1985.





Recently, Jones et al. (1999) redefined zonal and meridional indices for the SAAP region. The zonal index (**ZSAAP**), defined as the anomalous pressure difference between Stanley (51.46°S, 57.59°W) and Orcadas (60.70°S, 44.70°W), is a measure of the *zonal westerlies* between approximately 51° and 60°S, while the meridional index (**MSAAP**), corresponding to the differences in pressure anomalies between Punta Arenas (53.09°S, 70.48°W) and Stanley, measures *meridionality* across southern South America (58°W to 71°W).

### The vertical structure of the atmosphere

The atmospheric structure and motion in the vertical dimension has to be taken into account to understand the dust advection.

The extremely cold temperatures over the surface of Antarctica engender a temperature inversion within the first few thousand meters of atmosphere, whose thickness and amplitude varies with sites and seasons.

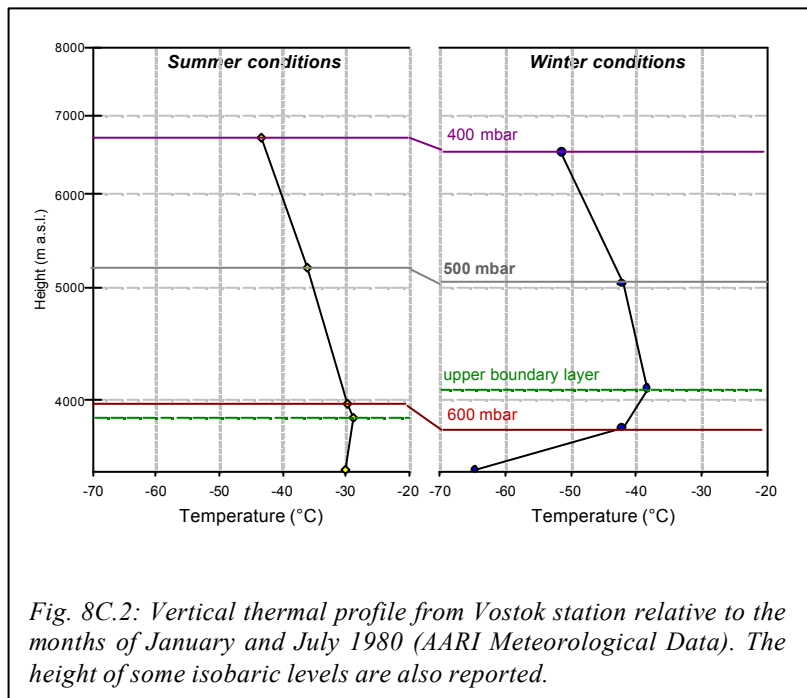


Fig. 8C.2: Vertical thermal profile from Vostok station relative to the months of January and July 1980 (AARI Meteorological Data). The height of some isobaric levels are also reported.

An example is reported in Fig. 8C.2, where two vertical thermal profiles from Vostok station are reported (January and July 1980, AARI Meteorological Data) with the altitude of the 600, 500 and 400 hPa levels.

In summer, the thermal inversion is weaker and isobars are higher than in winter. The annual average altitude of the 500 hPa isobar over Antarctica is 5,000 m, with seasonal variations of 150 m above, in summer, or below, in winter (Schwerdtfeger, 1984).

Seasonal variations in height are more important in the higher atmospheric levels (300 hPa, 100 hPa) and much more pronounced in the stratosphere than in the troposphere.

A thermal ridge is permanently present over the continent close to the surface, where the air is extremely stable, while the higher levels are characterized by more or less pronounced lows.

Air masses can penetrate into the Plateau from different altitudes within the mid-to-high troposphere, and their advection can be modulated, among other factors, by the local pressure structure. For instance, deep lows enhance air pumping from the high troposphere levels and allow it to penetrate into the plateau.

The convergence generated in the upper layers and the consequent air sinking are associated to divergence in the surface wind fields as the air moves towards the coast (permanent inversion winds and episodic katabatic winds blow off the Plateau according to the slope of the terrain).

In the cold regions of the Antarctic plateau the contribution from the advection of upper air to the heat budget of the atmosphere is important, while loss of heat from long-wave radiation and advective heating are minor components.

Dust advection from different altitudes can contribute to the dust size variability, since particle size decreases with height (Tagen and Lacis, 1996). Finer dust is preferentially transported by air masses travelling higher level in the atmosphere with respect to those of lower levels in the mid-troposphere carrying slightly coarser dust.

## **8C.2 Dust variability over East Antarctica: a response to atmospheric circulation patterns.**

### ***The Last Glacial Maximum***

During the LGM, sea ice cover was displaced equatorward and the polar front strengthened. The sharp latitudinal thermo-barometric gradients enhanced the zonal component of the atmospheric circulation in the circum Antarctic. This factor, associated to the continental aridity and to the reduced atmospheric humidity is responsible for the high dustiness of the atmosphere at that time and for the large dust input to the Antarctic (Petit et al., 1981).

Southern South America was the dominant source region for dust in glacial periods in the four East Antarctic sites investigated and likely overall the Plateau (Chap. 7).

During LGM, the position of cyclonic cells in the SO was probably displaced equatorward with respect to the Holocene. As the variable position of the atmospheric centres of influence in the SO affects dust advection (Chap. 8B) , it is possible that during the LGM the ocean-atmosphere configuration was prone to favour dust transport towards some sectors of the Plateau respect to others, thus generating the observed differences among the sites (DB, DC, KMS) .

Dust transport time depends also on the vertical path of air masses. Advection from higher or lower troposphere levels is modulated by the vertical structure of the atmosphere, altitude lows exerting a more or less pronounced pumping effect. The dust size decreases with altitude; therefore the configuration would led to advection of finer dust from longer (higher) paths and coarser dust from shorter (lower) paths.

The data evidence fluctuating but always coarser dust sizes at Dome B with respect to Dome C and KMS during the LGM. This could be associated to different times of transport between the sites, associated - in turn - to *shorter* horizontal dust trajectories from southern South America to Dome B and air advection from lower troposphere levels with respect to Dome C and KMS. At these two latter sites, on the opposite, *longer* trajectories and incursions of air masses from *higher* troposphere levels favoured deposition of finer particles.

In fig. 8C.3 and 8C.4 a tentative scenario of pressure fields (SLP and 500 hPa altitude) and hypothetic dust trajectories for the LGM are proposed. At present, there is a lack of data from ice cores for the 0°E - 90°E Antarctic sector, and therefore the reconstruction can be wrong for that area.

On the opposite, the average LGM-Holocene trend of dust size at Vostok seems quite similar to Dome B (Briat et al., 1982).

The cartoon in fig. 8C.5 emphasizes the differences in the vertical atmospheric structures between Dome B, Dome C and KMS.

Fig. 8C.3 and 8C.4: Theoretical LGM barometric configurations (SLP and 500 hPa altitude Gpdm) showing conditions over the Antarctic and the circum Antarctic favourable to advection of coarser dust towards Dome B and finer dust towards Dome C and KMS.

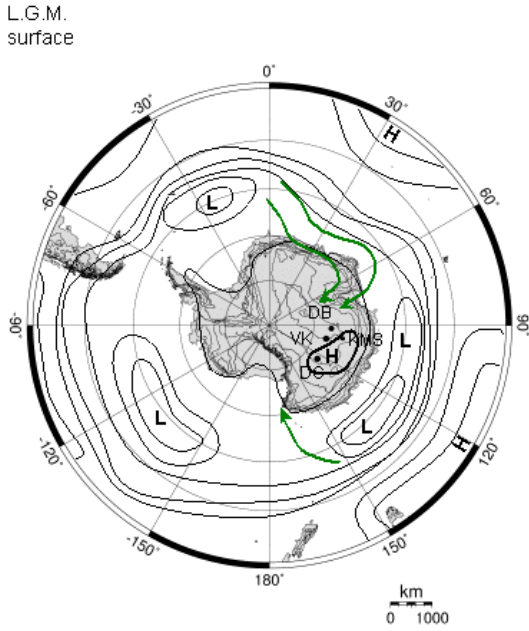


Fig. 8C.3

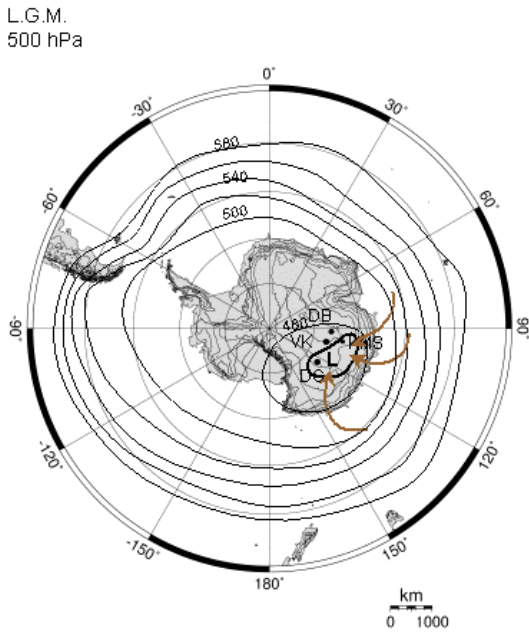


Fig. 8C.4

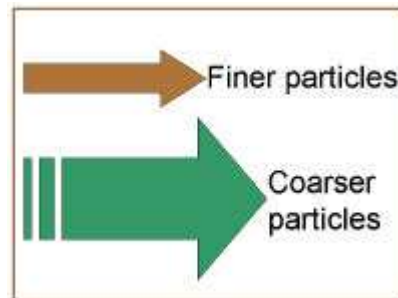
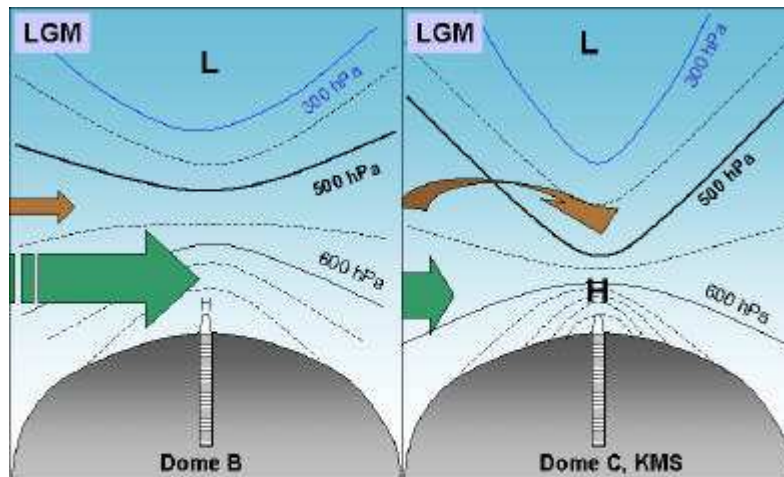


Fig. 8C.5 : Cartoons showing the vertical atmospheric structures (arbitrary scales, exaggerated) allowing penetration of tropospheric air masses from different altitudes (green arrows indicate advection from mid troposphere carrying slightly larger dust, brown arrows indicate high altitude dust transport, bringing finer dust).

### *The Holocene*

During the deglaciation the THC restarted and sea ice extent reduced. The meridional temperature gradient weakened, and consequently also the zonal component of the Westerlies. With the onset of the Holocene, the general atmospheric and continental humidity increased and the dust load of the atmosphere drastically lowered (Chap. 8A).

Within the deglaciation and the Holocene periods, the dust input varied quite uniformly over East Antarctica (§ 8A.1, 8A.3, 8B.2). However, the glacial/interglacial transition saw opposite regional changes in dust transport between Dome B, on one side, and Dome C and KMS, on the other (§ 8A.3). These changes were interpreted as a reorganization of the atmospheric circulation from an “LGM-type” to a “Holocene-type”, these two associated to different mean pressure fields in the Antarctic and circum-antarctic, and possibly to a different eccentricity of the polar vortex (wavenumber 1 component).

Overall the Holocene, the dust size shows oscillating variations in all ice records from the Plateau. The frequencies of such variations, spanning from millennial to centennial timescales, are almost in the same spectral band in the three cores investigated.

Our data and those from Basile (1997) for Dome C and Vostok sites suggest for the LGM Southern South America was the dominant source for dust to the Plateau, and during interglacials (Holocene and stage 5.5) an additional source (probably Australia) contributed.

Further isotopic studies would be needed to investigate if an enhanced contribution from one source with respect to the other occurs in some parts of the Holocene with respect to others or if the different sources contribute in the same proportions overall the interglacial period<sup>2</sup>.

Nevertheless, the size fluctuations reflect atmospheric circulation changes.

Holocene dust transport variations, in the line of the previous interpretation, are also related to the atmospheric conditions over and around Antarctica. Figures 8C.6 to 8C.9 report two examples of possible atmospheric configurations where Dome B receives finer dust than Dome C and KMS (Fig. 8C.6 and 8C.7) and viceversa (Fig. 8C.8 and 8C.9).

It is known that the perturbations of the more or less stationary waves associated to wavenumbers 1 to 3 extend to the middle and high troposphere and account for a large part of the total variance in the annual 500 hPa. The consequent distortion of the mean zonal circulation allows to enhance meridional exchanges and dust advection to the interior of the Plateau.

---

<sup>2</sup> In this respect, it would be interesting to sample Holocene sections of the EDC ice core with different modal value for particles and  $s$  (standard deviation of the lognormal distribution).

The climate anomalies (in atmospheric pressure fields, wind stress and sea ice) can propagate eastward through the Southern Ocean on a variety of timescales (Mikolajewicz and Maier-Reimer, 1990; White and Peterson, 1996), and this is possibly at the origin of the centennial to millennial changes observed in dust transport.

The dust size variations and their phasing among the sites can be interpreted as an indicators of the ocean-atmosphere conditions and their circumpolar propagation in the Southern Ocean; such assumption implies that the phasing of variations for a given frequency can differ from site to site (*wavering effect*).

The dust deposition in the inner plateau occurs exclusively through dry deposition processes. However, the dust carrying air masses advected from different altitudes carried different moisture content (Schwerdtfeger, 1984). Consequently, penetration of air masses from different atmospheric levels, can potentially affect the accumulation rate at each site. This qualitatively supports the presence of the same bands of variability in dust size and concentration spectra (§ 8B.3.3).

The frequency band around 200 years that is present in all dust size and concentration records (Chap. 8C) and found also in the  $^{10}\text{Be}$  record from Vostok BH1 ice core is primarily associated to the solar variability, despite a possible contribution from accumulation rate is possible.

As hypothesis, a sun-climate relationship could be established through an amplification of the faint external solar forcing by the ocean, and the circumpolar propagation of the anomaly.

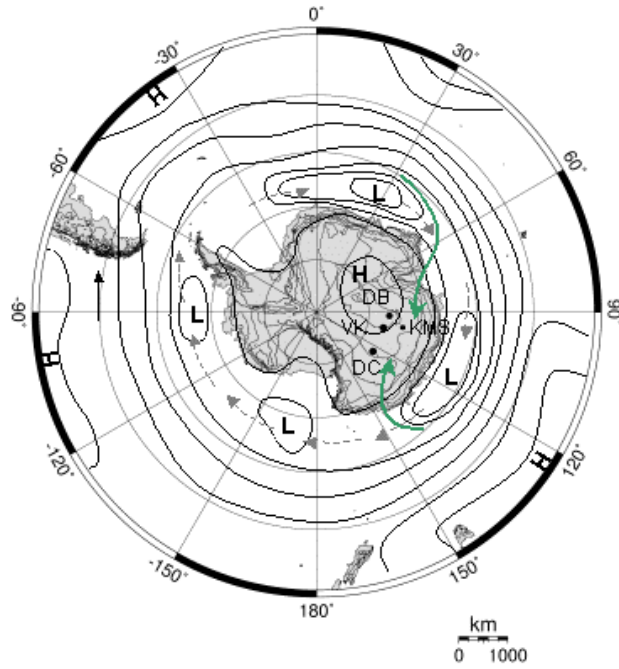
The SO in fact is an oscillatory system capable to amplify and combine frequencies in the 50-500 years band (Mikolajewicz and Maier-Reimer, 1990), and as W.H. Berger et al. (2002) suggested, “*a system that oscillates is a good candidate for amplification of a periodic stimulation*”.

*Fig. 8C.6 to 8C.9: Idealized Holocene pressure fields at sea level (SLP, charts 8C.6 and 8C.8) and at around 5000 m altitude (altitude of the 500 hPa isobar in Gpdm) over the Antarctic and the circum Antarctic. Holocene I scenario (Fig. 8C.6 and 8C.7) allows advection of fine dust towards Dome B and coarse dust towards Dome C and KMS; Holocene II scenario (Fig. 8C.8 and 8C.9) leads to opposite dust characteristics.*

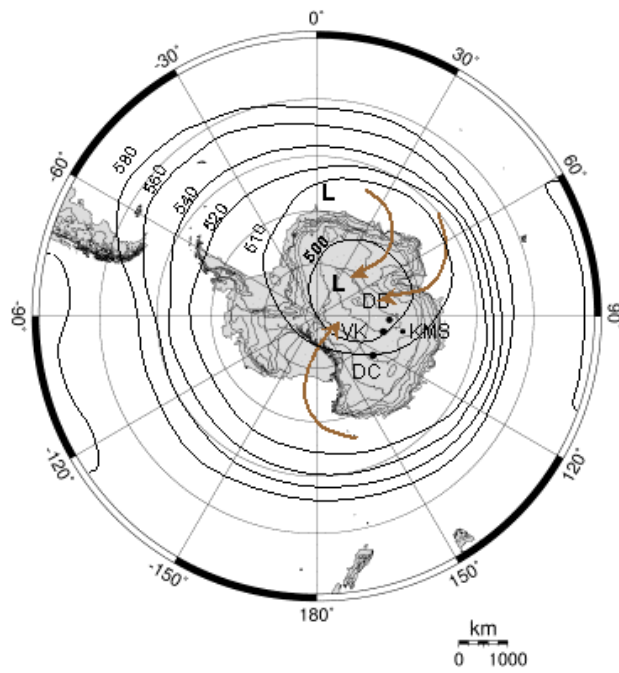
*The pressure fields are arbitrarily traced; the reconstruction can be inaccurate for the areas of the Plateau still not documented (0°E – 90°E sector). Intermediate situations are also possible.*



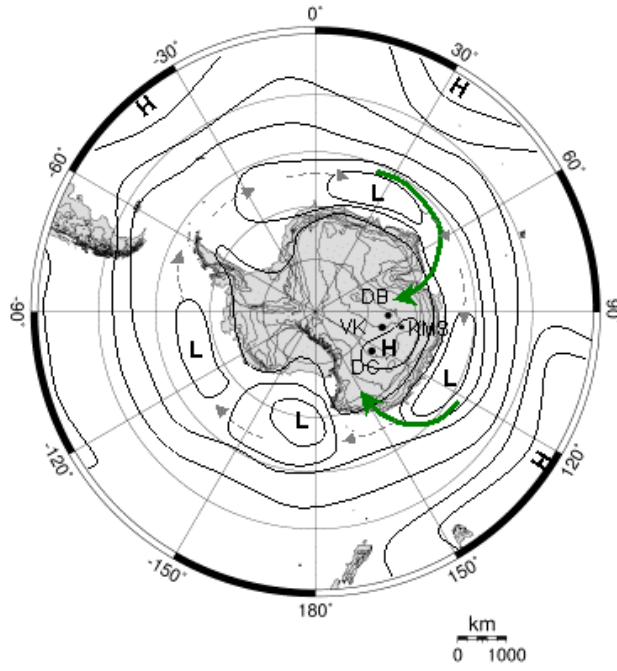
Holocene I  
surface



Holocene I  
500 hPa



Holocene II  
surface



Holocene II  
500 hPa

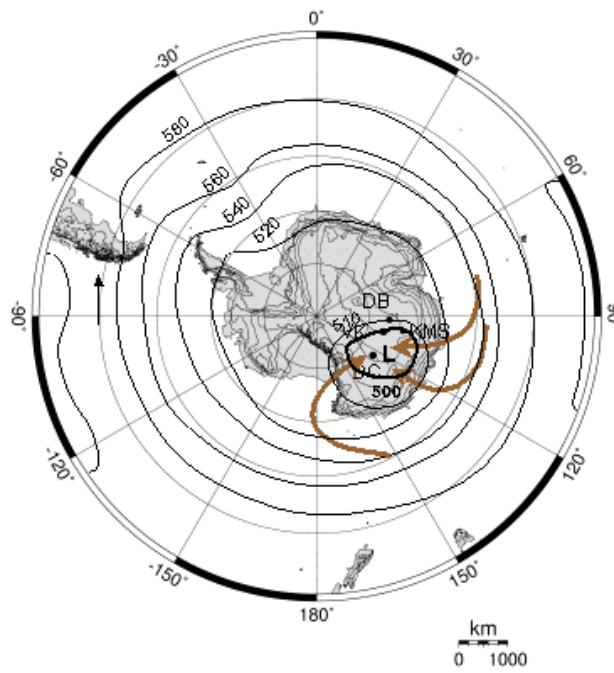
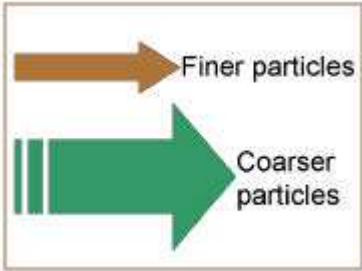
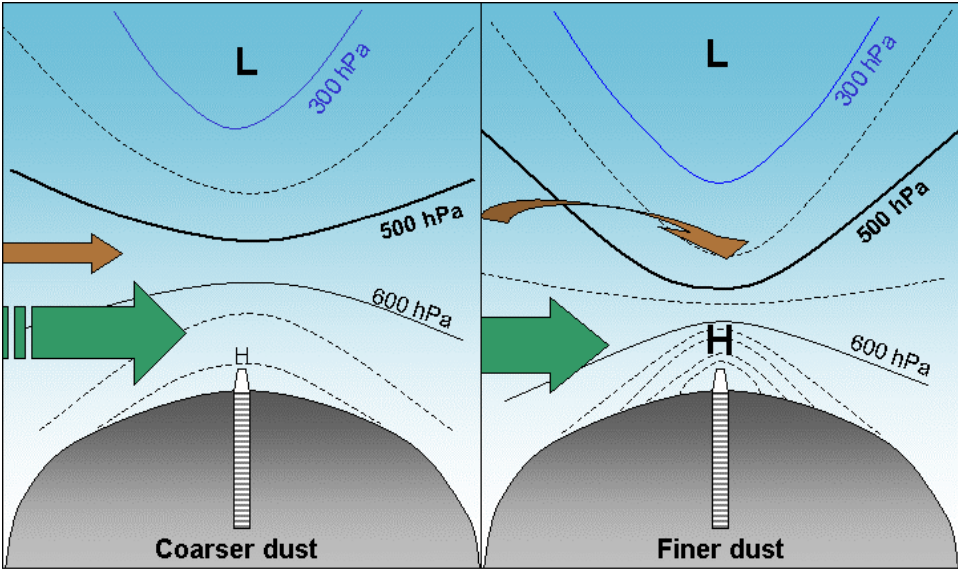


Fig. 8C.10 : Schematic representation of the vertical structure of the atmosphere favouring incursions of mid-troposphere air masses and coarser dust (left) or subsidence of upper air and advection of finer dust (right).



\*\*\*\*\*            \*\*\*\*\*            \*\*\*\*\*

### Summary

Dust transport pathways have to be considered in a three dimensional space. The horizontal dimension is the meridional component of the circumpolar atmospheric motion, the vertical dimension consists in the altitude of the advections and subsidence.

During the LGM/Holocene climatic transition the dust transport paths towards the Antarctic continent changed in response to the general reorganization of atmospheric circulation, and a displacement of the wavenumber 1 component of the Southern Hemisphere Westerlies is suggested.

Persistent millennial and secular scale variations in dust advection onto the Plateau, ubiquitous at all sites but with different phasing during Late glacial and Holocene times, can reflect the circumpolar propagation of ocean-sea ice-atmosphere anomalies at these timescales.

## 8.D LATE QUATERNARY EDC DUST RECORD

At the end of the 2002/2003 campaign the EPICA-Dome C drilling reached the depth of 3200 m. The ice from 2201 to 3138 m has been measured for dust concentration and size distribution with resolution of about 1 sample every 3.3 m.

The whole EDC record is shown in Fig. 8D.1; it clearly shows structures of high and low dust content, that can be associated to glacial/interglacial changes, dust peaks interpreted as glacial marine isotopic stages.

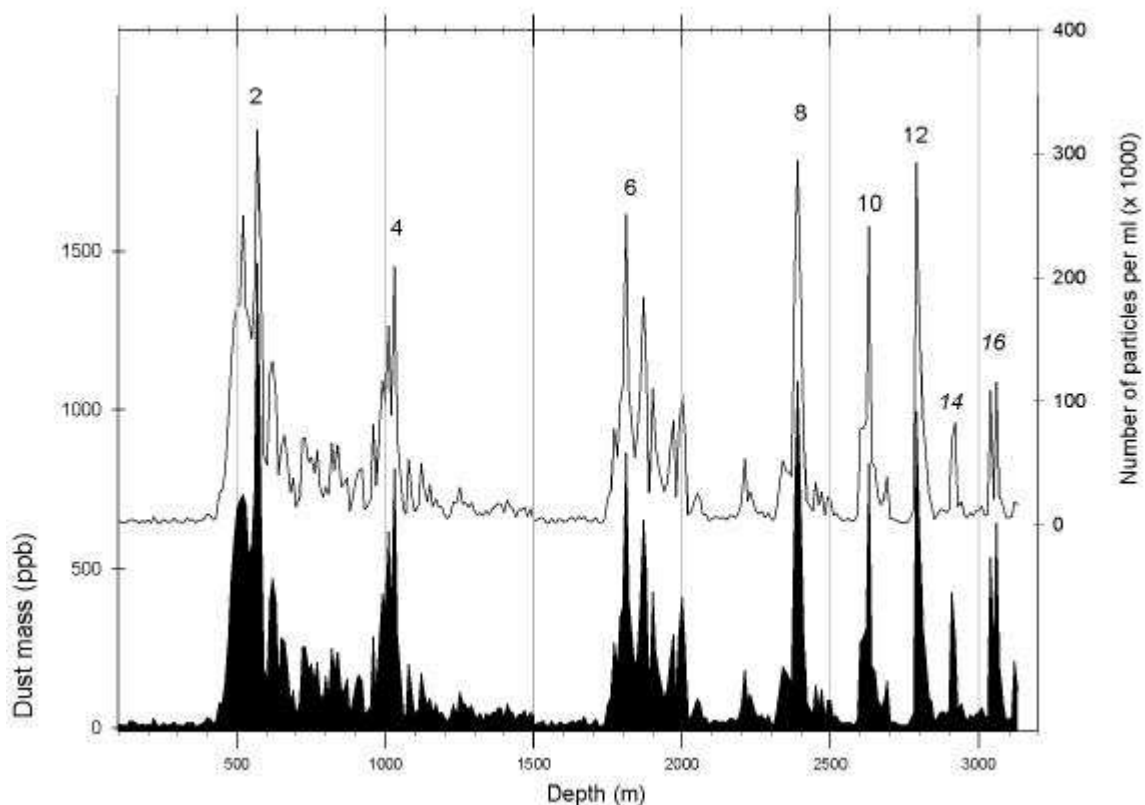


*Fig. 8D.1: EDC dust record for the first 3138 m of the ice core.*

The EDC and Vostok records are very similar, and a fine depth-to-depth relationship can be established through some major dust events reported in Table 8D.1. and in Fig. 8D.2; it can be observed that the deeper part of EDC core extends the climatic record beyond the Vostok one.

DUST event	Climatic Event	EPICA depth (m)	Vostok depth (m)
I	end of Stage 2	420	309
<sup>10</sup> Be peak		742	600
II	end Stage 4	947	849
III	Beginning Stage 4	1062	1000
IV		1123	1123
V		1415	1450
VI	end of Stage 6	1744	1906
VII		1970	2294
VIII		1997	2364
IX		2052	2444
X	end Stage 7.4	2201	2670
XI	end of Stage 8	2341	2807
XII		2367	2849
XIII	Beginning stage 8	2420	2897
XIV	end of Stage 10	2587	3128

Tab. 8D.1 Depth of 14 dust events common to EDC and Vostok ice cores, allowing to link the respective stratigraphies.

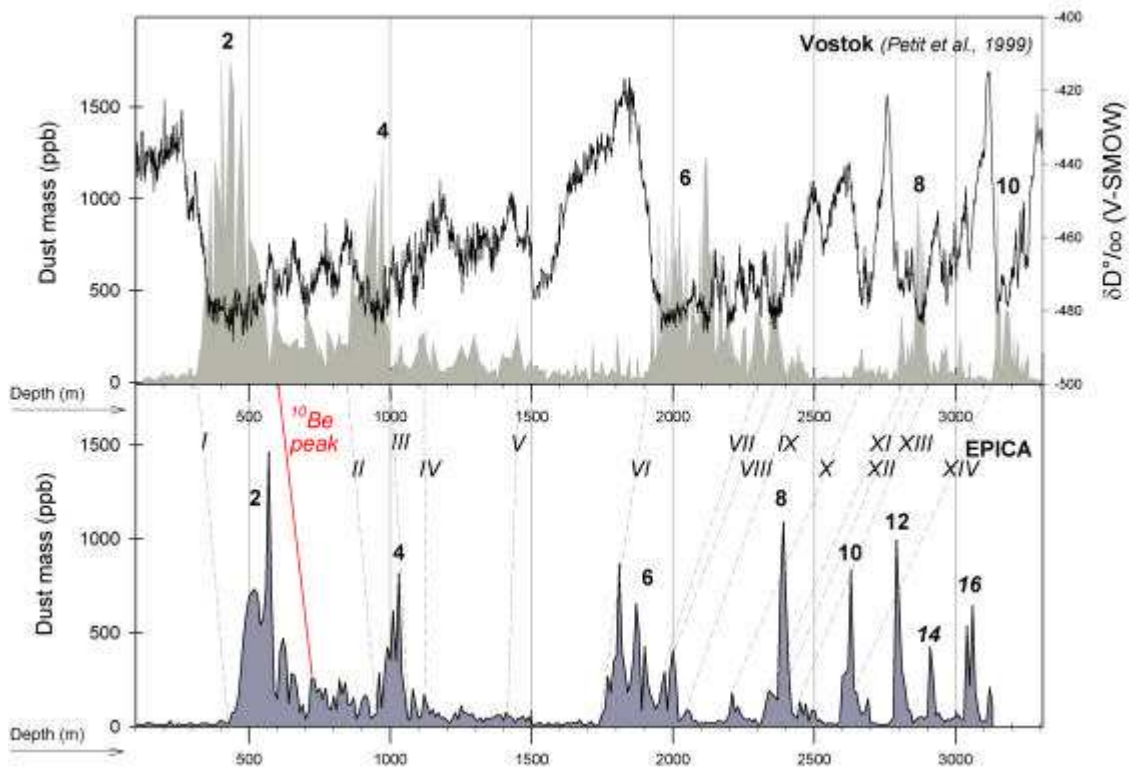


Fig. 8D.2: Vostok dust and isotope profiles (top) and EDC dust profile (bottom) versus depth. The fourteen common dust events that allow to link the stratigraphies are indicated by roman numbers.

The stratigraphical link with Vostok ice core has allowed to establish a preliminary dating (by transferring the Vostok GT4 timescale) for the first 2,780 m of EDC core (420 kyrs).

For the deeper part of EDC, a tentative dating has been made through comparison with the marine sediment record from Bassinot et al. (1994). The evident similarity of the two profiles for the main glacial/interglacial structures has allowed to estimate an age of about 750 kyrs B.P. for the deeper part of EDC (3138 m)<sup>1</sup>.

With such dating, the whole dust sequence would cover the last 7 climatic cycles (Fig 8D.3) and gives an overall pattern which is well comparable to dust from China (Kukla, 1990).

Fig 8D.3: Comparison of ice cores, marine and terrestrial records for the Late Quaternary.

[a] and [b]: Vostok ice core isotopic and dust records (from Petit et al., 1999);

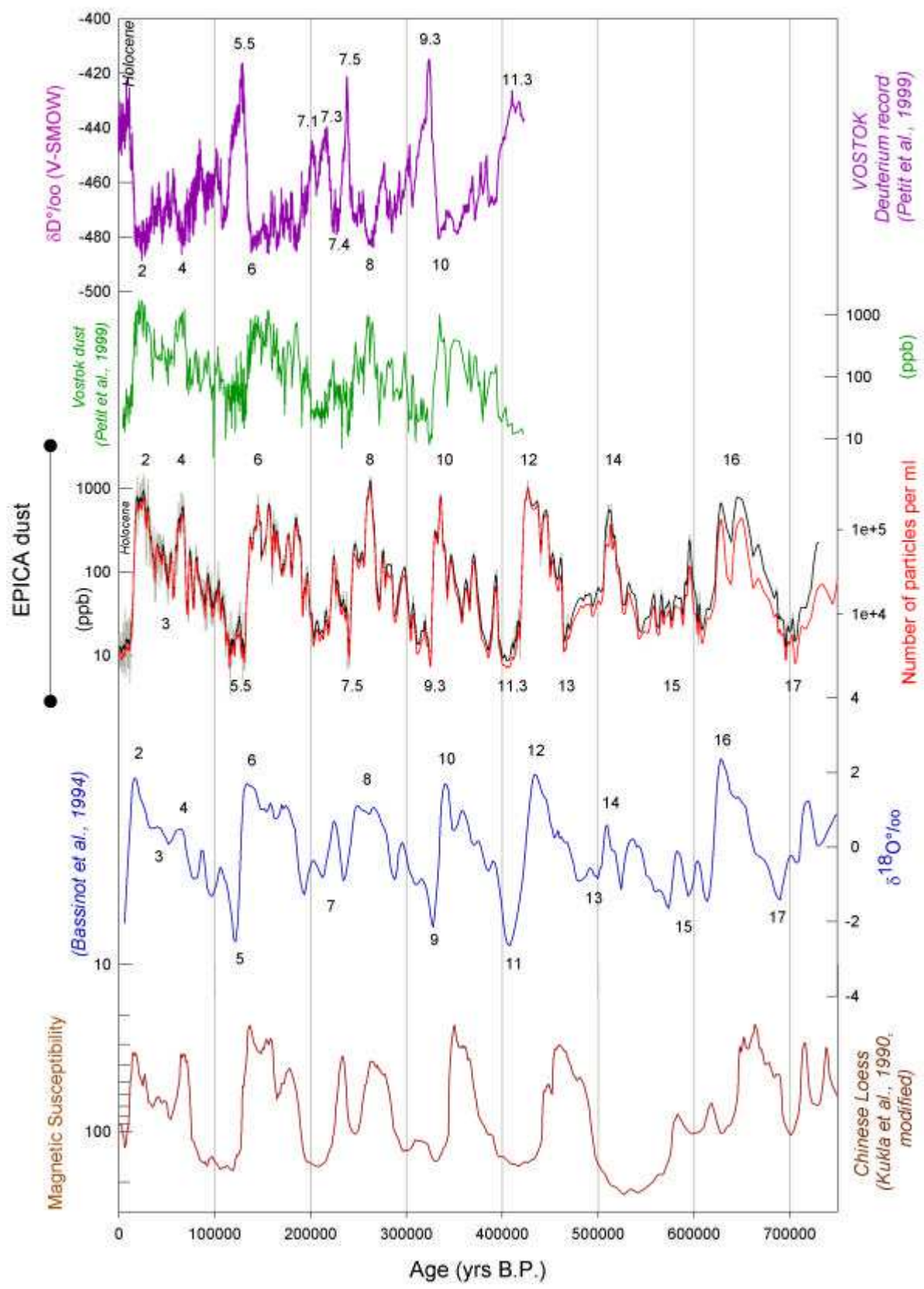
[c]: EDC dust concentration records (Number of particles per ml and ppb) versus age (see text).

[d]: Marine sediment record of  $d^{18}O$  from Bassinot et al (1994)

[e]: Magnetic susceptibility of Chinese loess/paleosol sequences (from Kukla et al., 1990).

---

<sup>1</sup> The MIS 17 (interglacial) is about 3102 m depth in EDC ice core.





### *The dust size record*

The EDC dust size profile (Fine Particle Percent, FPP) shows fluctuations overall the ice core length (Fig. 8D.4). The first 500 kyrs of record (2900 m) are characterised by FPP values oscillating around 45% ( $\pm 3$ ). Downward, the dust size profile shows alternation of fine-grained and coarse-grained layers. Very low FPP values (very coarse dust) have been retrieved in correspondence to glacial stages 14 and 16.

The horizontal green line at about 32% in Fig. 8D.4 marks the minimum<sup>2</sup> FPP values ever observed in the upper part of the core.

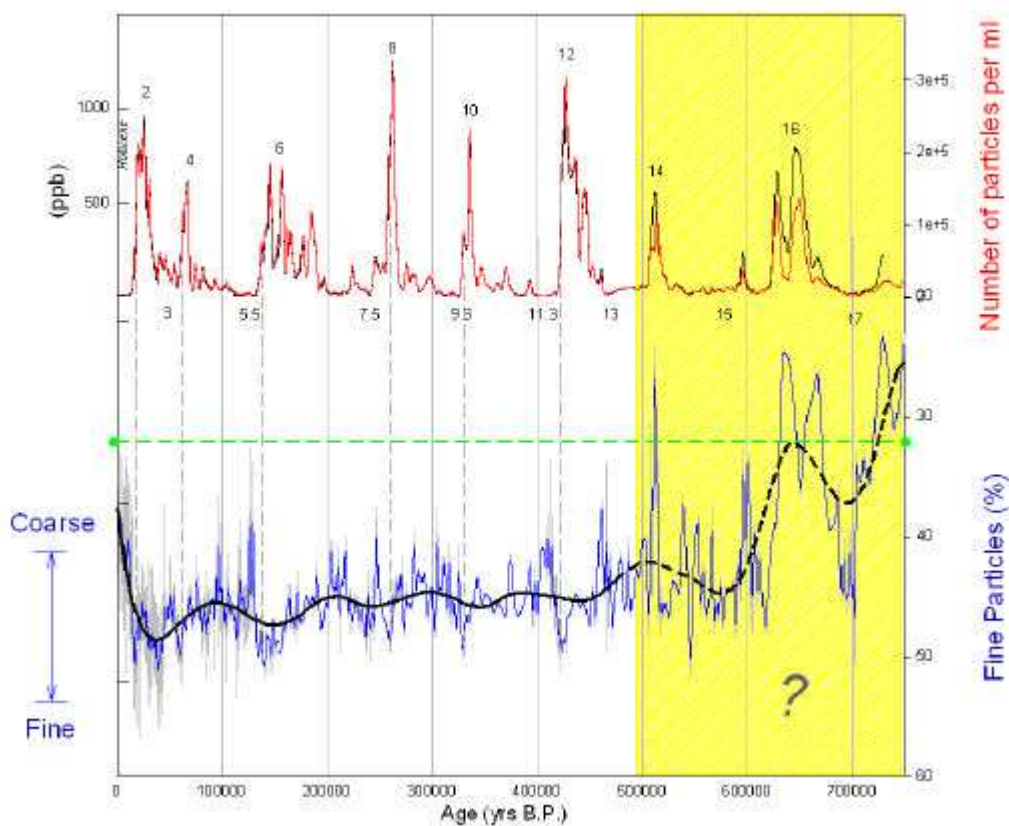


*Fig. 8D.4: EDC dust concentration and size records.*

The mass (volume) size distribution of samples corresponding to the peaks above this line show modal values around 3  $\mu\text{m}$ , as can be observed in Fig. 8D.5. Such values are extremely high for Aeolian particles reaching the East Antarctic, and have never been observed in the upper part of the core.

<sup>2</sup> Scale is inverted in the figure.

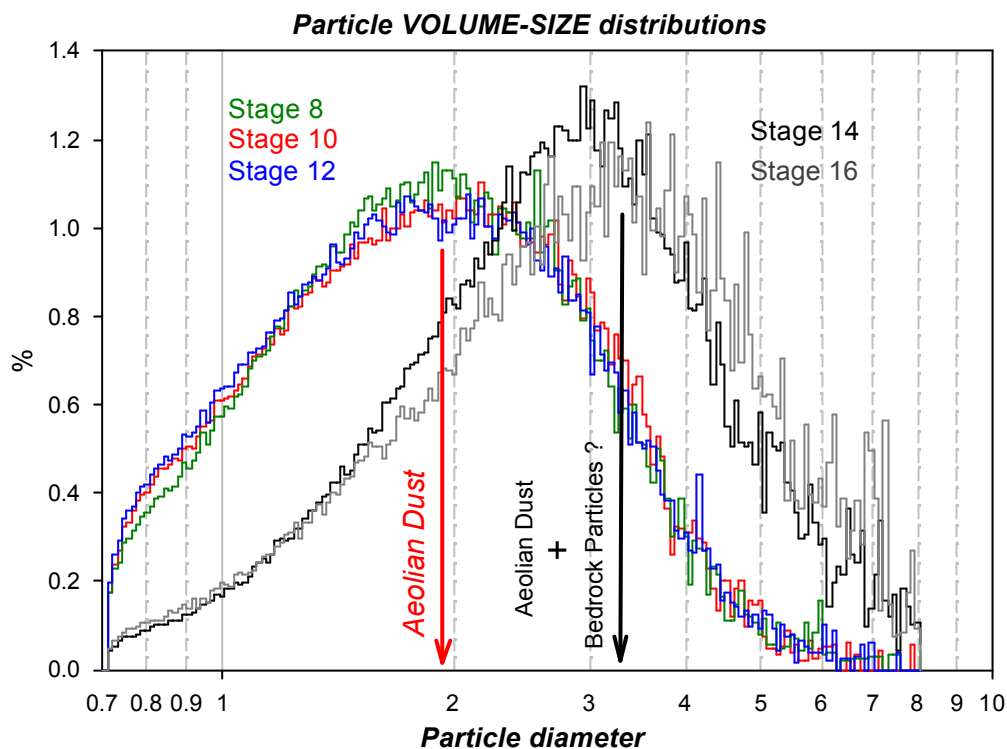


Fig. 8D.5: Volume size distribution (%) of samples from stage 8, 10 and 12 (modal value around 2 micron) and stage 14 and 16 (modal values >3 micron).

### Size changes

The EDC ice core profile of dust size (Fig. 8D.4 and 8D.6) evidences a general decreasing trend and a repeated pattern during the last ~500 kyrs, corresponding to the last five climatic cycles.

Particles are progressively finer during each cold stage until the beginning of the deglaciation, when minimum grain sizes are attained (Fig. 8D.6 and 8D.7). The subsequent warm interglacials are characterised by larger dust, as can be observed in Fig. 8D.6.

Such a pattern was first observed for EDC core during the last termination (§ 8A.3), documented at high temporal resolution, and was linked to the reorganization of atmospheric circulation during glacial/interglacial transition. The fine dust during glacial periods was attributed to enhanced advection and sinking of upper air (carrying finer dust) over the Dome C area in cold periods, and to the easier penetration of (mid troposphere) air masses during the interglacials (coarser dust).

The profile reported in Fig. 8D.6 suggests that the same dynamics of dust transport changes that characterised the last deglaciation could have been repeated during the last five climatic cycles.

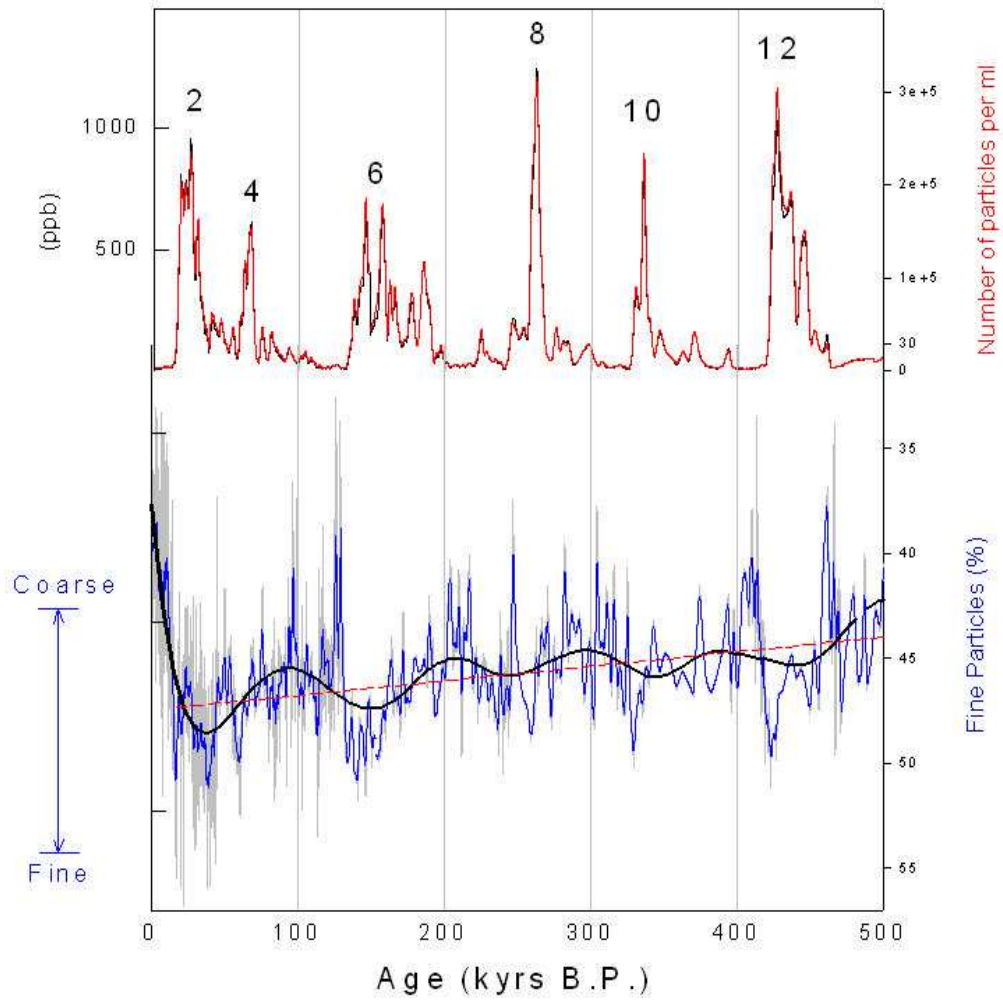
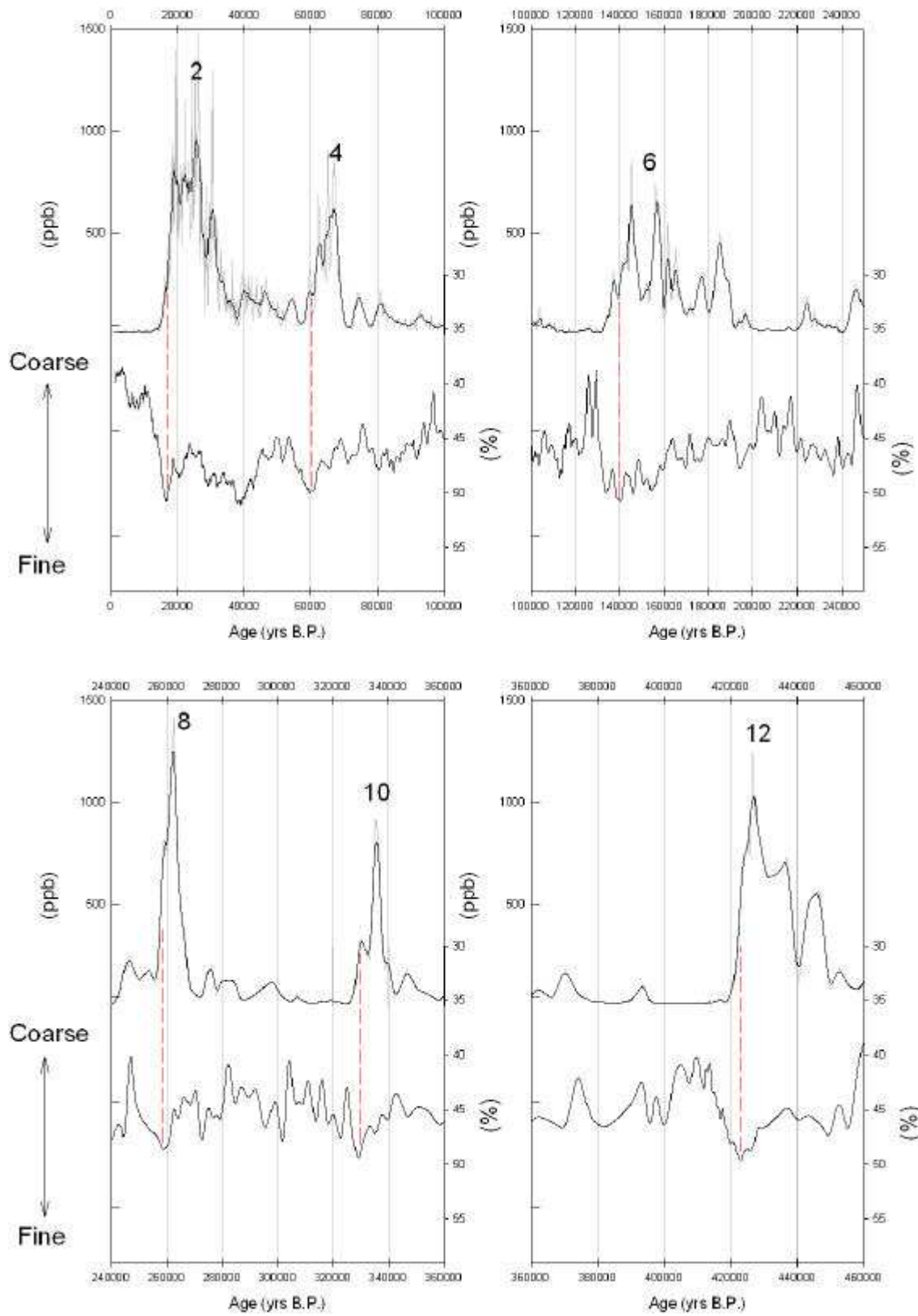


Fig. 8D.6: Pattern of dust concentration and size changes during the last five climatic cycles.

Fig. 8D.7: Dust size evolution during glacial stages. At the very beginning of each deglaciation, a minimum in dust size can be observed, followed by an increase to interglacial coarser dimensions. The pattern observed for the last climatic transition (§8A.3) seems to have been repeated during the last five cycles.



The particle size variations associated to glacial stages 14 and 16 appear different with respect to the previous transitions, as can be observed in Fig. 8D.7.

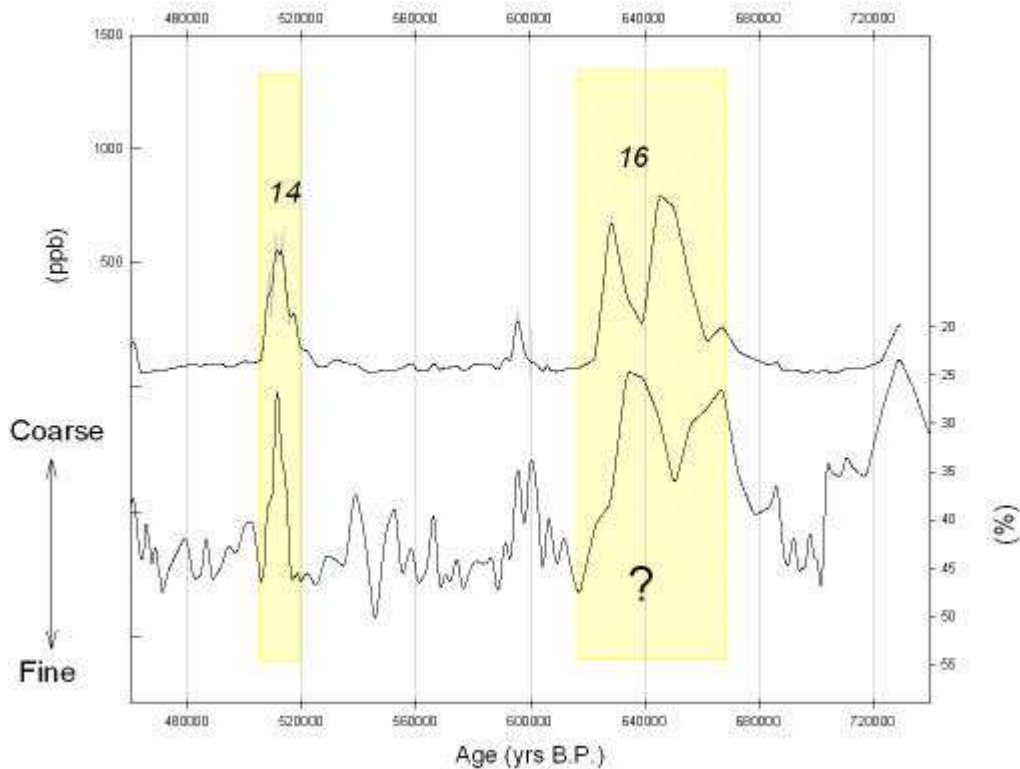


Fig. 8D.7: Dust concentration and size evolution during stages 14 and 16.

### **SEM observations**

It has been pointed out that the dust size and the dynamics of size changes during Stages 14 and 16 is quite anomalous with respect to the remaining part of the ice core profile. Further investigations have been performed through Scanning Electron Microprobe (SEM) observations coupled with X-ray spectrometer (EDX) analysis on three samples (2912 and 2917 m depth, corresponding to Stage 14 and 3137 m depth, corresponding to Stage 16) presenting modal values around 3-4 micron.

The presence of some big aggregates of mineral particles (Fig. 8D.7 a, b, c), very different from typical aeolian dust composed by small monocrystals (Fig. 8D.7 d), has been detected. EDX Elemental composition analysis (not reported) did not suggest for these large particles a particular composition.

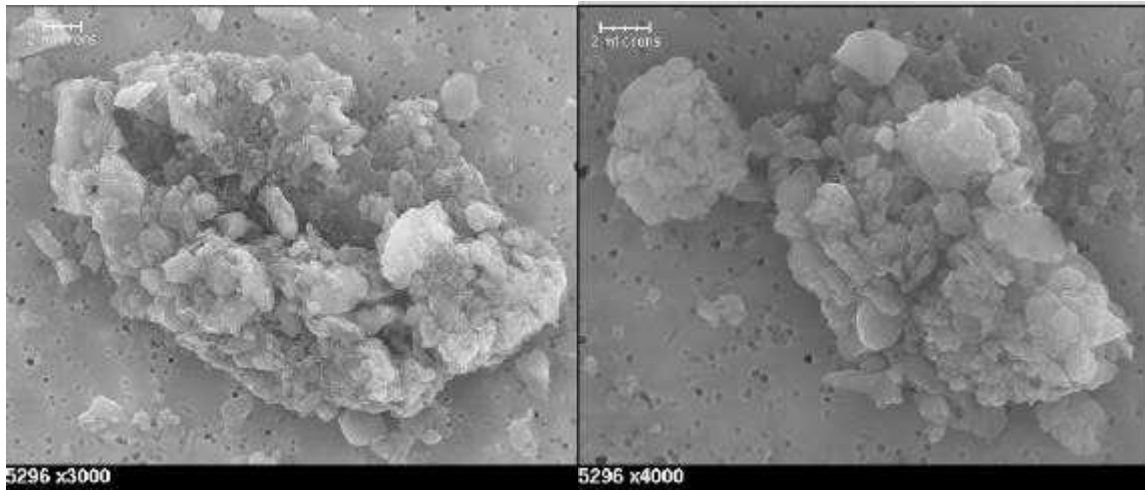


Fig. 8D.7a : SEM photographs of two coarse aggregates found in EDC sample #5296 (2912 m depth).

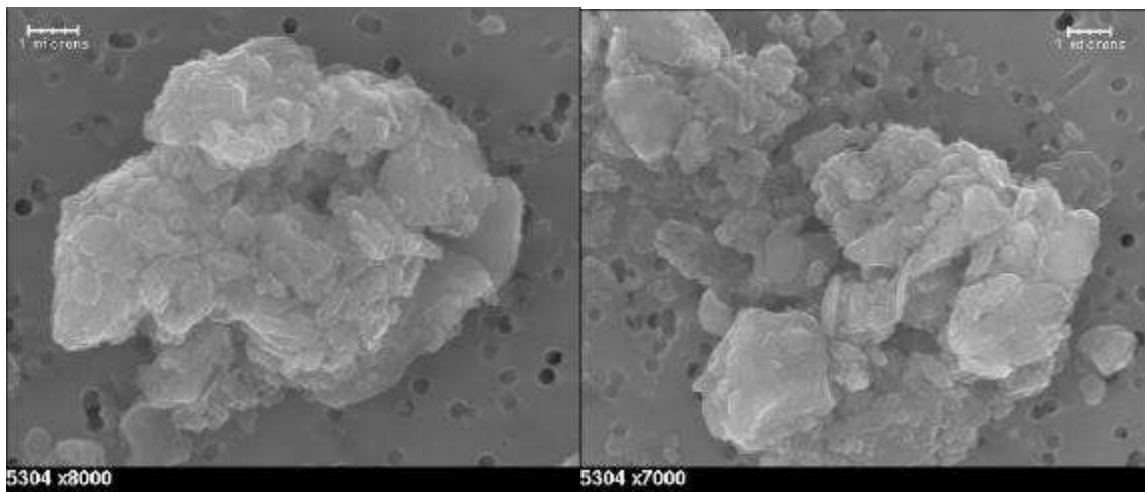


Fig. 8D.7b : SEM photographs of two coarse aggregates found in EDC sample #5304 (2917 m depth).



Fig. 8D.7c : SEM photograph of a coarse aggregate found in EDC sample #5704 (3137 m depth).

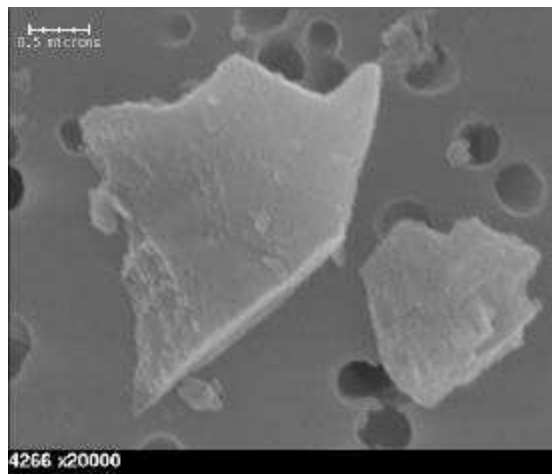
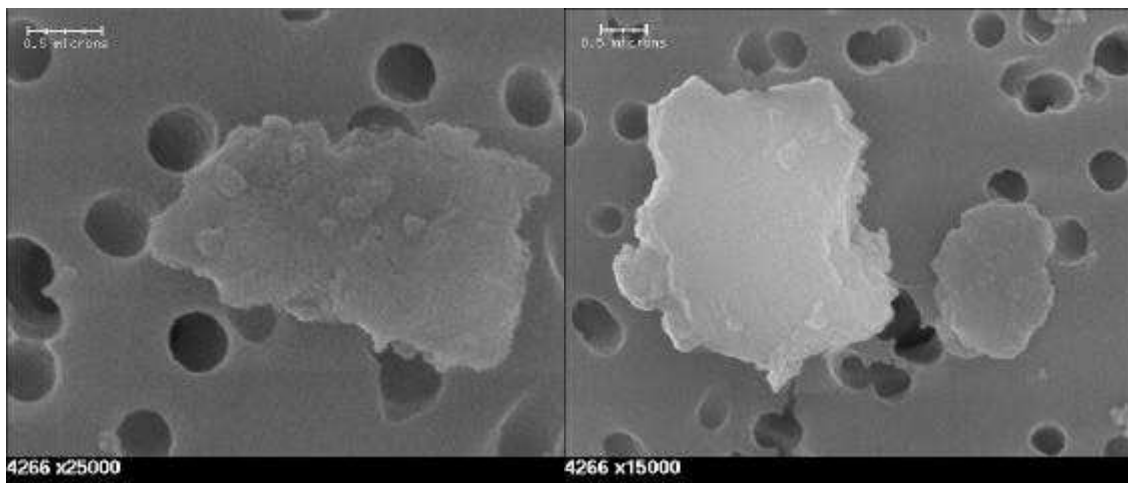
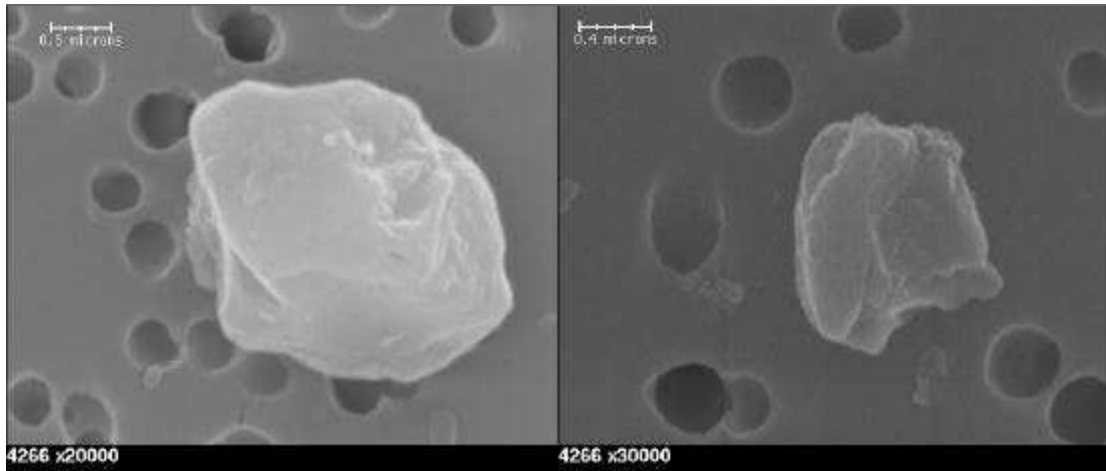


Fig. 8D.7d : SEM photographs of Aeolian dust from EDC sample #4266 (2346 m depth).

### **Three possible hypothesis**

The origin and the nature of the coarse aggregates observed in EDC ice core from 2900 m and downward has to be investigated in further detail in future.

Today, three possible hypothesis on their origin can be made:

- (1) Such particles could originate from the bedrock below the glacier. Their morphology reminds particles observed by Simoes et al. (2002) in the deepest 89 m of Vostok glacier ice, that were interpreted as glacial flour deriving from the mountainous sub-glacial topography during ice flow. The bedrock is located about  $3.309 \pm 22$  m below the drilling site and its topography is almost flat below the Dome. Nevertheless, shallow relieves are present at few tens of kilometres of distance. Supposing the coarse particles retrieved in Dome C ice derive from bedrock, this would imply that the ice interval containing the sediments has been close to it at some time. One hypothesis would be that the ice sections where sediments are entrapped (about 400 m above the bedrock depth at the drilling site) have been entrained elsewhere, possibly in correspondence to one of the sub-glacial ridges near the drilling site (Tabacco et al., 1998). Since glacial flow lines are vertical below a topographic dome, the scenario proposed would imply a shift of the topographic position of the Dome. This hypothesis however arises some questions about a realistic scenario leading to apparent preservation of the stratigraphic sequence within the deep layers. Moreover, preliminary  $^{87}\text{Sr}/^{86}\text{Sr}$  isotopic composition (E. Jagoutz, personal communication) of samples from Stage 14 and 16, evidence a signature typical for aeolian dust ( $0.711 \pm 0.003$  and  $0.7088 \pm 0.0015$  respectively) and markedly different from the bedrock inclusions of Vostok accretion ice (see Appendix I). This scenario therefore is quite improbable.
- (2) The large particles could be windblown from proximal (Antarctic) areas (as the Dry Valleys) exposed during glacial stages 14, 16 and likely 18. However, this hypothesis seems quite unlikely since it would make necessary to invoke mechanisms for dust uplift into the mid-to-high troposphere and transport to the interior of the East Antarctic Plateau during those cold periods.
- (3) Coarse aggregates might derive from agglomeration of aeolian minerals due to processes internal to the ice mass; this hypothesis is also coherent with their occurrence mainly in correspondence to shear layers (Durand, personal communication).



\*\*\*\*\*                    \*\*\*\*\*                    \*\*\*\*\*

### Summary

*The first 3138 m of EDC ice core provide a record of dust input to the Antarctic spanning the last 7 climatic cycles, i.e. ~730 kyr of climatic history, according to a preliminary chronology proposed here.*

*The sequence is comparable to the Vostok dust record for the last 420 kyr, to marine sediment records and to continental loess/paleosol sequences from China.*

*The pattern of dust size changes characterising the last termination in Dome C has been repeated at the end of each glacial stage during the last 500 kyr, suggesting the same scenario of atmospheric circulation reorganization for each glacial/interglacial transition.*

*Surprisingly, particles slightly coarser than typical aeolian dust are present from 2900 m and downward. Probably, they derive from aggregation of aeolian particles by internal processes occurring into the ice mass.*

## CONCLUSIONS

The novel and often surprising aspects of the paleo-dust cycle arising from this work raise several new questions about the dynamics of the atmospheric circulation changes in the Antarctic and circum-antarctic realm during the Late Quaternary.

Dust provenance has been investigated through the Sr-Nd isotopic method, refined according to some basic *guiding principles*; a new database for the isotopic signature of aeolian sediments from the potential source regions of the Southern Hemisphere has been produced specially for this purpose.

The geographical provenance of mineral particles has proven to be identical overall the East Antarctic Plateau and for all the glacial stages investigated. As already suggested more than ten years ago by Goussot (1992), and later by other authors (Basile, 1997; Gemmiti, 2000), the southern South America regions of the Pampas and Patagonia appear as the most important contributors.

However, interglacial dust is significantly different from that of glacial periods, and a mixed origin from south America and Australia is suggested.

In future, much effort has to be done in order to characterise sediments and aeolian deposits from the large and arid Australian continent in better detail, and further measurements on interglacial ice core dust have to be made. For these latter, the extremely low amount of dust available for the interglacial periods makes necessary to improve the efficiency of dust extraction by centrifugation and to develop new techniques for Neodymium isotopic measurements by Thermo Ionization Mass Spectrometry.

The dust influx has proven to be remarkably uniform over the East Antarctic, and for the first time a clear relationship between environmental conditions in the regions where dust originates and the dust input to Antarctica has become clear. During the last climatic transition, in fact, three independent ice cores within the Plateau evidence a drastic decrease in dust concentration, a shallow re-increase in correspondence to the cool ACR period, and a well marked 800-1000 years long “*Pre-Holocene dust minimum*”, this latter attributed to a humid phase at the source.

Such uniformity in dust flux, however, nests remarkable regional differences in transport patterns, especially during the LGM.

During the last climatic transition the reorganization of atmospheric circulation in the circum-antarctic generated opposite and asynchronous regional evolutions of transport patterns, and a change in the eccentricity of the polar vortex has been suggested. This

important and unexpected feature of the dynamics of dust changes during the last climatic transition is one of the most relevant results of this work. Moreover, the recent extension of the Dome C ice core dust record into the Pleistocene has shown repetition of the same *swinging pattern* for the last 500 kyrs.

Investigations on other sectors (e.g. 0°E-60°E) of the Plateau are needed in order to complete the scenario proposed. In this context, the new EPICA-Draunung Maud Land ice core (in course), and the Japanese Dome Fuji ice cores appear as good candidates.

If one has to choose the most important outcome of this thesis, there will be no doubt about the evidence for pervasive millennial and secular scale pulsations in dust advection to the Plateau during the Late glacial and the Holocene epochs.

Such rhythm suggests a circumpolar displacement of ocean-sea ice-atmosphere anomalies at these timescales, a wavering effect reminding that of present-day interannual propagation of Antarctic Circumpolar Wave.

This issue raises several questions about the identification and characterisation of the modes of variability around Antarctica, about the ability of the Southern Ocean to propagate oceanic anomalies through the three world oceans at different timescales, and finally about the origin of these anomalies and their link with the global Thermohaline circulation.

## APPENDIX I

### **GEOCHEMICAL (Sr-Nd) SIGNATURE OF BEDROCK INCLUSIONS FROM LAKE VOSTOK ACCRETION ICE AND SAMARIUM-NEODYMIUM MODEL AGE.**

The 3623 m deep Vostok (78°S, 106°E, 3480 m a.s.l.) ice core was obtained through a tri-partite Russia-US-France collaborative programme. Drilling operation are stopped 130 m above the ice-water interface of the underlying giant lake (Petit et al., 1999). Down to 3310 m, the Vostok ice core preserves climatic information for the last 420 kyrs. Below this depth, the horizontal layers of the climatic record appear disturbed by the glacier dynamics.

Simoes et al. (2002) observed microparticle and ionic content variations between glacial and interglacial values from 3350 to 3450 m depth, and thin bedrock particles as glacial flour entrapped in the ice matrix from 3450 m to 3538.7 m depth. Within this latter interval the proportion of coarse ( $>2.5 \mu\text{m}$ ) particles is very high with respect to the upper part of the core, and the modal values of dust mass-size distributions ( $\sim 3\text{-}4 \mu\text{m}$ ) appear significantly different from typical aeolian dust ( $\sim 2 \mu\text{m}$ ).

Glacial flour is supposed to have been released in the northern area of the lake, where glacier mostly melts and contributes to sediment accumulation. In the southern area, close to the Vostok station, the lake water freezes and the upstream glacial flour does not contribute to sedimentation.

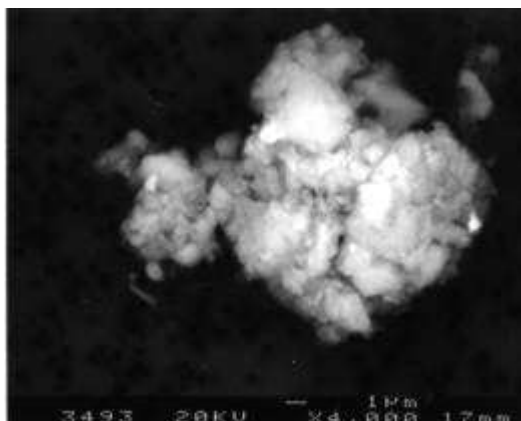


*Fig A1 : SEM photograph of glacial flour inclusions within the Vostok ice core in at 3493 m (from Simoes et al., 2002).*

Below the glacier ice, there is accreted ice, deriving from refreezing of the lake water.

Down to **3608** m the accretion ice (*Accretion ice 1 zone*) contains some visible sediments of 1-2 mm in diameter; below this depth and likely down to the ice-water interface ( $\sim 3750$  m) the ice is clear (*Accretion ice 2 zone*).

Inclusions from *Accretion ice 1* are samples of primary importance for the investigation of the geology of the East Antarctic basement. In fact, less than 3% of Antarctica is ice-free, and what is known about the geology of the continent comes from investigations on the

small rocks exposed either at the coast or at the top of mountain ranges extending above the ice.

In this work one sample from *Accretion ice 1* has been analysed for mineralogical composition through XRD, two samples have been analysed for their  $^{87}\text{Sr}/^{86}\text{Sr}$  versus  $^{143}\text{Nd}/^{144}\text{Nd}$  isotopic composition, and one of them has been dated through Sm-Nd method.

### ***XRD spectrum***

The XRD spectrum of sample 3551 suggests presence of Quartz, Clinocllore (chlorite group), muscovite and phlogopite (Mg-mica). The only bibliographic data available for comparison are those from Caparros (2000), which performed SEM and XRD analysis on fine inclusions within

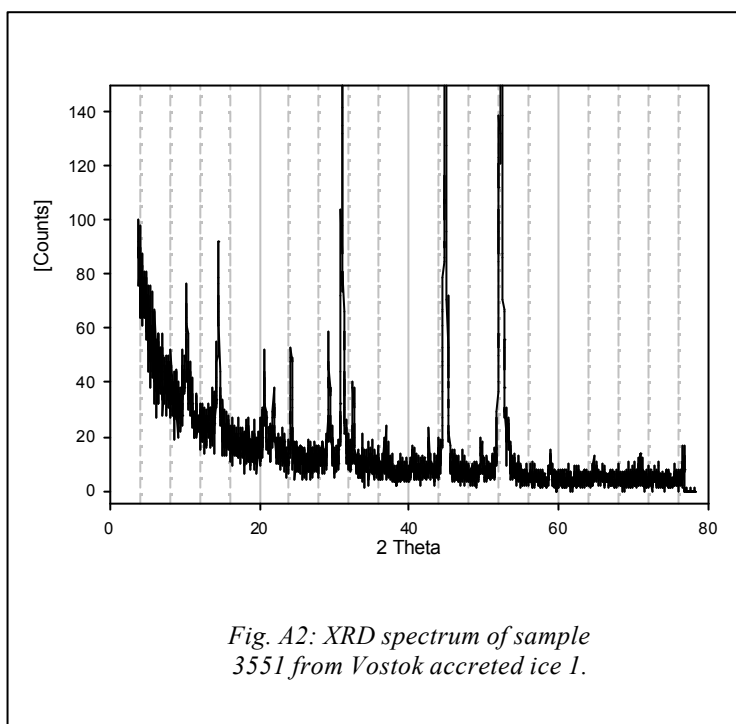


*Fig. A2: XRD spectrum of sample 3551 from Vostok accreted ice 1.*

*Accretion Ice 1* and showed abundance of quartz, feldspars and ferromagnesian phyllosilicates (probably chlorite or micas) with minor amounts of amphiboles, muscovite and dolomite.

The data suggests that metamorphic and sedimentary rocks could be present in the subglacial basement of East Antarctica.

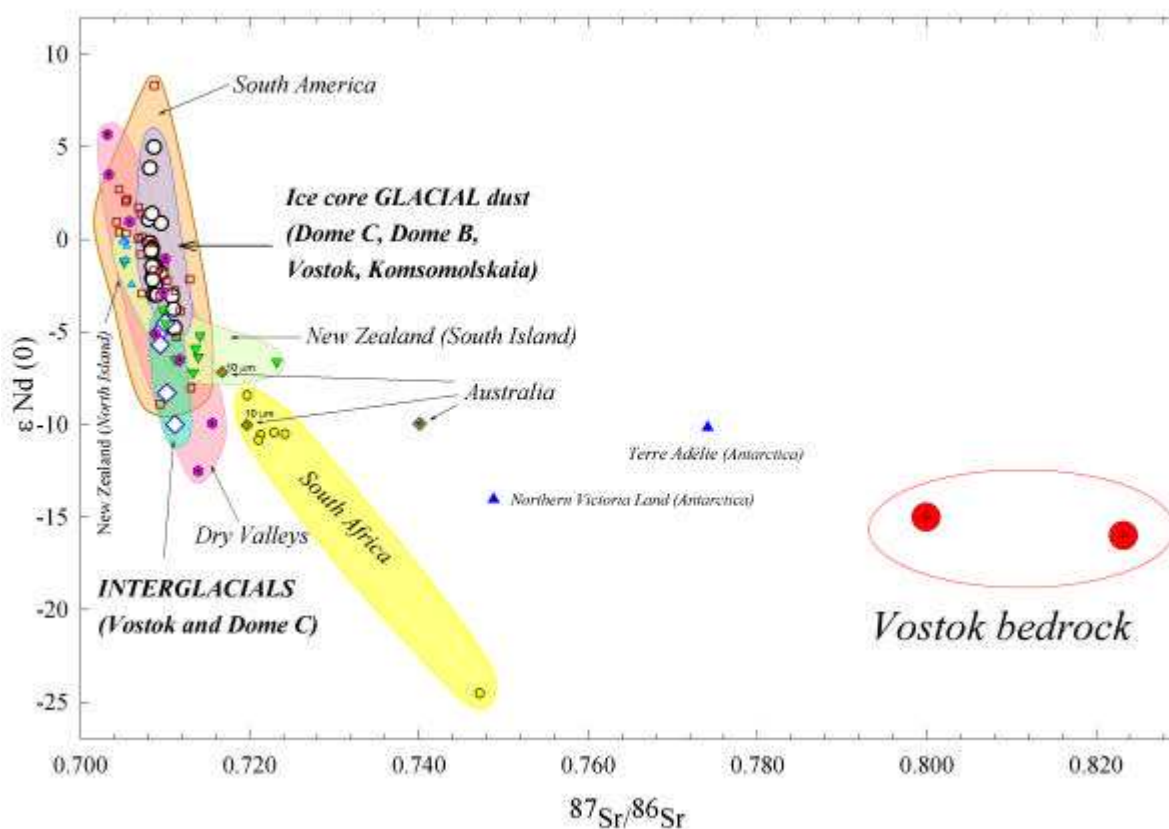
**$^{87}\text{Sr}/^{86}\text{Sr}$  and  $^{143}\text{Nd}/^{144}\text{Nd}$  isotopic composition**

Two samples from Vostok *Accretion ice 1* (3551 and 3607 m depth) have been analyzed for their  $^{87}\text{Sr}/^{86}\text{Sr}$  and  $^{143}\text{Nd}/^{144}\text{Nd}$  isotopic composition; the results are reported in the Tab.A1 and in Fig. A3. The bedrock inclusions appear extremely different from the ice core aeolian dust and show the typical signature of an old continental crust.

Tab. A1 :  $^{87}\text{Sr}/^{86}\text{Sr}$ ,  $^{143}\text{Nd}/^{144}\text{Nd}$  and  $\epsilon_{\text{Nd}}(0)$  isotopic values of Vostok samples

Vostok Sample	$^{87}\text{Sr}/^{86}\text{Sr}$ ( $\pm 2\sigma \times 10^6$ )	$^{143}\text{Nd}/^{144}\text{Nd}$ ( $\pm 2\sigma \times 10^6$ )	$\epsilon_{\text{Nd}}(0)$ ( $\pm 2\sigma \times 10^6$ )
3551	0.799910 (14)	0.511869 (10)	-15.00 (0.20)
3607	0.823218 (21)	0.511818 (12)	-16.00 (0.23)

Fig. A3: Comparison between Sr versus Nd isotopic composition of ice core dust (glacial and interglacial stages), the fine-grained fraction (<5  $\mu\text{m}$ ) of the potential source regions of the Southern Hemisphere, and the bedrock inclusions within the Vostok ice core.



### *Sm-Nd model age*

One of these inclusions (3607) has been dated by Sm-Nd method.

The Neodymium model age<sup>1</sup> has been estimated in **1.88 (+/-0.13) Ga** (DM model age) and **1.47 Ga** ( $T_{\text{CHUR}}$ ) [ $^{147}\text{Sm}/^{149}\text{Sm} = 2.14935$  and  $^{147}\text{Sm}/^{144}\text{Nd} = 0.1116$ ], corresponding to the Precambrian period. Results suggest therefore the presence of a subglacial old continental crust, as could be expected the geological history of the Antarctic continent.

In fact, East Antarctica was part of Gondwana, the large land mass made up of the present continents of Africa, India, Australia, and South America. Gondwana was part of the supercontinent Pangaea, that grouped all the major continents in the Paleozoic Era.

East Antarctic consists in a Precambrian to lower Paleozoic basement with a complex history and structure, intruded by granite and peneplained by weathering and glacial processes, underlying a large sequence of sediments of the Upper Paleozoic. Basic igneous rocks were intruded in Jurassic times within the basement rocks, along the contact plane between the basement and the sediments and within the sediments. In some places these rocks erupted at the surface forming basalt flows and tuffs. No younger rocks are known in East Antarctica except for the volcanics that may range in age from 10 Ma to the present, erupted after the onset of glaciation in East Antarctica (Campbell and Claridge, 1987).

Results from the mineralogical and isotopic investigations performed in this work are consistent with the geology of the East Antarctic basement and with the occurrence of prevalent Proterozoic units in coastal East Antarctica (Craddock, 1982).

---

<sup>1</sup> The Sm-Nd isotopic system can be used to evaluate crust-formation ages, reflecting the time at which samples of continental crust separated from the mantle. However, if the sample is composed by a mixture of materials segregated from the mantle at different times, the Sm-Nd provides only an *average* age with no direct geological information about timing of crustal formation and development.

## APPENDIX II

**Table I - Dust Concentration data for Holocene and LGM**

ICE CORE	Average Holocene dust mass (ppb)	Sampling Frequency Holocene (yrs)	Average LGM dust mass (ppb)	LGM/Holocene Concentration Ratio (*)
Old Dome C <i>(Royer et al., 1983)</i>	$23 \pm 10$	~900	$640 \pm 169$	28
<b>EPICA Dome C</b> <i>(this work)</i>	<b><math>14 \pm 8</math></b>	<b>~50</b>	<b><math>750 \pm 300</math></b>	<b>53</b>
VOSTOK <i>(Petit et al., 1999)</i>	$35 \pm 18$	~600	$849 \pm 471$	24
<b>VOSTOK BH7</b> <i>(this work)</i>	<b><math>18 \pm 8</math></b>	<b>~50</b>		
DOME B <i>(Jouzel et al., 1995)</i>	$25 \pm 12$	~300	$875 \pm 541$	35
<b>DOME B</b> <i>(this work)</i>	<b><math>14 \pm 9</math></b>	<b>~50</b>	<b><math>810 \pm 450</math></b>	<b>55</b>

(\*): An estimate of the LGM/Holocene dust flux can be obtained dividing by a factor 2.



**Table II - EPICA Dome C (this work) and Vostok (Petit et al., 1999) dust concentration and fluxes** for various climatic periods during the last 420 kyr; accumulation rate data have been taken from Parrenin (2002).

<b>EPICA</b>	<b>Dust Concentration</b>	<b>Acc. Rate cm/yr</b>	<b><math>g*cm^{-2}*yr^{-1}</math></b>
Holocene	15	2.7	40
Glacial Stage 2(20-31kyrs BP)	650	1.5	975
Glacial Stage 4(65-74 kyrs BP)	500	1.5	750
Interglacial stage 5.5	15	2.7	40
Glacial Stage 6 (136-156 kyrs BP)	300	1.5	450
Glacial Stage 8 (250-260 kyrs BP)	480	1.5	720
Glacial Stage 10 (330-340 kyrs BP)	390	1.5	585
<b>VOSTOK (Petit et al., 1999)</b>			
Holocene	35	2.2	77
Holocene VK-BH7 (This work)	18	2.2	40
Glacial Stage 2(20-31kyrs BP)	980	1.3	1274
Glacial Stage 4(65-74 kyrs BP)	750	1.3	975
Interglacial stage 5.5	55	3	165
Glacial Stage 6 (136-156 kyrs BP)	475	1.3	617.5
Glacial Stage 8 (250-260 kyrs BP)	370	1.8	666
Glacial Stage 10 (330-340 kyrs BP)	440	1.8	792

**Table III – Reproducibility of Sr-Nd measurements**

Tab. III-A

Sample	$^{87}\text{Sr}/^{86}\text{Sr}$ ( $\pm 2\sigma \times 10^6$ )	Sample A1 selected in size (<5 $\mu\text{m}$ fraction), separated chemically and analysed c/o CEREGE laboratory (Aix en P.ce) in this work is compared to the same sample selected by Gemmiti (2000), separated chemically c/o EPOC laboratory (Bordeaux) and analysed c/o CEREGE laboratory with the same TIMS.
A1 this work	0.712439(09)	
A1 measured by Gemmiti (2000)	0.713913(10)	

Tab. III-B

Sample	$^{87}\text{Sr}/^{86}\text{Sr}$ ( $\pm 2\sigma \times 10^6$ )	$^{143}\text{Nd}/^{144}\text{Nd}$ ( $\pm 2\sigma \times 10^6$ )	$\epsilon_{\text{Nd}}(0)$ ( $\pm 2\sigma \times 10^6$ )
A4 (this work)	0.709797(41)	0.512492(08)	-2.81(0.16)
A4 (Gemmiti 2000)	0.710038(23)	0.512585(11)	-0.99(0.21)

As in Tab. III-A, sample A4 has been selected in size (<5  $\mu\text{m}$  fraction), separated chemically and analysed c/o CEREGE laboratory (Aix en P.ce) in this work is compared to the same sample selected by Gemmiti (2000), separated chemically c/o EPOC laboratory (Bordeaux) and analysed c/o CEREGE laboratory with the same TIMS.

Tab. III-C

Sample	$^{87}\text{Sr}/^{86}\text{Sr}$ ( $\pm 2\sigma \times 10^6$ )	Samples CH9 and CH9-repeated have been separated chemically two times and analysed c/o CEREGE laboratory (Aix en P.ce) in this work.
CH9	0.709785(17)	
CH9 repeated	0.709880(19)	

Tab. III-D

Sample	$^{87}\text{Sr}/^{86}\text{Sr}$ ( $\pm 2\sigma \times 10^6$ )	One Sr sample deriving from a unique chemical separation has been split and analyzed two times c/o CEREGE laboratory (Aix en P.ce) in this work.
A4 leached	0.713281(16)	
A4 leached repeated	0.713259(23)	

## APPENDIX III

### List of publications outcome from this work

#### Papers

B. **Delmonte**, J.R. Petit, K.K. Andersen, I. Basile-Doelsch, V. Maggi, V. Ya Lipenkov Opposite regional changes and quasi-millennial oscillations in atmospheric circulation over East Antarctica during the last climatic transition. Submitted to *Climate Dynamics*.

B. **Delmonte**, J.R. Petit, G. Krinner, V. Maggi, G. Raisbeck, F. Yiou, J. Jouzel, V.Y Lipenkov, Secular variations in dust transport to Antarctica during the Holocene: an atmosphere-ocean response to solar forcing? Submitted to *Earth and Planetary Science Letters*.

B. **Delmonte**, I. Basile-Doelsch, J.-R. Petit, V. Maggi, M. Revel-Rolland, A. Michard, E. Jagoutz, F. Grousset, Comparing the EPICA and Vostok dust records during the last 220,000 years: stratigraphical correlation and origin in glacial periods. *Earth Science Reviews*, in press

F. Marino, V. Maggi, B. **Delmonte**, G. Ghermandi, J.R. Petit “Atmospheric dust elemental composition (Si, Fe, Ti) of the last 220 kyrs from the EPICA ice core (Dome C, Antarctica)” *Annals of Glaciology*, in press.

R. Udisti, S. Becagli, E. Castellano, B. **Delmonte**, J. Jouzel, J.R. Petit, J.Schwander, B. Stenni, E. Wolff “Stratigraphic correlations between EPICA-Dome C and Vostok ice core showing the relative variations of snow accumulation over the past 45 kyr” Submitted to *Journal of Geophysical Research (Atmosphere)*.

B. **Delmonte**, J.R. Petit, I. Basile-Doelsch, A. Michard, B.Gemmiti, V.Maggi, M.Revel-Rolland, (2003) Refining the isotopic (Sr-Nd) signature of potential source areas for glacial dust in East Antarctica, *Journal de Physique*, IV, 107, 365-368.

B. **Delmonte**, V.Maggi, I. Basile-Doelsch, A. Michard, J.R. Petit, B.Gemmiti, M.Revel-Rolland (2003) Sr-Nd signature of potential source areas for dust in East Antarctica: preliminary results. *Terra Antarctica Reports*, 8, 83-85.

**Epica Dome C 2001-02 science and drilling teams\*** (2002) Extending the Ice Core Record beyond half a million years, *EOS* 5-11-, 509,517.

(\*) List of authors including B.Delmonte

B. **Delmonte**, J.-R. Petit, V. Maggi (2002) “LGM-HOLOCENE changes and Holocene millennial-scale oscillations in dust revealed by EPICA-DOME C ice core (Antarctica)”. *Annals of Glaciology* 35, 306-312.

B. **Delmonte**, J.-R. Petit, V. Maggi (2002) “Glacial to Holocene implications of the new 27,000-year dust record from the EPICA Dome C (East Antarctica) ice core” , *Climate Dynamics* 18 (8), 647-660.

## Abstracts and Conference Proceedings

B. **Delmonte**, J.R. Petit, I. Basile-Doelsch, A. Michard, V. Lipenkov (2003) Samarium-Neodymium model age and geochemical (Sr-Nd) signature of a bedrock inclusion from Lake Vostok accretion ice. Geophysical research abstracts Vol. 5, 03580.

B. **Delmonte**, J.R. Petit, I. Basile-Doelsch, E. Jagoutz, A. Michard, V. Maggi, M. Revel-Rolland (2003) Origin of glacial dust in four East Antarctic ice cores. Geophysical research abstracts Vol. 5, 01432.

B. **Delmonte**, J.R. Petit, G. Krinner, V. Maggi, G. Raisbeck, F. Yiou, J. Jouzel, V.Y. Lipenkov, (2003) Holocene secular variations in dust transport to East Antarctica (Vostok and Dome C): a response to solar forcing? Geophysical research abstracts Vol. 5, 01896.

P. Gabrielli, C. Barbante, F. Planchon, C. Ferrari, B. **Delmonte**, C.F. Boutron, (2003) Changes in the occurrence of heavy metals in Antarctic ice during the last climatic cycles. Geophysical research abstracts Vol. 5, 01451.

F. Marino, B. **Delmonte**, G. Ghermandi, J.R. Petit, V. Maggi (2003) A 220 kyr record of insoluble atmospheric Si, Fe and Ti from EPICA-Dome C (East Antarctica) ice core using PIXE technique. Geophysical research abstracts Vol. 5, 13939.

C. Barbante, V. Gaspari, G. Cozzi, P. Cescon, C. Ferrari, B. **Delmonte**, J.R. Petit, C.F. Boutron (2003) Temporal variability of Iron and other bioreactive trace elements in Antarctic (Dome C) ice during the last 30,000 years. Geophysical research abstracts Vol. 5, 01457.

B. **Delmonte**, I. Basile-Doelsch, A. Michard, J.R. Petit, V. Maggi, B. Gemmiti, M. Revel-Rolland (2002) Sr-Nd signature of potential source areas for dust in East Antarctica: preliminary results. Geochimica e Cosmochimica Acta, A175, Goldschmidt conference Davos, Switzerland.

## *References*

- Andersen KK, Armengaud A, Genthon C (1998) Atmospheric dust under glacial and interglacial conditions. *Geophys Res Lett* 25:2281-2284
- Andersen KK (1998) Simulations of atmospheric dust in the glacial and interglacial climate. PhD Thesis, Niels Bohr Institute of Astronomy, Physics and Geophysics, University of Copenhagen, Copenhagen, 136 p.
- Anklin M, Barnola JM, Schwander J, Stauffer B, Raynaud D (1995) Processes affecting the CO<sub>2</sub> concentrations measured in Greenland ice. *Tellus* 47:461-470
- Arndt NT, Goldstein SL (1987) Use and abuse of crust formation ages. *Geology* 15:893-895
- Barrows TT, Stone JO, Fifield LK, Cresswell RG (2002) The timing of the last Glacial Maximum in Australia. *Quat Sci Rev* 21:159–173
- Basile I, Grousset FE, Revel M, Petit JR, Biscaye PE, Barkov NI (1997) Patagonian origin of glacial dust deposited in East Antarctica (Vostok and Dome C) during glacial stages 2, 4 and 6. *Earth Planet Sci Lett* 146:573-589
- Basile I (1997) Origine des aérosols volcaniques et continentaux de la carotte de glace de Vostok (Antarctique). PhD Thesis, LGGE-Université Joseph Fourier-Grenoble I, Grenoble, 254 p.
- Basile I, Petit JR, Touron S, Grousset FE, Barkov NI (2001) Volcanic tephra in Antarctic (Vostok) ice-cores: source identification and atmospheric implications. *J Geophys Res* 106:31915-31931
- Bassinot FC, Labeyrie LD, Vincent E, Quidelleur X, Shackleton NJ, Lancelot Y (1994) The astronomical theory of climate and the age of the Brunhes-Matuyama magnetic reversal. *Earth Planet Sci Lett* 126:91-108
- Berger AL (1978) Long Term Variations of Daily Insolation and Quaternary Climatic Changes. *J Atmosph Sci* 35:2362-2367
- Berger A, Loutre MF (1991) Insolation values for the climate of the last 10 million years. *Quat Sci Rev* 10:297-317
- Berger GW, Pillans BJ, Tonkin PJ (2001) Luminescence chronology of loess–paleosol sequences from Canterbury, South Island, New Zealand. *New Zealand Journal of Geology and Geophysics* 44:501–516
- Berger GW, Pillans BJ, Bruce JG, McIntosh PD (2002) Luminescence chronology of loess from southern South Island, New Zealand. *Quat Sci Rev* 21:1899-1913
- Berger WH, Patzold J, Wefer G (2002) A case for climate cycles: Orbit, Sun and Moon. In: Wefer G, Behre K.-E., Jansen E. (ed) *Climate development and History of the North Atlantic realm*. Springer Verlag, Berlin Heidelberg, p 101-123
- Birck JL (1986) Precision K-Rb-Sr isotopic analysis: application to Rb-Sr chronology. *Chem Geol* 56:73-83
- Birckle MJ (1994) The role of metamorphic decarbonation reactions in returning strontium to the silicate sediment mass. *Nature* 367:699-704

- Biscaye PE, Grousset FE, Revel M, Gaast SvD, Zielinski GA, Vaars A, Kukla G (1997) Asian provenance of glacial dust (Stage 2) in the Greenland Ice Sheet Project 2 ice core, Summit, Greenland. *J Geophys Res* 102:26765-26781
- Bogdanovski O (1997) Development of highly-sensitive techniques for Sm-Nd isotopic analysis and their application to the study of terrestrial and extraterrestrial objects. PhD Thesis, Cosmochemistry Dept. Max Plank Institute, Johannes Gutenberg Universitat, Mainz.
- Bond G, Showers W, Cheseby M, Lotti R, Almasi P, DeMenocal P, Priore P, Cullen H, Hajadas I, Bonani G (1997) A pervasive millennial scale cycle in the North Atlantic Holocene and glacial climates. *Science* 278:1257-1266
- Bond G, Showers W, Cheseby M, Lotti R, Almasi P, DeMenocal P, Priore P, Cullen H, Hajadas I, Bonani G (1997) A pervasive millennial scale cycle in the North Atlantic Holocene and glacial climates. *Science* 278:1257-1266
- Bory A J-M, Biscaye PE, Svensson A, Grousset FE (2002) Seasonal variability in the origin of recent atmospheric mineral dust at NorthGRIP, Greenland. *Earth Planet Sci Lett* 196:123-134
- Bowler JM (1976) Aridity in Australia: Age, origins and expression in aeolian landforms and sediments. *Earth Sci Rev* 12:279-310
- Bowler JM, Johnston H, Olley JM, Prescott JR, Roberts RG, Shawcross W, Spooner NA (2003) New ages for human occupation and climatic change at Lake Mungo, Australia. *Nature* 421:837-840
- Briat M, Royer A, Petit JR, Lorius C (1982) Late glacial input of eolian continental dust in the Dome C ice core: additional evidence from individual microparticle analysis. *Ann Glaciol* 3:27-30
- Broecker WS, Denton GH (1989) The role of ocean-atmosphere reorganizations in glacial cycles. *Geochim Cosmochim Acta* 53:2465-2501
- Broecker WS, Bond G, Klaus M, Bonani G, Wolffli W (1990) A salt oscillator in the glacial Atlantic? *Paleoceanogr* 5:469-477
- Campbell IB, Claridge GGC (1987) *Antarctica: soils, weathering processes and environment*, Vol 16. Elsevier
- Caparros P (2000) *Mineralogie du socle rocheux de Vostok*. Scientific and Technical Report, Universite Aix-Marseille III, 30 p.
- Carignano CA (1999) Late Pleistocene to recent climate change in Cordoba province, Argentina: geomorphological evidence. *Quat International* 57/58:117-134
- Carleton AM (1989) Antarctic sea-ice relationships with indices of the atmospheric circulation of the Southern Hemisphere. *Clim Dyn* 3:207-220
- Carrasco JF, Bromwich DH, Monaghan AJ (2003) Distribution and characteristics of mesoscale cyclones in the Antarctic: Ross sea eastward to the Weddel sea. *Mon Weather Rev* 131:289-301
- Chiquet A, Michard A, Nahon D, Hamelin B (1999) Atmospheric input vs in situ weathering in the genesis of calcretes: An Sr isotope study at Galvez (Central Spain). *Geochim Cosmochim Acta* 63:311-323

- Ciais P, Petit JR, Jouzel J, Lorius C, Barkov NI, Lipenkov V, Nicolaiev V (1992) Evidence for an early Holocene climatic optimum in the Antarctic deep ice-core record. *Clim Dyn* 6:169-177
- Clapperton CM (1993) *Quaternary Geology and Geomorphology of South America*, Elsevier, Amsterdam, 779 p.
- Claquin T, Schulz M, Balkanski Y, Boucher O (1998) Uncertainties in assessing radiative forcing by mineral dust. *Tellus B* 50:491-505
- Claquin T, Roelandt C, Kohfeld K, Harrison S, Tegen I, Prentice IC, Balkanski Y, Bergametti G, Hansson M, Mahowald N, Rodhe H, Schulz M (2003) Radiative forcing of climate by ice-age dust. *Clim Dyn* 20:193-202
- Claridge GCC, Campbell IB (1988) Loess sources and aeolian deposits in Antarctica. In: Eden and Furkert (ed) *Loess*, Rotterdam
- Clark CO, Cole JE, Webster PJ (2000) Indian Ocean SST and indian summer rainfall: predictive relationships and their decadal variability. *J Climate* 13:2503-2519
- COHMAP Project Members (1988) Climatic changes of the last 18000 years: observations and model simulations. *Science* 241:1043-1052
- Cooke DW, Hays JD (1982) Estimates of Antarctic seasonal sea-ice cover during glacial intervals. In: Craddock C (ed) *Antarctic geoscience*. University of Wisconsin Press, Madison
- Craddock C (1982) Geological map of Antarctica. In: Craddock C (ed) *Antarctic geosciences*. University of Wisconsin press, Madison, Wisconsin, USA
- Cragin JH, Herron MM, Langway CC, Klouda G (1977) Interhemispheric comparison of changes in the composition of atmospheric precipitation during the Cenozoic era. In: Dunbar MJ (ed) *Polar Oceans Conference*, Calgary, Alberta, p 617-641
- Crosta X, Pichon JJ (1998) Reappraisal of Antarctic seasonal sea-ice at the Last Glacial Maximum. *Geophys Res Lett* 25:2703-2706
- D'Almeida GA, L. Schutz (1983) Number, mass and volume distributions of mineral aerosol and soils of the Sahara. *J. Climate Appl. Meteorol.* 22:233-224
- Dansgaard W, Johnsen SJ, Clausen HB, Dahl-Jensen D, Gundestrup NS, Hammer CU, Oeschger H (1984) North Atlantic climate oscillations revealed by deep Greenland ice cores. In: Hansen, J.E. and Takahashi, T. (ed) *Climate processes and climate sensitivity*, Vol 29. AGU Geophysical Monograph, p 288-298
- DeAngelis M, Legrand M, Petit JR, Barkov NI, Korotkevitch YS, Kotlyakov VM (1984) Soluble and insoluble impurities along the 950 m deep Vostok ice core (Antarctica) - Climatic implications. *J Atmos Chem* 1:215-239
- DeAngelis M, Barkov NI, Petrov VN (1992) Sources of continental dust over Antarctica during the last glacial cycle. *J Atmos Chem* 14:233-244
- Delmonte B, Petit JR, Maggi V (2002a) Glacial to Holocene implications of the new 27,000-year dust record from the EPICA Dome C (East Antarctica) ice core. *Clim Dyn* 18:647-660

- Delmonte B, Petit JR, Maggi V (2002b) LGM-Holocene changes and Holocene millennial-scale oscillations of dust particles in the EPICA Dome C ice core, East Antarctica. *Ann Glaciol* 35:306-312
- DeMenocal P (1995) Plio-Pleistocene african climate. *Science* 270:53-59
- Dentener FJ, G.R. Carmichael, Zhang Y, Lelieveld J, Crutzen PJ (1996) Role of mineral aerosol as a reactive surface in the global troposphere. *J. Geophys. Res* 101:22,869-822,889
- Denton GH, Prentice ML, Burckle LH (1991) Cainozoic history of the Antarctic ice sheet. In: R.J. Tingey (ed) *The Geology of Antarctica*, Vol 17. Oxford Monogr. Geol. Geophys., p 365-433
- Denton GH, Hughes TJ (2002) Reconstructing the Antarctic ice sheet at the Last Glacial Maximum. *Quat Sci Rev* 21:193-202
- DePaolo DJ, Wasserburg GJ (1976) Nd isotopic variations and petrogenetic models. *Geophys Res Lett* 3:249-252
- Derry LA, France-Lanord C (1996) Neogene Hymalayan weathering history and river  $^{87}\text{Sr}/^{86}\text{Sr}$ : impact on the marine Sr record. *Earth Planet Sci Lett* 142:59-74
- Deser C, Blackmon M (1993) Surface climate variations over the North Atlantic ocean during winter: 1900-1989. *J Clim* 6:1743-1753
- Dickerson RR, Kondragunta S, Stenchikov G, Civerolo KL, Doddridge BG, Holben BN (1997) The impact of aerosols on solar ultraviolet radiation and photochemical smog. *Science* 278:827-830
- Dickin AP (1995) *Radiogenic isotope geology*, Cambridge University Press, Cambridge, U.K., 452 p.
- Ding Z, Xiong S, Sun J, Yang SL, Gu ZY, Liu TS (1999) Pedostratigraphy and paleomagnetism of a 7.0 Ma eolian loess-red clay sequence at Lingtai, Loess Plateau, north-central China, and the implications for paleomonsoon evolution. *Palaeogeogr Palaeoclimatol Palaeoecol* 152:49-66
- Dodson JR, Ono Y (1997) Timing of late Quaternary vegetation response in the 30-50° latitude bands in southeastern Australia and northeastern Asia. *Quat Internat* 37:89-104
- Duplessy JC, Labeyrie L, Jullet-Lerclerc A, Duprat J, Sarnthein M (1991) Surface salinity reconstruction of the North Atlantic ocean during the last glacial maximum. *Oceanol. Acta* 14:311-324
- EPICA-Dome C 2001-02 Science and Drilling teams (2002) Extending the Ice Core Record beyond half a million years, *EOS* 5-11-, 509,517.
- Falkowski PG, Barber RT, Smetacek V (1998) Biogeochemical controls and feedbacks on ocean primary production. *Science* 281:200-206
- Faure G (1986) *Principles of isotope geology*, John Wiley & Sons, New York
- Fisher DA (1979) Comparison of 105 years of oxygen isotope and insoluble impurity profiles from the Devon Island and Camp Century ice cores. *Quat Res* 11:299-305
- Francis PW, Moorbath S, Thorpe RS (1977) Strontium isotope data for recent andesites in Ecuador and North Chile. *Earth Planet Sci Lett* 37:197-202



- Fung I, Meyn S, Tegen I, Doney SC, John J, Bishop JKB (2000) Iron supply and demand in the upper ocean. *Global Biogeochem. Cycles* 14:281-296
- Futa K, Stern CR (1988) Sr and Nd isotopic and trace element composition of Quaternary volcanic centers of the southern Andes. *Earth Planet Sci Lett* 88:253-262
- Gallet S, Jahn B, Lanoe BVV, Dia A, Rossello E (1998) Loess geochemistry and its implications for particle origin and composition of the upper continental crust. *Earth Planet Sci Lett* 156:157-172
- Gallée H (1996) Mesoscale atmospheric circulations over the southwestern Ross Sea sector, Antarctica. *J. Appl. Meteor.* 35:1142-1152
- Gaudichet A, Petit JR, Lefevre R, Lorius C (1986) An investigation by analytical transmission electron microscopy of individual insoluble microparticles from Antarctic (Dome C) ice core samples. *Tellus*:250-261
- Gaudichet A, Angelis MD, Lefevre R, Petit JR, Korotkevitch YS, Petrov VN (1988) Mineralogy of insoluble particles in the Vostok Antarctic ice core over the last climatic cycle (150 Kyr). *Geophys Res Lett* 15:1471-1474
- Gaudichet A, Angelis MD, Jossasume S, Petit JR, Korotkevitch YS, Petrov VN (1992) Comments on the origin of dust in East Antarctica for present and ice age conditions. *J Atmos Chem* 14:129-142
- Gemmiti B (2000) Poussieres desertiques dans la glace Antarctique: variations des flux et sources. Report-Université Aix-Marseille III, INPL, Toulouse III, 44 p.
- Genthon C (1992) Simulations of desert dust and sea-salt aerosols in Antarctica with a general circulation model of the atmosphere. *Tellus, Ser. B*:371-389
- Gershunov A, Barnett T, Cayan D (1999) North Pacific interdecadal oscillation seen as factor in ENSO-related north American climate anomalies. *EOS* 80:25-30
- Gillette D (1978) A wind tunnel simulation of the erosion of soil: effect of soil texture, sandblasting, wind speed, and soil consolidation on dust production. *Atmos Environ* 12:1735-1743
- Gillette DA, Adams J, Muhs D, Kihl R (1982) Threshold friction velocities and rupture moduli for crusted desert soils for the input of soil particles into the air. *J. Geophys. Res* 87:9003-9015
- Gillette DA (1999) A qualitative geophysical explanation for "hot spot" dust emitting source regions. *Contrib Atmos Phys* 72:67-77
- Goudie A (1983) *Environmental change*, Second Edition. Clarendon Press, Oxford
- Goudie AS (1996) Climate, past and present. In: W.M. Adams, A.S. Goudie and A.R. Orme (ed) *The physical geography of Africa*. Oxford University Press, New York, p 44-59
- Gow AJ, Williamson T (1971) Volcanic ash in the Antarctic ice sheet and its possible climatic implications. *Earth Planet Sci Lett* 13:210-218
- Graham IJ, Glasby GP, Churchman GJ (1997) Provenance of the detrital component of deep-sea sediments from the SW Pacific Ocean based on mineralogy, geochemistry, and Sr isotopic composition. *Marine Geol* 140:75-96
- Graham IJ, Ditchburn RG, Whitehead NE (2001) Be isotope analysis of a 0-500 ka loess-paleosol

sequence from Rangitatu East, New Zealand. *Quat Internat* 76/77:29-42

- Grousset FE, Biscaye PE, Zindler A, Prospero JM, Chester R (1988) Neodymium isotopes as tracers in marine sediments and aerosols: North Atlantic. *Earth Planet Sci Lett* 87:367-378
- Grousset FE, Biscaye PE, Revel M, Petit JR, Pye K, Jossaume S, Jouzel J (1992) Antarctic (Dome C) ice-core dust at 18 k.y. B.P.: isotopic constraints and origins. *Earth. Planet. Sci. Lett.* 111:175-182
- Hamidi EM, Colin F, Michard A, Boulangé B, Nahon D (2001) Isotopic tracers of the origin of Ca in a carbonate crust from the Middle Atlas, Morocco. *Chem Geol* 176:93-104
- Hammer CU, Clausen HB, Dansgaard W, Neftel A, Kristinsdottir P, Johnson E (1985) Continuous impurity analysis along the Dye 3 deep core. In: C. C. Langway, H. Oeschger, W. Dansgaard (ed) *Greenland Ice Core: geophysics, geochemistry and the Environment.*, Vol 33. A.G.U., Washington D. C., p 90-94
- Hansson ME (1994) The Renland ice core. A northern hemisphere record of aerosol composition over 120,000 years. *Tellus Ser. B*:390-418
- Harrison SP, Dodson J (1993) Climates of Australia and New Guinea since 18,000 yr B.P. In: H.E. Wright, J.E. Kutzbach, T. Webb III, W.F. Ruddiman, F.A. Street-Perrott and P.J. Bartlein (ed) *Global climates since the Last Glacial Maximum.* University of Minnesota press, Minneapolis, p 265-293
- Hawkesworth CJ, Norry MJ, Roddick JC, Baker PE (1979)  $^{143}\text{Nd}/^{144}\text{Nd}$ ,  $^{87}\text{Sr}/^{86}\text{Sr}$ , and incompatible element variations in calc-alkaline andesites and plateau lavas from South America. *Earth Planet Sci Lett* 42:45-57
- Haxeltine A, Prentice IC (1996) BIOME3: an equilibrium terrestrial biosphere model based on ecophysiological constraints, resource availability, and competition among plant functional types. *Global Biogeochem. Cycles* 10:693-710
- Hays JD, Lonzo JA, Shackleton N, Irving G (1976) Reconstruction of the Antarctic and western Indian ocean sectors of the 18,000 B.P. Antarctic ocean. *Geol Society of America, Memoir* 145
- Heinrich H (1988) Origin and consequences of cyclic ice rafting in the northeast Atlantic Ocean during the past 130,000 years. *Quat. Res.* 29:142-152
- Hulton NRJ, Purves RS, McCulloch RD, Sugden DE, Bentley MJ (2002) The last glacial maximum and deglaciation in southern South America. *Quat Sci Rev* 21:233-241
- Hutchins DA, Brunland KW (1998) Iron-limited diatom growth and Si:N uptake ratios in a coastal upwelling regime. *Nature* 393:561-564
- Imbellone PA, Teruggi ME (1993) Paleosols in loess deposits of the Argentine pampas. *Quat Internat* 17:49-55
- Imbrie J, Boyle EA, Clemens SC, Duffy A, Howard WR, Kukla G, Kutzbach J, Martinson DG, McIntyre A, Mix AC, Molfino B, Morley JJ, Peterson LC, Pisias NG, Prell WL, Raymo ME, Shackleton NJ, Toggweiler JR (1992) On the structure and origin of major glaciation cycles. 1. Linear responses to Milankovich forcing. *Paleoceanogr* 7:701-738

- IPCC 2001 Intergovernmental Panel on Climate Change, J.T. Houghton, Y.Ding, D.J. Griggs, M. Noguer, P.J. Van der Linden, X. Dai, K. Maskell, C.A. Johnon (ed) Cambridge Univ. Press, New York
- Iriondo MH, Garcia NO (1993) Climatic variations in the Argentine plains during the last 18,000 years. *Palaeogeogr, Palaeoclimatol, Palaeoecol* 101:209-220
- Iriondo MH (1999) Climatic changes in South America plains: Records of a continent-scale oscillation. *Quat Internat* 57/58:93-112
- Iriondo MH (1999) Last glacial maximum and hypsithermal in the Southern Hemisphere. *Quat Internat* 62:11-19
- Jacobsen SB, Wasserburg GJ (1980) Sm-Nd isotopic evolution of chondrites. *Earth Planet Sci Lett* 50:139-155
- Jagoutz E, Vogel J, Jacob-Foley D (1990) Guideline for laboratory work, Max Plank Institut fur Chemie, Mainz, Germany
- James IN (1989) The Antarctic drainage flow: implications for hemispheric flow on the Southern hemisphere. *Antarctic Science* 1:279-290
- Jones DA, Simmonds I (1993) A climatology of southern hemisphere extratropical cyclones. *Clim Dyn* 9:131-145
- Jones PD, Salinger MJ, Mullan AB (1999) Extratropical circulation indices in the Southern Hemisphere based on station data. *Int. J. Climatol.* 19:1301-1317
- Joussaume S (1989) Desert dust and climate: an investigation using an atmospheric general circulation model. In: Sarnthein MLaM (ed) *Paleoclimatology and Paleometeorology: Modern and Past Patterns of Global Atmospheric Transport - NATO Workshop*, p 253-263
- Jouzel J, Vaikmae R, Petit JR, Martin M, Duclos Y, Stievenard M, Lorius C, Toots M, Melières MA, Burckle LH, Barkov NI, Kotlyakov VM (1995) The two-step shape and timing of the last deglaciation in Antarctica. *Clim Dyn* 11:151-161
- Jouzel J, Masson V, Cattani O, Falourd S, Stievenard M, Stenni B, Longinelli A, Johnsen SJ, Steffensen JP, Petit JR, Schwander J, Souchez R (2001) A new 27 kyr high resolution East Antarctic climate record. *J Geophys Res* 28:3199-3202
- Keeling RF, Stephens BB (2001) Antarctic sea ice and the control of Pleistocene climate instability. *Paleoceanogr* 16:112-131
- Keeling CD, Whorf TP (2003) Atmospheric CO<sub>2</sub> records from sites in the SIO air sampling network, Oak Ridge National Laboratory, U.S. Department of Energy, Oak Ridge, Tenn., U.S.A.
- Kohfeld K, Harrison SP (2001) DIRTMAP: the geological record of dust. *Earth Sci Rev* 54:81-114
- Kohfeld KE, Harrison SP (in press) Glacial-interglacial changes in dust deposition on the Chinese Loess Plateau. *Quat Sci Rev*
- Kukla G (1989) Long continental records of climate - an introduction. *Palaeogeogr, Palaeoclimatol, Palaeoecol*, 72:1-9

- Kukla G, An ZS, Melice JL, Gavin J, Xiao JL (1990) Magnetic susceptibility record of Chinese loess. *Transactions Royal Society of Edinburgh Earth Sciences* 81:263-288
- Kyle PR, Jezek PA, Thompson EM, Thompson L (1981) Tephra layers in the Byrd Station ice core and the Dome C ice core, Antarctica and their climatic importance. *J. Volcanol. Geotherm. Res.* 11:29-39
- Lancaster N (1995) *Geomorphology of desert dunes*, Routledge, New York, 279 p.
- Legrand M, Mayewski P (1997) Glaciochemistry of polar ice cores: a review. *Rev. Geophys.* 35:219-243
- Legrand M, Hammer C, DeAngelis M, Savarino J, Delmas R, Clausen H, Johnsen SJ (1997) Sulfur-containing species (methanesulfonate and SO<sub>4</sub>) over the last climatic cycle in the Greenland Ice Core Project (central Greenland) ice core. *J Geophys Res* 102:26663-26679
- Lugmair GW, Marti K (1978) Lunar initial <sup>143</sup>Nd/<sup>144</sup>Nd: differential evolution of the lunar crust and the mantle. *Earth Planet Sci Lett* 39:349-357
- Lunt DJ, Valdes PJ (2002) Dust deposition and provenance at the Last Glacial Maximum and present day. *Geophys. Res. Lett.* 29:2085-2089
- Maggi V (1997) Mineralogy of atmospheric microparticles deposited along the GRIP ice core. *J Geophys Res* 102: 26,725-26,734
- Mahowald N, Kohfeld K, Hansson M, Balkanski Y, Harrison SP, Prentice IC, Schulz M, Rodhe H (1999) Dust sources and deposition during the Last Glacial Maximum and current climate: a comparison of model results with paleodata from ice cores and marine sediments. *J Geophys Res* 104:15895-15916.
- Markgraf V (1991) Younger Dryas in South America? *Boreas* 20:63-69
- McCulloch MT, Black LP (1984) Sm-Nd isotopic systematics of Enderby Land granulites and evidence for the redistribution of Sm and Nd during metamorphism. *Earth Plan. Sci. Lett.* 71:46-58
- McGlone MS, Salinger MJ, Moar NT (1993) Paleovegetation studies of New Zealand's climate since the Last Glacial Maximum. In: H.E. Wright, J.E. Kutzbach, T. Webb III, W.F. Ruddiman, F.A. Street-Perrott and P.J. Bartlein (ed) *Global climates since the Last Glacial Maximum*. University of Minnesota press, Minneapolis, p 294-317
- McGlone MS, Salinger MJ, Moar NT (1993) Paleovegetation studies of New Zealand's climate since the Last Glacial Maximum. In: H.E. Wright, J.E. Kutzbach, T. Webb III, W.F. Ruddiman, F.A. Street-Perrott and P.J. Bartlein (ed) *Global climates since the Last Glacial Maximum*. University of Minnesota press, Minneapolis, p 294-317
- Measures CI, Vink S (2000) On the use of dissolved aluminium in surface waters to estimate dust deposition to the ocean. *Global Biogeochem. Cycles* 14:317-328
- Mikolajewicz U, Maier-Reimer E (1990) Internal secular variability in an ocean general circulation model. *Clim Dyn* 4:145-156
- Mitchell JM (1976) An overview of climatic variability and its causal mechanisms. *Quat Res* 6:481-493

- O'Nions RK, Hamilton PJ, Evensen NM (1977) Variations in  $^{143}\text{Nd}/^{144}\text{Nd}$  and  $^{87}\text{Sr}/^{86}\text{Sr}$  ratios in oceanic basalts. *Earth Planet Sci Lett* 34:13-22
- Orombelli G (1996) Climatic records in ice cores. *Terra Antarctica* 3:63-75
- Parrenin F (2002) Datation glaciologique des forages profonds en Antarctique et modelisation conceptuelle des paleoclimats: implications pour la theorie astronomique des paleoclimats. LGGE-CNRS, Universite' Joseph Fourier-Grenoble I, Grenoble, 230 p.
- Partridge TC (1993) Warming phases in southern Africa during the last 150 000 years: an overview. *Palaeogeogr, Palaeoclimatol, Palaeoecol* 101:237-244
- Petit JR, Briat M, Royer A (1981) Ice Age aerosol content from East Antarctic ice core samples and past wind strength. *Nature* 293:391-394
- Petit JR, Mounier L, Jouzel J, Korotkevich YS (1990) Paleoclimatological and chronological implications of the Vostok core dust record. *Nature* 343:56-58
- Petit JR (1999) Climate and atmospheric history of the past 420000 years from the Vostok ice core, Antarctica. *Nature* 399:429-436
- Pittock AB (1980) Patterns of climatic variation in Argentina and Chile. I. Precipitation, 1931-1960. *Mon Weather Rev* 108:1347-1361
- Prentice IC, III TW (1998) BIOME6000: reconstructing global mid-Holocene vegetation patterns from paleoecological records. *J. Biogeogr.* 25:995-1005
- Prospero JM, Ginoux P, Torres O, Nicholson SE (2002) Environmental characteristics of global sources of atmospheric soil dust derived from the NIMBUS-7 TOMS absorbing aerosol product. *Rev. Geophys.* 40:1002, doi:10.1029/2000RG000095
- Pye K (1984) Loess. *Progress in Physical Geography* 8:176-217
- Pye K (1987) Aeolian dust and dust deposits, Academic Press, San Diego, California, 265 p.
- Rahmstorf S (2001) Abrupt Climate Change. In: J. Steele ST, and K. Turekian (ed) *Encyclopedia of Ocean Sciences*. Academic Press, London, p 1-6.
- Raisbeck GM, Yiou F, Jouzel J, Petit JR (1990)  $^{10}\text{Be}$  and  $\text{d}^2\text{H}$  in polar ice cores as a probe of the solar variability's influence on climate. *Phil Trans R Soc Lond A330*:463-470
- Raymo ME, Ruddiman WF, Shackleton NJ, Oppo DW (1990) Evolution of Atlantic-Pacific  $\text{d}^3\text{C}$  gradients over the last 25 m.y. *Earth Planet Sci Lett* 97:353-368
- Raynaud D, Blunier T, Ono Y, Delmas RJ (2003) The Late Quaternary history of atmospheric trace gases and aerosols: interactions between climate and biogeochemical cycles. In: K.D. Alverson, R.S. Bradley, T.F. Pedersen (ed) *Paleoclimate, global change and the future*. Springer Verlag, Berlin Heidelberg
- Rea DK (1994) The paleoclimatic record provided by eolian deposition in the deep sea: the geologic history of wind. *Rev. Geophys.* 32:159-195
- Revel M, Sinko JA, Grousset FE, Biscaye PE (1996) Sr and Nd isotopes as tracers of North Atlantic lithic particles: paleoclimatic implications. *Paleoceanogr* 11:95113

- Richard P, Shimizu N, Allegre CJ (1976)  $^{143}\text{Nd}/^{144}\text{Nd}$ , a natural tracer: an application to oceanic basalts. *Earth Planet Sci Lett* 31:269-278
- Roeckner E, et al (1992) Simulation of the present climate with the ECHAM model: impact of model physics and resolution. Report No. 93, Max-Planck-Inst. for Meteorol., Hamburg, Germany
- Rogers RR, Yau MK (1989) A short course in cloud physics, Pergamon Press, 293 p.
- Rollinson H (1993) Using Geochemical Data: evaluation, presentation, interpretation. Longman Singapore Publishers, Singapore
- Royer A, Angelis MD, Petit JR (1983) A 30000 year record of physical and optical properties of microparticles from an East Antarctic ice core and implications for paleoclimate reconstruction models. *Clim Change* 5:381-412
- Ruth U, Wagenbach D, Steffensen JP, Biggler M (2003) Continuous record of microparticle concentration and size distribution in the central Greenland NGRIP ice core during the last glacial period. *J. Geophys. Res* 108:4098-4110
- Sarnthein M (1978) Sand deserts during glacial maximum and climatic optimum. *Nature* 272:43-46
- Sarnthein M, Kennett JP, Allen J, Beer J, Grootes P, Laj C, McManus J, Ramesh R, 117 S-IWG (2002) Decadal-to-millennial-scale climate variability - chronology and mechanisms: Summary and recommendations. *Quat Sci Rev* 21:1121-1128
- Sayago JM (1995) The argentine neotropical loess: an overview. *Quat Sci Rev* 14:755-766
- Sayago JM, Collantes MM, Karlson A, Sanabria J (2001) Genesis and distribution of the Late Pleistocene and Holocene loess of Argentina: a regional approximation. *Quat International* 76/77:247-257
- Schulz M, Balkanski YJ, Guelle W, Dulac F (1998) Role of aerosol size distribution and source location in a three-dimensional simulation of a Sahara dust episode tested against satellite-derived optical thickness. *J Geophys Res* 103:10579-10592
- Schutz L, Seibert M (1987) Mineral aerosol and source identification. *J Aerosol Sci* 18:1-10
- Shulz M, Paul A (2002) Holocene climate variability on centennial to millennial time scales: 1. climate records from the North Atlantic realm. In: G. Wefer, W. Berger, K.-E. Behre, E. Jansen (ed) *Climate development and history of the North Atlantic realm*. Springer-Verlag, Berlin, Heidelberg
- Schwander J, Jouzel J, Hammer CU, Petit JR, Udisti R, Wolff E (2001) A tentative chronology for the EPICA-Dome Concordia ice core. *Geophys. Res. Lett.* 28:4243-4246
- Schwerdtfeger W (1984) *Weather and climate in the Antarctic*, Vol 15, Elsevier Science, Amsterdam, 261 p.
- Shackleton NJ (1987) Oxygen isotopes, ice volume and sea level. *Quat Sci Rev* 6:183-190
- Shulmeister J (1999) Australasian evidence for mid-Holocene climate change implies precessional control of Walker Circulation in the Pacific. *Quat International* 57/58:81-91
- Simoes JC, J.R. Petit, Souchez R, Lipenkov VY, Angelis MD, Liu L, Jouzel J, Duval P (2002) Evidence of glacial flour in the deepest 89 m of the Vostok glacier ice core. *Ann Glaciol*

- Smith BJ, Wright JS, Whalley WB (2002) Sources of non-glacial, loess-size quartz silt and the origins of "desert loess". *Earth Sci Rev* 59:1-26
- Sokolik IN, Toon OB (1996) Direct radiative forcing by anthropogenic airborne mineral aerosols. *Nature* 381:681-683
- Steele LP, Krummel PB, Langenfelds RL (2002) Atmospheric CH<sub>4</sub> concentrations from sites in the CSIRO Atmospheric Research GASLAB air sampling network (October 2002 version). Oak Ridge National Laboratory, U.S. Department of Energy, Oak Ridge, TN, U.S.A.
- Steffensen JP (1997) The size distribution of microparticles from selected segments of the GRIP ice core representing different climatic periods. *J Geophys Res* 102 (C12):26755-26763
- Steiger RH, Jager E (1977) Subcommittee on geochronology: convention on the use of decay constants on geo- and cosmochronology. *Earth Planet Sci Lett* 36:359-362
- Swap R, Garstang M, Greco S, Talbot R, Kallberg P (1992) Saharan dust in the Amazon Basin. *Tellus Ser.B*:133-149
- Tabacco IE, Passerini A, Corbelli F, Gorman M (1998) Determination of the surface and bed topography at Dome C, East Antarctica. *J Glaciol* 44:185-191
- Talbot MR (1980) Environmental responses to climatic change in the West African Sahel over the past 20000 years. In: M.A.J. W, H. Faure (ed) *The Sahara and the Nile*, Balkema, Rotterdam, p 37-62
- Taylor SR, McLennan SM (1985) *The Continental crust: its composition and evolution*, A. Hallam (ed) Blackwell Scientific Publications, 312 p.
- Tegen I, Fung I (1994) Modeling of mineral dust in the atmosphere: sources, transport, and optical thickness. *J. Geophys. Res* 99:22,897-822,914
- Tegen I, Lacis AA (1996) Modeling of particle size distribution and its influence on the radiative properties of mineral dust aerosol. *J. Geophys. Res* 101:19,237-219,244
- Tegen I, Harrison SP, Kohfeld K, Prentice IC, Coe M (2002a) The impact of vegetation and preferential source areas on global dust aerosol: Results from a model study. *J Geophys Res* 107, doi:10.1029/2001JD000963.
- Tegen I, Harrison SP, Kohfeld KE, McTainsh G (2002b) Modeling the role of Mineral Aerosol on Global Climate cycles. *EOS* 83 (36).
- Tegen I (*in press*) Modeling soil dust aerosol in the climate system: An overview. *Quat Sci Rev*
- Thirlwall MF (1997) Thermal ionisation mass spectrometry (TIMS). In: R. Gill (ed) *Modern analytical geochemistry*. Longman, Singapore
- Thompson LG, Mosley-Thompson E (1981) Microparticle concentration variations linked with climatic change: evidence from polar ice. *Science* 246:812-815
- Thompson LG, Mosley-Thompson E, Davis ME, Bolzan JF, Dai J, Yao T, Gundestrup N, Wu X, Klein L, Xie Z (1989) Holocene-Late Pleistocene climatic ice core records from Qinhai-Tibetan plateau. *Science* 246

- Thompson LG, Mosley-Thompson E, Davis ME, Lin P-N, Henderson KA, Cole-Dai J, Bolzan JF, Liu K-b (1995) Late glacial stage and Holocene tropical ice core records from Huascarán, Peru. *Science* 269:46-50
- Thompson LG (1998) A 25,000-year tropical climate history from Bolivian ice cores. *Science* 282:1858-1864
- Trombotta D (1996) The old cryogenic structures of Northern Patagonia: the Cryomere Penfordd. *Z. Geomorph. N.F.* 40:385-399
- Tyson PD (1986) *Climatic change and variability in southern Africa*, Oxford University Press, Cape Town, 220 p.
- Tzedakis PC, Andrieu V, Beaulieu JLD, Crowhurst S, Follieri M, Hooghiemstra H, Magri D, Reille M, Sadori L, Shackleton NJ, Wijmstra TA (1997) Comparison of terrestrial and marine records of changing climate of the last 500,000 years. *Earth Planet Sci Lett* 150:171-176
- Unnerstad L, Hansson M (2001) Simulated airborne particle size distribution over Greenland during Last Glacial Maximum. *Geophys. Res. Lett.* 28:287-290
- Venegas SA, Drinkwater MR, Shaffer G (2001) Coupled oscillations in Antarctic sea ice and atmosphere in the South Pacific sector. *Geophys Res Lett* 28:3301-3304
- Venegas SA, Drinkwater MR (2001) Sea ice, atmosphere and upper ocean variability in the Weddel sea, Antarctica. *J Geophys Res* 106:16747-16766
- Villalba R, Cook ER, D'Arrigo RD, Jacoby GC, Jones PD, Salinger MJ, Palmer J (1997) Sea-level pressure variability around Antarctica since A.D. 1750 inferred from subantarctic tree-ring records. *Clim Dyn* 13:375-390
- Wasson RJ (1986) *Geomorphology and Quaternary history of the Australian continental dunefields*. *Geographical Review of Japan*: 55-67
- Watanabe O, Jouzel J, Johnsen S, Parrenin F, Shoji H, Yoshida N (2003) Homogeneous climate variability across East Antarctica over the past three glacial cycles. *Nature* 422: 509-512
- Werner M, Tegen I, Harrison SP, Kohfeld KE, Prentice IC, Balkanski Y, Rodhe H, Roelandt C (2002) Seasonal and interannual variability of the mineral dust cycle under present and glacial climate conditions. *J Geophys Res* 107: doi:10.1029/2002JD002365
- White WB, Peterson RG (1996) An Antarctic circumpolar wave in surface pressure, wind, temperature and sea-ice extent. *Nature* 380:699-702
- Williams MAJ, Dunkerley DL, Dekker PD, Kershaw AP, Stokes TJ (1993) *Quaternary environments*, Edward Arnold, London, 329 p.
- Wright HE, Kutzbach JE, III TW, Ruddiman WF, Street-Perrott FA, Bartlein PJ (1993) *Global climates since the Last Glacial Maximum*, University of Minnesota, Minneapolis
- Young NW, Pourchet M, Kotlyakov VN, Korolev PA, Dyugero MB (1982) Accumulation distribution in the IAGP area, Antarctica: 90°E-150°E. *Ann Glaciol* 3: 333-338
- Zhang Y, Carmichael GR (1999) The role of mineral aerosol in tropospheric chemistry in East Asia - a model study. *J. Appl. Meteor.* 38:353-366



Zindler A, Hart SR (1986) Chemical Geodynamics. *Ann Rev Earth Planet Sci* 14:493-571